Vaccinia virus as a tool to study novel mechanisms of host cell contraction and blebbing

Charlotte Hope Durkin

University College London

and

Cancer Research UK London Research Institute

PhD Supervisor: Michael Way

A thesis submitted for the degree of

Doctor of Philosophy

University College London

September 2012

Declaration

I, Charlotte Durkin, confirm that the work presented in this thesis is my own. Where information has been derived from other sources, I confirm that this has been indicated in the thesis.

Abstract

Vaccinia is a widely studied member of the poxvirus family. Throughout its life cycle, vaccinia manipulates cellular processes of the host to aid its replication and spread. Early in infection vaccinia stimulates transient host cell contraction, associated with dynamic plasma membrane blebbing and migration, reminiscent of the RhoA-ROCK regulated amoeboid migration of cancer cells. Cell contraction required the expression of early vaccinia genes whilst subsequent re-spreading required late vaccinia genes. Using a virus that does not express the vaccinia protein F11, I showed that F11 was required for virus infection to stimulate contraction. However, using a highly attenuated vaccinia strain rescued with wild type F11, MVA-F11, I found that cell contraction additionally required other vaccinia proteins. Live cell imaging of F11-GFP revealed that F11 is recruited to the plasma membrane during blebbing, further supporting a role for F11 in regulating these membrane events. Despite previous evidence from this laboratory showing F11 interacts with RhoA, I found that cell contraction was independent of RhoA. Instead vaccinia induced contraction required RhoC to ROCK signalling. Furthermore, using a small siRNA screen of several Rho GTPases, I discovered that RhoD negatively regulates vaccinia-induced contraction. I suggest that RhoD can supress cell contraction in uninfected and ΔF11L-infected cells by inhibiting RhoC activation, and suggest that RhoD signalling is inhibited during infection to allow for efficient cell contraction.

Acknowledgements

I have just signed a declaration to say this work is my own but I would like to acknowledge the people that have helped me get there by offering scientific advice, technical help, encouragement or just general comic relief!

Firstly, I would like to give a big thanks to my supervisor Michael. Thank you for all your advice and support during the past four years but especially recently with help on the thesis and the long job hunt!

Sara, we have taken this PhD journey together! Thank you, I don't think I would have made it without you! I hope I have given you the same support, with our alternating waves of despair and reassurance. How am I going to do a PostDoc without you next to me? Ashley, I am so glad you were lured to the lab. It has been lovely working with you and you have become a great friend, why do you have to go off to the States as well? Theresa, thank you for being the heart of the lab family, for organising us all and keeping us in line. You also make a mean cocktail and throw the now world-famous Burn's Night suppers. I will be in London, can I still come? Jasmine, thank you for always giving great scientific insights and suggestions but more importantly for making me laugh and being my bench buddy! Thank you to my virology teacher, Antonio, for always asking the challenging questions and for providing comic relief with stories and photos of you beautiful daughter! Judy, it was 'quite' nice to work with you. Of course by that I mean it was a joy to work with you and I missed you very much when you left! Dave I owe you a beer (or several hundred!) for all your help with imaging and blebs, and patiently explaining image analysis to a layperson! Xenia, thank you for making me feel I was good at explaining techniques (even if you were pretending)! Good luck with the PhD, you will be great! Joe for lowering the tone of the lab, I'm not sure that warrants thanks?! Yutaka, thank you for the helpful discussions on F11. To Morag, Amy and Mark, I loved working with you and was extremely sad when you all left! I hope you all realise how grateful I am for you for all the help you gave me during my PhD! Joao, you were a great teacher and despite leaving 3 months after I started, you have always answered all my questions and provided continued reassurance and encouragement!

Thank you to everyone in the LRI equipment park for their expertise, saving me so much experimental time and explaining techniques with lots of patience. Thank you to Sally and Sophie (and Sabina and Erin), the graduate team at the LRI, for making the graduate programme so enjoyable and organised and for tirelessly answering all our questions and concerns.

And finally, I would like to thank my cheerleaders, this includes lots of friends and family members but especially my parents, my sisters and most of all Mike who has had to put up with more of my stress than anyone else!

Table of Contents

Table of figures

List of tables

Abbreviations

ADF	Actin depolymerisation factor
ADP	Adenosine 5'-diphsphate
Arp 2/3	Actin related proteins 2 and 3
ATP	Adenosine 5'-triphsphate
BTB	Bric-a-brac Tramtrack Broad-complex
Cdc	Cell division cycle
CEF	Chicken embryo fibroblast
CEV	Cell-associated enveloped virus
CRIB	Cdc42/Rac interactive binding
CVA	Chorioallantois vaccinia virus Ankara
DAPI	4',6 diamidino-2-phenylindole
DMSO	Dimethyl sulfoxide
dNTP	Deoxynucleoside 5'-triphosphate
DRF	Diaphanous related formin
E.coli	Escherichia coli
EEV	Extracellular enveloped virus
FBS	Foetal bovine serum
FRET	Förster/Fluorescence resonance electron transfer
GAG	Glycosaminoglycan
GAP	GTPase activating protein
GDI	Guanine dissociation inhibitor
GDP	Guanine diphosphate
GEF	Guanine nucleotide exchange factor
GFP	Green fluorescent protein
GTP	Guanine triphosphate
hpi	Hours post infection
IEV	Intracellular enveloped virus
IMV	Intracellular mature virus
IV	Immature virion
kb	kilobase
kDa	kiloDalton
LB	Luria Bertani

MEF	Mouse embryo fibroblasts
MEM	Minimal essential medium
MLC2	Myosin light chain 2
MOI	Multiplicity of infection
MVA	Modified vaccinia Ankara
PAK	p21 associated kinase
PBS	Phosphate buffered saline
PCR	Polymerase chain reaction
PFA	Paraformaldehyde
PH	Pleckstrin homology
RBD	Rho binding domain
RFP	Red fluorescent protein
Rho	Ras homolog gene family
ROCK	Rho-associated coiled-coil containing protein kinase
SDS	Sodium dodecyl sulphate
SH	Src homology
siRNA	Small interfering ribonucleic acid
TGN	Trans-golgi network
v/v	Volume per volume
w/v	Weight per volume
WASP	Wiskott-Aldrich-Syndrom protein
WAVE	WASP Verprolin homologous protein
WR	Western Reserve

Chapter 1. Introduction

1.1 Rho Family GTPases

1.1.1 Overview of Rho GTPases - history and biology

The first *rho* gene was discovered by accident in the molluscs Aplysia and was identified as a *ras*-related gene (Madaule and Axel, 1985). *Rho* was subsequently found to be evolutionary conserved (with up to 70% amino acid homology) between molluscs, *drosophila* and humans, with multiple *rh*o genes (*rhoA, rhoB* and *rhoC*) identified in humans (Madaule and Axel, 1985). Rac1 and Cdc42 were later identified as *ras*-related genes and Rho, Rac1 and Cdc42 were clustered as the Rho sub family, based on sequence identity (Didsbury et al., 1989; Hall, 1990; Shinjo et al., 1990). Studies with the *Clostridium botulinium* toxin C3 (an ADP-ribosylating enzyme) provided the first indication of the biological function of the Rho family of GTPases. Several studies had confirmed RhoA and RhoC as the substrates for C3 (Aktories et al., 1989; Braun et al., 1989; Chardin et al., 1989). ADP ribosylation renders Rho biologically inactive (Paterson et al., 1990). In parallel, it was observed that actin stress fibres were completely abolished in Vero cells following treatment with C3 (Chardin et al., 1989). This led to the elucidation of specific cytoskeletal regulatory roles for RhoA, Rac1 and Cdc42. Microinjection of activated RhoA into mammalian cells stimulated stress fibres and focal adhesion assembly (Paterson et al., 1990; Ridley and Hall, 1992). Overexpression and microinjection of activated Rac1 induced a reorganisation of actin to the leading edge plasma membrane to form membrane ruffles and focal adhesions (Ridley et al., 1992). Finally, Cdc42 was found to induce long filopodia (Nobes and Hall, 1995).

Since the initial studies on Rho, Rac and Cdc42, the Rho GTPase family has expanded to encompass 22 family members with diverse biological functions. These family members have now been implicated is a wide range of biological functions including but not limited to the cytoskeleton, transcription, cell cycle, cytokinesis and membrane trafficking. As the work presented in this thesis is mainly concerned with the RhoA-related subfamily of GTPases and their role in cell migration, the regulation and signalling of this family will be discussed in more detail.

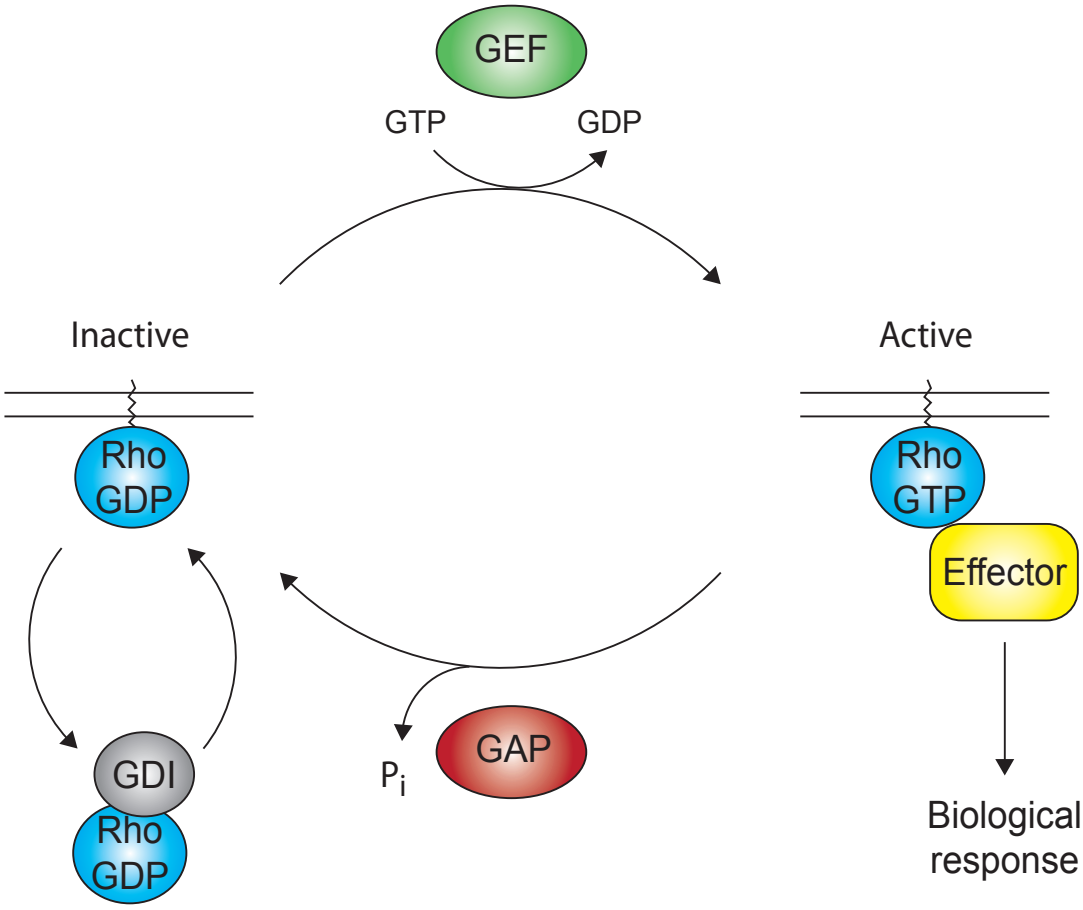

Figure 1.1 The Rho GTPase cycle

Rho GTPases cycle between GTP bound active and GDP bound inactive states. Three groups of proteins regulate the cycle: GEFs catalyse the exchange of GDP for GTP, GAPs stimulate GTP hydrolysis and GDIs sequester GDP bound Rho in the cytosol. GTP and GDP bound Rho are localised at membranes using isoprenoid lipid moieties and the polybasic region. GTP bound Rho binds to effector molecules to elicit a biological response.

1.1.2 The molecular switch and Rho GTPase structure

1.1.2.1 The molecular switch

Rho GTPases are 20-25kDa proteins with intrinsic GTPase activity. These proteins act as molecular switches that can cycle between a GTP bound active state and a GDP bound inactive state. In the GTP bound state Rho GTPases bind to and activate effector molecules to stimulate downstream signalling (Bishop and Hall, 2000). The activity of Rho GTPases is regulated by three sets of molecules, GEFs, GAPs and GDIs. Guanine nucleotide exchange factors (GEFs) catalyse the exchange of GDP for GTP and therefore stimulate Rho activity (Bos et al., 2007). GTPase activating proteins (GAPs) enhance the rate of GTP hydrolysis, which is intrinsically very slow, resulting in the inactive Rho state (Bos et al., 2007). Guanine dissociation inhibitors (GDIs) maintain a cytosolic GDP bound inactive pool of Rho GTPase (Garcia-Mata et al., 2011). Nearly all Rho family members are post-translationally modified at the C terminus CAAX box with an isoprenoid lipid, this allows Rho proteins to localise to membranes (Figure 1.1) (Boulter et al., 2012).

1.1.2.2 Rho GTPase structure

Rho GTPases have a conserved structural fold of a mixed six-stranded β-sheet (β1-6) surrounded by five α-helices (α1-5), called the G domain fold, common to all guanine nucleotide-binding proteins (Figure 1.2) (Vetter and Wittinghofer, 2001). Rho GTPases are distinguished from other GTPase proteins by a 13-residue insertion called the 'Rho Insert domain' (Valencia et al., 1991). The guanine base of the nucleotide is buried within a hydrophobic pocket formed by the conserved motifs GXKXDL (residues 116-121 in RhoA) and SAK residues (106-162 in RhoA) (Ihara et al., 1998). In the GTP bound conformation, the triphosphate groups form 21 direct and 9 water mediated hydrogen bonds with residues in the switch 1 (residues 28-44 between α1 and β2 in RhoA) and switch 2 regions (residues 62-69 between β3 and β4 in RhoA) and the phosphate binding loop (P loop) (residues 13-20 in RhoA) (Figure 1.3 A) (Ihara et al., 1998). The nucleotide binding site contains a Mg^{2+} ion, which co-ordinates the correct orientation of the P loop, switch 1 and switch 2 with β- and γ-phosphates, as such the Mg^{2+} ion is critical to nucleotide binding and GTP hydrolysis (Ihara et al., 1998; Shimizu et al., 2000). The switch 1 and 2 regions are flexible and exist in different structural conformations depending on the whether they bind GTP or GDP (Hakoshima et al.,

2003). The GTP bound form is in a ‘loaded spring’ conformation where the γ-phosphate oxygen atoms stabilise the main chain NH groups of Threonine 37 and Glycine 62. Upon hydrolysis of the bond between β- and γ-phosphates, these interactions are lost and switch 1 and 2 revert to a relaxed conformation (Figure 1.3 B) (Vetter and Wittinghofer, 2001). The conformation of the switch 1 and switch 2 regions determines GTPase signalling as they represent the main binding interface between the GTPase and effector molecules. GTPase effector molecules only bind to the GTP bound ‘loaded spring’ conformation (Hakoshima et al., 2003).

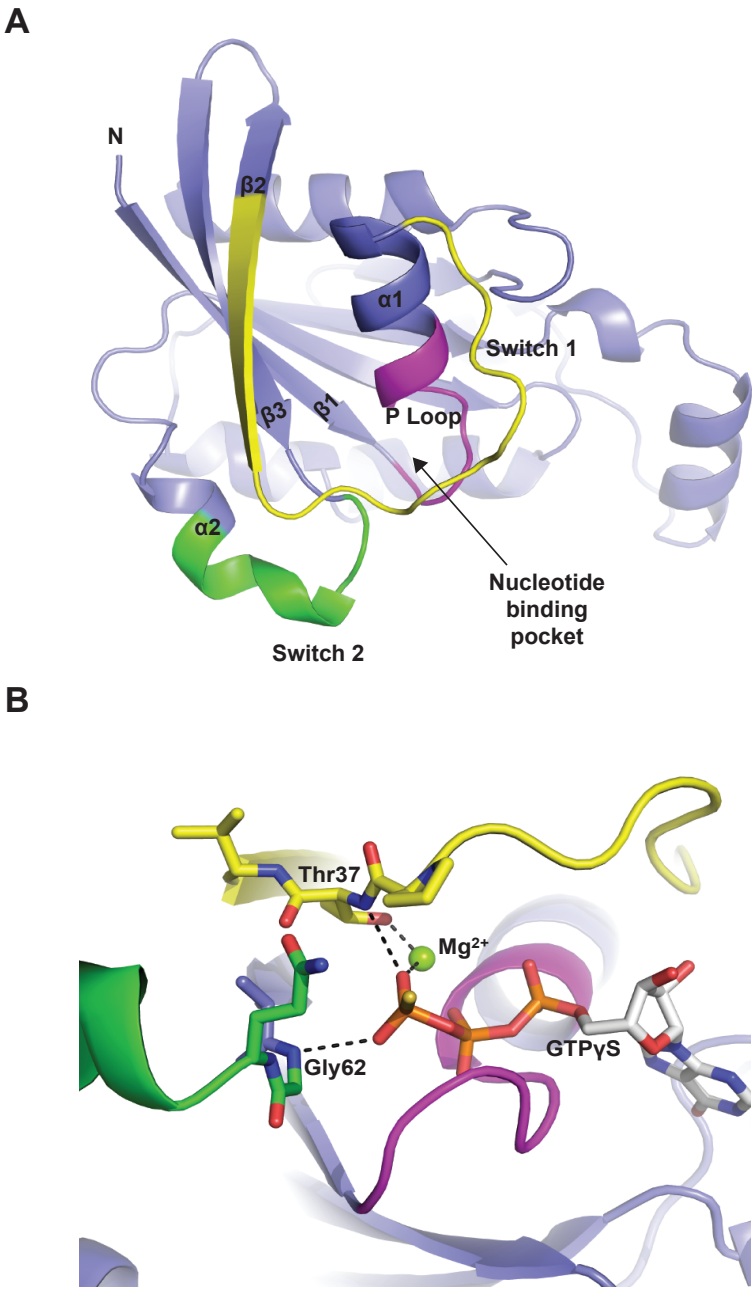

Figure 1.2 Crystal structure of RhoA

A. The crystal structure of RhoA is made up of a six-stranded β sheet surrounded by five α-helices. The nucleotide-binding site is formed by the switch 1 (yellow) and switch 2 (green) and the P loop (magenta). **B**. A close up of the nucleotide-binding site with GTPγS (orange) and Mg^{2+} ion (light green). The oxygen atoms of the γ-phosphate group of GTP hydrogen bond with the main chain NH (blue) groups of Threonine 37 and Glycine 62. Images were created using PyMol from PBD 1S1C (Dvorsky et al., 2004)

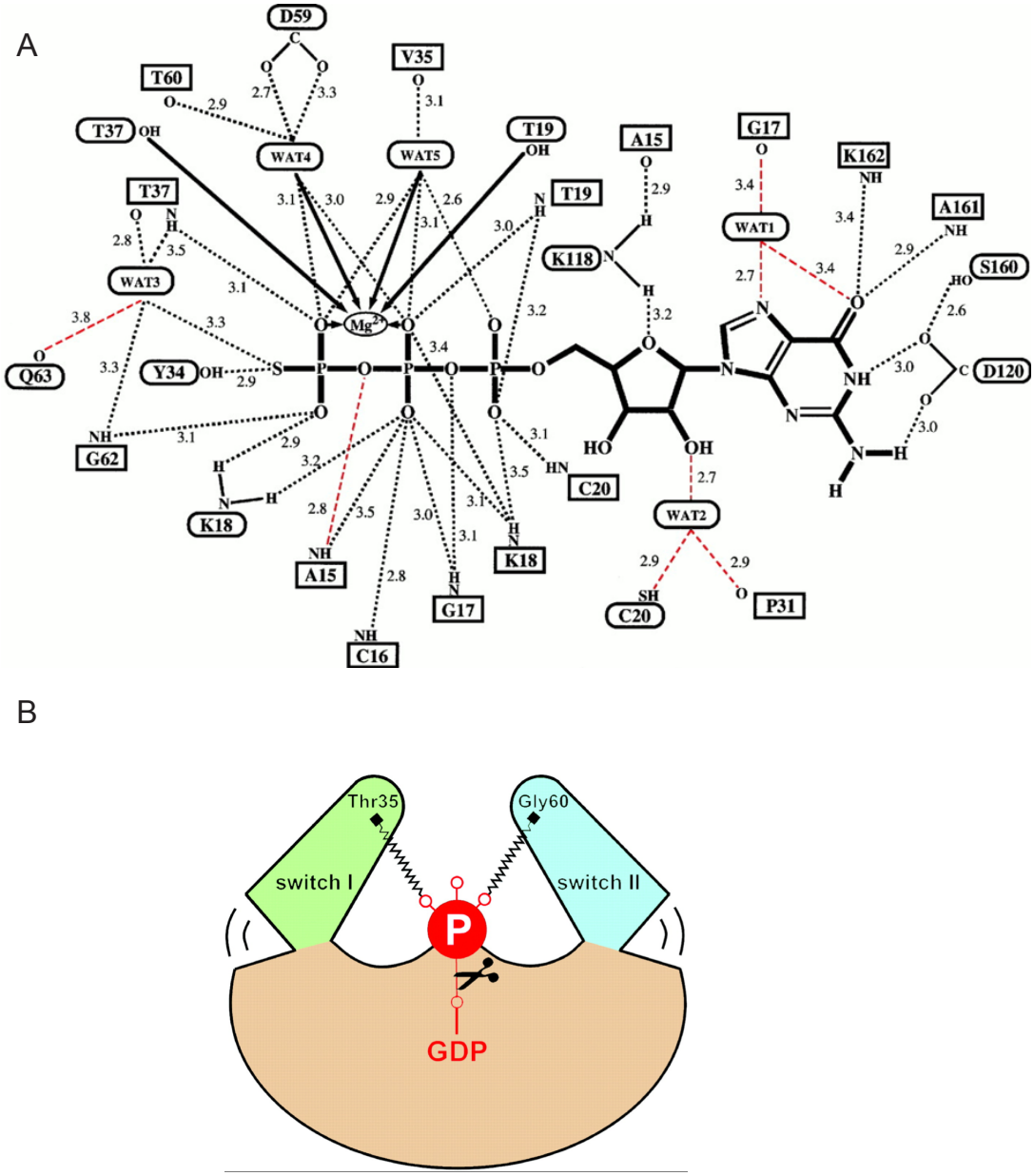

Figure 1.3 The "loaded spring"

A. An illustration of the interactions formed between RhoA and GTPγS as determined from the crystal structure. Dashed lines represent hydrogen bonds. Hydrogen bonds can form between GTPγS and amino acid main chains (residues in rectangles) or side chains (residues in ovals). This figure was originally published in Journal of Biological Chemistry. Ihara, K *et al.,* Crystal structure of Human RhoA in a Dominantly Active Form Complexed with a GTP Analogue. *J Biol Chem,* 273**,** 9656-66 © the American Society for Biochemistry and Molecular Biology. **B** A schematic of the "loaded spring" conformation. The γ phosphate oxygen atoms of GTP hydrogen bond with the main chains of a threonine residue in switch 1 (Thr37 in RhoA) and a glycine residue in switch 2 (Gly 62 in RhoA). This figure was originally published in Science. Vetter and Whittinghofer (2001) The guanine nucleotide-binding switch in three dimensions. Science 294: 1299-304. Reprinted with permission from AAAS.

1.1.2.3 Effector binding

The crystal structures of GTP bound RhoA, Rac1 and Cdc42 in complex with Rho binding domains of specific effectors have provided essential molecular insights into the structural elements required for effector binding (reviewed in (Dvorsky and Ahmadian, 2004)). The Rho binding domains (RBD) of Rho associated kinase (ROCK) and protein kinase N (PKN) form α-helical coiled-coil dimers to complex with RhoA. The RBD of ROCK binds predominantly to residues in the α2 helix, switch 1 and 2 regions (Dvorsky et al., 2004). PKN interacts with two contacts sites within RhoA. The first site is formed from α1, β2/β3 and α5 regions, the second site from the C-terminal half switch 2, β3 and switch 1 (Maesaki et al., 1999). Meanwhile, the GTPase binding domains (GBD) of activated Cdc42-associated kinase (ACK), Wiskott-Aldrich syndrome protein (WASP) and p21 associated kinase (PAK1) interact with the Cdc42 α1 and α5 helices and both switch regions using a β-hairpin and a C-terminal α-helix (Abdul-Manan et al., 1999; Morreale et al., 2000; Mott et al., 1999). Additionally the Cdc42/Rac–interactive binding (CRIB) motif, a feature found in these Cdc42/Rac effectors, forms an intermolecular β-sheet with β2 strand of the GTPase (Abdul-Manan et al., 1999; Morreale et al., 2000; Mott et al., 1999). The crystal structure of $p67^{phox}$ reveals a different mechanism for Rac1 binding. $p67^{phox}$ interacts with α1, switch 1 and the loop between β6 and α5 of Rac1 via four α-helical tetratrico-peptide (TPR) motifs (Lapouge et al., 2000). There is clearly a great divergence in the mechanism by which effector molecules bind to Rho GTPases, however, the majority of effectors interact with Rho GTPases over the switch 1 and 2 regions (reviewed in (Dvorsky and Ahmadian, 2004)). The switch regions experience the greatest conformational changes between GDP and GTP binding, therefore, specific binding of effectors to these regions must form the basis of GDP/GTP selectivity.

Rho GTPases frequently activate effector proteins by disrupting auto inhibitory interactions within the effector molecule (Bishop and Hall, 2000). The PAK family of kinases contain a regulatory domain that binds to the kinase domain and maintains a closed, inactive conformation (Lei et al., 2000). This intramolecular interaction is disrupted upon binding to GTP bound Rac or Cdc42, which allows the kinase domain to bind substrates (Lei et al., 2000; Parrini et al., 2002; Tu and Wigler, 1999). PAK kinases can then auto-phosphorylate to release the GTPase and stabilise the active conformation (Jung and Traugh, 2005; Manser et al., 1994). ROCK, PKN and DRFs (Diaphanous related formins) also exist in an auto-inhibited conformation, which is

disrupted upon RhoA binding (Amano et al., 1999; Maiti et al., 2012; Watanabe et al., 1996; Yoshinaga et al., 1999). In many cases, full activation of effectors is only achieved by additional signalling inputs. For example, the activation of N-WASP by Cdc42 is enhanced upon synergistic binding to SH3 adapter molecules and PIP_2 (Rohatgi et al., 2001; Tomasevic et al., 2007).

1.1.3 Regulation of Rho GTPases

1.1.3.1 Guanine nucleotide exchange factors (GEFs)

Rho GTPases, as with all members of the Ras superfamily of small GTPases, have extremely high affinity for guanine nucleotides and as a result the half-life of nucleotide dissociation is in the range of one or more hours (Bos et al., 2007). This is not practical for molecules that act as molecular switches to transduce rapid signals. The problem is overcome by a family of proteins called Rho Guanine nucleotide exchange factors (GEFs) that catalyse nucleotide exchange. The mechanism of GEF action on Rho GTPases involves conformational changes within the nucleotide binding site, specifically within switch 1, switch 2 and the P loop, to reduce the affinity of the GTPase for the nucleotide (Boriack-Sjodin et al., 1998; Worthylake et al., 2000). Upon GTPase:GEF complex formation steric changes physically block the Mg^{2+} binding site and disrupt interactions between the Mg^{2+} ion and the nucleotide. Additionally, GEF binding disturbs the interaction between the P loop and nucleotide phosphate groups (Boriack-Sjodin et al., 1998; Bos et al., 2007; Rossman et al., 2002; Worthylake et al., 2000). The GEF then stabilises the transient nucleotide free GTPase intermediate (Vetter and Wittinghofer, 2001). This intermediate has roughly equal affinity for either GTP or GDP, but the cellular concentration of former is 10 times higher and therefore GTP binding is favoured (Bos et al., 2007; Traut, 1994). GTP binding to the GTPase reduces its affinity for the GTPase for the GEF, which subsequently dissociates (Yang et al., 2009).

Rho GEFs fall into two major groups, the conventional DH-PH family and the atypical DOCK180 family. The DH-PH family is the largest group, comprising 69 predicted members in the human genome. The minimal requirements are a Dbl homology (DH) domain (the GEF domain), which was first identified in Dbl, and a C terminal pleckstrin homology (PH) domain (Hart et al., 1991; Rossman et al., 2002). The DOCK180-

related proteins comprise 11 members that all contain a DOCK homology region (DHR)-2 domain (the GEF domain) and an N-terminal DHR-1 domain (Brugnera et al., 2002; Cote and Vuori, 2002, 2007). Rho GEFs from both families also contain additional domains, such as protein-protein interaction domains (PDZ, SH2 and SH3 domains) or protein lipid interaction domains (PH, BAR and FYVE domains)(Bos et al., 2007; Cote and Vuori, 2002; Lemmon, 2008; Yaffe, 2002). The modular structure means that GEFs can be tightly regulated by translocation and allosteric structural changes and also act to integrate multiple signalling pathways or as signalling scaffolds (Bos et al., 2007).

1.1.3.2 GTPase activating proteins

GTPases are actually very inefficient at hydrolysing GTP so require GTPase activating proteins (GAPs) to catalyse the reaction (Leonard et al., 1998; Trahey and McCormick, 1987; Zhang et al., 1999). GAPs allows for tight control over Rho signalling, as downstream signalling can be turned off rapidly and in response to upstream signals. There are between 59-70 predicted Rho GAPs in the human genome (based on sequence searches for the Rho GAP domain) of which half have been characterised *in vivo* or *in vitro* (Peck et al., 2002; Tcherkezian and Lamarche-Vane, 2007). In comparison there are only 22 Rho GTPases. Therefore multiple GAPs should activate a single GTPase, presumably in response to specific signalling pathways in specific cellular locations or tissues. Rho GAPs are themselves tightly controlled by a number of mechanisms, including protein-protein and protein-lipid interactions, phosphorylation and protein degradation (reviewed in(Tcherkezian and Lamarche-Vane, 2007)).

Rho GAPs catalyse GTP hydrolysis by stabilising switch 1 and 2 in a reaction transition state and by contributing an arginine residue ('arginine finger') into nucleotide-binding site. In the transition state the GAP arginine residue stabilises the side chain of a GTPase glutamine residue (Gln63 in RhoA), to co-ordinate the correct orientation of the nucleophilic water molecule and the β and γ phosphates of GTP (Rittinger et al., 1997). GAP binding accelerates GTPase activity by some 10^5 fold (Rittinger et al., 1997). This GAP mechanism is a general mechanism that applies to other GTPase families within the Ras-superfamily. This is despite strikingly little structural similarity between the different GAPs for different GTPase families (Bourne, 1997).

1.1.3.3 Post-translational modifications of Rho GTPases

The proper subcellular localisation of Rho GTPases, namely to different membrane compartments, is essential for their biological function. This is achieved through post translation modification with the addition of isoprenoid lipid moieties (Hancock et al., 1991b; Hancock et al., 1990; Michaelson et al., 2001). The C terminus of Rho GTPases is a CAAX box, where C is Cysteine, A is an aliphatic residue and X any residue. The CAAX box undergoes a series of post-translational modifications (Hancock et al., 1991a). Firstly, a farnesyl or geranylgeranyl group is covalently attached to the cysteine residue, catalysed by farnesyltransferase or geranylgeranyltransferase, respectively (Clarke, 1992). The nature of the X residue in the CAAX box determines the lipid moiety added to the Rho protein. When X is Leu, Phe, Ile or Val the protein is geranylgeranylated, when X is Gln, Cys, Ser, Thr or Ala the protein is farnesylated (Boulter et al., 2012). RhoA, Rac1 and Cdc42 are all geranylgeranylated. Subsequently, the –AAX motif is removed by the Ras converting enzyme 1 (Rce1) endopeptidase. Finally the isoprenylated cysteine is methylated by isoprenylcysteine carboxyl methyltransferase (Imct) (Clarke, 1992). This results in a highly hydrophobic C terminus (whereas the remainder of the protein is hydrophilic) that targets the Rho GTPase to hydrophobic membranes. In addition, Rho GTPases contain a polybasic region (PBR) immediately upstream of the CAAX box (Hancock et al., 1990; Wheeler and Ridley, 2004). The PBR is a stretch of positively charged residues that associate with negative phospholipids in the membrane to help stabilise the Rho GTPase at the membrane (Hancock et al., 1990). The PBR also directs localisation to different membrane compartments, depending on the electrostatic properties of the PBR and the composition of the membrane (Boulter et al., 2012). The region differs significantly within the Rho family and regulates specific localisation of family members to distinct membrane compartments (Michaelson et al., 2001).

Rho GTPase can be further regulated by the addition of post-translational modifications, including, phosphorylation, oxidation, and ubiquitination/degradation. Phosphorylation can negatively regulate specific Rho proteins. Seven of the 22 Rho proteins, including RhoA, Cdc42 and RhoG, have a serine residue between the CAAX motif and PBR (Ser188 in RhoA), which can be phosphorylated (Wheeler and Ridley, 2004). This weakens the association of the Rho GTPase with the membrane as it introduces a negative charge adjacent to the PBR, which disturbs the electrostatic interactions with the negatively charged phospholipids (Ellerbroek et al., 2003). In addition,

phosphorylation at Ser188 increases the affinity of RhoGDI for RhoA and the GTPase is extracted from the membrane (Boulter et al., 2012; Garcia-Mata et al., 2011) (Ellerbroek et al., 2003).

1.1.3.4 Guanine dissociation inhibitors

90-95% of each Rho GTPase is maintained in the cytoplasm in a soluble inactive (GDP bound) state by Rho guanine dissociation inhibitors (GDIs) (Boulter et al., 2010). There are three RhoGDI proteins (RhoGDI1-3), RhoGDI1 is the most abundant and is ubiquitously expressed (DerMardirossian and Bokoch, 2005). The structural basis of RhoGDI1 and GTPase binding was elucidated from studies with RhoA, Rac1 and Cdc42 (Grizot et al., 2001; Hoffman et al., 2000; Longenecker et al., 1999). In a two-step mechanism of binding, the GDI N-terminal regulatory arm interacts with the GTPase switch 1 and 2 regions. Subsequently, the GTPase isoprenoid moiety burrows into a geranylgeranyl hydrophobic binding pocket at the C terminus of the GDI. In addition, an acidic patch in the hydrophobic binding pocket interacts with the GTPase polybasic region (Grizot et al., 2001; Hoffman et al., 2000; Longenecker et al., 1999).

RhoGDIs are classically perceived as negative regulators of Rho GTPase, because they preferentially bind the GDP bound GTPase and sequester GTPase in the cytoplasm away from the site of activation (Leonard et al., 1992). In addition, RhoGDIs may also provide an additional regulatory mechanism in Rho GTPase cycle, by functioning as chaperones to maintain a reservoir of GTPase ready for rapid activation in response to stimulation (Garcia-Mata et al., 2011). In the absence of RhoGDI1, Rho GTPases are rapidly degraded, as mature GTPases are insoluble as a result of the hydrophobic prenylated C terminus (Boulter et al., 2010). The release of GDP bound GTPase from RhoGDI1 can regulated by lipid or protein interactions (Rose et al., 2005b; Takahashi et al., 1997). In addition, phosphorylation of RhoGDI1 reduces its affinity for Rho GTPases, conversely phosphorylation of the GTPase at Ser188 (in RhoA) increases the affinity of the interaction (DerMardirossian et al., 2004; Ellerbroek et al., 2003). At any one time the pool of RhoGDI1 is bound to multiple different Rho GTPases, but it is not clear how an individual Rho protein can be released from the GDI in response to specific signals. It has been hypothesised that this is mediated by

phosphorylation at specific sites in the GDI or by recruitment to the correct cellular compartments (Garcia-Mata et al., 2011).

1.2 RhoA and cell migration

There are four main types of actin structures in the mesenchymal mode of cell migration; lamellipodia, filopodia, focal adhesions and stress fibres (Figure 1.4) (Ridley, 2011). Lamellipodia and filopodia drive protrusion of the plasma membrane at the front of the cell, the leading edge. Focal adhesions form at the basal surface of the leading edge to form contracts with the substratum to provide traction to pull the cell forward. As the cell pulls forward focal adhesions mature and grow. Stress fibres provide contractile force to bring the rear of the cell forward towards the leading edge, this force also promotes detachment from the substrate at the rear. Rho GTPases play a significant role in regulating these actin structures during cell migration. Rac activates WAVE to stimulate Arp2/3 driven actin polymerisation at the leading edge to form dendritic arrays of actin filaments in lamellipodia (Eden et al., 2002; Ridley et al., 1992; Svitkina and Borisy, 1999; Vinzenz et al., 2012). Cdc42 also stimulates Arp2/3 dependent actin polymerisation at the leading edge, but instead uses the nucleation-promoting factor WASP/N-WASP to drive filopodia formation (Miki et al., 1998; Nobes and Hall, 1995; Rohatgi et al., 2000; Rohatgi et al., 1999). RhoA drives the formation and contraction of actin myosin arrays in stress fibres or in the cell cortex (Paterson et al., 1990; Ridley and Hall, 1992). Other Rho GTPases can also regulate these structures and this will be discussed in more detail in later sections (1.2.5).

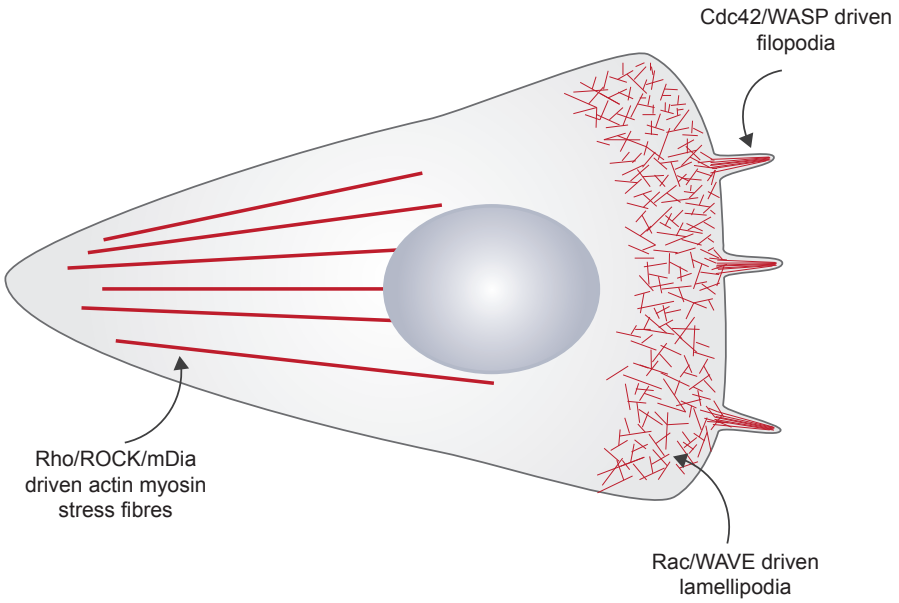

Figure 1.4 Actin structures

Three types of actin structures that are regulated by Rho GTPases in a migrating cell. Filopodia are bundles of unbranched actin filaments that are induced by Cdc42 using VASP, Formins and Arp2/3 activation by N-WASP. Lamellipodia are formed by a dendritic array of branched actin driven by Rac activation of Arp2/3 actin polymerisation via WAVE. Stress fibres comprised of actin and myosin II filaments are formed in response to RhoA signalling to ROCK and mDia.

1.2.1 RhoA signalling and cell migration

RhoA regulates the formation and contraction of actin stress fibres and contraction of the cell cortex through synergistic activation of multiple signalling pathways (Figure 1.4). RhoA stimulates the activity of the kinase ROCK, which then phosphorylates myosin light chain (MLC) and MLC phosphatase (Bishop and Hall, 2000). Phosphorylation of MLC leads to the activation of the non-muscle myosin II motor protein and the consequential contraction of actin fibres in actin-myosin bundles (Vicente-Manzanares et al., 2009). Additionally, ROCK activates LIM kinase (LIMK), which in turns inactivates cofilin leading to actin filament stabilisation (Bishop and Hall, 2000). RhoA can regulate the *de novo* formation and elongation of actin filaments by activating the mammalian diaphanous formins (mDia1-3) (Goode and Eck, 2007). Each of the downstream signalling pathways illustrated in Figure 1.5 will now be discussed in more detail. Although this section specifies signalling downstream of RhoA, the same can be considered to be true downstream of RhoB and RhoC as the three proteins share 85% sequence identity and bind to ROCK and mDia1 (Ihara et al., 1998; Rose et al., 2005b).

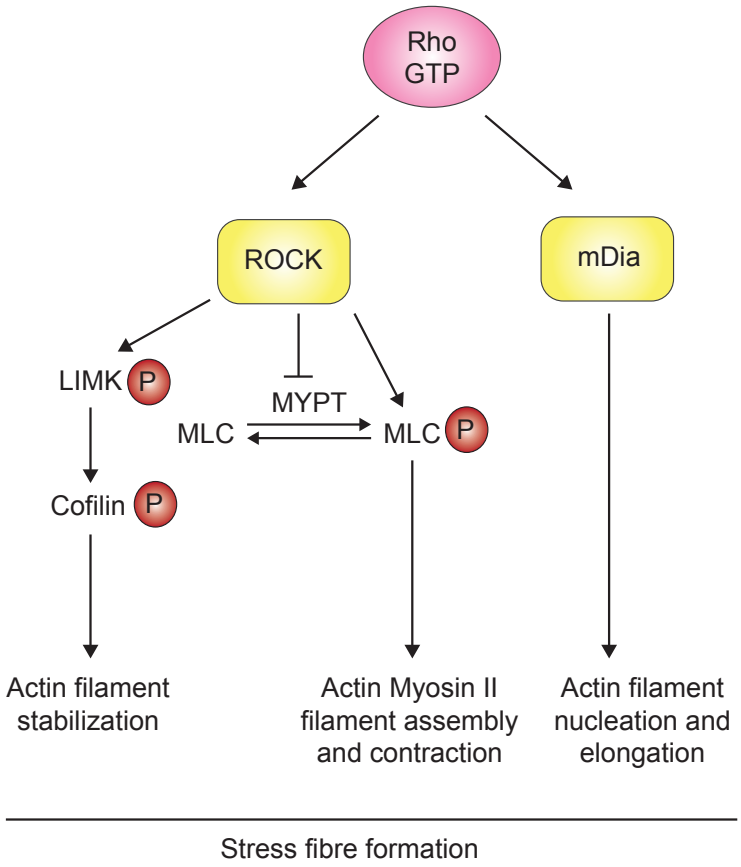

Figure 1.5 RhoA signalling in stress fibre formation

GTP bound RhoA binds to and activates ROCK and mDia. ROCK phosphorylates MLC and MYPT to increase the levels of phosphorylated MLC and stimulates actin myosin fibre assembly and contraction. ROCK also phosphorylates LIMK, which in turn phosphorylates cofilin and prevents cofilin from severing actin filaments. mDia nucleates actin filaments and remains bound to the barbed end to elongate actin filaments. Adapted with permission from The Biochemical Journal. Bishop, A.L., and Hall, A., Rho GTPases and their effector proteins. 2000; *348 Pt 2*, 241-255 © **the Biochemical Society**

1.2.2 RhoA and ROCK

The two ROCK proteins, ROCKI (Rokβ/p160 ROCK) and ROCKII (Rokα/Rho kinase), were initially identified as RhoA interacting proteins that preferentially interact with GTP bound RhoA (Ishizaki et al., 1996; Leung et al., 1995; Matsui et al., 1996; Nakagawa et al., 1996). The two proteins possess a N-terminal serine/threonine kinase domain, a central α-helical coiled-coil domain with an internal Rho binding domain (RBD) and a C-terminal pleckstrin homology domain (PH) (Figure 1.6 A) (Fujisawa et al., 1996;

Ishizaki et al., 1996; Matsui et al., 1996; Nakagawa et al., 1996). ROCKI and ROCKII share 64% overall sequence identity with 92% identity in the kinase domains (Leung et al., 1996; Nakagawa et al., 1996). ROCK is believed to exist in an inactive auto inhibited conformation as the C-terminal portion, containing the RBD and PH domains, inhibits kinase activity and deletion of the PH domain results in constitutively active ROCK (Amano et al., 1997; Amano et al., 1999; Ishizaki et al., 1996; Leung et al., 1995). It has been suggested that this intramolecular interaction is disrupted upon binding of RhoA to the RBD (Amano et al., 1997; Amano et al., 1999; Ishizaki et al., 1996; Leung et al., 1995) (Figure 1.6 B). The coiled-coil region mediates the dimerization of ROCK as a parallel dimer, and structural analysis of this region revealed a discontinuity in the coiled-coil dimer that could act as a hinge to allow the putative folded auto inhibitory conformation (Figure 1.6 B)(Shimizu et al., 2003; Tu et al., 2011). The RBD resides within the coiled-coil domain and binds to two RhoA molecules as a coiled-coil dimer using a combination of hydrophobic and electrostatic interactions. One face of the coiled-coil dimer interacts with the switch 1 and 2 regions of one RhoA molecule, while complementary interactions are formed on the opposite face of the dimer with a second RhoA molecule (Dvorsky et al., 2004). The minimal RBD of ROCK1 is a 13-residue motif (residues 998-1010), which is highly conserved between ROCK proteins from other organisms (Figure 1.6 A) (Dvorsky et al., 2004). In addition to RhoA, both RhoB and RhoC can also directly interact with ROCKII (Leung et al., 1996). The residues through which RhoA interacts with ROCK1 are entirely conserved with RhoB and RhoC, suggesting that these proteins interact with ROCK through the same mechanism (Dvorsky et al., 2004).

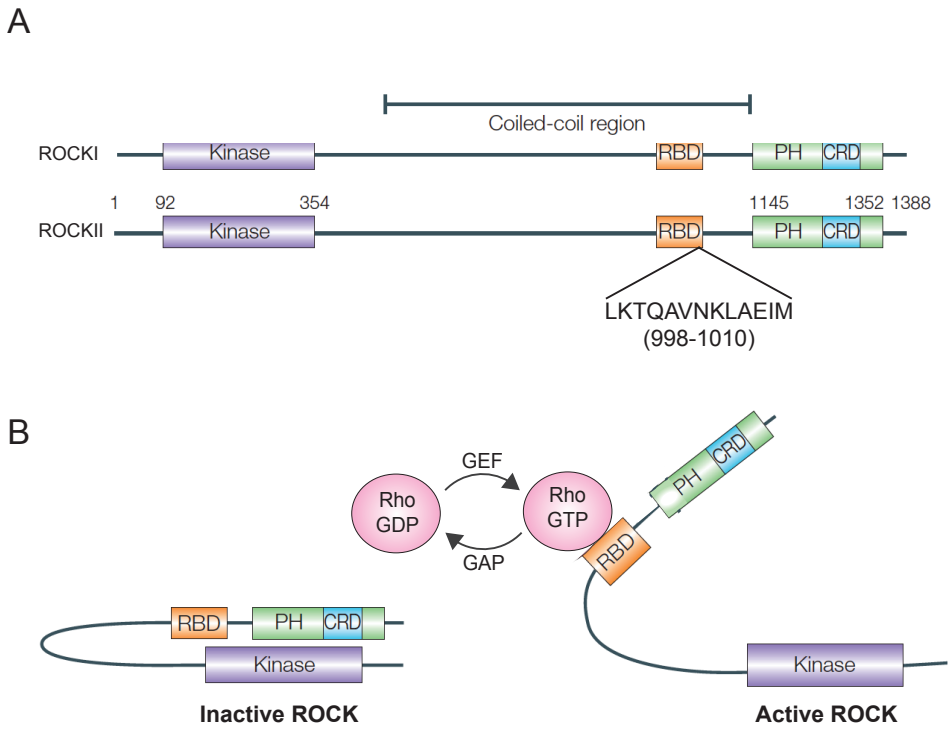

Figure 1.6 The activation of ROCK

A. ROCK proteins are comprised of a kinase domain, a coiled-coil region, a Rho binding domain (RBD) and a pleckstrin homology domain. **B.** The N-terminal kinase domain is inhibited by the C-terminal RBD and PH domains. Auto-inhibition is relieved when ROCK binds to GTP bound RhoA. Both A and B are adapted with permission from Macmillan Publishers Ltd: Riento, K and Ridley, A. Nat Rev Mol Cell Biol. 2003 Jun;4(6):446-56. Copyright 2003

1.2.2.1 ROCK and Actin myosin fibre assembly

Stress fibres are actin myosin structures that loosely resemble the sarcomeric arrays in muscle cells. The fibres comprise approximately 10-30 actin filaments per fibre that are bundled by crosslinking proteins, such as α-actinin, and bipolar non-muscle myosin II filaments (Cramer et al., 1997; Verkhovsky and Borisy, 1993). α-actinin and Myosin II array between actin filaments in alternating bands, and α-actinin crosslinking dictates spacing between actin filaments to allow the insertion of myosin bundles (Langanger et al., 1986). The polarity of the actin filaments is generally ordered, such that the fast-growing/barbed ends are pointed outwards (Cramer et al., 1997). Myosin filaments progressively walk along actin filaments towards the barbed ends in an ATP dependent manner to generate contractile force by dragging actin filaments of opposite polarity

towards each other (Figure 1.7) (Vicente-Manzanares et al., 2009). Functional myosin II is a complex consisting of two heavy chains, two essential light chains (ELC) and two regulatory light chains (MRLC or MLC). The heavy chains have a globular head domain, a coiled-coil rod dimerization domain and a non-helical tail. Myosin II molecules oligomerize using the rod domain into bipolar filaments (Vicente-Manzanares et al., 2009). The ELC and MLC bind to the heavy chain at the neck region between the head and rod domains (Vicente-Manzanares et al., 2009). The heavy chain head is an ATPase motor domain and responsible for actin binding and progressive motility along the filament. The activity of myosin II is regulated by phosphorylation of MLC predominantly at serine 19 but additionally threonine 18 (Ikebe et al., 1988). Phosphorylation of MLC alters the conformation of myosin heads and consequently increases the ATPase activity of the motor (Amano et al., 1996a; Sellers et al., 1982). Non-phosphorylated myosin II monomers do not assemble into filaments, as they are folded by head-head and head-tail interactions (Burgess et al., 2007). Phosphorylation of MLC disrupts the folding and enables the formation of filaments comprising 14-20 myosin molecules that can interact with actin (Li et al., 2000; Vicente-Manzanares et al., 2009). Several kinases can phosphorylate MLC including ROCK and myosin light chain kinase (MLCK) (Amano et al., 1996a). ROCK can also indirectly increase MLC phosphorylation as it phosphorylates and inhibits the myosin phosphatase-targeting subunit 1 (MYPT1), of the major myosin light chain phosphatase, on Thr696 and Thr853 (Kawano et al., 1999). To further exert control over the system, ROCK phosphorylates and activates myosin light chain phosphatase inhibitor CPI-17 (Kitazawa et al., 2000). In addition, ROCK phosphorylates ZIPK, which in turn phosphorylates CPI-17, MLC and MYPT (Hagerty et al., 2007).

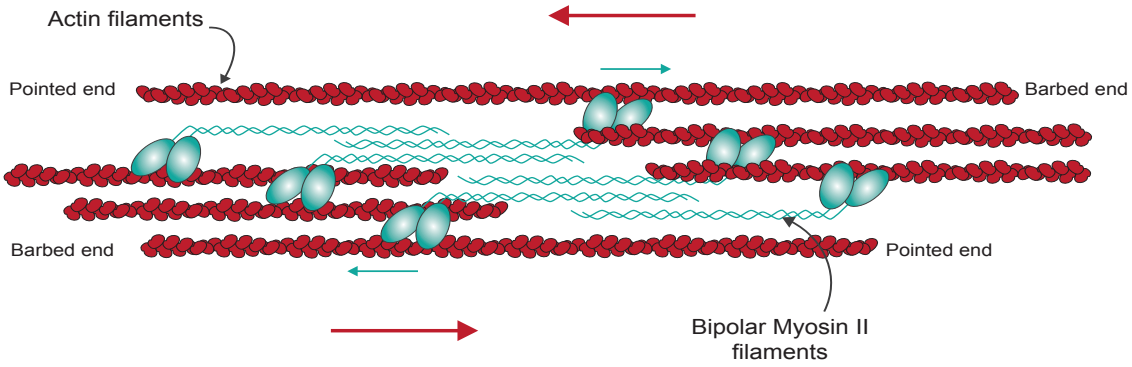

Figure 1.7 Actin stress fibres

Myosin II molecules (with phosphorylated MLC) assemble into bipolar bundles. In stress fibres, the actin filaments are arranged in an antiparallel fashion, with barbed ends directed outwards. The globular head domains of the myosin II bind to F-actin filaments and move progressively, in an ATP-dependent manner, towards the barbed end of actin filaments (the direction of travel is shown by green arrows), this drags antiparallel actin filaments towards each other resulting in contractile force (direction of actin filament contraction is represented by red arrows). Adapted with permission from Macmillan Publishers Ltd: Vicente-Manzanares, M., Ma, X., Adelstein, R.S., and Horwitz, A.R. Nat Rev Mol Cell Biol. 2009 *10*:778-790. Copyright 2003

1.2.2.2 ROCK and the stabilisation of actin filaments

Monomeric actin (G-actin) is an ATP/ADP interacting globular protein of 42kDa, which can assemble into filamentous polymers (F-actin) (Dominguez and Holmes, 2011). F-actin comprises two chains of G-actin that are twisted into a helical filament. F-actin exhibits structural polarity with a barbed end and a pointed end, as defined from the appearance of filaments decorated with Heavy meromyosin subfragment 1 by electron microscopy (Huxley, 1963; Woodrum et al., 1975). G-actin monomers preferentially associate with the barbed end of the filament (Dominguez and Holmes, 2011). Upon binding of G-actin to the barbed end of the filament ATP is hydrolysed to ADP and Pi, following which Pi slowly dissociates and is released (Dominguez and Holmes, 2011). Release of Pi alters the local structural properties of the filament and facilitates the dissociation of ADP bound actin monomers from the pointed end (Dominguez and Holmes, 2011).

Cofilin-1 is the ubiquitously expressed member of actin depolymerizing factor (ADF)/cofilin family. Cofilin associates with actin filaments by binding to ADP-actin. There are two proposed activities of cofilin. Firstly, cofillin is proposed to increase the rate of dissociation of G-actin at the pointed end by facilitating the release of Pi. This increases the concentration of free G-actin available for ADP:ATP exchange and

subsequent addition to the barbed end, indirectly stimulating filament growth (Carlier et al., 1997). Secondly, cofillin binding to ADP bound actin alters the intrinsic twist of the filament resulting in a weakened filament more susceptible to severing; leading to more free barbed ends available for growth (Ichetovkin et al., 2002; McGough et al., 1997). Filaments servered by cofilin are good substrates for Arp2/3 dependent actin polymerisation (Ichetovkin et al., 2002). Cofilin activity can be regulated by phosphorylation and subsequent de-phosphorylation (Arber et al., 1998; Moriyama et al., 1996). The LIM kinases, LIMK1 and LIMK2, phosphorylate cofilin on serine 3, this inhibits F-actin binding and the actin severing activity by cofilin (Arber et al., 1998; Moriyama et al., 1996). The RhoA effector ROCK phosphorylates LIMK1 and LIMK2 on a conserved threonine to stimulate kinase activity (Amano et al., 2001; Sumi et al., 2001; Sumi et al., 1999). Increased LIMK activity results in increased stress fibre formation, focal adhesions and membrane blebbing, all structures implicated in Rho-ROCK signalling (Sumi et al., 2001; Sumi et al., 1999). In these actin structures, cofilin activity may be detrimental and a stable actin filament is preferential to dynamic branched actin networks.

1.2.3 RhoA and DRF

The formin family comprises 15 members in mammals, and is subdivided into seven groups, the Diaphanous formins (mDia), the formin-related proteins identified in leucocytes (FRL/FMNL), the dishevelled-associated activators of morphogenesis (DAAM), Delphilin, the inverted formins (INF), the formin homology domain-containing proteins (FHOD) and the original namesake formins (FNM) (Goode and Eck, 2007). The common defining features of the formin family are a C-terminal 400-residue Formin homology-2 (FH2) domain and an adjacent proline-rich FH1 domain (Campellone and Welch, 2010). The DRFs, which include the mDia, DAAM and FRL subfamilies, are the best-studied members of the formin family (Goode and Eck, 2007). DRFs exist in an auto-inhibited conformation through an intramolecular interaction between the C-terminal Diaphanous autoinhibitory domain (DAD) and the N-terminal regulatory domain, which consists of a Rho binding domain (RBD) and a Diaphanous-inhibitory domain (DID) (Alberts, 2001; Li and Higgs, 2005; Rose et al., 2005a). In mDia1, the DAD interacts with the N-terminal diaphanous inhibitor domain (DID), which occludes the actin binding surfaces of the FH2 domain (Maiti et al., 2012). Active Rho binds to the GBD domain, and directly occludes the DAD binding site whilst also

altering the conformation of the GBD and neighbouring DID (Figure 1.8) (Nezami et al., 2006; Rose et al., 2005a). This interaction is not completely sufficient to activate DRFs raising the possibility that other co-operative signals are required (Maiti et al., 2012). Outside of the FH1 and FH2 domains the formin family are quite divergent but the auto-inhibition mechanism seems to be well conserved (Campellone and Welch, 2010). Formins nucleate actin filaments as a dimer using these FH1 and FH2 domains (Pruyne et al., 2002; Sagot et al., 2002). The FH2 domains homo-dimerise to form a donut structure that encircles the actin dimer or growing actin filament and each FH2 domain binds to an actin monomer (Otomo et al., 2005; Xu et al., 2004). The FH1 domain binds to profilin:actin dimers to direct and orient G-actin towards the FH2 dimer and actin filament (Figure 1.8) (Paul and Pollard, 2008). Formins can nucleate filaments and promote filament elongation, as they remain progressively bound to barbed ends of actin filament. This has an additional benefit of protecting the barbed ends from capping proteins and facilitates the generation of long, unbranched filaments (Kovar and Pollard, 2004; Pruyne et al., 2002; Zigmond et al., 2003).

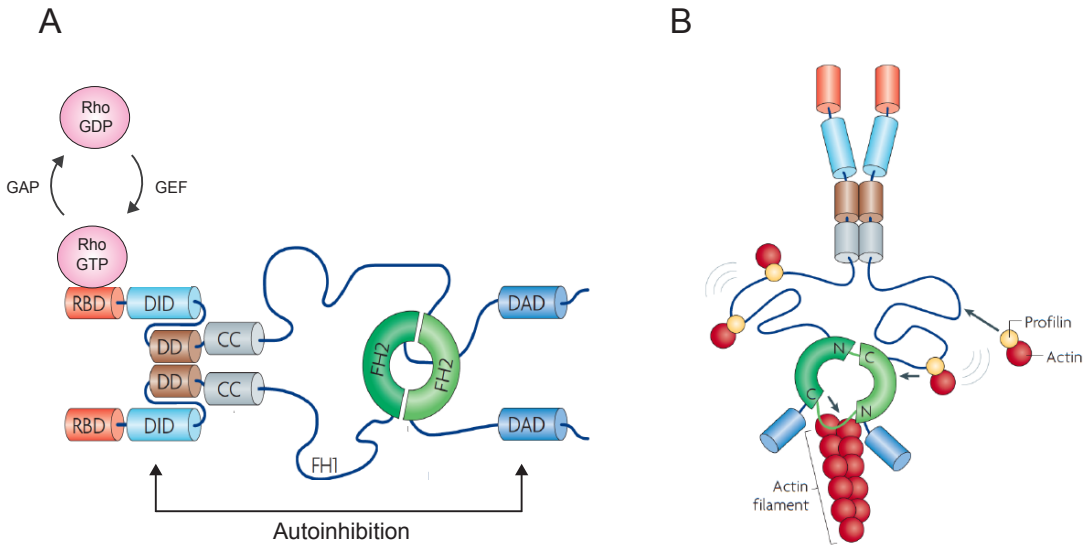

Figure 1.8 The domain structure of mDia1

A. Formins exist as a dimer and contains a Rho binding domain (RBD), a Diaphanous inhibitory domain (DIF), a dimerization domain (DD), coiled coil domain and two formin homology domains (FH1 and FH2). The FH2 domains homo-dimerise in a donut conformation. The DID and DAD interact in an auto-inhibited conformation, this is disrupted upon binding of Rho to the RBD. **B.** The FH1 domains orient profilin:actin complexes towards the FH2 donut and growing actin filament. The FH2 donut encircles the growing filament and stays associated with the barbed end as the filament grows. Adapted with permission from Macmillan Publishers Ltd: Chesarone, M. *et al.,* (2010). Nat Rev Mol Cell Biol. 2010 Jan;11(1):62-74. Copyright 2010

1.2.4 Cortical contraction and blebbing

In addition to their role in stress fibre contraction, actin and myosin II play an important role in the cell cortex beneath the plasma membrane, which is a thin actin mesh intrinsically linked to the membrane with linker proteins. The mesh is under tension due to myosin II driven actin contraction, this exerts hydrostatic pressure on the cell to maintain cell shape or drive cell shape changes required for various biological functions such as cytokinesis and locomotion (Bray and White, 1988; Charras et al., 2006; Morone et al., 2006). The cortex can become highly contractile under Rho-ROCK signalling and force the cell into a rounded morphology. The previous section highlighted the four types of actin structures that contribute to mesenchymal cell migration; lamellipodia, filopodia, stress fibres and focal adhesions. In contrast, rounded migration (also often called amoeboid migration) is dependent on membrane bleb protrusions that are formed by myosin II dependent contraction of the actin cortex (Friedl and Wolf, 2003; Lorentzen et al., 2011; Pinner and Sahai, 2008a; Wolf et al., 2003). This section will focus on membrane blebbing during cell contraction and its contribution to cell migration *in vivo*.

1.2.4.1 Plasma membrane blebbing

Membrane blebs are transient spherical membrane protrusions filled with cytosol and initially devoid of actin cortex. The bleb life cycle consist of four distinct steps, nucleation, growth, stabilisation and retraction. The nucleation of a bleb occurs when the membrane splits from the underlying actin cortex or through localised rupture of the cortex itself (Figure 1.9) (Charras et al., 2005; Keller et al., 2002; Paluch et al., 2005). In both cases, bleb nucleation results from an intracellular pressure build up induced by actin myosin II dependent cell contraction (Charras et al., 2008; Tinevez et al., 2009). The hydrostatic pressure is not equalised quickly enough throughout the cell and a bleb forms by rupture or tearing at sites of localised pressure build up (Charras et al., 2005). Blebs can also nucleate at points where the cortex or membrane-actin adhesion is weak, suggesting that the properties of the cortex are not uniform (Paluch et al., 2006). The site of nucleation only becomes a bleb if it reaches a threshold size. This is dependent on the extent of cortical tension, the strength of actin-membrane adhesion and membrane rigidity (Charras et al., 2008). Following nucleation, cytosol is forced

though the rupture point by cortical contraction. The bleb membrane grows to accommodate cytosol movement using a bulk flow of lipids to the bleb membrane and additional tearing away from the cortex at the bleb neck. The force of bleb expansion is opposed by extracellular osmotic pressure and membrane rigidity. The bleb membrane is initially devoid of cell cortex and therefore has low rigidity (Charras et al., 2006). Bleb expansion slows and stops when a new actin cortex assembles beneath the plasma membrane, which lends rigidity to the membrane. Bleb expansion will also slow when intracellular local hydrostatic pressure no longer exceeds the opposing forces (Charras et al., 2008). The actin cortex reassembles sequentially. Initially actin membrane linkers such as ezrin and moesin are recruited to the bleb membrane. Actin is then recruited, quickly followed by actin crosslinking proteins α-actinin, tropomyosin and coronin to form a layered actin mesh beneath the bleb membrane (Charras et al., 2006). It is not yet known how actin filaments form in the new cortex. Arp2/3 and mDia1 are not localised to the bleb membrane so perhaps it is not through *de novo* actin polymerisation, although mDia2 may play a role (Charras et al., 2006; Eisenmann et al., 2007). Finally, myosin II arrives and drives contraction of the newly formed actin cortex. The membrane wrinkles during retraction due to crumpling of the underlying actin cortex. This is mediated by increasing recruitment of myosin II motors during retraction. In addition, to allow cortex crumpling, localised spots of the actin mesh must collapse because of the transient loss and reattachment of actin bundling proteins (Charras et al., 2008).

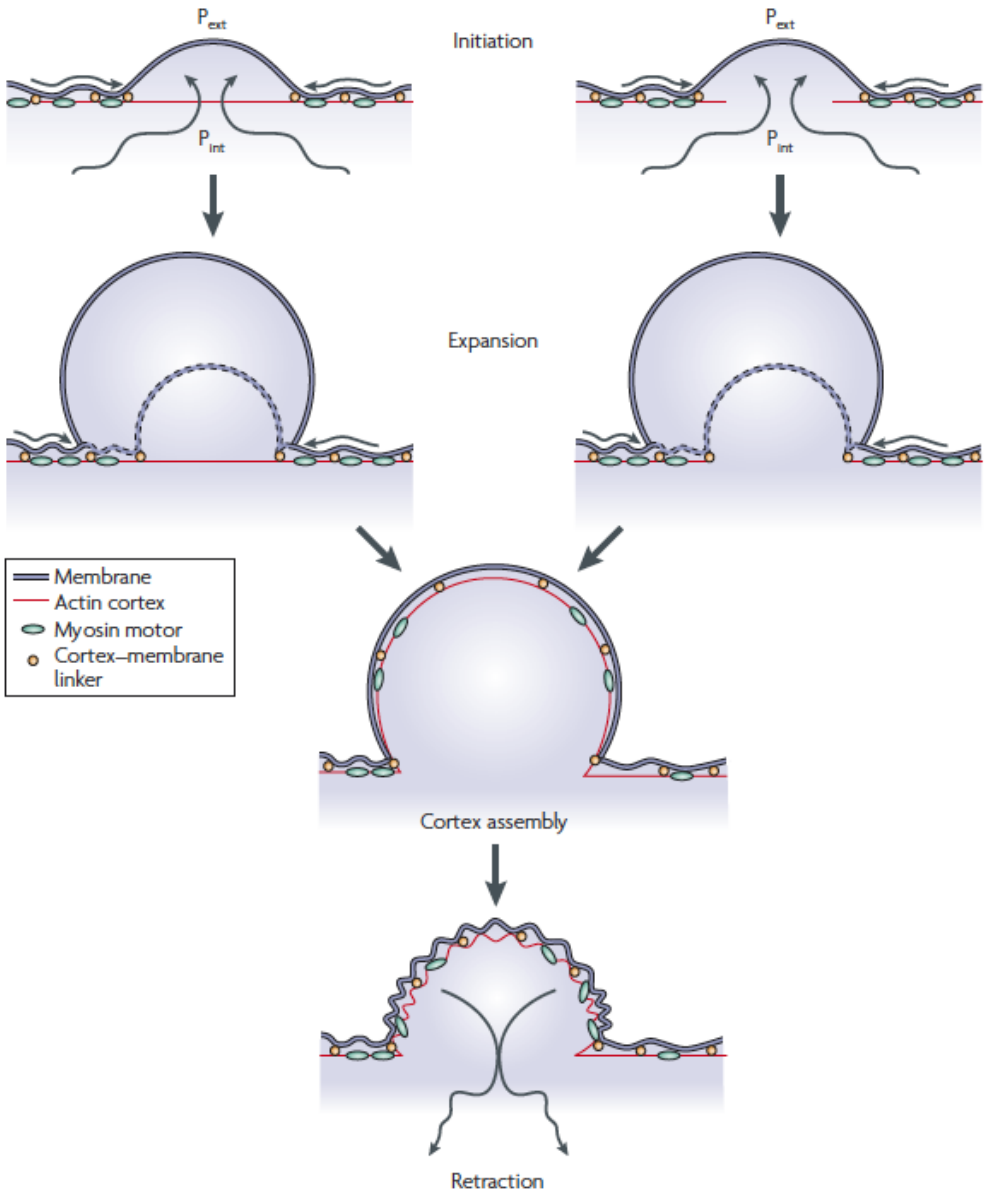

Figure 1.9 The lifecycle of a bleb

The four steps of the bleb lifecycle are nucleation, growth, stabilisation and retraction. Blebs nucleate following localised detachment of the membrane from the actin cortex (left hand image) or localised rupture of the actin cortex (right hand image). Taken with permission from Macmillan Publishers Ltd: Charras, G and Paluch, E. Nat Rev Mol Cell Biol. 2008 Sep;9(9):730-6. Copyright 2008

1.2.4.2 Cell contraction and blebbing in vivo

Cancer cell migration *in vivo* is highly heterogeneous with migrating cells adopting a variety of shapes and modes of migration from mesenchymal to rounded (Friedl and Wolf, 2010). Mesechymal is the classically defined mode of migration where the migratory protrusive force is provided by Arp2/3 dependent lamellipodia formation. Cells are tightly adhered to the substrate and require ventral stress fibres to contract the cell body as the cell moves forward. This type of migration requires degradation of the surrounding extracellular matrix (ECM) by matrix metalloproteases (MMPs) (Friedl and Wolf, 2003; Sahai and Marshall, 2003). Lamellipodia require WAVE dependent activation of Arp2/3, therefore mesenchymal migration often correlates with high Rac activity (Bergert et al., 2012; Sanz-Moreno et al., 2008). Rounded migration in contrast is characterised by little adherence to the extracellular substrate, a rounded morphology and plasma membrane blebbing (Friedl and Wolf, 2010). This mode of migration is driven by RhoA-ROCK activation of myosin II mediated contraction of the cortex (Gutjahr et al., 2005; Pinner and Sahai, 2008b; Sahai and Marshall, 2003; Sanz-Moreno et al., 2008). Rounded migration is independent of proteolytic degradation of the ECM (Wolf et al., 2003). This is because, in contrast to lamellipodia in mesenchymal migration, the flexible, actin-devoid blebs are able to squeeze through small gaps in the ECM. In order to drive directional cell migration *in vivo* blebbing must be polarised. Polarisation of blebbing can be established by altering the local properties of the cortex, because bleb nucleation is influenced by the strength of membrane cortex attachments (Charras et al., 2008). Ezrin is an essential membrane-actin linker protein. The overexpression of activated ezrin can prevent bleb nucleation. In contrast, the FERM domain of ezrin and dominant negative ezrin can induce frequent large distended blebs (Charras et al., 2008; Charras et al., 2006; Diz-Munoz et al., 2010). In cancer cells lines that exhibited persistent movement, ezrin was frequently localised to the rear of the cell while the leading edge was relatively devoid of ezrin. These cells displayed polarised cell blebbing in areas devoid of ezrin, presumably because membrane attachment to the cortex is weaker here (Lorentzen et al., 2011; Rossy et al., 2007). Alternatively, polarised blebbing might also occur through localised weakening of the actin cortex, as blebs can also nucleate by cortex rupture (Tinevez et al., 2009). Polarisation of blebbing could also be mediated by localised changes in intracellular hydrostatic pressure, membrane rigidity or

extracellular osmolality (Charras et al., 2005). A polarised blebbing leading edge is propagated because the newly formed cortex and membrane attachments are weak, as highlighted by the appearance of blebs on blebs or new blebs in close proximity to an earlier bleb (Charras and Paluch, 2008; Charras, 2008).

As mentioned, numerous studies attribute mesenchymal migration or rounded migration to Rac or Rho signalling, respectively (Gutjahr et al., 2005; Pinner and Sahai, 2008b; Sahai and Marshall, 2003; Sanz-Moreno et al., 2008). However, it is often not as simple as this as the distinction between mesenchymal and rounded migration methods is blurred. For example, cells moving by rounded migration can form lamellipodia, or highly adherent cells can bleb at the leading edge. It is also apparent that cells can switch migration modes to adapt to the extracellular environment or in response to a change in upstream signalling (Bergert et al., 2012; Sahai and Marshall, 2003). This is very important for metastatic cancer cells, as during the processes of extravasation and subsequent colonisation of new tissues the migrating cell will encounter very different extracellular environments (Friedl and Wolf, 2010).

1.3 Rho GTPase subfamilies

Since the discovery of the first Rho protein, the family has expanded to encompass 22 members. The Rho family is divided into smaller subfamilies based on sequence homology, structure and biological function; Rho-A related subfamily, Rac1-related family, Cdc42-related family, the Rnd family, the Rho BTB subfamily, and the Miro subfamily and an additional three proteins, Rif, RhoD and RhoH that do not fall into a particular family (Wennerberg and Der, 2004). This next section will describe the subfamilies and their biological function with particular reference to cell migration.

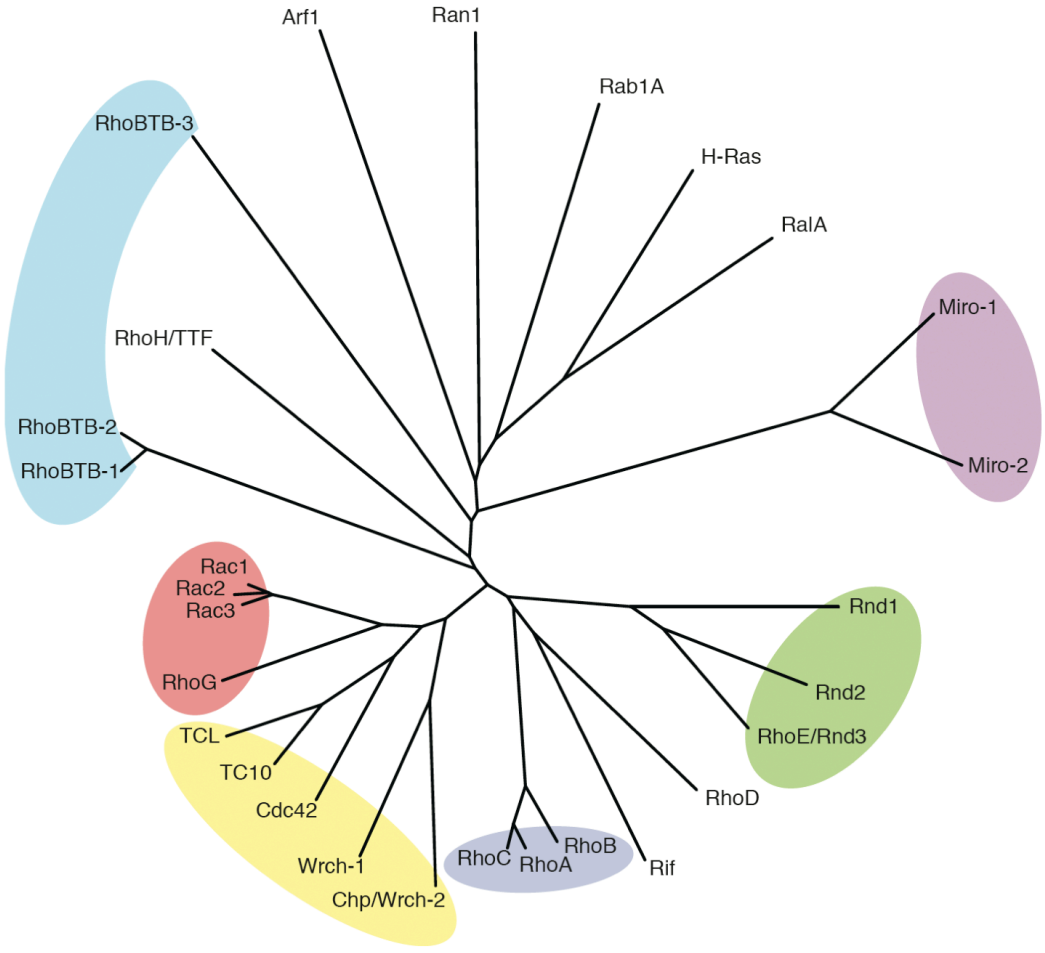

Figure 1.10 The phylogenetic tree of Rho GTPases

The 22 members of the Rho GTPases family are divided into six sub families based on amino acid sequence; RhoA-related family (dark blue), Rac1-related family (red), Cdc42-related family (yellow), Rnd family (green), RhoBTB family (light blue) and Miro family (purple). RhoH, Rif and RhoD are sufficiently different that they do not fall into a specific subfamily. Reproduced with permission from Journal of Cell Science Wennerberg, K., and Der, C.J. (2004). J Cell Sci *117*, 1301-1312.

1.3.1.1 RhoA-related proteins

RhoA, RhoB and RhoC share 85% amino acid sequence identity (Figure 1.11) (Wheeler and Ridley, 2004). The three Rho proteins likely arose by gene duplication, but have diverged and so are not functionally redundant. The three proteins only differ substantially in the C terminus around the PBR and the CAAX box (Figure 1.11) (Wheeler and Ridley, 2004). RhoA and RhoC are geranylgeranylated, which directs plasma membrane localisation upon release from Rho GDI (Adamson et al., 1992a; Michaelson et al., 2001). In contrast, RhoB can be geranylgeranylated or farnesylated (Adamson et al., 1992a). In addition RhoB has additional cysteine residues upstream of CAAX that permits palmitoylation (Adamson et al., 1992a). RhoB is localised to late endosomes, lysosomes and the plasma membrane (Adamson et al., 1992b). This is dependent on the isoprenoid modification, as the proportion of RhoB within different subcellular compartment changes if the farnesyltransferase is inhibited (Wherlock et al., 2004).

Differential localisation alone will determine how Rho proteins are regulated and their downstream biological functions. However, the principle way Rho proteins mediate different effects is by specific regulation by GEFs and GAPs and binding to different effectors molecules. Therefore, it is important to understand how regulatory molecules and effectors distinguish RhoA, RhoB and RhoC. GEFs and GAPs interact with Rho GTPases via the switch 1. In this region, the three proteins have almost identical sequences, with only a single change for each of RhoB (Q29E) and RhoC (V43I) (Figure 1.11) (Wheeler and Ridley, 2004). This small change may affect binding specificities for regulatory proteins and therefore, may allow for specific signalling. Structural analysis of RhoA in complex with the LARG, PDZ-RhoGEF, or p63RhoGEF revealed that Val43 participates in van der Waals interactions at the GTPase:GEF interface (Chen et al., 2010; Kristelly et al., 2004; Lutz et al., 2007; Oleksy et al., 2006). A bulkier isoleucine residue at this point could sterically block the interaction between the GTPase and GEF. Indeed, GEF XPLN interacts with RhoA and RhoB but not RhoC, the distinguishing feature being the isoleucine residue at position 43 in RhoC (Arthur et al., 2002; Sloan et al., 2012).

As with GEFs and GAPs, Rho effectors bind over the switch 1 and 2 of Rho. The X-ray crystal structures of PKN1 or ROCK1, in complex with activated RhoA (G14V mutation or with the GTP mimic, GppNHp), and mDia1 in complex with GppNHp bound RhoC

indicated the specific residues required for effector binding (Dvorsky et al., 2004; Maesaki et al., 1999; Rose et al., 2005a). The Rho residues that mediate binding to ROCK1 and mDia1 are entirely conserved between RhoA, RhoB and RhoC (Dvorsky et al., 2004; Rose et al., 2005a), suggesting that RhoA-related family bind effectors in the same way. However, Val43 in RhoA contributes to the interaction with PKN1 (Maesaki et al., 1999). The importance of this residue for PKN binding is yet to be determined as the possibility of a direct interaction between PKN1 and RhoC has not been studied (Amano et al., 1996b; Watanabe et al., 1996). More recently, the structure of RhoC with two GTP analogues (GppNHp or GTPγS) was determined (Dias and Cerione, 2007). This analysis revealed that RhoC had two putative activation conformations; a partially active conformation where only switch 2 is moved relative to RhoC:GDP and a fully active conformation which is analogous to the available RhoA GTP bound structure (Dias and Cerione, 2007; Ihara et al., 1998). If these two distinct conformations exist *in vivo* then this could form the basis of effector specificity for RhoA and RhoC. However, this variation could be an artefact of the different GTP analogues used (Dias and Cerione, 2007; Ihara et al., 1998). In addition, a full comparison between RhoA and RhoC is not possible because structural analysis of RhoA with both GTP analogues has not been conducted (Ihara et al., 1998).

Historically, it has been difficult to discern the individual effects of the three proteins, because many of the early studies focused on RhoA only, or used non-specific reagents such as the C3 enzyme (which targets all three proteins) and constitutively active mutants. These methods assigned the general functions of cell contraction, stress fibre formation and focal adhesion regulation to this family (Aktories et al., 1989; Aktories and Hall, 1989; Aspenstrom et al., 2004; Ridley and Hall, 1992). However, more recent studies have begun to delineate specific functions of RhoA, RhoB or RhoC with regards to cell migration and cancer.

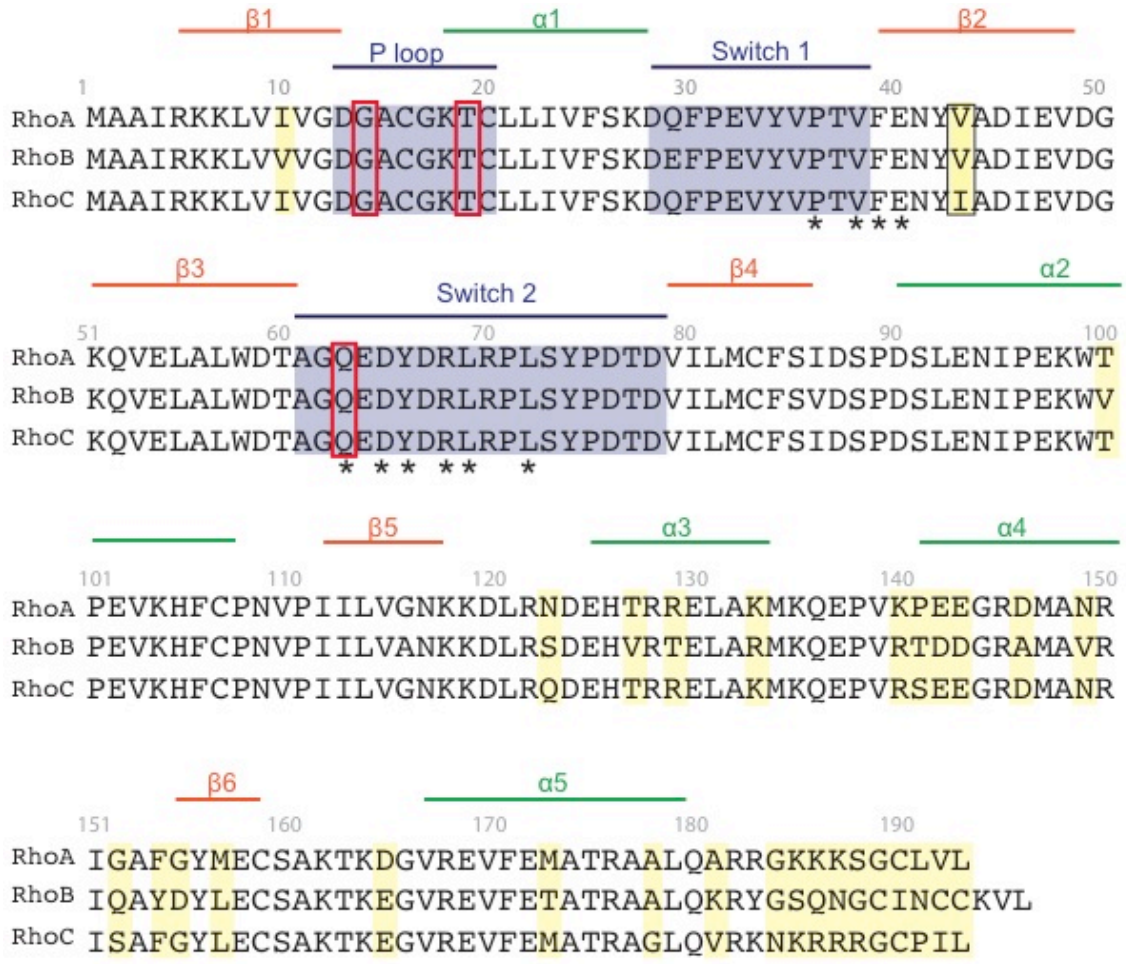

Figure 1.11 Sequence alignment of RhoA-related subfamily

The conserved residues between the three proteins are in white, while any differences are highlighted in yellow. The Val43Ile substitution is shown by the black box. The α helices are highlight by green lines, β strands by orange lines. The P loop, switch 1 and switch 2 regions are highlighted in blue (Ihara et al., 1998). Black stars show the residues that participate in ROCK1 binding (Dvorsky et al., 2004). Boxed in red are the residues that can be mutated to give constitutively active and dominant negative mutants.

1.3.1.1.1 RhoA and RhoC

The loss of either RhoA or RhoC, either by genetic ablation or siRNA-mediated depletion, reduces the ability of cancer cell lines in culture to migrate and invade (Hakem et al., 2005; Kitzing et al., 2010; Sahai and Marshall, 2003; Vega et al., 2011). While, the overexpression of either RhoA or RhoC in tumour cells significantly increased invasion *in vitro* (Horiuchi et al., 2003; Iiizumi et al., 2008). This indicates that RhoA and RhoC are important for cancer cell migration and unsurprisingly, RhoA and RhoC are associated with metastatic potential of tumours (Iiizumi et al., 2008; Kamai et al., 2003a). Of the three Rho proteins, RhoC is most often associated with migration and invasion of tumours. RhoC up-regulation has been shown to correlate with highly metastatic cells, following *in vivo* selection of metastases derived from a poorly metastatic cell line (Clark et al., 2000). In contrast, RhoA expression was unchanged in the selected cell lines. In addition, ectopic expression of RhoC, but not RhoA, drives metastasis (Clark et al., 2000). High RhoC expression has been shown in a variety of human cancers including breast and head and neck cancers (Islam et al., 2009; Rosenthal et al., 2012). In other tumour types, high RhoC correlates with high ROCK expression, and this indicates poor prognosis (Abe et al., 2008; Kamai et al., 2003b). RhoA mRNA and protein levels are also elevated in certain cancers, and this is associated with muscle invasion and metastasis (Kamai et al., 2003a). Therefore, mRNA levels of RhoA and RhoC could be a useful prognostic markers (Horiuchi et al., 2003; Kamai et al., 2003a).

RhoA presumably regulates migration and invasion through the mechanisms described previously, such as ROCK and mDia1 signalling. RhoC also interacts directly with ROCK and mDia1 and so is likely to regulate migration through the same mechanisms (Leung et al., 1996; Rose et al., 2005a). RhoA and RhoC appear to have many overlapping functions with regards to cell migration, but some examples of their unique functions have been uncovered. Depletion of RhoA or RhoC in the prostate cancer cell line, PC3, caused distinctive cell morphologies and had differential effects on migration and invasion in cell culture models (Vega et al., 2011). Loss of RhoA induced an elongated morphology of cells and increased migration and invasion, this was phenocopied by the loss of both ROCK1 and ROCK2 (Vega et al., 2011). In contrast, siRNA of RhoC induced cell spreading and inhibited cell migration and invasion. These effects were mediated by newly identified specific effector for RhoC, FMNL3, but did not involve ROCK1 or ROCK2 (Vega et al., 2011). However, the independence of

ROCK in this RhoC phenotype is not universal. ROCK interacts more strongly with RhoC than with RhoA. This appears to be particularly important in ROCK mediated disruption of adherens junctions, where RhoC is more effective than RhoA in regulating ROCK activity (Sahai and Marshall, 2002). Another formin family member, FMNL2, interacts with RhoC only and is proposed as another specific effector of RhoC, driving amoeboid invasion *in vitro* (Kitzing et al., 2010).

Invasive cancer cell lines in cell culture form protrusive F-actin structures called invadopodia that have capacity to degrade the local basement membrane matrix (reviewed in (Murphy and Courtneidge, 2011)). These structures are believed to aid invasion and intravasation *in vivo.* Both RhoA and RhoC can regulate the ability of invadopodia to degrade the matrix, albeit by different mechanisms, therefore this might represent another mechanism by which the proteins regulate cancer cell invasion (Sakurai-Yageta et al., 2008). RhoA regulates IQGAP1 and exocyst mediated delivery of matrix metalloproteases (MMPs) to the invadopodia tip (Bravo-Cordero et al., 2011; Sakurai-Yageta et al., 2008). In contrast, RhoC can spatially restrict invadopodia formation by activating ROCK and LIMK signalling to inhibit cofilin mediated actin-severing ability. This improves the efficiency of invadopodia protrusion (Bravo-Cordero et al., 2011).

1.3.1.1.2 RhoB

RhoB has the most diverse function in the RhoA-related subfamily. RhoB has a crucial pro-apoptotic role in response to DNA damage and mitotic block in transformed cells (Liu et al., 2001; Liu et al., 2011). RhoA and RhoC activity is predominantly regulated by GEFs, GAPs and post-translational modifications (Wheeler and Ridley, 2004). In contrast, RhoB levels are endogenously low and the protein has a short half-life, this allows for the regulation of RhoB activity mainly at the level of transcription (Zalcman et al., 1995). RhoB expression is quickly activated in response to UV, cytokines, growth factors and DNA damaging agents to mediate apoptosis (reviewed in (Huang and Prendergast, 2006)).

Several studies have implicated RhoB in cell migration. RhoB-/- macrophages exhibit reduced adhesion and cell spreading (Wheeler and Ridley, 2007). RNAi mediated loss of RhoB, resulted in small, rounded cells that were less well adhered to the substrate

and displayed abnormal focal adhesion dynamics (Vega et al., 2012). In both situations, this phenotype was attributed to the role of RhoB in endosome trafficking (Vega et al., 2012; Wheeler and Ridley, 2007). RhoB is recruited to endosomes with its putative effectors mDia1 and PKN1 (Fernandez-Borja et al., 2005; Mellor et al., 1998). It has been shown that RhoB regulates EGF receptor trafficking by linking actin polymerisation to endosomes through mDia1 (Fernandez-Borja et al., 2005; Mellor et al., 1998). Loss of RhoB results in decreased cell surface expression of β1, β2 and β3 integrins as a result of reduced membrane trafficking (Vega et al., 2012; Wheeler and Ridley, 2007). Therefore, RhoB indirectly regulates cell adhesion, spreading and migration by regulating membrane trafficking. In cancer, RhoB acts as a migration suppressor and decreased expression often correlates with increased invasion and metastasis (Forget et al., 2002; Mazieres et al., 2004).

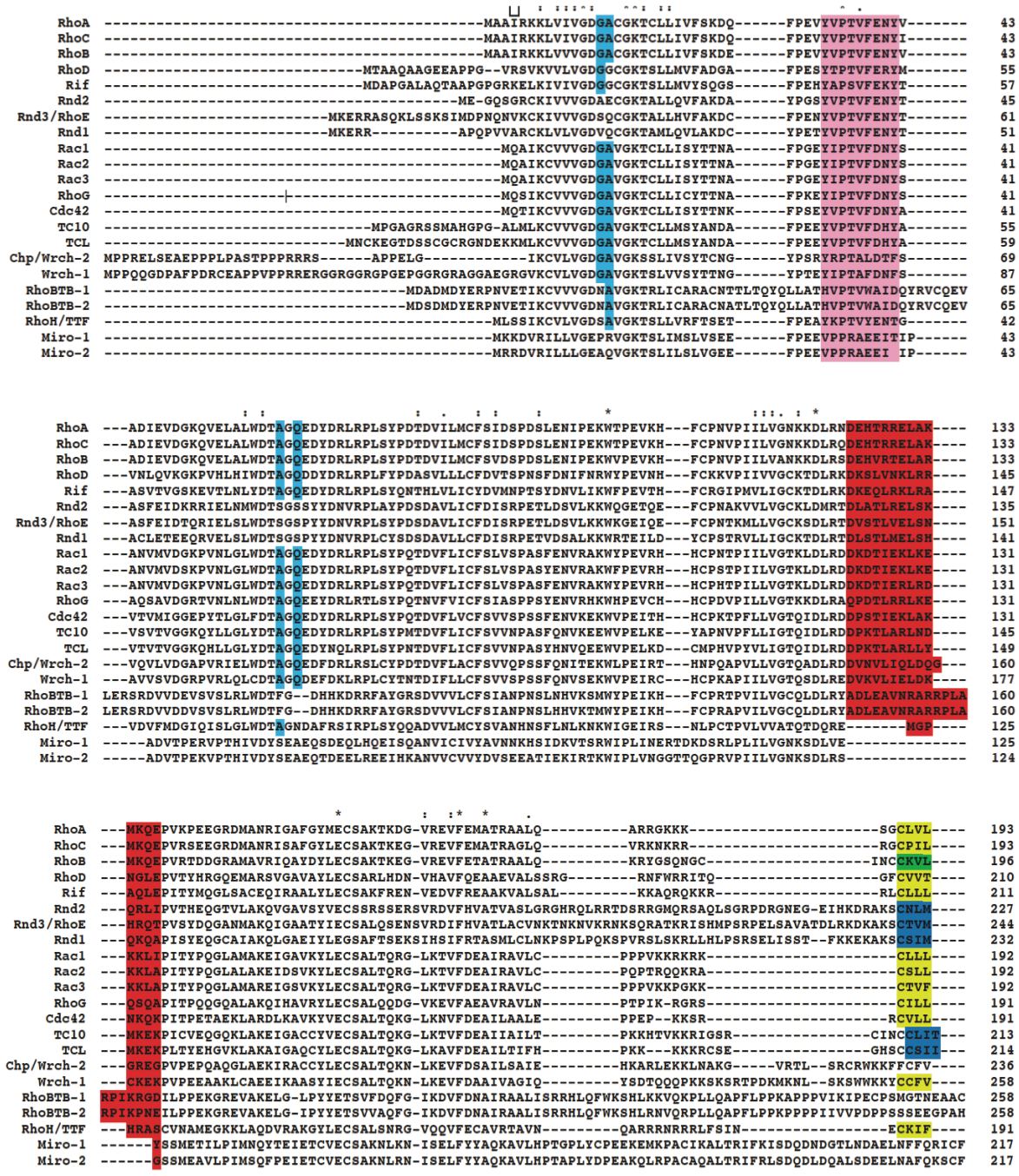

Figure 1.12 Sequence alignment of all members of the Rho GTPase family

The Rho proteins sequences were aligned by ClustalW. Highlighted in light blue are the residues that are important for GTP hydrolysis. The Rho insert domain is in red. The CAAX boxes are highlighted in yellow, blue and green for proteins that are geranylgeranylated, farnesylated or geranylgeranylated and farnesylated, respectively. Only the sequences that align with the rest of the family are shown for RhoBTB-1, RhoBTB-2, Miro-1 and Miro-2. Reproduced with permission from Journal of Cell Science Wennerberg, K., and Der, C.J. (2004). J Cell Sci *117*, 1301-1312.

1.3.1.2 Rac1-related proteins

This sub family comprises Rac1, Rac2, Rac3 and RhoG. Many of the functions attributed to this family arise principally from studies on Rac1. Rac1-3 have 88% sequence identity, with the differences between the proteins occurring in the PBR and CAAX boxes (Figure 1.12). RhoG is more divergent with 72% sequence identity to Rac1 (Vincent et al., 1992; Wennerberg and Der, 2004). The overexpression of constitutively active mutants of all four proteins can stimulate lamellipodia (Aspenstrom et al., 2004; Didsbury et al., 1989). Rac1 stimulates actin nucleation for lamellipodia by activating the WAVE complex (WRC) (Eden et al., 2002). It is assumed that the other Rac proteins are also capable of activating the WRC to induce lamellipodia formation (Aspenstrom et al., 2004). Rac1 is ubiquitously expressed and the genetic knockout in mice is embryonic lethal, because of motility and adhesion defects in the germ layers during gastrulation (Sugihara et al., 1998). In contrast, Rac2 is only expressed in cells of a haematopoietic lineage (Roberts et al., 1999). Rac2 knockout mice develop normally but are susceptible to infection and have haematopoietic cell defects, including reduced neutrophil migration and NADPH oxidase function (Roberts et al., 1999). Rac1 and Rac2 have an actin independent role as both proteins can bind to and activate the NADPH oxidase complex via the $p67^{phox}$ component (Dorseuil et al., 1996). Rac2 is believed to be the main interacting GTPase as it has a higher affinity for $p67^{phox}$ than Rac1 and also because it is expressed in the cells where superoxide production is most required (Dorseuil et al., 1996). Combined conditional knockout of Rac1 and Rac2 exacerbated haematopoietic cell defects in adhesion and migration (Gu et al., 2003). Rac3 is mainly expressed in the brain. There is no obvious defect in the development of Rac3 knockout mice (Corbetta et al., 2005). However, combined neuronal specific knockout of Rac1 and Rac3 led to defective development of the central nervous system (Corbetta et al., 2009). Rac3 can also be up regulated and hyperactive in breast cancers leading to increased cell migration and gene transcription of pro-growth and pro-migration genes (Walker et al., 2011). RhoG is highly expressed in lymphocytes (Vigorito et al., 2004). There is no obvious defect in the lymphocyte development in RhoG knockout mice (Vigorito et al., 2004). This is despite the fact that overexpression of active RhoG can dramatically induce lamellipodia, ruffles and filopodia (Gauthier-Rouviere et al., 1998). RhoG can regulate migration by activating the Rac and Cdc42 specific DOCK180 GEF (Katoh et al., 2006; Katoh and Negishi, 2003; Meller et al., 2008). There is controversy over whether RhoG has a specific role in regulation of cell migration. The major differences in the extent of RhoG mediated

effects vary between studies using activation mutants of RhoG or genetic knockout/ depletion (Katoh et al., 2006; Katoh and Negishi, 2003; Meller et al., 2008).

1.3.1.3 Cdc42-related proteins

The five members of this subfamily are Cdc42, TCL, TC10, Wrch-1, Wrch-2. Every member is believed to regulate the formation of filopodia (Abe et al., 2003; Aspenstrom et al., 2004; Nobes and Hall, 1995). Cdc42 induces filopodia formation by activating the actin nucleators N-WASP and mDia2 (Miki et al., 1998; Rohatgi et al., 2000; Rohatgi et al., 1999). Cdc42 has two isoforms that arise from the same gene as a result of slight variation in exon splicing (Nicole et al., 1999). The two variants differ only in the last 10 amino acids. Cdc42a is ubiquitously expressed and has been most highly studied, while Cdc42b is only expressed in the brain (Nicole et al., 1999). TC10 and TCL have overlapping functions with Cdc42, probably because TC10 and TCL can bind similar effectors to Cdc42. In the GTP bound active forms both TC10 and TCL bind to CRIB domains in effector molecules (Vignal et al., 2000);(Neudauer et al., 1998). In contrast to Cdc42, which is only geranylgeranylated, TC10 and TCL can be geranylgeranylated or farnesylated, which may provide some specificity in their function by directing their recruitment to specific cellular locations (Munemitsu et al., 1990; Vignal et al., 2000) (Neudauer et al., 1998). TC10 is also palmitoylated, which prevents any interaction with RhoGDI1, and eliminates one mode of regulation (Neudauer et al., 1998). However, despite overlapping functions it is clear that Cdc42 has essential specific functions, as Cdc42 knock out mice are embryonic lethal (Chen et al., 2000). TC10 has an important role in glucose uptake by adipocytes in response to insulin as it is activated upon insulin signalling and regulates GLUT4 containing vesicle trafficking to the plasma membrane and GLUT4 vesicle fusion (Chang et al., 2007; Kanzaki and Pessin, 2003). Cdc42, TC10 and TCL have been implicated in neurite extension by activating N-WASP (Abe et al., 2003). In addition, TC10 is believed activate neurite extension by an N-WASP independent exocyst mediated mechanism (Pommereit and Wouters, 2007).

Wrch-1 and Wrch-2 are very divergent from the other three members of the family, having only 52 to 57% sequence identity with Cdc42 (Shutes et al., 2006; Tao et al., 2001). Both Wrch-1 and Wrch-2 have extended N and C terminal sequences flanking the GTPase domain (Wennerberg and Der, 2004). In addition, Wrch-2 lacks a

functional CAAX box and membrane targeting is instead mediated by palmitoylation at a C-terminal cysteine residue (Chenette et al., 2006). Wrch-1 mainly exists in a GTP bound conformation, not because of a lack of GTPase activity but because it has an extremely high intrinsic GTP exchange activity (Saras et al., 2004). Both proteins can induce filopodia formation (Ruusala and Aspenstrom, 2008). Wrch-1 can interact with the Rho GTPase activating proteins ARHGAP30 and cdGAP, but these interactions do not regulate its own activity. ARHGAP30 displays GAP activity towards Rac1 and RhoA, suggesting Wrch-1 may mediate some biological functions via Rho GTPase crosstalk (Naji et al., 2011). Activated Wrch-2 can bind to the PAK kinase and N-WASP, and is proposed to regulate filopodia formation by a similar mechanism to Cdc42 (Aspenstrom et al., 2007).

1.3.1.4 The Rnd subfamily

This subfamily comprises three members Rnd1, Rnd2, RhoE (Rnd3). Rnd proteins are always bound to GTP. This is for two reasons, firstly Rnd proteins do not possess intrinsic GTPase activity as they lack conserved glycine and glutamine residues required for GTP hydrolysis (G14 and Q63 in RhoA) (Foster et al., 1996). Secondly, Rnd proteins have approximately 100 times higher affinity for GTP than GDP, and there is approximately 10 times more GTP than GDP in the cell, which reduces the possibility of GDP binding (Nobes et al., 1998; Traut, 1994). Rnd proteins have between 45-49% sequence identity with RhoA. The additional differences arise in an 8-18 amino acid N-terminal extension and a 30-32 amino acid C-terminal extension (Wennerberg and Der, 2004). The N-terminal region is important for Rnd localisation to the membrane. An additional difference is that Rnd proteins are farnesylated rather than geranylgeranylated at the C terminus (Foster et al., 1996; Nobes et al., 1998). As these proteins are always GTP bound, GEFs and GAPS have no role in regulating Rnd activity. In addition, Rnd proteins do not interact with RhoGDI1 and are predominantly associated with membranes (Oinuma et al., 2012). Rnd protein activity is modified by other modes of regulation including regulation of expression and phosphorylation. These will be briefly discussed with particular reference to RhoE, as it is the most highly studied member of this family. RhoE is regulated at the level of transcription by several different signalling pathways. RhoE is up regulated in response to cAMP levels via PKA (Collett et al., 2012). RhoE mRNA can be down regulated in colorectal cancer as it is targeted by the micro RNA mi-17 (Luo et al., 2012). In hypoxic conditions RhoE can be up regulated through hypoxia-inducible factor (HIF)-1α binding to hypoxia

responsive element (HRE) in the RhoE promoter (Zhou et al., 2011). In addition, RhoE is up regulated in response to UV radiation and DNA damaging chemotherapy drugs (Chardin, 2006). Rnd1 and RhoE, but not Rnd2, overexpression results in a dramatic loss of focal adhesions and stress fibres, indicating an antagonism with RhoA family signalling (Nobes et al., 1998). All three Rnd proteins can interact with p190 RhoGAP, however only Rnd1 and RhoE can inhibit RhoA activity by increasing the GAP activity towards RhoA (Wennerberg et al., 2003). This activity of Rnd1 and RhoE is regulated by specific localisation to lipid rafts through a KERRA motif in the N-terminal extension; Rnd2 lacks this motif, which could explain the lack of effect over RhoA with Rnd2 (Oinuma et al., 2012). In addition, RhoE antagonises RhoA signalling by binding to the kinase domain of ROCK1 and inhibiting its kinase activity (Komander et al., 2008; Riento et al., 2003). ROCK in turn regulates RhoE through phosphorylation at multiple residues. Two of the ROCK phosphorylation sites in RhoE, serine 11 and serine 240, are located in regions that mediate binding to the membrane. It is likely that RhoE phosphorylation reduces its affinity for the negative membrane, and in turn its localisation. Phosphorylated RhoE is exclusively in the cytosol, while non-phosphorylated RhoE is membrane bound (Riento et al., 2005). RhoE activity can additionally be regulated through competition with PDK1 for ROCK binding. The presence of PDK1 prevents RhoE binding to ROCK and allows ROCK downstream signalling (Pinner and Sahai, 2008b).

1.3.1.5 RhoD

RhoD is a widely expressed member of the Rho family that is most highly related to Rif, with 48% sequence similarity between the two GTPases (Murphy et al., 1996). RhoD has a 14 residue N-terminal extension relative to Rho, Rac and Cdc42 family proteins (Wennerberg and Der, 2004). It is believed that RhoD and Rif derive from a common ancestral gene and RhoD arose by gene duplication of Rif (Boureux et al., 2007). RhoD is localised to the plasma membrane and early endosomes (Murphy et al., 1996). RhoD regulates endosome dynamics via a GTP dependent interaction with the DRF formin hDia2C, a novel splice variant of hDia2 (mDia3) (Gasman et al., 2003). This is dependent on hDia2C activation of Src. The RhoD/hDia2C/Src pathway is important for the association of Rab5 positive early endosomes to actin filaments, which may regulate the balance between actin and microtubule transport of endosomes (Gasman et al., 2003). Very recently, RhoD was found to signal through another DRF family member, mDia1, to regulate centrosome duplication (Kyrkou et al., 2012). hDia2C and

mDia1 are currently the only confirmed effectors of RhoD (Gasman et al., 2003; Kyrkou et al., 2012). Overexpression of active RhoD induces long peripheral actin rich protrusions. Although resembling filopodia, these structures are longer and thinner (Aspenstrom et al., 2004; Murphy et al., 1996) and so are distinct from the Cdc42 controlled structures. Overexpression or microinjection of wild type or active RhoD causes disassembly of focal adhesions at the cell periphery concomitant with a loss of actin myosin stress fibres. In agreement, expression of active RhoD led to suppression cell migration *in vitro* (Tsubakimoto et al., 1999). The disruption of actin stress fibres by RhoD is suggested to act via antagonism of RhoA signalling, as active RhoD reduces LPA or active RhoA induced stress fibre formation (Tsubakimoto et al., 1999). This hypothesis has not been further studied or confirmed, but alludes to an interesting mechanism for Rho crosstalk (see 1.3.2). Rho GTPases can regulate the activity of other Rho proteins. As a specific example Rac1 can supress RhoA activity through the inactivation of RhoA GEFs by the Rac effector PAK kinases. RhoD has been shown to bind PAK5 and localise it to endosomes (Wu and Frost, 2006). PAK5 has not been shown to contribute to RhoA suppression (Wells and Jones, 2010). However, if RhoD can interact with other PAK family members, it could provide a mechanism for RhoA suppression.

1.3.1.6 Rif

Rif (RhoF) is most closely related to Rac2 and RhoD, with 49 and 48% sequence similarity, respectively. Rif localises to the plasma membrane (Ellis and Mellor, 2000). Rif overexpression stimulates the formation of thin peripheral and apical actin rich protrusions (Ellis and Mellor, 2000). Expression of dominant negative components of the Cdc42/WASP/Arp2/3 pathway blocked filopodia induced by Cdc42 but not Rif, which indicate these structures can arise by distinct modes of actin regulation (Pellegrin and Mellor, 2005). Rif can directly interact with two formins, mDia1 and mDia2, *in vitro* (Fan et al., 2010; Goh et al., 2011; Pellegrin and Mellor, 2005). mDia1 and mDia2 have been independently implicated in Rif induced filopodia, and are localised at the tip and along the filopodia length (Goh et al., 2011; Pellegrin and Mellor, 2005). Overexpression of Rif stimulates the formation of actin stress fibres in a ROCK and mDia1 dependent manner. This is presumably through the interaction between Rif and mDia1, and a hypothesised interaction with ROCK (Fan et al., 2010). Rif induced

stress fibres were independent of RhoA, but this study does not rule out RhoB or RhoC (Fan et al., 2010).

1.3.1.7 RhoH

RhoH is an atypical, haematopoietic specific Rho GTPase (Li et al., 2002). Despite sequence similarity within the switch 1 and switch 2 regions and the presence of a CAAX box and PBR, RhoH is not regulated by GAP activity as it is GTPase deficient. This is because the residues required for GTP hydrolysis, G14 and Q63 in RhoA, are not conserved in RhoH (Li et al., 2002). RhoH is instead regulated at the level of transcription or via localisation through interactions with RhoGDIs (Li et al., 2002). Initially, RhoH was not implicated in regulation of the actin cytoskeleton (Aspenstrom et al., 2004). However, this appears to be cell context dependent, as it is now apparent that RhoH can regulate cell migration and cell-ECM interactions in haematopoietic cell lineages (Gu et al., 2005; Troeger et al., 2012).

1.3.1.8 The RhoBTB subfamily

This is another atypical sub group of the Rho family that consists of three family members, RhoBTB-1, RhoBTB-2, RhoBTB-3. The RhoBTB family have additional domains following the GTPase domain, these include a proline rich region, a tandem repeat of the broad-complex, tramtrack, bric a brac (BTB) domain and a long C-terminus (Wennerberg and Der, 2004). The GTPase domain in RhoBTB-3 is very poorly conserved and is therefore not usually included in the Rho family (Gu et al., 2005). Rho BTB-1 and 2 do not have the conserved glycine and glutamine (G14 and Q63 in RhoA) required for GTP hydrolysis, it is therefore unlikely that they can hydrolyse GTP, and may not bind GTP at all (Chang et al., 2006). RhoBTB may instead be regulated by protein-protein interactions as BTB domains mediate homo and heteromeric associations with other proteins containing BTB domains (Berthold et al., 2008). The overexpression of RhoBTB-1 or 2 had no effect on the actin cytoskeleton (Aspenstrom et al., 2004; Berthold et al., 2008). Instead, these proteins may have a role in vesicle trafficking (Aspenstrom et al., 2004; Berthold et al., 2008). Rho BTB-2 was initially identified as a gene deleted in cancer and a putative tumour suppressor. Consistent with this, RhoBTB proteins negatively regulate cell proliferation (Berthold et al., 2008).

1.3.1.9 The Miro subfamily

Miro-1 and Miro-2 were initially characterised as atypical members of the Rho family. Miro proteins are 60% identical to each other and contain two GTPase domains and two EF-hand motifs (Fransson et al., 2003). Only the N-terminal GTPase domain has similarity to Rho GTPases. Miro proteins do not contain a CAAX box but use an intrinsic C-terminal trans-membrane domain to localise to the outer mitochondrial membrane (Fransson et al., 2006). Miro proteins regulate mitochondrial morphogenesis and trafficking (Fransson et al., 2006). Overexpression of Miro-1 had no effect on the actin cytoskeleton (Aspenstrom et al., 2004). Given the sequence and functional diversity, these proteins now form a separate GTPase family (Reis et al., 2009).

1.3.2 Crosstalk between Rho GTPases

Some of the previous sections have alluded to examples of cross talk between different Rho GTPases, where one GTPase can activate or inhibit the activity of another. Crosstalk can take place at the level of GEFs and GAPs, expression and protein stability or downstream signalling (Guilluy et al., 2011). Rho GTPase cross regulation can have positive or negative outcomes on the downstream signalling.

There are many biological examples of negative crosstalk between Rho GTPases. The first mechanism is by Rho GTPase mediated activation of GAP activity. RhoA can decrease Rac activity through the effector ROCK, which phosphorylates the Rac specific GAP filGAP to increase the GAP activity towards Rac (Ohta et al., 2006). ROCK can also activate the Rac GAP ARHGAP22 to inhibit Rac (Sanz-Moreno et al., 2008). Rnd1 and RhoE bind to p190RhoGAP to localise it to specific compartments and increase its catalytic GAP activity towards RhoA (Oinuma et al., 2012; Wennerberg et al., 2003). Rac1 can bind directly to p190RhoGAP to negatively regulate RhoA activity (Bustos et al., 2008). Rac can also indirectly increase the activity of this GAP, through the regulation of ROS production, which leads to increased GAP catalytic activity (Nimnual et al., 2003). The second negative cross talk mechanism occurs through the inhibition of GEFs. It is well documented that Rac inhibition of RhoA can also proceed through the inactivation of Rho GEFs. The predominant mechanism is

through the Rac effectors, the PAK family kinases. PAK1 and PAK4 phosphorylate multiple RhoA-related family GEFs including; p115 RhoGEF, GEF-H1, PDZ-RhoGEF and the RhoA specific Net1 (Alberts et al., 2005; Barac et al., 2004; Rosenfeldt et al., 2006; Zenke et al., 2004). Phosphorylation of GEFs either inhibits exchange activity, alters protein stability or causes mis-localisation. Finally, negative crosstalk can occur at the level of effectors and targets. For example, RhoE further antagonises RhoA signalling by binding to and inhibiting ROCK1 (Komander et al., 2008; Riento et al., 2003). A major output of RhoA-ROCK signalling is increased phosphorylation of MLC, PAK1 has been shown to antagonise MLC phosphorylation by negatively regulating MLC kinase (MLCK) (Sanders et al., 1999).

There are fewer examples of positive crosstalk between Rho GTPases, and the only characterised examples are via GEFs or at the level of downstream effectors. RhoG can enhance Rac1 activity by localising the ELMO:DOCK180 complex (a Rac specific GEF) to the membrane (Katoh and Negishi, 2003). Rac can activate RhoA activity through an interaction with the PH domain of the GEF Dbs, which increases GEF activity towards RhoA (Cheng et al., 2004). Rac and RhoA can in some cases positively regulate the same target molecules. A specific example of this is the synergistic activation of LIMK by Rac-PAK1 and RhoA-ROCK mediated phosphorylation (Edwards et al., 1999; Sanders et al., 1999).

The RhoGDI family regulate Rho GTPase signalling by sequestering inactive GDP bound Rho GTPase in the cytoplasm (Boulter et al., 2010). Additionally, RhoGDIs protect GTPases from degradation and therefore enhance protein stability (see 1.1.2.4). RhoGDI1 is ubiquitously expressed and binds to most typical Rho GTPases. It has been suggested that RhoGDI1 protein levels are equal to the combined protein levels of Rac1, Cdc42 and RhoA (Michaelson et al., 2001). This would suggest that there is a limited supply of GDI to act as a stability reservoir to Rac, Cdc42 and RhoA (Michaelson et al., 2001). When a Rho GTPase is individually overexpressed the concentration of this protein vastly exceeds the pool of GDI in the cell. This leads to a competition for GDI occupancy and a consequential decrease in the stability of other Rho GTPases (Boulter et al., 2010). In contrast, siRNA of one Rho GTPase can lead to an increase in the protein levels of others (Boulter et al., 2010). Specifically this has been observed with the RhoA-related subfamily (Giang Ho et al., 2011).

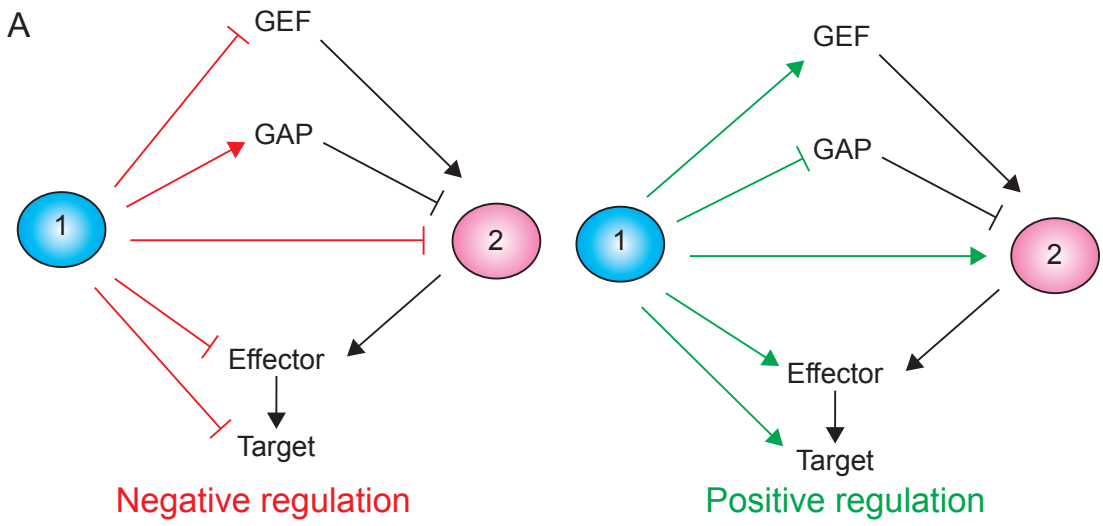

Figure 1.13 Potential mechanisms of Rho GTPase crosstalk

A. The possible modes of Rho GTPase cross talk. The right hand scheme illustrates negative regulation. Rho GTPase 1 can inhibit GEFs, activate GAPs or alter GDI occupancy of GTPase 2. Additionally, GTPase 1 can inhibit effectors and downstream targets of GTPase 2. Positive regulation (left hand side) could theoretically proceed by the opposite mechanism although specific examples only exist for inhibition of GAPs and synergistic activation of downstream targets (Guilluy et al., 2011). Adapted from Trends in Cell Biology, *21*, Guilluy, C., Garcia-Mata, R., and Burridge, K., Rho protein crosstalk: another social network?, 718-726 Copyright (2011), with permission from Elsevier

1.4 Vaccinia virus

1.4.1 Poxviruses

Viruses within the Poxviridae family (Poxviruses) are double strand DNA viruses. The poxvirus genomes encode their own replication and transcription enzymes and as a consequence can replicate entirely within the cytoplasm of the host cell. The genomes are between 130-360kb in size and encode more than 150 genes (Lefkowitz et al., 2006; Upton et al., 2003). The poxvirus intracellular life cycle is complex and produces three forms of infectious progeny virus particles: intracellular mature virus (IMV), cell associated extracellular virus (CEV) and extracellular enveloped virus (EEV). The Poxviridae family is subdivided into two subfamilies; *Entomopoxvirinae and Chordopoxvirinae,* which can infect invertebrates and vertebrates, respectively (Hughes et al., 2010). Eight different genera make up the *Chordopoxvirinae* subfamily; *Orthopoxvirus, Parapoxvirus, Avipoxvirus, Capripoxvirus, Leporipoxvirus, Suipoxvirus, Molluscipoxvirus* and *Yatapoxvirus* (Table 1) (Poxvirus Bioinformatics Resource Center www.poxvirus.org*)*.

Table 1 The viruses within the Poxviridae family

Subfamily	Genus	Species
Chordopoxvirinae	*Orthopoxvirus*	Variola
		Vaccinia
		Camelpox
		Cowpox
		Ectromelia
		Monkeypox
	Parapoxvirus	Orf
	Avipoxvirus	Fowlpox
	Capripoxvirus	Sheeppox
	Leporipoxvirus	Myxoma
	Suipoxvirus	Swinepox
	Molluscipoxvirus	Molluscum contagiosum virus
	Yatapoxvirus	Yaba like disease virus
Entomopoxvirinae	*Entomopoxvirus A*	Melolontha melolontha virus
	Entomopoxvirus B	Amsacta moorei virus
	Entomopoxvirus C	Chironomus luridus virus

The Orthopoxvirus genus (OPV) has been very highly studied because of the pathogenicity and interesting biology of some of its members. The OPV genus is made up of Variola, Vaccinia, Cowpox, Camelpox, Ectromelia and Monkeypox (Table1) (Poxvirus Bioinformatics Resource Center www.poxvirus.org*)*. Variola virus caused the devastating disease Smallpox, which is estimated to have killed more than 500 million people in the 20th Century. Fortunately, smallpox was officially eradicated in 1980 largely due to a global vaccination program organized by the World Health Organization (http://www.who.int/mediacentre/factsheets/smallpox/en/). This was made possible by almost 200 years of research, which was initiated by Edward Jenner and his innoculation of milkmaids with Cowpox. Vaccinia virus was eventually used in the WHO eradication program as the live vaccine to mediate immunity against variola virus. Despite the eradication of smallpox, vaccinia virus is still widely studied for a variety of reasons. Firstly, there is a perceived threat of bioterrorism that could originate from known stocks of variola, of which there are only two held by WHO collaborating laboratories in the USA and Russian Federation (Mayr, 2003). Secondly, the monkeypox virus has recently caused outbreaks of fatal human disease (Hutin et al., 2001; Learned et al., 2005). Thirdly, vaccinia virus and derivatives are in development as oncolytic viruses (Thorne, 2008). As vaccinia virus is only rarely pathogenic to humans, it is studied to give insights into the mechanism of other members of the *Chordopoxvirus* subfamily and OPV genus, including variola virus and monkeypox. In addition vaccinia virus is a useful tool to study host cell biology, as it manipulates host cell processes, is genetically tractable and easy to visualize.

1.4.2 Vaccinia virus

Vaccinia virus is an extremely large brick shaped particle with dimensions of 350 x 270 x 250nm (Cyrklaff et al., 2005). The virus genome, virus transcription factors and enzymes are surrounded by a protein core, which is altogether enveloped by host cell derived membrane. There are multiple strains of vaccinia virus including Western Reserve (WR), Chorioallantois vaccinia virus Ankara (CVA) and Copenhagen (Herrlich and Mayr, 1957; Parker et al., 1941). WR in the most frequently used in laboratories and throughout this thesis wild type vaccinia virus will be referred to as WR. During the efforts to eradicate smallpox the highly attenuated vaccinia strains, MVA (derived from CVA) and NYVAC (derived from Copenhagen), were created by serial passage through chicken embryo fibroblasts or targeted deletions in the genome, respectively

(Mayr et al., 1978) (Tartaglia et al., 1992). The genomes of 16 different vaccinia virus strains have been sequenced and are between 178-212kb in size (http://poxvirus.org/viruses.asp). Comparison of the genomes reveals a highly conserved central 100kb portion flanked by variable inverted terminal repeated regions (Wittek, 1982). The conserved region encodes approximately 90 genes that are conserved in all members of the *Chordopoxvirus* family (Gubser et al., 2004; Upton et al., 2003). These genes are essential for replication and morphogenesis, while the terminal regions encode proteins responsible for virulence and immune evasion in specific hosts (Smith and Law, 2004). Interestingly, the genome terminates in hairpins, therefore, the genome is a self-complementary circular strand of DNA (Figure 1.14) (Baroudy and Moss, 1982; Goebel et al., 1990). Vaccinia virus strain Copenhagen was the first strain sequenced and encodes 263 predicted open reading frames (ORFs). Vaccinia gene nomenclature is derived from the HindIII restriction map of Copenhagen, which is comprised of 16 fragments named A-P according to decreasing size. ORFs are named according to the HindIII fragment and additionally by the direction of transcription (Right or Left), as both DNA strands are used for transcription (Goebel et al., 1990). To use an example, E2L is the 2nd ORF from the 5' end of the E HindIII fragment and is transcribed towards the left (Figure 1.14). Vaccinia genes do not contain introns and each gene is under transcriptional control from its own promoter, which usually occurs within 30 bases upstream of the initiating ATG. As the genome is very tightly packed, the promoter for one gene may overlap with the upstream gene (Broyles, 2003; Davison and Moss, 1989a, b). Vaccinia promoter sequences and transcription factors are well conserved in the poxvirus family and it is possible to express a poxvirus gene, controlled by the endogenous promoter, during infection with another poxvirus (Dodding and Way, 2009).

Vaccinia genes fall into three categories depending on the promoter sequence and expression kinetics within the vaccinia replicative cycle: early, intermediate and late (Assarsson et al., 2008; Broyles, 2003). Early, intermediate and late gene mRNA is detected from 20, 100, and 140 minutes post infection in HeLa cells, respectively (Baldick and Moss, 1993). The early class of genes is further sub categorised into immediate-early and early. Additionally, a group of genes, called early/late, have elements of early and late promoters and are transcribed at the same time as other early genes but have sustained expression throughout infection (Assarsson et al., 2008). Early genes are functionally associated with DNA replication, intermediate gene

transcription, nucleotide biosynthesis and immune evasion. Intermediate and late genes are associated with virus morphogenesis (Assarsson et al., 2008). Vaccinia gene expression is regulated at the level of transcription and control achieved by a cascade mechanism, whereby intermediate gene transcription factors are early proteins, late transcription factors are intermediate proteins and early transcription factors are late proteins (and are required to initiate transcription in the subsequent infected cell) (Figure 1.14). In addition to the expression of early genes, intermediate and consequently late gene expression is dependent on DNA genome replication and newly synthesised RNA polymerase from early genes (Assarsson et al., 2008; Broyles, 2003; Moss, 2007; Rubins et al., 2008).

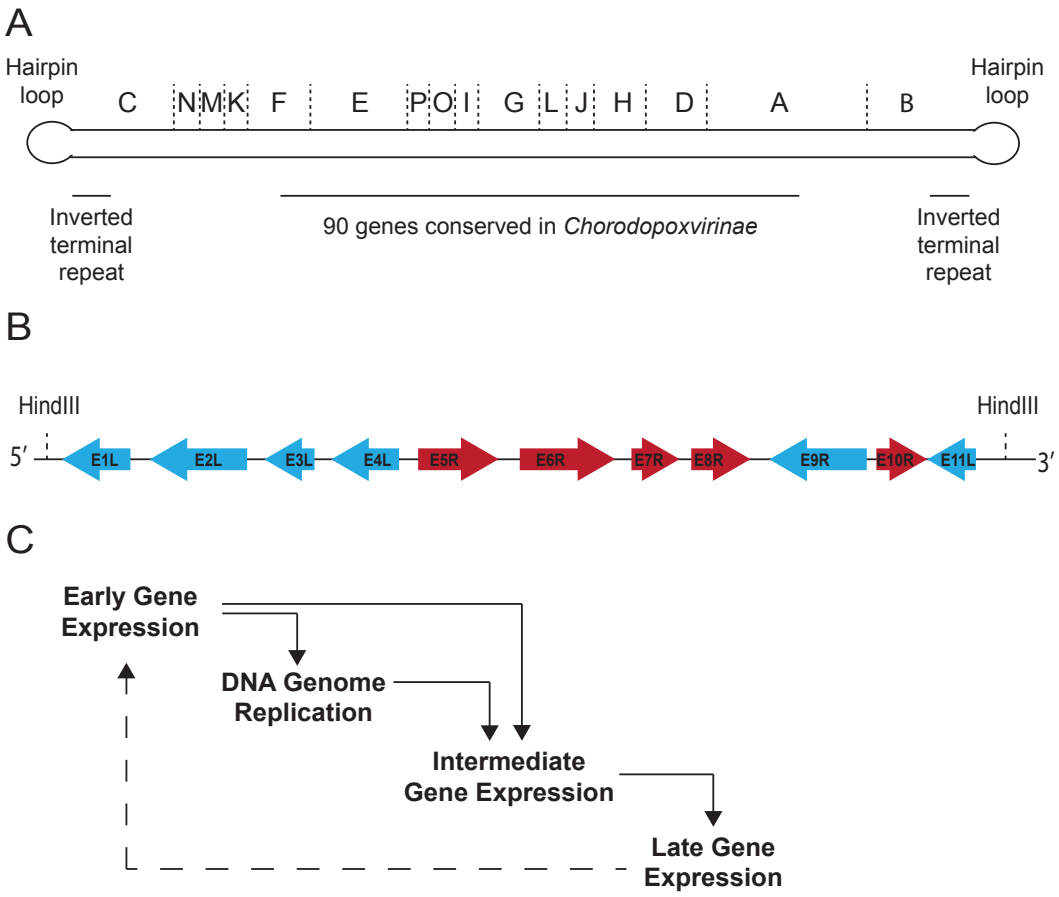

Figure 1.14 The vaccinia virus genome

A. The vaccinia virus genome is a self-complementary circular strand of DNA. Each terminus is a hairpin loop of 101 nucleotides. The ITRs are comprised of tandem repeat sequences. The core of the genome is very well conserved within the *Chordopoxvirus* subfamily. Dashed lines indicate the HindIII restriction sites. The 16 fragments that arise from HindIII digest are labeled A-P. **B.** The E HindIII fragment consists of 11 genes represented by red or blue arrows. The direction of the arrows indicates the direction of transcription. **C**. A schematic to illustrate the gene expression cascade that occurs during vaccinia infection.

1.4.3 Vaccinia life cycle

1.4.3.1 Entry

The entry of vaccinia virus into the host cell cytoplasm is mediated by virus and host membrane fusion (Figure 1.15). The virus core is subsequently released into the cytoplasm. Poxvirus entry is complicated by the fact that there are two distinct infectious virus particles, the intracellular mature virus (IMV) and extracellular enveloped virus (EEV), which are enveloped by one or two membranes, respectively. The external membranes of the two particles contain different subsets of virus proteins that are available to mediate virus attachment and entry. IMVs and EEVs are therefore, structurally and antigenically different and enter the host cell by distinct mechanisms (Mercer and Helenius, 2008; Schmidt et al., 2011; Schmidt et al., 2012). IMVs attach to the cell plasma membrane using four vaccinia proteins that interact with different plasma membrane glycoproteins/glycolipids; A27 and H3 bind to heparin sulphate, A26 to laminin and D8 to chondroitin sulphate (Chiu et al., 2007; Chung et al., 1998; Hsiao et al., 1999; Lin et al., 2000). It is not clear how EEVs attach to host cells, but it has been suggested that unknown virus proteins bind to cell membrane glycosaminoglycans (GAG). IMVs and EEVs enter the cell either through direct fusion of the virus membrane with the plasma membrane (Armstrong et al., 1973; Carter et al., 2005), or after endocytosis through fusion with the endocytic membrane (Huang et al., 2008; Townsley et al., 2006). The main route of entry for both IMVs and EEVs is likely to be through macropinocytosis, a specific form of endocytosis (Laliberte and Moss, 2009; Mercer and Helenius, 2008; Sandgren et al., 2010). IMV and EEV particles are enveloped at the plasma membrane by large actin dependent membrane blebs, which involves Rac1 and PAK1 signalling to promote the required actin rearrangements (Laliberte and Moss, 2009; Mercer and Helenius, 2008; Schmidt et al., 2011). IMV uptake is stimulated by phosphatidylserine in the virus membrane, a phospholipid that is normally associated with apoptotic bodies (Mercer and Helenius, 2008). At the plasma membrane or following uptake into macropinosomes, the entry-fusion complex (EFC) mediates the fusion of the IMV membrane with the host cell membrane (Laliberte et al., 2011). The EFC is a multi-meric protein complex made up of trans-membrane and membrane associated vaccinia proteins (A16, A21, A28, F9, G3, G9, H2, J5, L1, L5 and O3) (Laliberte et al., 2011; Moss, 2012; Senkevich et al., 2005; Wolfe et al., 2012). As EEV particles possess one additional membrane, cell entry of EEVs particles presents a topological problem. It has been suggested that acidification

of the endosome disrupts the outer EEV membrane, resulting in an IMV particle that may fuse with the macropinosome membrane by a similar mechanism to IMVs (Schmidt et al., 2011).

1.4.3.2 Replication and assembly

After entry into the cell cytoplasm, vaccinia virus cores are transported within the cell to sites of transcription on microtubules, using as yet unknown cellular motors and vaccinia core proteins (Carter et al., 2003; Mallardo et al., 2001). Early gene transcription factors are enclosed in the virus core and direct early gene expression. It has been suggested that the complete transcription machinery is assembled onto early gene promoters during viral morphogenesis (Broyles, 2003). This could allow for immediate early gene expression upon infection of the host cell (Baldick and Moss, 1993). Early mRNAs are synthesised within a partially disrupted core and extruded into the cytoplasm from the core (Mallardo et al., 2001). Early proteins then mediate core uncoating to allow DNA release and subsequent replication (Moss, 2007). DNA replication of the vaccinia genome is apparent, using microscopy, by the appearance of DNA positive structures (early virus replication sites) in the cytoplasm. These early DNA sites first appear in the periphery of the cell and over time grow and accumulate in the perinuclear region of the cell to form the mature virus factory (Domi and Beaud, 2000; Schepis et al., 2006). The virus factory is devoid of cellular organelles and almost completely enclosed by an ER derived membrane (Tolonen et al., 2001). Intermediate and late gene expression occurs in virus factories after DNA replication (Broyles, 2003), following which the assembly of immature progeny virus particles can begin. This is characterised by the appearance (by electron microscopy) of a crescent of lipid and virus protein. The crescent encloses newly synthesised virus cores and DNA genome to form a barrel shaped immature virion (IV) (Rodriguez et al., 1998; Zhang and Moss, 1992). There has been considerable controversy in the field regarding the derivation of the IV membrane and whether one or two membranes enclose the progeny virus particles. It is now clear that a single lipid bilayer surrounds the particle and this derives from *de novo* membrane biogenesis (Carter et al., 2005; Heuser, 2005; Hollinshead et al., 1999). IVs mature to form brick-shaped IMVs through condensation, proteolytic processing and reorganisation of the core proteins (Roberts and Smith, 2008). For the majority of virus particles this is where the life cycle finishes and these particles are released from the infected cell upon cell lysis.

1.4.3.3 Release

A small proportion of IMVs are transported from the virus factory to sites where the particles become wrapped by an additional double membrane derived from the trans-Golgi or endosomal network to form intracellular enveloped virus (IEV) (Figure 1.15) (Hiller and Weber, 1985; Schmelz et al., 1994; Tooze et al., 1993). Therefore, three membranes envelop IEV particles. The outer IEV membranes contain IEV specific integral membrane proteins A33, A34, A36, A56 and B5 and membrane associated proteins E2, F12 and F13, nearly all of which are required for IEV formation and/or transport to the cell periphery on microtubules (Roberts and Smith, 2008). Two of the IEV proteins, F12 and A36, have been suggested to mediate IEV transport to the periphery via kinesin-1 dependent microtubule movement (Herrero-Martinez et al., 2005; Rietdorf et al., 2001; Ward and Moss, 2004). However, recently it has been shown that F12 is also required for the earlier event of IMV membrane wrapping to form IEVs, in association with E2, while A36 is absolutely required for microtubule movement through a direct interaction with kinesin light chain (Dodding et al., 2009; Ward and Moss, 2004). In addition to direct movement along microtubules, virus proteins stimulate increased peripheral microtubule dynamics and a coincidental increase in the frequency with which microtubule tips reach the cell periphery. Upon reaching the cell periphery, virus particles negotiate the dense network of cortical actin by altering actin dynamics. Both of these peripheral processes are dependent on F11 and will be discussed in more detail in later sections (see 1.4.7) (Arakawa et al., 2007a; Arakawa et al., 2007b). IEV particles exit the infected cell through fusion of the outer most IEV membrane and the plasma membrane in a process that resembles exocytosis (reviewed in (Roberts and Smith, 2008)). Virions are released from the cell as EEVs or can remain associated with the plasma membrane, as CEV. EEVs are thought to mediate long-range dissemination *in vivo*. CEVs can stimulate the formation of an actin tail beneath the particle to propel particles towards neighbouring cells to mediate local cell-to-cell spread (Cudmore et al., 1995; Doceul et al., 2010). CEVs locally activate Src and Abl family kinases beneath the virus particle (Newsome et al., 2004). This family of kinases phosphorylate the cytoplasmic domain of the integral membrane protein A36 at two tyrosine residues Y112 and Y132 (Newsome et al., 2006). The phosphorylation of A36 mediates the release of kinesin-1 from CEVs (Newsome et al., 2004). After kinesin-1 release, phosphotyrosine residues on A36 recruit a complex of Nck, Grb2, WIP (WASP-interacting protein) and N-WASP to

stimulate actin polymerisation via the Arp2/3 complex (Frischknecht et al., 1999; Moreau et al., 2000; Scaplehorn et al., 2002).

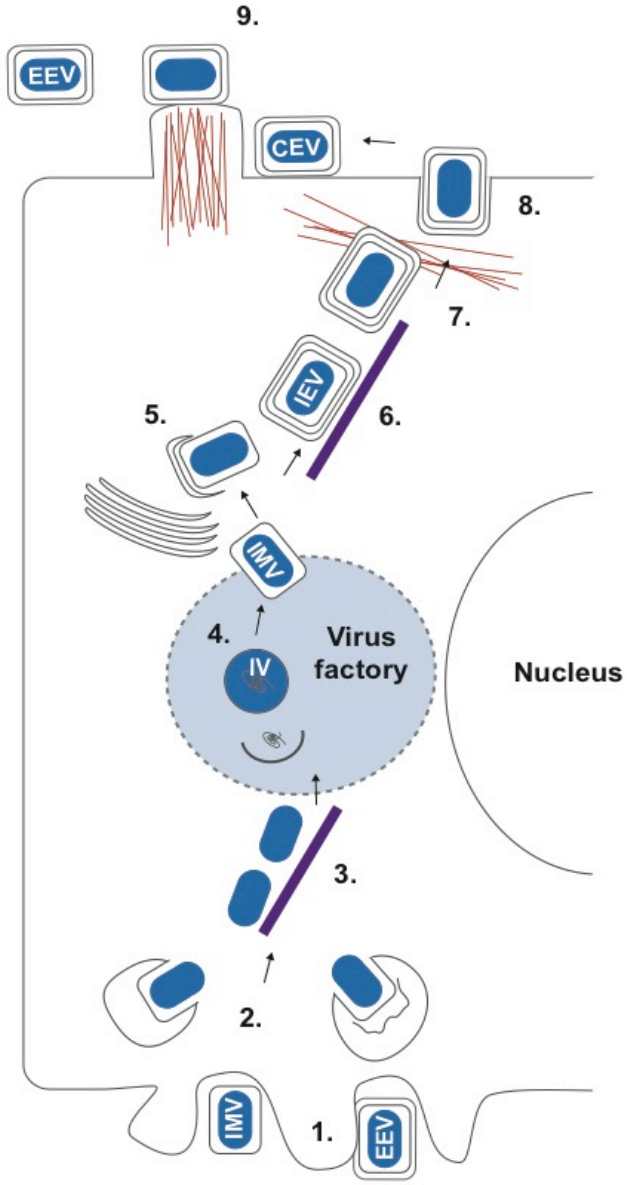

Figure 1.15 The vaccinia replicative cycle

1. IMV and EEV attach to the cell and stimulate macropinocytosis. 2. The virus membrane fuses with the macropinocytic membrane and the virus core is released into the cytoplasm. 3. Virus cores move to the perinuclear region on microtubules. 4. In the virus factory, crescents of lipid and virus protein form, which encloses newly made virus core and genome to form IVs. IVs mature to IMVs. 5. IMVs can become wrapped by a double membrane from the TGN or endosomal network to form IEVs. 6. IEVs move to the periphery on microtubules. 7. IEVs move through the cortical actin layer to reach the plasma membrane. 8. The outer IEV membrane fuses with the plasma membrane. 9. CEVs stimulate outside-in signalling to form an actin tail beneath the particle. (Roberts and Smith, 2008). Adapted from Trends in Microbiology, *16*, Roberts, K.L., and Smith, G.L., Vaccinia virus morphogenesis and dissemination. 472-479, Copyright (2008), with permission from Elsevier.

1.4.4 Virus induced migration

Upon vaccinia virus infection, in addition to the previously described local changes in the actin cytoskeleton, dramatic changes in cell morphology occur. This was first documented with cell contraction at early stages of infection, followed by sequential re-spreading, cell migration and extension of peripheral long, thin projections (Figure 1.16) (Bablanian et al., 1978; Sanderson and Smith, 1998; Schepis et al., 2006; Schramm et al., 2006).

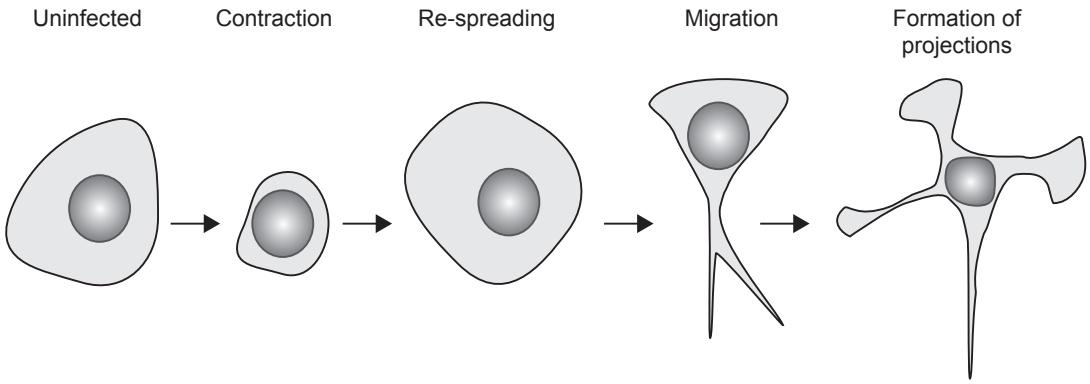

Figure 1.16 Sequential cell morphology changes during vaccinia infection

Early stage cell contraction (also called cell rounding) and cell migration requires virus transcription and subsequent protein expression, as inactivation of the virus particle with UV or inhibition of protein synthesis with cycloheximide completely blocks cell contraction (Bablanian et al., 1978; Sanderson and Smith, 1998; Schepis et al., 2006). More specifically, cell contraction and migration requires the expression of early genes as preventing intermediate and late gene expression, by blocking DNA replication, had no aberrant effect on cell contraction (Sanderson et al., 1998). Dynamic microtubules are necessary for cell contraction (Schepis et al., 2006). In contrast, F-actin, rather than microtubules, is required for cell re-spreading (Sanderson et al., 1998).

At later stages of infection cells become stellate, due to the extension of multiple lamellipodia that laterally collapse to form thin long neurite-like projections. F-actin and microtubule bundles extend throughout the projection and are associated with focal adhesions in the lamellipodium at the end of the projection (Sanderson et al., 1998).

Additional thin projections are formed through vaccinia-induced cell migration as the cell is unable to retract the rear end (Valderrama et al., 2006). Rear end retraction in migrating cells is mediated through contraction of stress fibres and proteolysis of focal adhesions, usually stimulated by Rho and ROCK signalling (see 1.2.2). Similar phenotypes are observed when Rho or ROCK are inhibited, suggesting that defective rear end retraction is due to vaccinia inhibition of Rho and ROCK (Totsukawa et al., 2004; Valderrama et al., 2006; Vega et al., 2011; Worthylake et al., 2001). These cell projections cannot form if intermediate and late gene expression is blocked. Additionally, projections do not form when actin polymerisation is inhibited or if microtubules dynamics are disrupted (Sanderson et al., 1998).

It is not clear if or how cell morphology changes contribute to vaccinia replication and spread. Co-ordinated changes in cell morphology are suggested to enhance vaccinia spread: cell contraction disrupts cell-cell adhesions early in infection to enable infected cells to migrate, form multiple new adhesions and increase the frequency of encountering uninfected cells (Cordeiro et al., 2009; Morales et al., 2008; Sanderson et al., 1998). Cell contraction may also aid intracellular virus replication, as it has been hypothesised that contraction can coalesce peripheral DNA factories and cellular organelles to the perinuclear region to establish an efficient zone for vaccinia replication and morphogenesis (Schepis et al., 2006; Schramm et al., 2006). However, this hypothesis was formed by blocking cell contraction with microtubule depolymerising drugs, which could have a vast range of additional deleterious effects on virus replication that are quite distinct from contraction.

1.4.5 MVA versus WR

It is important to note that the studies mentioned have been conducted with the WR strain of vaccinia virus. Modified vaccinia Ankara (MVA) is a highly attenuated vaccinia strain, derived from Chorioallantois vaccinia virus Ankara (CVA) after approximately 570 passages in chicken embryo fibroblasts (Mayr et al., 1978). This serial passage has led to multiple genomic deletions or point mutations and approximately one third of the genome is not expressed. Analysis of the MVA genome revealed six major deletions within the terminal regions, relative to CVA. In addition, there are numerous small deletions and point mutations within MVA (Antoine et al., 1998; Meisinger-Henschel et al., 2007). As a result MVA cannot replicate in human cells (Wyatt et al.,

1998). IV particles can form in HeLa cells but these do not mature to become IMVs (Gallego-Gomez et al., 2003; Sancho et al., 2002). Several studies have shown that MVA does not stimulate cell contraction, migration or the formation of projections (Gallego-Gomez et al., 2003; Morales et al., 2008; Schepis et al., 2006; Schramm et al., 2006; Valderrama et al., 2006). This would suggest that genes deleted or mutated in the MVA genome with reference to CVA and WR are required to induce cell morphology changes seen during WR infection (Gallego-Gomez et al., 2003).

1.4.6 F11 and cell migration

It was hypothesised that by examining the differences between WR and MVA it would be possible to identify vaccinia proteins involved in cell migration and the formation of projections. To this end, Ferran Valderrama and colleagues used a series of recombinant MVA strains, rescued with portions of the parental (CVA) genome, to identify proteins required for virus induced cell migration (Valderrama et al., 2006; Wyatt et al., 1998). This approach identified that the viral gene F11L, which is fragmented in MVA, was required for cell migration (Antoine et al., 1998; Valderrama et al., 2006). F11 can rescue the formation of cellular projections when it is overexpressed in cells infected with MVA (Valderrama et al., 2006). F11 expression from its endogenous promoter in a recombinant MVA virus (MVA-F11L) can also rescue cell migration (Zwilling et al., 2010). Additionally, F11 is required for the cell contraction that is observed when vaccinia virus spreads through confluent monolayer of cells, and for the disruption of cell-cell contacts (Cordeiro et al., 2009; Morales et al., 2008). In uninfected and MVA-F11 infected cells the expression of F11 causes a loss of stress fibres (Valderrama et al., 2006; Zwilling et al., 2010). This is similar to the phenotype seen in WR infection (Valderrama et al., 2006). Conversely, infection with a recombinant WR strain that does not express F11 (ΔF11L) maintains stress fibre formation, confirming that F11 is required to disrupt stress fibres (Cordeiro et al., 2009). The loss of stress fibres is characteristic of the inhibition of Rho proteins (Chardin et al., 1989; Valderrama et al., 2006). Consistent with this, F11 was found to bind and inhibit RhoA, but not Rac or Cdc42 (Cordeiro et al., 2009; Valderrama et al., 2006). The interaction between F11 and RhoA mimics the interaction between ROCK and RhoA, as F11 contains five conserved residues with the Rho binding motif of ROCK1 (Figure 1.17) (Dvorsky et al., 2004; Valderrama et al., 2006). Mutation of a valine and lysine in this motif (F11-VK mutant) completely abrogated RhoA binding (Figure 1.17) Like

ROCK, F11 preferentially binds activated RhoA. In addition, F11 can dimerise, which is consistent with ROCK forming a coiled coil to bind RhoA (Cordeiro et al., 2009; Dvorsky et al., 2004; Valderrama et al., 2006). F11 has very little sequence similarity with any human proteins or any conserved functional domains, outside of the RhoA binding motif (Valderrama et al., 2006). F11L is, however, very highly conserved amongst the Orthopoxvirus genus (Kato et al., 2004). Secondary structural predictions suggest that F11 is globular and has a predominantly β-sheet N terminal domain (1-222) and a α-helical C terminus (223-348) (Joao Cordeiro, unpublished data).

A

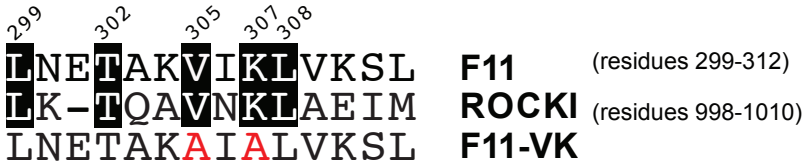

B

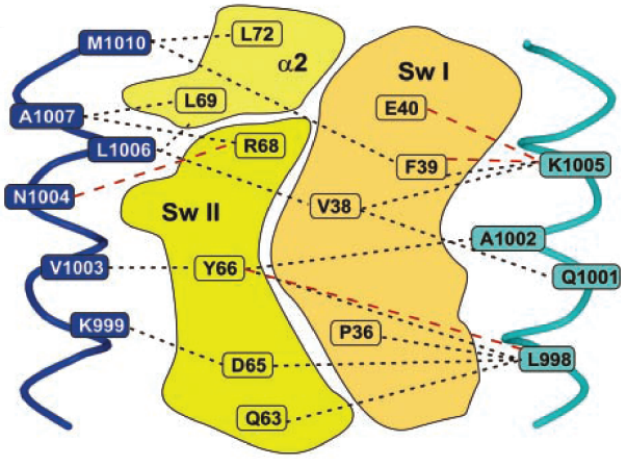

Figure 1.17 Sequence alignment of F11 and ROCK1

A. F11 has five conserved residues with the Rho binding domain of ROCK1. The conserved residues are highlighted in black. Mutation of a valine and lysine residues forms the Rho binding mutant of F11, F11-VK (residues highlighted in red). Adapted from Cordeiro, J.V. (2008). Modulation of Rho GTPase signalling during vaccinia virus infection (UCL). **B**. A schematic of the RhoA-ROCK1 interface. ROCK1 dimerises through a coiled coil motif (blue and green ribbons) and uses this motif to bind the switch 1 and switch 2 motifs in RhoA. The highlighted residues are those known to participate in the RhoA-ROCK1 interaction. The lines indicate hydrophobic (black) and electrostatic (red) interactions. This figure was originally published in Journal of Biological Chemistry: Dvorsky, R et al., (2004). Structural insights into the interaction of ROCKI with the switch regions of RhoA. J Biol Chem *279*, 7098-7104.© the American Society for Biochemistry and Molecular Biology

1.4.7 The role of F11 in virus release and spread

Newly assembled vaccinia IEV particles travel on microtubules to the cell periphery (Herrero-Martinez et al., 2005; Rietdorf et al., 2001; Ward and Moss, 2004). The efficiency of this process is augmented by dynamic peripheral microtubules that increase the delivery of virus particles to the cell cortex. F11 has been shown to enhance microtubule dynamics and peripheral targeting of microtubule tips (Arakawa et al., 2007b). F11 inhibition of RhoA signalling is responsible for increased microtubule dynamics, by inhibiting RhoA signalling to the formin mDia1 (Arakawa et al., 2007b). On reaching the cell cortex, IEV must negotiate the dense mesh of cortical actin to reach the plasma membrane. Virus particles have similar dimensions to exocytic vesicles (Cyrklaff et al., 2005). Reorganisation of the actin cortex facilitates exocytic vesicle trafficking to the cell periphery (Eitzen, 2003; Malacombe et al., 2006). Due to the large size of IEV particles, it is likely that cortical actin changes are also required to facilitate virus release (Arakawa et al., 2007a). F11 regulates local cortical actin, once again by inhibiting RhoA signalling to mDia1 (Arakawa et al., 2007a). F11-dependent inhibition of RhoA signalling therefore promotes virus release through modulation of microtubule and actin dynamics at the cell periphery (Arakawa et al., 2007a; Arakawa et al., 2007b; Cordeiro et al., 2009).

The role of F11 in virus spread was investigated in cell culture plaque assays and an *in vivo* mouse model of vaccinia infection. The spread of WR in a confluent monolayer of cells forms a large plaque with a clearance in the centre due to loss of cell-cell adhesion and cell migration away from the centre of the plaque (Cordeiro et al., 2009). Consistent with the role of F11 in virus release, the absence of F11 attenuated virus spread in the plaque assay and the characteristic plaque clearance was not observed (Cordeiro et al., 2009). The WR F11 protein also greatly enhances virus spread, in confluent monolayers, when it is introduced into the *Leporipoxvirus* Myxoma genome, which lacks a functional F11L gene (Irwin and Evans, 2012). In an *in vivo* model, WR infection in C57/BL6 mice resulted in acute sequential infection of the trachea, lungs and spleen followed by 100% mortality after 8 days. In the absence of F11, virus infection was restricted to the trachea and there was limited mortality (Cordeiro et al., 2009). The spread of F11-VK, the RhoA binding mutant, in confluent monolayers of cells and *in vivo*, was intermediate to WR and ΔF11L infection (Cordeiro et al., 2009). Taken together, the plaque assay and *in vivo* data suggest that RhoA independent F11

functions are required for efficient virus spread from cell-cell and through the infected host (Cordeiro et al., 2009).

1.5 The aims of this thesis

F11 is required for vaccinia induced cell contraction, cell migration and the formation of cellular projections (Morales et al., 2008; Sanderson et al., 1998; Valderrama et al., 2006). However, we lack molecular understanding of the host cell mechanisms involved in vaccinia induced cell morphology changes. The aim of this thesis was to characterise vaccinia induced cell contraction in more detail, elucidate the vaccinia proteins required and to understand which host cell mechanisms are required for vaccinia induced cell contraction. Ultimately, the aim is to use vaccinia virus as a tool to understand cell contraction in other pathogenic situations.

Chapter 2. Materials & Methods

2.1 General buffers and culture media

Routine media and buffers used in this thesis were prepared by Cell Services at the LRI, the recipes for which are listed below. The use of additional solutions or buffers is described within the relevant protocols.

2.1.1 General Buffers

Phosphate Buffered Saline A (PBSA)
8.00 g NaCl
0.25 g KCl
1.43 g Na_2HPO_4
0.25 g KH_2PO_4,

These reagents were dissolved in distilled water; adjusted to pH 7.2 before the solution was adjusted to a total volume of 1L. The solution was autoclaved to sterilise.

10x Tris Buffered Saline (TBS)
88.0 g NaCl
2.0 g KCl
30.0 g Tris Base

These reagents were dissolved in distilled water, the solution adjusted to pH 7.2 and made to a total volume of 1L. The solution was autoclaved to sterilise.

2.1.2 Cell Culture Media

Versene Solution
8.00 g NaCl
0.20 g KCl
1.15 g Na_2HPO_4
0.20 g KH_2PO_4, pH 7.2
0.20 g EDTA
1.50 ml 1% (w/v) Phenol red solution

Versene solution was made by dissolving the above reagents in distilled water, the pH was adjusted to 7.2 with HCl and the solution was made up to 1L and autoclaved to sterilise.

Trypsin Solution
0.25% in Tris Saline

Tris Saline (TS)
8.00 g NaCl
2.00 ml 19% (w/v) KCl solution
0.10 g $Na_2H_2PO_4$
1.00 g D-Glucose
3.00 g Trizma Base
1.50 ml 1% (w/v) Phenol red solution
0.06 g Penicillin
0.10 g Streptomycin

The Tris Saline reagents were dissolved in distilled water, adjusted to pH 7.7 and made to a total volume of 200 ml. Penicillin and streptomycin were then added. 2.5g of trypsin (Difco 1:250) was dissolved up to a total volume of 200 ml in distilled water (pH 7.7). The trypsin was added to Tris saline and made to a final volume of 1L with distilled water. The final solution was filter sterilised through a 0.22µm filter.

To make a 0.05% trypsin solution for cell culture, 0.25% trypsin was diluted 1:5 in versene and filter sterilised through a 0.22µm filter.

Minimal Essential Medium (MEM)
9.68g MEM powder
3.70g Sodium bicarbonate (NaHCO3)

MEM powder and sodium bicarbonate were dissolved in 10 L of distilled water and adjusted to pH 7.0 with carbon dioxide (CO_2). The final solution was filter sterilised through a 0.22µm filter

2.1.3 Bacteriological Media

Luria-Bertani (LB) Medium
10 g Bacto-tryptone
5 g Bacto-yeast extract
10 g NaCl

The above reagents were dissolved in distilled water, the solution adjusted to pH 7.2 with 1M NaOH and made to a total volume of 1L. The solution was autoclaved to sterilise. Ampicillin was added to 100µg/ml if required.

LB Agar plates
15 g of Bacto-agar was dissolved in 1L of LB medium and autoclaved. To make LB agar plates, LB Agar was melted in a microwave and allowed to cool to 50ºC, following which ampicillin was added at 100µg/ml.

2.2 Cell culture

2.2.1 Cell culture and freezing stocks

Cell lines were maintained in 10cm^2 cell culture dishes in the indicated media at 5% CO_2/37°C (Table 2). Cells were sub-cultured by washing once with PBSA, adding 0.05% trypsin/versene solution and incubating at 37°C for 5 minutes. Trypsinised cells were re-suspended in warm media and sub-cultured at the indicated ratio or counted using a haemocytometer and seeded at the appropriate cell density. For microscopy-based assays, cells were seeded onto fibronectin-coated dishes. To coat a dish, fibronectin was diluted 1:500 in PBSA and added to cell culture dish for 1 hour at room temperature, after which the dish was washed three times with PBSA.

Table 2 Cell lines and culture conditions

Cell Line	Species	Media	Sub-culture ratio	Supplements
HeLa	Human	MEM [1]	1:3-1:6	10% FBS[4] Pen/Strep[5]
HEK 293	Human	DMEM High glucose[2]	1:10-1:20	10% FBS[4] Pen/Strep
BS-C-1	African Green Monkey	DMEM Low glucose[3]	1:5-1:10	10% FBS[4] Pen/Strep[5]
U-2 OS	Human	DMEM High glucose[2]	1:5-1:10	10% FBS[4] Pen/Strep[5]
Ptk2	Rat Kangaroo	DMEM High glucose[2]	1:5-1:10	10% FBS[4] Pen/Strep[5]
MEF	Mouse	DMEM High glucose[2]	1:5-1:10	10% FBS[4] Pen/Strep[5]

Notes

1 Minimal essential medium provided by CRUK media services

2 Dulbecco's modified eagle medium 1000mg/l Sigma (D6046)

3 Dulbecco's modified eagle medium 4500mg/l Sigma (D6429)

4 Fetal Bovine Serum PAA laboratories (A15-101)

5 100 units/ml penicillin, 100 µg/ml streptomycin from 100x stock, Invitrogen (15140-122)

To prepare cells for liquid nitrogen storage, cells were trypsinised as above, re-suspended in warm culture media and then centrifuged at 120g for 5 min at room temperature. The cell pellet was then re-suspended in FBS plus 5% DMSO, aliquoted into cryo vials and transferred to the -80°C freezer. Several days later the frozen cells were transferred to liquid nitrogen. Cells were recovered by re-suspending the frozen pellet in warm media. Eight hours later media was replaced with fresh warm media.

2.2.2 Transfection

The method of transfection varied depending on the assay and nucleic acid. Fugene6 (Roche) and HiPerfect (Qiagen) were frequently used and are described here.

Lipofectamine2000 (Invitrogen) and calcium phosphate mediated transfections were also used in specific cases and these are described in the appropriate section.

2.2.2.1 Fugene 6

Fugene 6 (Roche) was used, according to the manufacturers instructions, to transfect HeLa cells with GFP-tagged genes of interest in CB6 vectors for confocal or wide field microscopy. Briefly, HeLa cells were seeded at $1.5x10^4$ cells per well in a fibronectin coated 12 well dish. After eight hours, Fugene 6 reagent and cDNA were added at a ratio of 3µl:1µg to 100µl Opti-MEM, briefly vortexed and incubated for 15 minutes at room temperature. The transfection mixture was added dropwise to cells. Imaging began 14-24 hours after transfection.

2.2.2.2 HiPerfect

HiPerfect (Qiagen) was used, according to the manufacturer's fast forward protocol, to transfect HeLa cells with siRNA oligonucleotides for RNA mediated interference. In summary, 6µl of HiPerfect reagent and 1µl of 20µM siRNA were diluted in 100µl MEM, briefly vortexed and incubated for 5 minutes. Meanwhile, 1ml of HeLa cells was seeded into a well of a fibronectin coated 12 well dish at a density of $1x10^4$ cells per ml. Immediately after seeding, the transfection mixture was added to the HeLa cells. 72 hours after transfection, HeLa cells were infected with vaccinia virus and imaged, or collected for immuno blotting or mRNA extraction.

Table 3 Target sequences of siRNA oligos

Gene	Target sequence	Dharmacon Cat No.
RHOA	AUGGAAAGCAGGUAGAGUU	D-003860-01
	GAACUAUGUGGCAGAUAUC	D-003860-02
	GAAAGACAUGCUUGCUCAU	D-003860-03
	GAGAUAUGGCAAACAGGAU	D-003860-04
RHOC	GGAGAGAGCUGGCCAAGAU	D-008555-01
	AUAAGAAGGACCUGAGGCA	D-008555-02
	GGAUCAGUGCCUUUGGCUA	D-008555-03
	GAGAGCUGGCCAAGAUGAA	D-008555-04
RHOD	UGAACAAGCUCCGAAGAAA	D-008940-01
	GAUUGGAGCCUGUGACCUA	D-008940-02
	CCGAACAGCUUUGACAACA	D-008940-03
	AGACGUCGCUGCUGAUGGU	D-008940-04
ARHE (RHOE)	GAACGUGAAAUGCAAGAUA	D-007794-02
	GAAAUUAUCCAGCAAAUCU	D-007794-03
	UAGUAGAGCUCUCCAAUCA	D-007794-04
	AGAAUUACACGGCCAGUUU	D-007794-05
RHOF (RIF)	GGGAGAAUGUGGAGGACGU	D-008316-04
	CGGCCGGGCAAGAAGACUA	D-008316-05
	AGAUCGUGAUCGUGGGCGA	D-008316-06
	ACGACAACGUCCUCAUCAA	D-008316-07
ROCK1	GCCAAUGACUUACUUAGGAUU	D-003536-05
ROCK2	GCAAAUCUGUUAAUACUCGUU	D-004610-05
Non-targeting	AllStars Negative Control	Qiagen

2.2.3 Generation of stable cell lines

Two HeLa cell lines that stably expressed fluorescent proteins were generated for this thesis, Lifeact-cherry and MLC2-RFP. Each gene was sub-cloned into the pLVX puro vector (ClonTech) (see 2.3.4), which contains a puromycin resistance cassette and all the necessary elements for the production of infectious but non-replicative lentivirus.

HEK 293t cells were seeded at a density of $2x10^6$ cells in a 6cm dish. The following day the media was replaced with 3.5ml of fresh warm complete MEM. Three hours later, 5ug each of pLVX vector, pRRE, pREV and pVSV-G were mixed in a total volume of 500µl 250mM $CaCl_2$. DNA/$CaCl_2$ mixture was then added dropwise to an equal volume of HBS (280mM NaCl, 10mM KCl, 1.5mM Na_2HPO_4, 12mM glucose and 50mM HEPES) whilst slowly vortexing to agitate and incubated for 15 minutes. The transfection mix was added dropwise to HEK293t cells. The following day the media

was replaced with complete MEM supplemented with 10mM Sodium Butyrate, this was then replaced with normal media 8 hours later. The next day, the media was removed and passed through a 0.45μM filter. The infectious media was added to sub confluent HeLa cells in a 12 well dish. Two days later, the media was replaced with complete MEM supplemented with 1μg/ml puromycin. After 24 hours incubation with puromycin, the cells were sub-cultured and subsequently analysed for Cherry/RFP fluorescence.

2.3 Molecular Biology

2.3.1 General Buffers/Methods

10 x DNA Loading Buffer

0.25% (w/v)	Bromophenol Blue
30% (v/v)	Glycerol

5 x TBE

445mM	Tris Base
445mM	Boric Acid
10mM	EDTA

2.3.1.1 Ethanol precipitation of DNA

DNA was precipitated with 0.3M sodium acetate and 2.5 volumes of ice cold 100% ethanol and incubated at -20°C for 20 minutes. DNA was pelleted by centrifugation at 13,00rpm at 4°C and washed with 70% ethanol. The DNA pellet was vacuum dried and re-suspended in dH_2O or EB buffer (Qiagen).

2.3.2 Expression vectors

The CB6 vector and pLVX vectors (Clontech) were used to express protein in mammalian cells using a CMV promoter (Reckmann et al., 1997).

Table 4 Expression vectors used in the thesis

Vector	Used in figure	Created by
pCB6 GFP-RhoC WT	5.5A	J. Cordeiro
pCB6 GFP-RhoC T19N	5.5A	J. Cordeiro
pCB6 GFP-RhoD G26V	5.9A	J. Cordeiro
pCB6 GFP-RhoD T31N	5.9A	J. Cordeiro
pCB6 GFP.	5.5A	M. Way
pLVX hygro GFP-RhoD WT siRNA Res	5.8A	C. Durkin
pLVX hygro GFP-RhoD G26V siRNA Res	5.8A	C. Durkin
pLVX hygro GFP-RhoD T31N siRNA Res	5.8A	C. Durkin
pLVX puro Lifeact Cherry	3.9	C. Durkin
pLVX puro MLC2 RFP	3.9	C. Durkin
pBS II F11-GFP WT targeting vector	3.8	C. Durkin

2.3.3 Polymerase chain reaction

PCR reactions were used to amplify DNA from vaccinia genomic DNA or DNA vectors. A standard 100µl PCR reaction contained 0.5µM of each primer, 1mM dNTP mix (0.25mM each nucleotide), 1 x Phusion HF buffer, 20U/ml Phusion High Fidelity DNA Polymerase (NEB) and up to 100ng of template DNA. PCR reactions were performed using Applied Biosystems GeneAmp PCR machine using the following conditions.

95°C 5 min

Denaturation 95 °C 30 sec

Annealing 55 °C 30 sec 25 cycles

Extension 72 °C 1 min

---

72 °C 10 min

---

12 °C ∞

Reactions were resolved on a 1% (w/v) agarose gel (made up in 1x TBE) containing 1:10,000 SYBR safe DNA Gel Stain (Invitrogen) and visualized at 470nm using a Safe Imager (Invitrogen).

2.3.4 Sub-cloning

Insert and vector plasmids were digested at a ratio of approximately 3µg:1µg in separate 20µl reactions containing 10-20U restriction enzyme (NEB) and 1 x NEBuffer at 37ºC for 1 hour. The digestion reaction was resolved on a 1% agarose gel (made in TBE) with 1:10,000 SYBR safe DNA Gel Stain (Invitrogen) and visualised at 470nm using a Safe Imager (Invitrogen) and cut out from the gel. DNA was purified in 30µl H_2O using Qiagen QIAquick gel extraction kit. Insert DNA was vacuum dried and re-suspended in 7µl H_2O. Insert was added to 1µl vector DNA, 1x T4 ligase buffer and 200U T4 ligase (NEB) and incubated for 30 minutes at room temperature. Ligation reaction was transformed into chemically competent XL-10 cells (2.3.6).

2.3.5 Chemically competent *E.Coli*

A 5ml preculture of XL-10 gold *Escherichia coli* was incubated overnight in LB media at 37°C at 220 rpm. 2ml of the preculture was subsequently added to 500ml of LB with constant shaking at 37 ºC until an OD_{600} of 0.5 was reached. The culture was then centrifuged for 12 min at 2500 rpm. The pellet was re-suspended in 20 ml of cold RF1 buffer, incubated on ice for 15 min and centrifuged for 9 min at 2500 rpm. Finally, the pellet was re-suspended in 7 ml cold RF2 buffer, divided into 100µl aliquots, snap frozen and stored at -80ºC.

RF1 Buffer
12.00 g Rubidium chloride, RbCl
9.00 g Manganese chloride, $MnCl_2$
2.94 g Potassium acetate
150.00 g Glycerol

Dissolved in 1L of H_2O made to a final pH of 5.8 with acetic acid and sterilized through a 0.22µm filter.

RF2 Buffer
2.09 g 3-(N-morpholino)propanesulfonic acid (MOPS)
1.20 g Rubidium chloride, RbCl
11.00 g Calcium chloride, $CaCl_2$
150.00 g Glycerol

Dissolved in 1L of H_2O made to a final pH of 6.8 with sodium hydroxide and sterilized through a 0.22µm filter.

2.3.6 Transformation of bacteria

Chemically competent XL-10 cells were thawed on ice and then incubated with DNA on ice for 20 minutes. Cells were heat shocked at 42°C for 45 seconds, incubated on ice for 2 minutes, and then incubated at 37°C with constant shaking for 45 minutes in 100µl LB media. The bacteria solution was spread onto LB-agar plates containing ampicillin and incubated at 37°C overnight.

2.3.7 Colony screening by PCR

Colony screening by PCR was performed to identify XL-10 colonies containing the insert of interest, following the transformation of cloning ligation reactions. Colonies were picked with a pipette tip and transferred to a 25µl PCR reaction containing 1x PCR buffer, 1.5mM $MgCl_2$, 0.5µM of each primer, 1mM dNTP mix (0.25mM each nucleotide) and 50 U/ml Simpler Red DNA Polymerase (Thermo Scientific). PCR reactions were analyzed as before (2.3.3).

	95°C 10 min	
---	---	---
Denaturation	95 °C 30 sec	
Annealing	55 °C 30 sec	30 cycles
Extension	72 °C 1 min	
---	---	---
	72 °C 10 min	
---	---	---
	12 °C ∞	

2.3.8 Plasmid DNA purification

DNA was purified from XL-10 cultures using Plasmid Miniprep and Midiprep Kits (Qiagen) according to the manufacturers instructions. XL-10 cultures derived from a single colony and were grown overnight at 37°C and 220rpm in LB-ampicillin. DNA was purified from 5ml or 50ml of XL-10 for Miniprep or Midiprep, respectively.

2.3.9 DNA sequencing

To sequence regions of interest in purified plasmid DNA or PCR products from vaccinia genomic DNA, primers were designed to match DNA sequence flanking the region on sense or antisense strand and every 500 bases throughout the region of interest. The 20µl sequencing PCR reaction contained 3.2 pmole primer, 8µl BDTv3.1 reaction mix (Big Dye Terminator Cycle sequencing kit) and 200ng of plasmid DNA or 60ng-100ng of 3kb-4kb PCR product.

	95°C 1 min	
---	---	
Denaturation	95 °C 10 sec	
Annealing	55 °C 5 sec	25 cycles
Extension	60 °C 4 min	
---	---	
	12 °C ∞	

PCR products were purified with DyeEx columns (Qiagen) and vacuum dried. Sequencing was performed by the LRI equipment park.

2.3.10 Site directed mutagenesis

Point mutations were introduced into genes of interest using a protocol based on QuikChange site-directed mutagenesis (Agilent Technologies/Stratagene). Forward and reverse complimentary primers were designed to introduce single or multiple point mutations. The point mutation was in the centre of the primer with at least 15 bases on either side. The site-directed mutagenesis PCR was performed in a 100µl reaction containing 125ng of each primer, 1mM dNTP mix (0.25mM each nucleotide), 1 x Phusion HF buffer, 20U/ml Phusion High Fidelity DNA Polymerase (NEB) and up to 50ng of template/parental DNA, using the following conditions.

95°C 5 min

Denaturation 95 °C 30 sec

Annealing 55 °C 30 sec 12-18 cycles

Extension 68 °C 1 min per kb plasmid

---

72 °C 10 min

---

12 °C ∞

The number of cycles varied between 12 cycles for a single point mutation and 18 for multiple amino acid changes. Following the PCR, the reaction was incubated with 20U Dpn1 (NEB) to digest methylated/hemi-methylated parental DNA, for 1 hour at 37°C. DNA was then ethanol precipitated and re-suspended in 5µl H_2O. The DNA was transformed into XL-10 cells. XL-10 clones were cultured and the DNA was purified by Miniprep. DNA carrying the desired mutation was confirmed by sequencing.

2.4 Vaccinia virus

The wild type virus used in this thesis is the Western Reserve strain (WR). The recombinant viruses generated in this study are in a WR genomic background. The attenuated virus modified vaccinia Ankara (MVA) was also used. The viruses used in this study are listed below.

Table 5 Viruses used in the thesis

Virus name	Generated by/received from	Genomic backbone
ΔF11L	Y. Arakawa	WR
F11 VK	J. Cordeiro	WR
F11 IV-KNS	J. Cordeiro	WR
F11 VK/IV-KNS	J. Cordeiro	WR
MVA	G. Sutter (Zwilling et al., 2010)	
MVA F11	J. Zwilling (Zwilling et al., 2010)	MVA
F11-GFP	C. Durkin	WR

2.4.1 General buffers for virology

Tris buffer
10mM Tris-HCl pH 9
2mM MgCl2
in distilled water and filter sterilised using a 0.22µm filter.

Sucrose cushion
35% sucrose (w/v) in Tris buffer

Crystal violet
0.1% crystal violet (w/v)
20% ethanol

Virus lysis buffer
10mM Tris-HCl pH 9
10mM KCl
3mM $Mg(CH_3COO)_2$
in distilled water and filter sterilised using a 0.22µm filter.

2.4.2 Sucrose Purification of vaccinia virus

HeLa cells were grown in 15cm^2 culture dishes to a confluency of 90%. The cells were infected with 0.1 multiplicity of infection (MOI) of vaccinia virus and left to grown for 48-72 hours until all cells displayed obvious cytopathic effect (CPE). The infected cell media was removed and cells were harvested in 10ml of PBSA and centrifuged for 7 minutes at 1,700rpm. The cell pellet was washed once in PBSA. Subsequently, infected cells were re-suspended in 7mls of Tris Buffer and sheared by 15 strokes of a 7ml Dounce homogeniser (Wheaton). The resulting solution was clarified at 1,700rpm for 7 minutes, to remove nuclei and cell membrane, and the supernatant was saved and stored at -20ºC overnight. The virus supernatant was layered onto an 8ml 35% sucrose cushion in Beckman SV40 ultracentifuge tubes, made to a total of 25ml with Tris buffer and centrifuged at 24,000rpm in a Beckman Optima L-100 XP ultracentifuge for 30 mins. The pellet was re-suspended in Tris buffer and stored in 100µl aliquots at -80°C.

2.4.3 Virus titre

BS-C-1 cells were grown to a confluent monolayer in 6 well dishes. The virus preparation was serially diluted 1:10 in 1ml of serum free MEM. The culture media was removed from the BS-C-1 cells and replaced with 10^{-5}, 10^{-6} and 10^{-7} dilutions of virus. After 1 hour the media was removed and replaced with an overlay of 1 x MEM, 5% FBS and 0.9% agarose. Following a two day incubation, the cells were fixed with 4% paraformaldehyde (PFA) in PBSA for 1 hour, the overlay was removed and cells were stained with crystal violet solution for 30 mins. Virus titre or plaque forming unit per ml (PFU/ml) was determined by counting the number of virus plaques within the virus dilution where plaques are both discernible and isolated.

2.4.4 Infection

The multiplicity of infection (MOI) for an experiment was calculated from the PFU of the virus stock and the number of cells in the particular experiment. A MOI of 5 was used for all experiments unless otherwise stated. Prior to infection, the virus aliquot was sonicated in a water bath for 30 seconds. Cells were washed with serum free media and the appropriate volume of virus was added to the cells in serum free media. Cells were incubated for 20 mins with virus at 37°C after which the media was replaced for complete media. Cells were incubated at 37°C until the termination of the experiment.

2.4.5 Drug treatments during infection

HeLa cells were treated with inhibitors for the indicated time prior to infection and throughout infection, at the indicated concentrations.

Table 6 List of inhibitors

Compound	Concentration	Incubation time prior to infection	Reference
Z-VAD-fmk	10μM	30 minutes	(Postigo and Way, 2012)
Y27632	10μM	30 minutes	(Sanz-Moreno et al., 2008)
H1152	5μM	30 minutes	(Sanz-Moreno et al., 2008)
GSK429286A	5μM	30 minutes	(Nichols et al., 2009)
C3	0.5μg/ml	1 hour	Cytoskeleton Inc.
AraC	50μM	0	
Psoralen	5μg/ml	-	(Tsung et al., 1996)

2.4.6 UV irradiation of vaccinia

$4x10^4$ plaque forming units (PFU) of virus was suspended in 500µl of serum free media in a 6 well dish. 5µg/ml Psoralen was added to the virus solution and this was then exposed to 0.4J/cm-2 ultraviolet (UV) light. The 500µl solution was used to infect one well HeLa cells in a 12 well dish.

2.4.7 Preparation of vaccinia genomic DNA

Vaccinia genomic DNA was prepared from one 100µl aliquot of sucrose-purified virus or alternatively from the post-nuclear supernatant of infected cell lysates, which was prepared as follows. A $10cm^2$ dish of infected cells was collected in PBS, centrifuged at 1,700rpm for 5 minutes and washed with PBS. The cell pellet was re-suspended in 100µl virus lysis buffer, sheered and centrifuged at 1,700rpm for 5 minutes. The 100µl of virus containing supernatant was used for DNA preparation. Virus preparations were incubated at 37°C for 4 hours with 0.5mg/ml Proteinase K and 0.5% SDS. DNA was then isolated by phenol/chloroform extraction. Briefly, the virus preparation was added to an equal volume of phenol:chloroform, incubated with rotating for 5 minutes and centrifuged at 13,000rpm for 5 minutes. The top supernatant was again added to phenol:chloroform and the previous steps were repeated twice. The DNA was then purified by ethanol precipitation and the pellet was re-suspended in 20µl of H_2O.

2.4.8 Amplification of vaccinia DNA

2.4.8.1 Touch-down PCR

Touch down PCR was used to amplify DNA from vaccinia genomic DNA. Approximately 1µl of vaccinia genomic DNA was added to a standard PCR mix (2.3.3) and the PCR reaction was performed using the following conditions.

95°C 1 min

Denaturation 95 °C 20 sec

Annealing 65 °C 20 sec - 1°C per cycle for 10 cycles

Extension 72 °C 1 min

Denaturation 95 °C 20 sec

Annealing 55 °C 20 sec 25 cycles

Extension 72 °C 1 min

---

72 °C 10 min

---

12 °C ∞

2.4.8.2 Analytical PCR from plaque picks

The picked focus was re-suspended in 100µl serum free media and freeze/thawed three times. 8µl of this suspension was incubated with 40µg/ml proteinase K, 3µl of 10x Simpler Red DNA polymerase PCR buffer (Thermo Scientific) in a 25µl volume for 20 minutes at 56°C followed by 10 minutes at 85°C. The mixture was then supplemented with 1mM dNTPs, 0.5µM of each primer, 1.5mM MgCl2 and 50 U/ml Simpler Red DNA polymerase. The PCR reaction was performed as (2.3.3) using the following conditions and the reaction product was analysed on a 1% agarose gel as before.

95°C 10 min

Denaturation 95 °C 30 sec

Annealing 55 °C 30 sec 30 cycles

Extension 72 °C 1 min

---

72 °C 10 min

---

12 °C ∞

2.4.9 Generation of recombinant F11-GFP virus

The F11-GFP virus was generated by homologous recombination between a targeting vector and ΔF11L virus. The targeting vector consisted of F11-GFP between two arms of recombination; which mimic the flanking regions of the F11L locus within the WR genome (Figure 3.8A).

The targeting vector for the F11-GFP viruses was created as follows. F11 was cloned into a pE/L vector using BglII and Not1. GFP was amplified by PCR, with an additional 30bp (encoding GAAAWGGGGW) upstream of the GFP start codon to generate a flexible linker between F11L and GFP, and added to the C terminus of F11L with Not1 and BamH1 restriction sites. The final 25bp of F11L sequence was re-codonised to prevent recombination with the F10L promoter using site directed mutagenesis. The left and right arms of recombination were generated by touchdown PCR from purified WR genomic DNA. First, the left arm comprised the 600bp upstream of F11L start codon (F12L coding sequence) and was cloned into the targeting vector using BglII restriction sites. Subsequently, the right arm comprised the terminal 25bp of F11L (the F10L promoter) and a further 575bp downstream of F11L (F10L coding sequence), and was cloned using BamH1 restriction sites.

HeLa cells were seeded into a 35mm^2 culture dish at 90% confluency. Cells were infected with ΔF11L virus at MOI 0.1. At 2hpi cells were transfected with the 4μg of targeting vector using Lipofectamine 2000 (Qiagen), according to the manufacturer's protocol. Briefly, 10μl of Lipofectamine 2000 was added to 250μl Opti-MEM, whilst separately 4μg DNA was added to 250μl Opti-MEM and both solutions were incubated for 5 mins. The two solutions were mixed, incubated for 20 mins and added dropwise to the cells. At one day post infection, the media was removed and cells were scraped into 500μl of virus lysis buffer. The infected cell lysate was then freeze/thawed three times in liquid nitrogen/37°C incubator. Confluent monolayers of BS-C-1 cells in 35mm^2 dishes were infected with 1:10 serial dilutions of the infected cell lysate in serum free media, and then overlayed with agarose (2.4.3). At 24 hours post infection, the cells were observed on a widefield microscope using phase contrast to search for plaques and fluorescence to identify GFP positive plaques. Plaques were 'picked' with a p1000 pipette tip into 250μl virus lysis buffer, which was then freeze/thawed as before. For the second round of plaque purification 50μl of the picked plaque solution was used to infect BS-C-1 as before. Plaque purification continued until only fluorescent plaques

could be seen. Recombinant virus purity was confirmed by analytical PCR using primers pairs that amplified the target region and distinguished between parental and recombinant virus, by size or by the presence/absence of a PCR product.

2.5 Biochemistry

2.5.1 2 x Final sample buffer (FSB)

125mM	Tris HCl pH6.8
4%	SDS
20%	Glycerol
10%	B-mercaptoethanol

+ a pinch of Bromophenol blue

2.5.2 SDS-PAGE

For antibody tests and assessing the efficiency of siRNA knockdown, cells were lysed directly into 2 x FSB. Samples were boiled for 10 minutes at 95ºC. Samples were loaded onto 4-12% Bis-Tris or 8% Tris-actetae NuPAGE pre cast gels (Invitrogen), with reference to SeeBluePlus2 protein standards (Invitrogen) and resolved for 1 hour at 150V.

2.5.3 Immuno blotting

2.5.3.1 ECL immuno blotting

Proteins resolved by SDS-PAGE were transferred onto nitrocellulose membranes using the iBlot semi-dry transfer system (Invitrogen) at 23V for 7 minutes or 20V for 9 minutes for large proteins. Successful transfer onto the membrane was observed with Ponceau S staining (Pierce). The membrane was incubated in blocking buffer consisting of 5% BSA or 5% Milk in TBS-T (Tris-buffered saline + 0.1% Tween20) for 30 minutes and then incubated overnight with primary antibody in blocking buffer at 4ºC. The membrane was washed four times with TBS-T, and then incubated with HRP conjugated secondary antibody (Jackson ImmunoResearch) diluted to 1:5000 in blocking buffer for 30 minutes at room temperature. The membrane was washed as

before. Finally, the membrane was incubated in ECL reagent (Amersham Biosciences) for 1 minute and exposed on Hyperfilm-ECL (Amersham Biosciences).

2.5.3.2 Quantitative infra red immuno blotting

For quantitative immuno blot, membranes were blocked and antibodies diluted in Odyssey blocking buffer (LiCor). All immuno blotting steps were performed as above, until secondary antibody incubation where the membrane was incubated with Infrared secondary antibody (Rockland) diluted to 1:5000 for 1 hour. The membrane was washed as before and visualised on the Odyssey Infrared scanner (LiCor).

Table 7 Primary antibodies used in immuno blotting

Antibody	Raised in	Concentration	Blocking	Supplier
GST (G-7781)	Rabbit	1:2000	Milk	Sigma
ROCK1 (C8F7)	Rabbit	1:1000	BSA	Cell signalling
ROCK2 (D1B1)	Rabbit	1:1000	BSA	Cell signalling
RhoA (67B9)	Rabbit	1:1000	BSA	Cell signalling
RhoC (D40E4)	Rabbit	1:1000	BSA	Cell signalling
RhoD	Rabbit	1:1000	Milk	AnboBio
F11-N	Rabbit	1:2000	SuperBlock (Thermo Scientific)	C. Durkin and Y. Handa
F11-C	Rabbit	1:2001	SuperBlock (Thermo Scientific)	C. Durkin
P14/A27L	Mouse	1:1000	Milk	
A36	Mouse	1:2000	Milk	S. Cudmore
Actin (ac-74)	Mouse	1:2000	Milk	Sigma
α-Tubulin	Mouse	1:2000	Milk	Sigma
Grb2	Mouse	1:1000	Milk	BD Transduction
GFP (3E12)	Mouse	1:2000	Milk	In House CRUK
N1	Rabbit	1:1000	Milk	A. Postigo

Table 8 Secondary antibodies used in immuno blotting

Antibody	Raised in	Label	Supplier
Mouse	Goat	HRP	Jackson ImmunoResearch
Rabbit	Goat	HRP	Jackson ImmunoResearch
Mouse	Rabbit	IRDye800CW	Rockland
Rabbit	Goat	IRDye800CW	Rockland

2.5.4 Rhotekin Pull down assays

2.5.4.1 Rho activity in infected cells

U-2 OS cells were seeded into a 15cm^2 to achieve 80% confluency on the day of the assay. Cells were infected with WR or ΔF11L at an MOI 5 in serum free DMEM for 30 minutes, after which the media was replaced for complete DMEM. At 3hpi, cells were washed with 10ml of ice-cold TBS, lysed in 750µl 1x Mg^{2+} lysis buffer (MLB) (Millipore) on ice and clarified at 13,000rpm for 3 minutes. The lysate was incubated with 15µl of Rho assay reagent (Rhotekin RBD agarose, Millipore) for 1 hour at 4ºC whilst rotating. The beads were washed three times with MLB, and boiled in FSB. The bound and input samples were resolved by SDS-PAGE and analysed by quantitative infrared immuno blot using anti-RhoA or anti-RhoC antibodies (Table 7). The proportion of Rho.GTP in the cell lysate was determined by normalising the intensity of bands in the bound sample to the input, using LiCor Odyssey software. Each sample was further normalised to the mean of the uninfected control.

2.5.4.2 RhoC activity in cells expressing GFP-RhoD

U-2 OS cells were transfected with pCB6 GFP or pCB6 GFP-RhoD. Six hours later, the media was replaced with serum free DMEM. 24 hours after starvation, cells were stimulated in 20% FBS for 3 minutes. Cells were lysed and assay performed as above.

2.5.5 Generation of polyclonal F11 antibodies

2.5.5.1 Generation of bleeds

Peptides with a free sulfhydryl group were synthesised by the peptide synthesis facility at the LRI and conjugated to maleimide-activated mariculture Keyhole limpet hemocyanin (mcKLH) (Thermo Scientific) according to the manufacturer's instructions. Briefly, 2mg of the peptide was dissolved in 500µl of conjugation buffer, mixed with 2mg of maleimide-activated mcKLH (reconstituted in 200µl dH_2O) and incubated for 2 hours at room temperature. The peptide-KLH conjugate was applied to a desalting column (Thermo Scientific) and eluted with 0.5ml aliquots of purification buffer (Thermo Scientific). Aliquots that contained eluted peptide were identified by absorbance measurements at OD_{280} and these were pooled and made up to a total volume of 4.2ml in sterile PBSA. The immunogen solution was separated into six 1.2ml aliquots, one double strength aliqout and the remaining five diluted 1:1 with PBSA. Immunogen

aliquots were sent to Pettingill Technologies for injection into two rabbits over a 77-day schedule. The ability of the resulting antisera to detect F11 was tested by immuno blot analysis on HeLa cell lysates infected with WR or ΔF11L.

Table 9 Peptides used to generate polyclonal antibodies.

Name	Region	Sequence	Immuno blot	IF
F11-C	323-334	CGGNFITKEIKNRDK	Yes	No
F11-N	101-120	PDIKLDAVLDRDGNFRPADC	Yes	No

2.5.5.2 Coupling peptides to SulfoLink column

Peptides were coupled to a SulfoLink column (Thermo Scientific) according to the manufacturer's instructions. Briefly, 1mg of peptide was dissolved in 2 ml of Coupling buffer and incubated for 30 minutes at room temperature. The peptide was added to the prepared and washed SulfoLink column and the column washed three times. Finally, non-specific sites in the coulumn were blocked by the addition of 50mM L-Cysteine.HCl and washed three times with PBSA.

2.5.5.3 Affinity purification

The affinity column was prepared by sequential washing with 20ml of the following buffers; 100mM Triethylamine (TEA) pH 11.5, PBSA, 100mM Glycine pH 2.5 and finally PBSA +250mM NaCl. The antisera from the two rabbits were pooled and centrifuged for 15 minutes at 2500rpm, the supernatant was filtered through a Millex-HV 0.45µm filter and then diluted 1:1 in PBSA +250mM NaCl. The diluted antiserum was passed through the column three times. The column was washed once with PBSA +250mM NaCl and PBSA. Bound antibody was eluted using 1 ml aliquots of glycine and then 1ml aliquots of TEA. Elutions were immediately neutralised with 1M Tris.HCl pH 8.8, then measured for absorbance at OD_{280} to detect the fractions that contained antibody. These fractions were tested as before and those with similar specificity were pooled and stored either at 4°C or diluted 1:1 with glycerol at -20°C.

2.6 Microscopy

2.6.1 Cell contraction assay

Hela cells were seeded onto 6 well dishes at a density of $3x10^4$ cells per well one day prior to infection. Hela cells were infected at a MOI of 5 in serum free MEM. The media was replaced at 20 minutes post infection with complete MEM supplemented with 40mM HEPES. Imaging started at 40 minutes post infection and images were acquired every 5 minutes for 10 hours.

Images were acquired using a Plan-Apochromate 10x/0.25 Ph1 lens and a Photometrics Cool Snap HQ cooled CCD camera on a Zeiss Axiovert 200 Microscope. The system was controlled by MetaMorph software version 6.3r7 (Universal Imaging Corporation Ltd). The average area of infected cells was determined at 1 hour intervals post acquisition using MetaMorph software version 6.3r7. The average cell area at each time point was normalized to the original mean and in all experiments is represented as the percentage of the original cell area.

2.6.2 Cell blebbing assays

HeLa cells (and stable cell lines expressing RFP tagged cortical components) were seeded onto fibronection coated $35mm^2$ Matek dishes. Depending on the experiment, cells were transfected using Fugene6 with pCB6 GFP or pLVX RFP 8 hours later. The following day cells were infected at a MOI of 5. Live cell imaging was started at 3hpi using a Plan-Achromat 63x/1.40 Ph3 M27 Oil lens (Carl Zeiss, Germany) and an Evolve 512 camera (Photometrics, AZ) on an Axio Observer Microscope controlled by Slidebook (3i intelligent imaging innovations, USA). Images were collected at 1.0Hz or 3.7Hz as indicated. Cell blebbing movies were analysed by David Barry in ImageJ. The perimeter of the cell was determined from the GFP or RFP cytoplasmic signal, which allowed for accurate segmentation of the cell from the background. The membrane protrusion velocity at every point on the cell perimeter was determined, by following the temporal change in pixel intensity, using an ImageJ plugin created by David. This plugin was based on work by Dobereiner *et al.,* (Dobereiner et al., 2006). The cell perimeter was then used as a reference to determine the fluorescence intensity of LifeAct-cherry, MLC-RFP or F11-GFP at the plasma membrane.

2.6.3 Immunofluorescence (IF)

2.6.3.1 Buffers for IF

Blocking buffer

1% BSA

2% FCS

Mowiol

2.4g Mowiol and 6g glycerol were dissolved in 6 ml distilled water and the mix was incubated for 2 hours at room temperature with constant stirring. Subsequently, 12 ml of 200mM Tris-HCL (pH8.5) was added and the solution incubated at 55ºC until Mowiol was dissolved. Finally the solution was clarified at 4000rpm for 20 minutes.

4% Paraformaldehyde (PFA)

PBSA was pre-heated to 50ºC. 4% PFA (w/v) and one NaOH pellet were added and the solution was stirred until fully dissolved. The solution was adjusted to a final pH of 7.5 and the solution was passed through a 0.22µm filter.

2.6.3.2 Fixation and staining

HeLa cells were seeded at $4x10^4$ onto fibronectin coated glass coverslips in a 6 well dish. 8 hours later cells were transfected with pCB6/pLVX GFP of pCB6/pLVX GFP-RhoD. 24 hours post transfection HeLa cells were washed once with PBSA, fixed with 4% PFA for 10 minutes at room temperature and washed three times with PBSA. Cells were permeabilised with 0.1% saponin in PBSA for 5 minutes, following which the coverslips were three times with PBSA. Coverslips were incubated in blocking buffer for 20 minutes, washed three times with PBSA and incubated in 568-phalloidin (Molecular probes, Invitrogen) diluted to 1:1000 in blocking buffer for 20 minutes. Coverslips were washed again before incubation in 300nM DAPI, diluted in PBS, for 5 minutes. Finally coverslips were washed in PBS then H_2O and affixed to microscope slides using Mowiol.

Fixed samples were imaged using a Zeiss Axioplan2 equipped with a Photometrics Cool Snap HQ cooled CCD camera, external Prior Scientific filter wheels (DAPI; FITC; Texas Red; Cy5) and a 63x/ 1.4 Plan Apochromat objective. The system was controlled by MetaMorph software version 6.3r7 (Universal Imaging Corporation Ltd).

2.6.4 Statistical analysis of microscopy data

In all graphs the data is the mean value from at least three independent experiments (unless stated). Error bars represent the standard error of the mean. Statistical analysis was determined using Prism 5.0 (GraphPad Software, CA). A Student's T-test was used to compare two data sets. When more than two data sets were analyzed a One Way ANOVA test was performed followed by Tukey post test to compare all pairs of samples. A P value of >0.05 is not considered statistically significant. * indicates $P<0.05$, ** indicates $P<0.01$ and *** indicates $P<0.001$.

Chapter 3.

Vaccinia stimulates F11 dependent cell contraction and blebbing

3.1 Introduction

Several groups have previously documented the changes in host cell morphology during vaccinia infection. Briefly, infected cells contract early in infection, re-spread, migrate and extend actin-rich peripheral projections (Bablanian et al., 1978; Sanderson et al., 1998; Schramm et al., 2006; Valderrama et al., 2006). Originally, this lab documented a role for F11 in vaccinia induced cell migration and cell projections. Subsequent studies with two different ΔF11L viruses suggested that F11 was additionally involved in cell contraction and/or loss of cell-cell adhesion (Cordeiro et al., 2009; Morales et al., 2008). However, we now lack molecular understanding of the host cell mechanisms involved in cell contraction. Using live cell imaging and a combination of different inhibitors, recombinant viruses and cell lines, I sought to characterise vaccinia induced cell contraction and the involvement of F11 in more detail.

3.2 Results

3.2.1 Vaccinia stimulates temporal cell contraction and blebbing.

I sought to confirm the occurrence of vaccinia stimulated cell contraction and to characterise the temporal nature of this phenotype. Previous observations have suggested that cell contraction and associated membrane blebbing occurs early in vaccinia infection (Morales et al., 2008; Sanderson et al., 1998). I decided to synchronise vaccinia infection in HeLa cells to ensure contractile events happened simultaneously. This method had the additional benefit of enabling time-lapse microscopy to start as early as 40 minutes post infection to capture very early events. Synchronised infection is obtained by adding a high number of virus particles per cell (termed multiplicity of infection or MOI) to HeLa cells for a period of 20 minutes (this is in contrast to previous published methods from this laboratory where the virus is added for 1-2 hours). I infected HeLa cells at an MOI of 5 with the Western Reserve (WR) wild type vaccinia strain and followed cell morphology changes from 40 minutes post infection (pi) until 10 hours 40 minutes pi using phase time-lapse microscopy with a

10X objective lens (Figure 3.1A). I measured cell contraction by quantifying the cell area at 1 hour intervals, and normalising to the average cell area at the start of acquisition. In all experiments the change is cell area is expressed as a percentage of the original cell area. All subsequent cell contraction experiments were conducted in this manner unless otherwise stated. Cell contraction started as early as 1 hour post infection (hpi) and rapidly continued to increase until it reached maximal contraction at 3:40hpi, with the normalised average cell area at 25.3 ± 0.48% (Figure 3.1 B). The decrease in cell area was associated with transient plasma membrane blebbing (83% cells bleb between 2:40-3:40hpi, 86% between 3:40-4:40hpi) (Figure 3.1 C). From 4:40hpi onwards cells started to re-spread, this was associated with a gradual reduction in the number of cells making plasma membrane blebs (Figure 3.1 C). To follow plasma membrane blebbing at a higher resolution, I infected HeLa cells with WR and imaged infected cells at 3:40hpi on a spinning disc microscope with a 63X objective. Infected cells were unpolarised and exhibited multiple membrane blebs around the whole cell perimeter. Occasionally, long distended blebs and blebs on blebs were observed (Figure 3.1 D)

Host cell plasma membrane blebbing has been observed upon vaccinia attachment and entry (Mercer and Helenius, 2008). Although, cell contraction and associated blebbing occurs several hours after initial infection, I wondered whether it was associated with virus entry. To determine whether vaccinia induced contraction is dependent on the expression of viral genes or is a cellular response to virus attachment and entry, I infected HeLa cells with inactivated virus, which is unable to express vaccinia genes. To inactivate the virus I treated virus solutions with ultraviolet light (UV) and psoralen, a chemical that intercalates into and crosslinks DNA upon exposure to UV. This method inactivates the viral nucleic acids whilst preserving the antigenicity of the virus and its ability to enter the host cell (Tsung et al., 1996). The irradiation of vaccinia with UV alone blocked the expression of the vaccinia early gene N1L but not A36R, as shown by the immuno blot analysis performed by Antonio Postigo (Figure 3.2 A). Treatment with psoralen coupled with UV irradiation effectively blocked expression of both N1L and A36R (Figure 3.2 A). UV irradiation and psoralen treatment should therefore render the virus non-replicative (Tsung et al., 1996). To verify this, I performed plaque assays to measure the number of replication competent vaccinia virions following treatment with UV and psoralen. I infected confluent monolayers of BS-C-1 cells with $4x10^4$ plaque forming units (PFU) of irradiated or non-

irradiated virus. The PFU used in the plaque assay is equivalent to the PFU used in the cell contraction assay when infecting HeLa cells at an MOI of 5. Infected cells were overlaid with agarose, fixed at 48hpi and stained with crystal violet. The agarose overlay prevents virus spread through the media and only allows for direct cell-cell spread. Therefore, a single plaque will derive from a single infected cell. The number of clearances (plaques) in the crystal violet stained monolayer is the measure of the number of replicative vaccinia virions (Figure 3.2 B upper panel). No plaques were observed in monolayers infected with irradiated virus (Figure 3.2 B lower panel). Taken together this indicates that UV and psoralen treatment efficiently blocks gene expression and hence genome and virus replication. I then infected HeLa cells with UV and psoralen irradiated virus. Cells infected with irradiated virus did not contract, indicating that the expression of vaccinia genes is required for cell contraction. Therefore, cell contraction and membrane blebbing is not associated with the similar membrane events seen during vaccinia entry (Mercer and Helenius, 2008)(Figure 3.2C).

Vaccinia genes are categorised as early, intermediate and late genes, depending on when their expression begins in the vaccinia life cycle. Intermediate and late gene expression is dependent on the expression of early genes and vaccinia DNA genome replication (Broyles, 2003). It is likely that cell contraction and re-spreading are temporally regulated by the onset of expression of a specific subset of genes. To block intermediate and late gene expression, I treated HeLa cells with arabinosyl cytosine (AraC), an inhibitor of DNA synthesis, at the start of infection. Treatment of cells with AraC blocked the expression of the late gene A27L, but not the early gene F11L (Figure 3.3 C). Infected HeLa cells that were treated with AraC contracted as robustly as DMSO treated cells, but did not re-spread after 4:40hpi (Figure 3.3 A and B). Taken together my results demonstrate that WR induced cell contraction is a transient event that is dependent on the expression of virus early genes whilst re-spreading requires intermediate and/or late gene expression after genome replication.

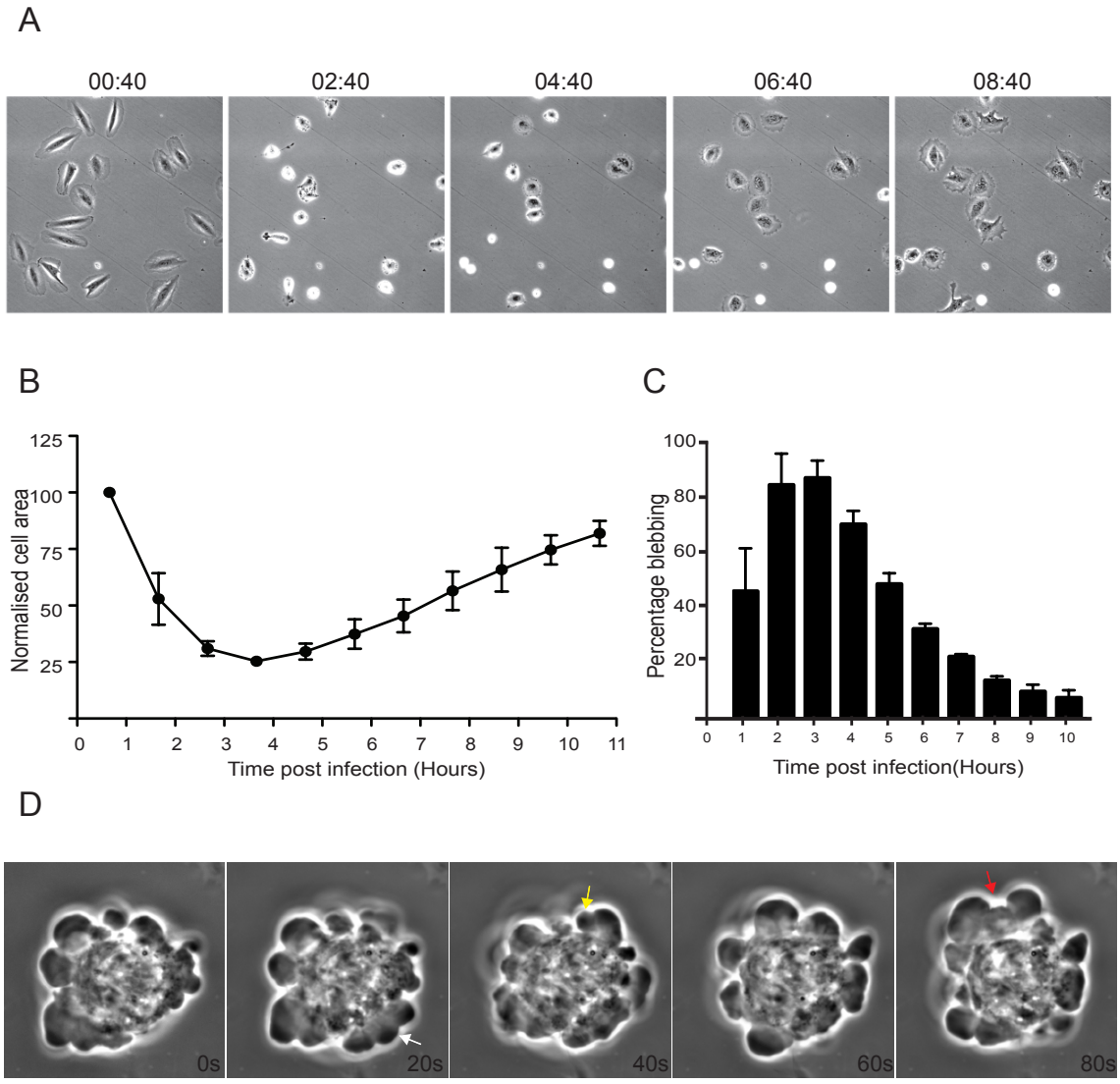

Figure 3.1 WR stimulates temporal cell contraction

A Representative still images from a phase time-lapse movie following HeLa cells infected with WR. The movie starts at 40 minutes post infection and continues for 10 hours. **B** A graph showing the change in average area of HeLa cells (normalised to cell area at the start of acquisition) during the course of infection. Cell area was quantified using MetaMorph software from the time-lapse movies described in A. Data is from three independent experiments, in which a total of 60 cells were analysed. Errors bars represent standard error of the mean (SEM). **C** A graph showing the percentage of cells that bleb during 1 hour time intervals in time lapse movies described in A and B. **D** Stills from a phase time-lapse movie of HeLa cells infected with WR at 3:40hpi. Time is indicated in seconds. The white arrow indicates long distended blebs, the yellow arrow indicates secondary blebs forming on a primary bleb and the red arrow indicates sites where multiple blebs protrude simultaneously.

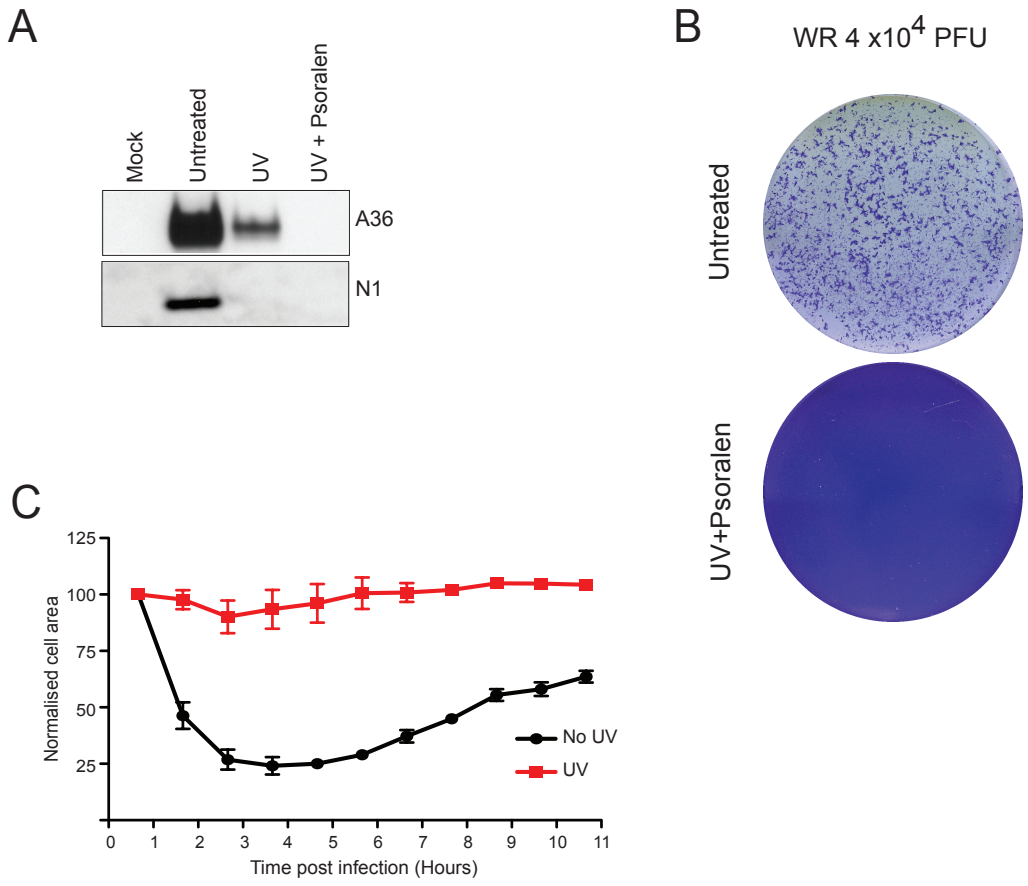

Figure 3.2 The expression of vaccinia genes is required for cell contraction

A Immuno blot analysis showing the expression of A36 and N1, which are expressed early during vaccinia infection, at 6 hpi with UV, UV/psoralen treated or untreated WR. **B** Representative images of vaccinia plaque analysis in confluent monolayers of BS-C-1 cells. Cells were infected with UV/psoralen treated or untreated WR, then fixed and stained with the cell stain crystal violet at 48 hpi. White regions represent vaccinia plaques. **C** A graph showing the change in average area of HeLa cells during the course of infection with UV/psoralen treated or untreated WR. Data is from three independent experiments, in which 78 and 80 cells respectively were analysed. Error bars represent SEM.

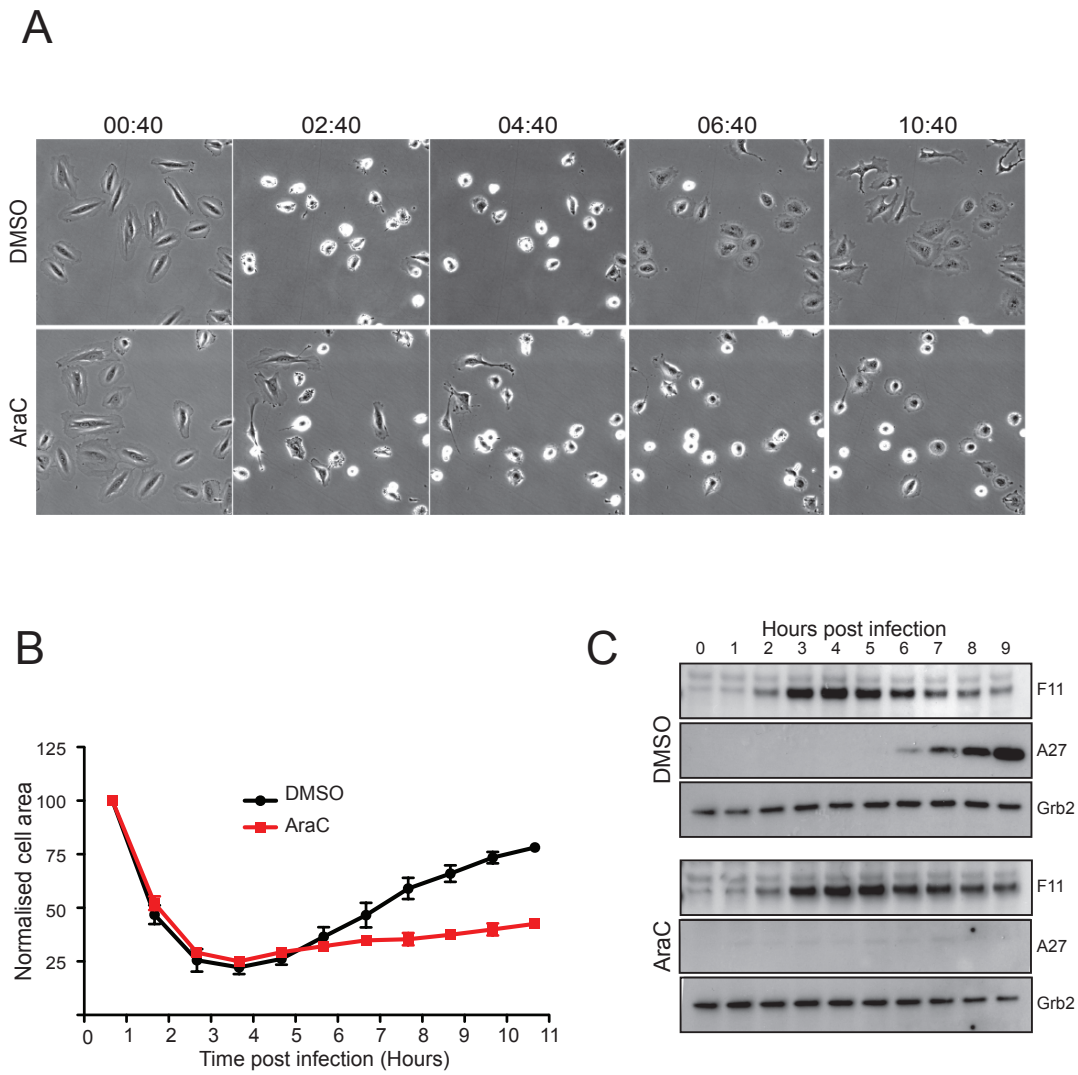

Figure 3.3 Vaccinia late genes are required for re-spreading but not contraction

A Still images from a phase time-lapse movie following HeLa cells infected with vaccinia virus in the presence of DMSO or AraC. **B** A graph showing the change in average area of HeLa cells during the course of infection with WR in the presence of DMSO or AraC. Data is from three independent experiments in which 70 cells in each condition were analysed. Error bars correspond to SEM. **C** Immuno blot analysis of the expression of F11 (an early viral protein) and A27 (a late viral protein) in the presence of either DMSO or AraC. F11 was detected with an antibody raised against a peptide corresponding to amino acids 323-334. Grb2 was used as an endogenous loading control.

3.2.2 F11 is necessary for cell contraction

It has previously been suggested that the vaccinia protein F11 is required for the loss of cell-cell attachment but not for cell contraction and migration in Ptk2 cells. This study used a combination of WR, Modified vaccinia Ankara (MVA) and a recombinant WR virus that does not express F11L (Morales et al., 2008), but a lack of quantification and direct comparisons makes it difficult to be fully confident in the results. I decided to re-evaluate the contribution of F11 to vaccinia-induced contraction. A previous lab member, Yoshiki Arakawa, generated an alternative recombinant virus that does not express F11 (ΔF11L), due to deletion of the F11L gene (Cordeiro et al., 2009). I infected HeLa cells with ΔF11L and investigated the extent of cell contraction. In contrast to the previously published observations, I found that F11 is required for cell contraction in HeLa cells. Infected cells contracted to 25.3 ± 0.48% and 91.5 ± 4.0% at 3:40hpi during infection with WR or ΔF11L, respectively (Figure 3.4 A, B). There is very little change in cell area over the course of infection with the ΔF11L virus, although there was obvious and dynamic peripheral membrane ruffling. (Figures 3.4 A, B). The difference in results between my work and Morales *et al.,* could be due to the cell type. To investigate this possibility, I infected a variety of cell lines derived from different animals with WR and ΔF11L viruses. I used U-2-OS, a human osteosarcoma cell line, Ptk2, rat kangaroo (also known as the long-nosed potoroo) kidney cells, and mouse embryonic fibroblasts (MEFs) (Figure 3.5). All the cell lines contracted when infected with WR. U-2-OS and MEFs did not contract upon infection with ΔF11L virus as in HeLa cells. However, in agreement with Morales *et al.,* Ptk2 cells contracted upon infection with both viruses, although neither virus induced a loss in cell-cell attachments as recorded previously (Morales et al., 2008). Ptk2 cells contracted into dense clumps of cells, as a result it was not possible to accurately quantify the cell area changes over time. By visual observations, it appeared that cell contraction was more robust and prolonged with WR in comparison to ΔF11L in this cell line. Therefore, it is possible that there is more than one vaccinia determinant required for cell contraction and in PtK2 cells the contribution of F11 is less important.

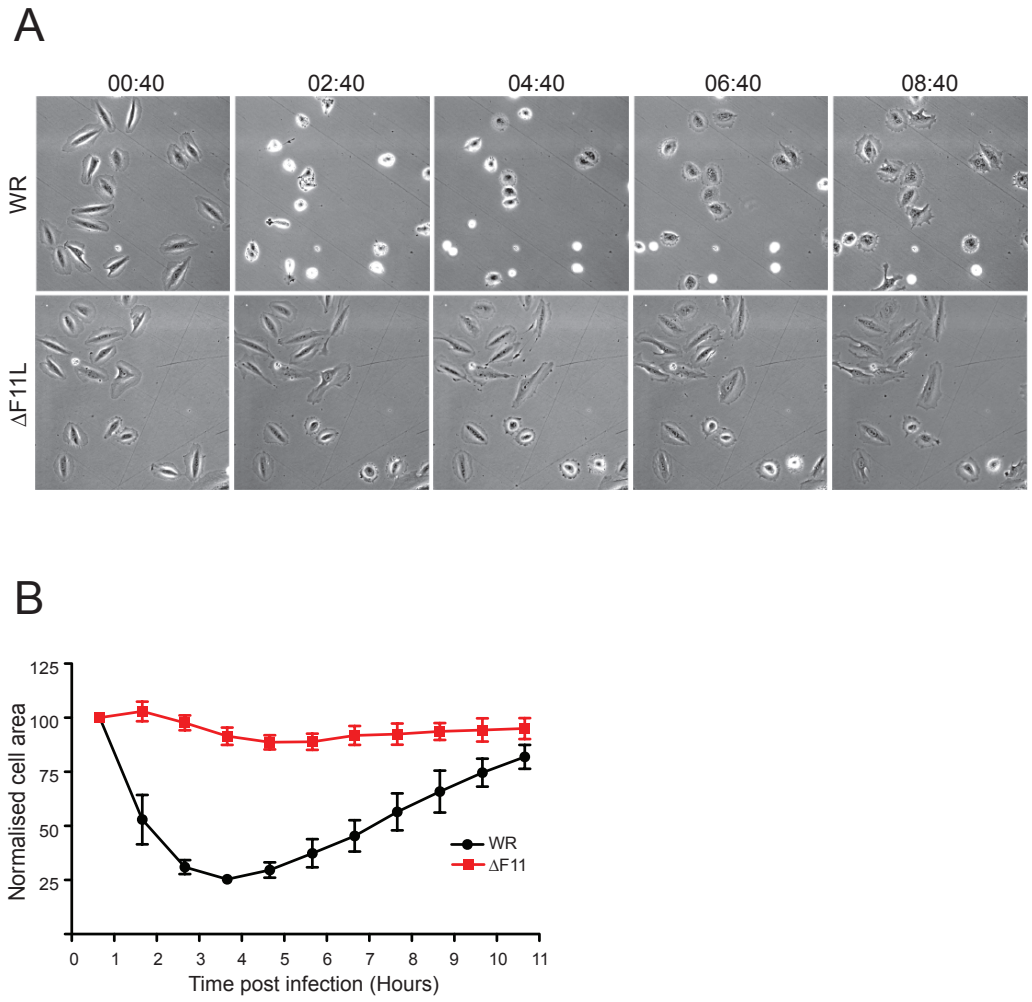

Figure 3.4 The vaccinia protein F11 is required for cell contraction

A Still images from a phase time-lapse movie following HeLa cells infected with WR or ΔF11L (a virus lacking the F11L gene). **B** The graph shows the change in average area of HeLa cells infected with either WR or ΔF11L. Data is from three independent experiments. A total of 60 and 68 cells were analysed respectively. Error bars represent SEM.

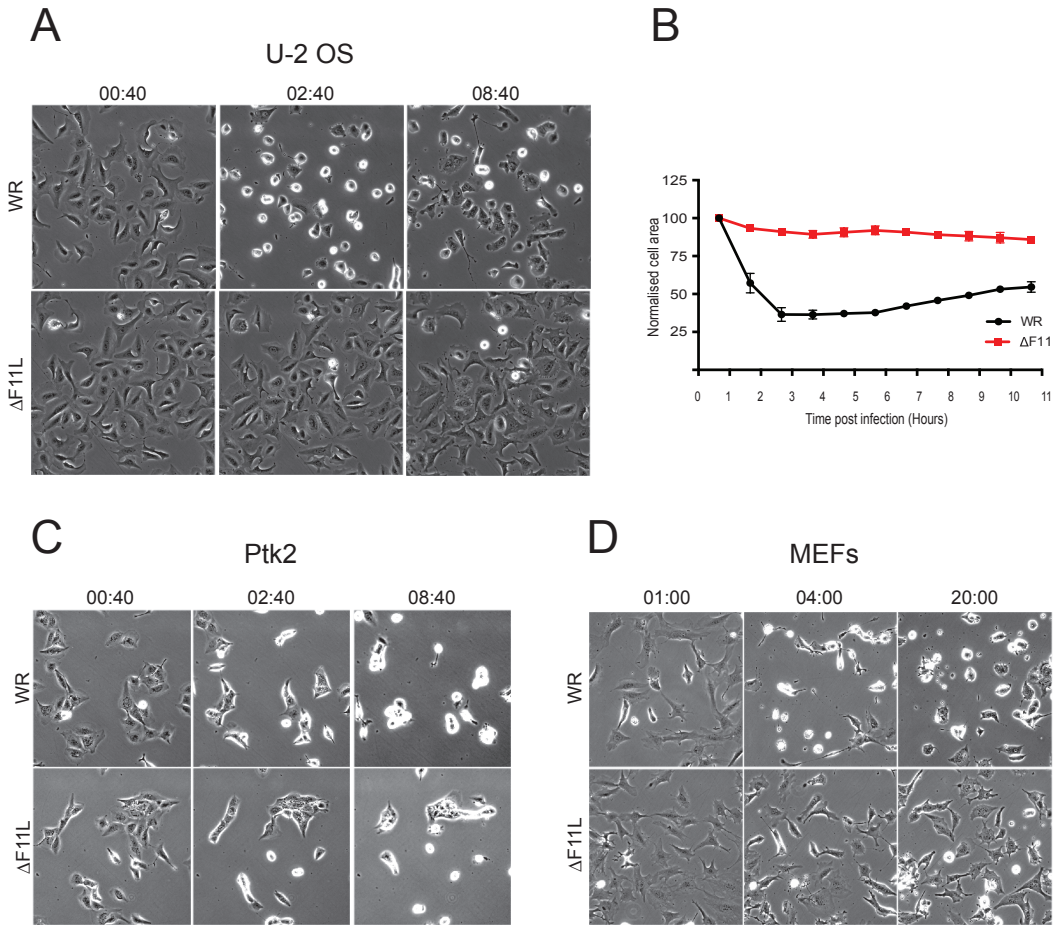

Figure 3.5 F11 is required for virus induced contraction in U-2 OS and MEFs but not Ptk2 cells

A Still images from a phase time-lapse movie following U-2 OS cells infected with WR or ΔF11L. **B** A graph showing the change in average area of U-2 OS cells infected with either WR or ΔF11L. Data is from three independent experiments. A total of 107 and 110 cells were analysed respectively. Error bars represent SEM. **C** Still images from a time-lapse movie following Ptk2 cells infected with WR or ΔF11L. **D** Still images from a time-lapse movie following mouse embryo fibroblasts (MEFs) infected with WR or ΔF11L. The movie began at 1 hour post infection and continued for 20 hours.

3.2.3 Generation of F11 antibodies

To follow the dynamics of F11 protein levels over the course of infection, I generated two F11 specific antibodies. F11-N was generated against a peptide spanning amino acids 101-120 and F11-C was generated against a peptide corresponding to residues 323-334 (Figure 3.6 A). These particular peptide sequences were selected based on predicted solubility. To test whether F11 specific antibodies were present in the terminal bleeds, I performed immuno blot analysis with HeLa cell lysates infected with WR or ΔF11L. Serum from all rabbits detected a protein at the estimated molecular weight of F11 (40kDa) in the WR infected lysate only, however there were also numerous non-specific bands (Figure 3.6 B and C left panels). I pooled the serum from rabbits immunised with the same peptide and affinity purified the serum through a SulfoLink column coupled to the corresponding peptide. I tested the elutions that showed absorbance at 280nm by immuno blot. For F11-N, the TEA elution number 3 was highly specific to F11L and did not detect non-specific bands (Figure 3.6 B). For F11-C, the glycine elutions 2-6 were highly immunogenic to F11, but all detected bands at 20kDa and 28kDa, however this was far enough away from the predicted molecular weight of F11 to be a useful antibody (Figure 3.6 C). I used these antibodies to investigate the temporal nature of F11 expression. In immuno blot analysis of a time course of WR infected HeLa lysates, F11 could be detected from 2 hpi onwards. F11 protein levels peak between 3-4 hpi and then decrease from 5 hpi onwards (Figure 3.6 C). Thus, F11 protein levels coincide strikingly with the onset and termination of cell contraction and blebbing. This suggests that a threshold level of F11 is required for cell contraction. Previous data indicated that the expression of intermediate or late genes is required for re-spreading (Figure 3.3 B). Interestingly, the level of F11 in cells treated with AraC did not decrease as dramatically from 5 hpi onwards suggesting that the expression of a late vaccinia protein could direct the decline in F11 protein levels (Figure 3.3 C). This data could explain why AraC treated cells remain contracted, as levels of F11 have not dropped sufficiently below the threshold to permit re-spreading (Figure 3.3 B). I used the F11-N and F11-C antibodies to investigate whether the decrease in protein levels from 5hpi onwards was due to cleavage of F11. Both antibodies showed a similar protein pattern by immuno blot. The molecular weight of the proteins did not visibly change and there were no observed bands at a lower molecular weight (not shown). This would suggest that the loss in protein that occurs from 5hpi onwards is not due to F11 cleavage (Figure 3.6 D).

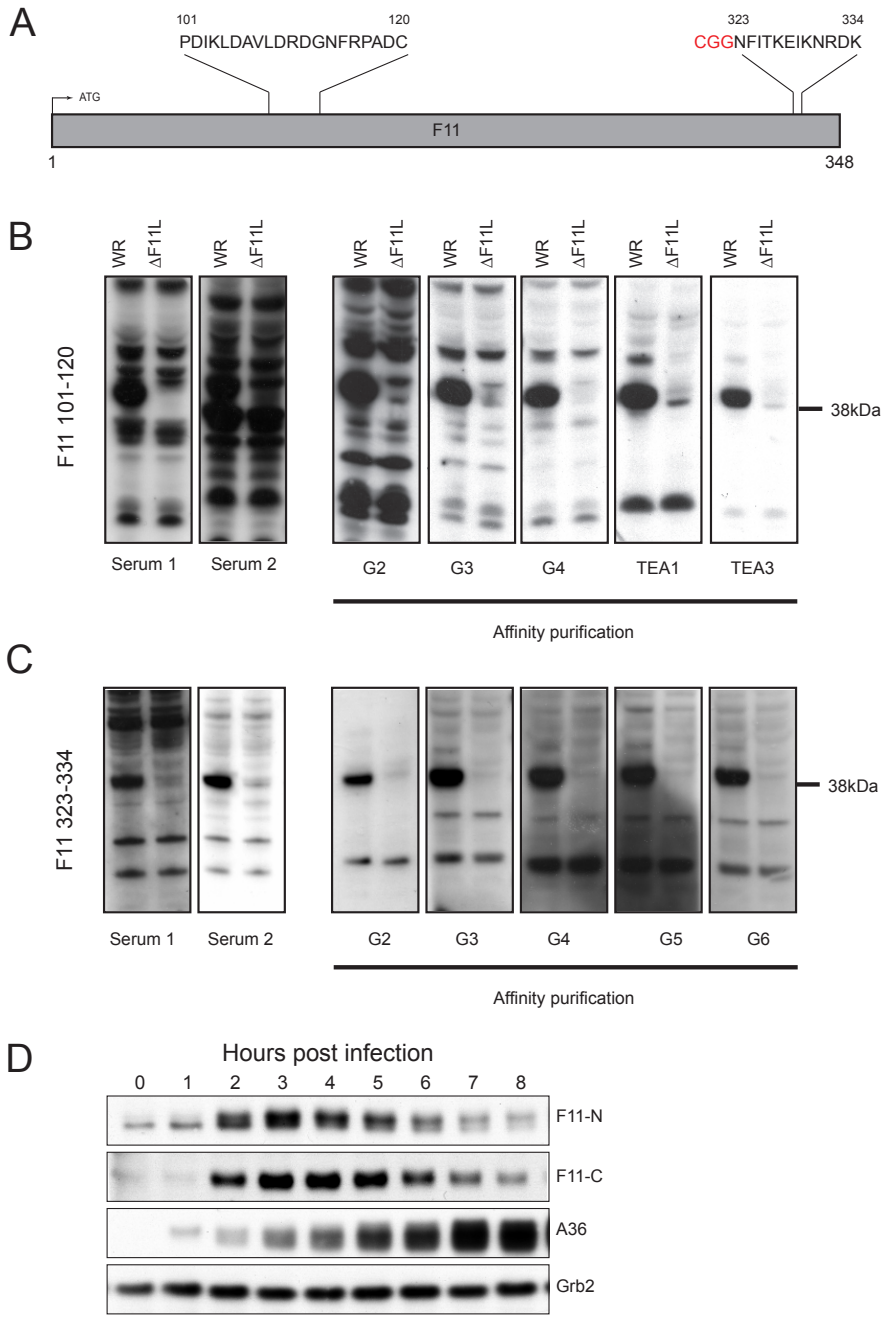

Figure 3.6 Purification of F11 antibodies

A The peptide sequences used to generate F11 antibodies. **B** Immuno blot analysis of HeLa cell lysates infected with WR or ΔF11L showing the purification of an antibody raised against a peptide corresponding to amino acids 101-120 in F11. The serum from the terminal bleeds of two rabbits immunized with F11 101-120 was tested for F11 specific antibodies. Following affinity purification with the F11 101-120 peptide, elutes that contained protein were tested for F11 specific antibodies. F11 has a predicted molecular weight of 40kDa. **C** Immuno blot analyses, as above, for the peptide corresponding to amino acids 323-334 in F11. **D** Immuno blot analysis showing the levels of F11 over the course of infection in HeLa cells. F11 was detected with F11-N (101-120) and F11-C (323-334) antibodies. A36 was used as a control for vaccinia infection and Grb2 was used as an endogenous loading control.

3.2.4 F11 is necessary but not sufficient for cell contraction

Modified Vaccinia Ankara (MVA) is a strain of vaccinia derived from the Chorioallantois vaccinia virus Ankara (CVA) strain, which has been highly attenuated for human infection by passaging 570 times in chicken embryo fibroblasts (Meyer et al., 1991). Genomic analysis of MVA revealed six major deletions within the terminal fragments, relative to CVA. In addition, there are numerous short deletions and point mutations within MVA (Antoine et al., 1998; Meisinger-Henschel et al., 2007). The open reading frame of F11 is fragmented in MVA, due to 15 and 16bp deletions in the centre of the ORF (Antoine et al., 1998; Zwilling et al., 2010). HeLa cells infected with MVA do not contract (Figure 3.6 A, B) (Schepis et al., 2006). I was interested if F11 could rescue cell contraction in MVA infected cells. To do this, I made use of a MVA recombinant virus where the WR F11L coding sequence has been rescued (MVA-F11L) and was introduced under the control of the WR F11L endogenous promoter. However, F11 is not re-introduced between F12L and F10L, instead it is inserted into the MVA deletion III region (Zwilling et al., 2010). When HeLa cells were infected with MVA-F11L cell contraction is partially rescued. However, in comparison to WR, MVA-F11L stimulated cell contraction was not as robust or prolonged. During MVA-F11 infection, HeLa cells contracted to 54.2% ± 4.0 and 48.4% ± 2.0 at 1:40hpi and 2:40 hpi, respectively, before re-spreading. This is in contrast to the degree of cell contraction in WR infection; 41.9% ± 6.8, 31.8% ± 2.5 and 34.4% ± 5.0 at time points 2:40hpi, 3:40hpi and 4:40hpi respectively. The difference between MVA-F11 and WR infection indicates F11 is required but not sufficient for virus induced cell contraction and that another protein or proteins, which are also lost in MVA, also contribute to efficient cell contraction. Interestingly, F11 protein levels do not decrease in cells infected with MVA-F11L (Figure 3.6C). As the cells do not contract as efficiently when infected with MVA-F11L, it is difficult to interpret the contribution of F11 levels to re-spreading. As many genes are lost in MVA, the late proteins I assume control F11 levels may not be expressed, explaining the steady levels of F11L throughout the time course. Alternatively, expressing F11L from an alternative locus in the genome may effect expression.

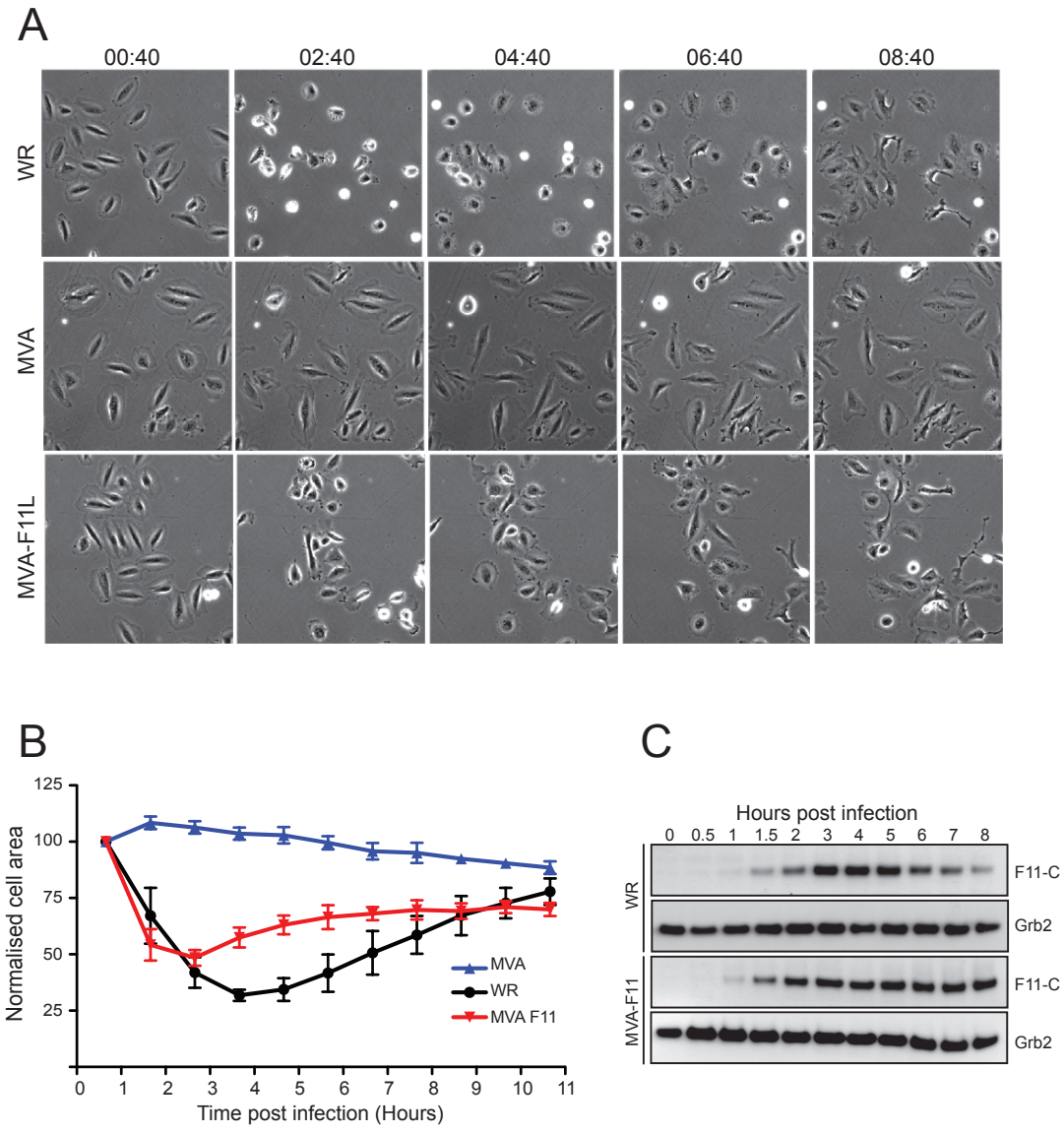

Figure 3.7 F11 is necessary but not sufficient for cell contraction

A Still images from a time lapse movie following HeLa cells infected with vaccinia virus strains WR, MVA or MVA-F11L. **B** A graph showing the change in average area of HeLa cells infected with WR, MVA or MVA-F11L. Data is from three independent experiments. A total of 78, 68 and 73 cells were analysed, respectively. **C** Immuno blot analysis following F11 protein levels over the course of infection. F11 was detected with F11-C. Grb2 was used as an endogenous loading control.

3.2.5 F11 localises to the cortex

After determining that F11 was necessary but not sufficient for vaccinia induced cell contraction, I was interested in studying the localisation of F11 during this phenotype. The F11 antibodies that I generated (Figure 3.6) were extensively tested for suitability in detecting F11 by immunofluorescence. I tried multiple fixation methods; 4% paraformaldehyde (PFA), methanol, acetone and finally, sequential PFA and methanol. On cells fixed with PFA I tried several permeabilisation methods using 0.01% Triton X-100, 0.1% saponin or PHEM + 0.05% Triton X-100. However, neither antibody was able to detect endogenous F11 in infected cells (data not shown). I decided to make a recombinant vaccinia virus that expressed F11 conjugated to GFP, to ascertain the localisation F11. The fluorescent virus would have the additional benefit of enabling live analysis of F11 localisation. The generation of the F11-GFP virus in the ΔF11L backbone is described in section 2.4.9 and Figure 3.8 A. To confirm that F11 was rescued in the recombinant virus, I collected HeLa cell lysates at 1 hour intervals during infection with the F11-GFP virus and analysed the lysates by immuno blotting with GFP. The GFP antibody detected a product at 65kDa, the expected molecular weight of F11 with a GFP tag (Figure 3.8 B). The 65kDa protein was also detected by the F11-C antibody (data not shown). F11-GFP was expressed with the same temporal dynamics as F11 in WR infection (Figure 3.6 D, Figure 3.8 B). From 6hpi onwards a lower band, migrating with the 28kDa marker, emerged. The lower band was not detected by the F11-C antibody, which suggests it could be cleavage of GFP from F11-GFP (data not shown). I additionally analysed the levels of the early vaccinia protein A36 to ensure that virus gene expression was not affected in the recombinant virus. The kinetics of A36 expression is not changed relative to WR infection (Figure 3.6 D and Figure 3.8 B).

To gain an understanding of the localisation of F11, I infected HeLa cells expressing RFP, as a cytoplasmic marker, with F11-GFP and imaged at 3hpi. In cells that were contracted and blebbing, F11-GFP localises to the plasma membrane and cortex (Figure 3.8 C). Previous studies on plasma membrane blebbing have shown that actin, MLC2 and ezrin are recruited to the membrane at different stages during the bleb life cycle, and this is indicative of the re-formation of the cortex beneath the plasma membrane (Charras et al., 2006). I wanted to study the localisation of F11 with reference to actin (using LifeAct) and MLC2. I generated HeLa cells stably expressing LifeAct-Cherry, and MLC2-RFP, using a lentivirus system to incorporate the gene of

interest into the genome of the HeLa cells. The use of stable cells lines overcomes various problems related to transient expression such as heterogeneity in expression levels, poor transfection efficiency and cytotoxicity from transfection methods. I confirmed that Cherry/RFP fluorescence in the resulting stable cell lines corresponded to the localisation of the protein of interest by immunofluorescence using phalloidin for comparison with LifeAct-cherry or a MLC2 antibody for comparison with MLC2-RFP (Figure 3.9A). In addition I confirmed that the cell lines expressed Cherry/RFP tagged proteins at the correct molecular weight by immuno blot analysis (Figure 3.9B).

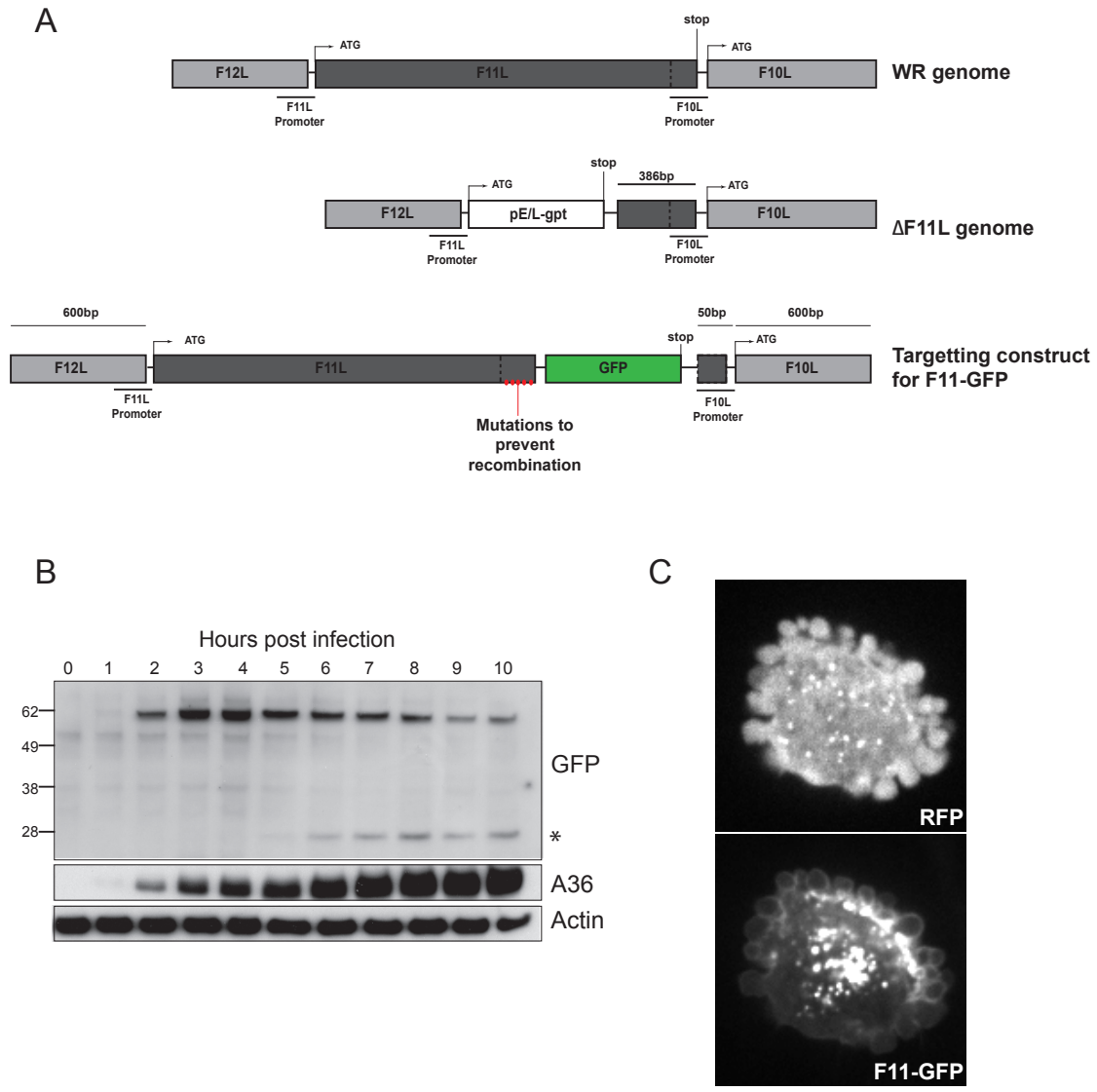

Figure 3.8 The generation of recombinant F11-GFP virus

A An illustration of the method used to introduce F11-GFP into ΔF11L. The F12L, F11L and F10L locus is depicted in the WR and ΔF11L virus genomes. F11-GFP was knocked in to the genome of ΔF11L by homologous recombination using 600bp arms of recombination identical to the C-terminus of F12L (left arm) and the N-terminus of F10L (right arm). The right arm includes 50bp upstream of the F10L start codon (including the C terminal 25bp of F11L), which contains the F10L promoter. The 25bp region that was mutated in F11-GFP is highlighted in red. **B** Immuno blot analysis of F11-GFP, actin and A36 at 1 hour intervals post infection during infection with F11-GFP virus. * indicates the appearance of a smaller band as infection progressed. **C** A representative HeLa cell expressing RFP and infected with F11-GFP at 3hpi. F11-GFP appears to localises to the plasma membrane and cortex.

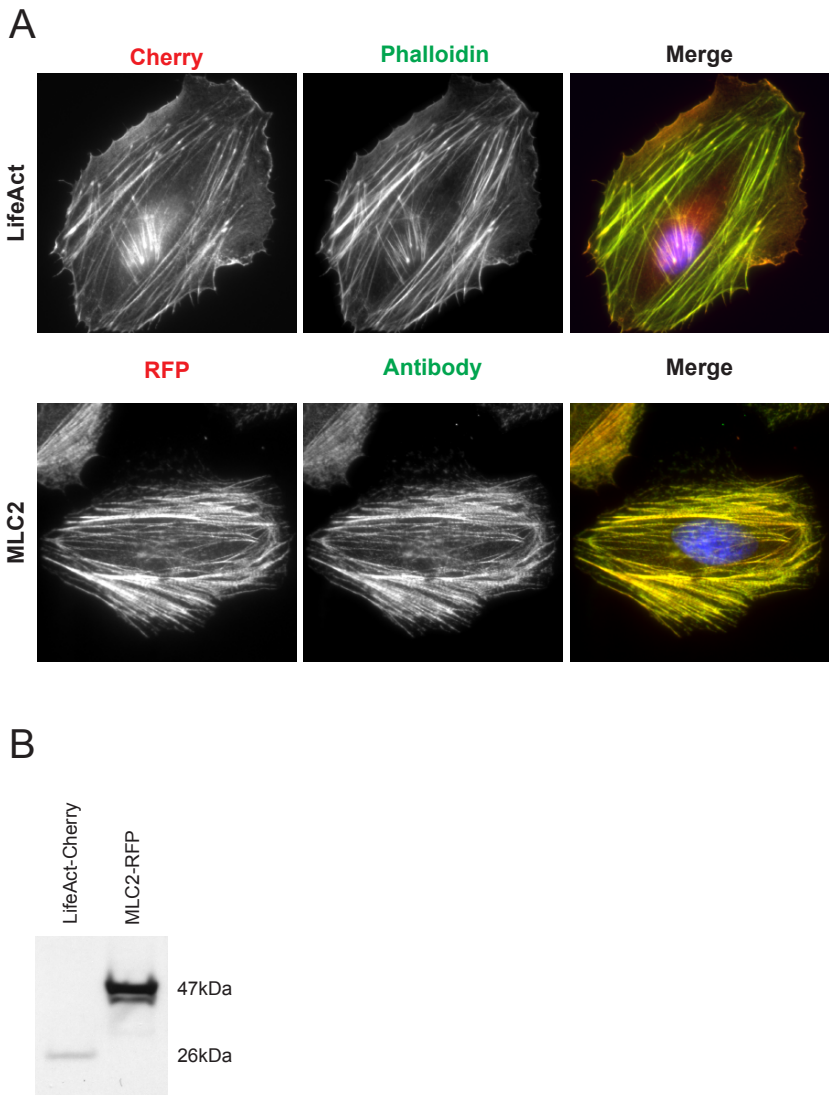

Figure 3.9 The generation of Cherry/RFP stable cell lines

A Immunofluorescence of LifeAct-Cherry and MLC2-RFP stable HeLa cells. LifeAct-Cherry HeLa were stained with 488 Phalloidin, while MLC2-RFP HeLa were stained with a MLC2 antibody. **B** Immuno blot analysis of lysates from the indicated stable cell lines. The overexpressed proteins were detected with an RFP antibody, which additionally recognises Cherry, albeit more weakly than RFP. The approximate molecular weights of the LifeAct-cherry and MLC2-RFP and are 26kDa and 47kDa, respectively.

3.2.6 F11 is recruited to the plasma membrane during blebbing

I infected HeLa cells expressing RFP with F11-GFP or the Cherry/RFP stable cell lines expressing GFP with WR. At 3hpi, when cells were contracted and blebbing, I acquired images at 1 (F11-GFP) or 3.7 (Cherry/RFP stables) frames per second in both fluorescent channels. The strength of F11-GFP signal was far lower than LifeAct or MLC2, therefore it was necessary to acquire F11-GFP images at a higher exposure and consequently a lower frame rate. In collaboration with a post-doctoral researcher, David Barry, we analysed the fluorescence intensity of F11-GFP, LifeAct-Cherry and MLC2-RFP at the membrane and the velocity of membrane bleb protrusion and retraction (Figures 3.10 and 3.11). We determined the mean membrane velocity and the mean rate of change in membrane velocity based on an analysis of 435 blebs in 29 cells (Figure 3.11 A, B). The bleb membrane protrudes with increasing velocity for approximately 3 seconds, following which the membrane extends with decreasing velocity for an additional 10 seconds. Bleb extension ceases approximately 13 seconds after initiation and the membrane then begins to retract. F11-GFP, LifeAct-Cherry and MLC2-RFP are lost from the membrane at bleb initiation. However, this appears as a gradual decline in fluorescent signal because of a combination of the application of noise reduction (smoothing) to the data, the cytosolic F11/LifeAct/MLC signals and the analysis of a 3D event in 2D (Figures 3.10 and 3.11). We can determine when each protein is recruited back to the membrane from the point where the rate of change in signal intensity becomes positive. Because of the smoothing referred to above, caution is advised in assigning specific time-points to protein recruitment. However, it is clear that F11-GFP is recruited first relative to LifeAct and MLC (Figure 3.11 A, B). In previous work investigating the assembly of the cortex during membrane blebbing, the only cortical component that was recruited to the membrane prior to actin was Ezrin, an actin-membrane linker protein that tethers the actin cortex to the membrane (Charras et al., 2006). The fact that F11-GFP re-localises to the membrane prior to the cortical components actin and MLC, suggests that F11 might function in the upstream regulation of actin and myosin recruitment or cortical contraction. The dynamics of F11 localisation with respect to LifeAct and MLC2 presented here should however be interpreted with caution, as the signal strength of F11-GFP was relatively low, resulting in a narrow dynamic range. The lower signal-noise-ratio necessitated a lower frame rate, which may have contributed to the differences in F11 signal dynamics relative to LifeAct and MLC2 evident in Figure 3.11B. Considerable efforts will be made in the future to improve the signal of F11-GFP.

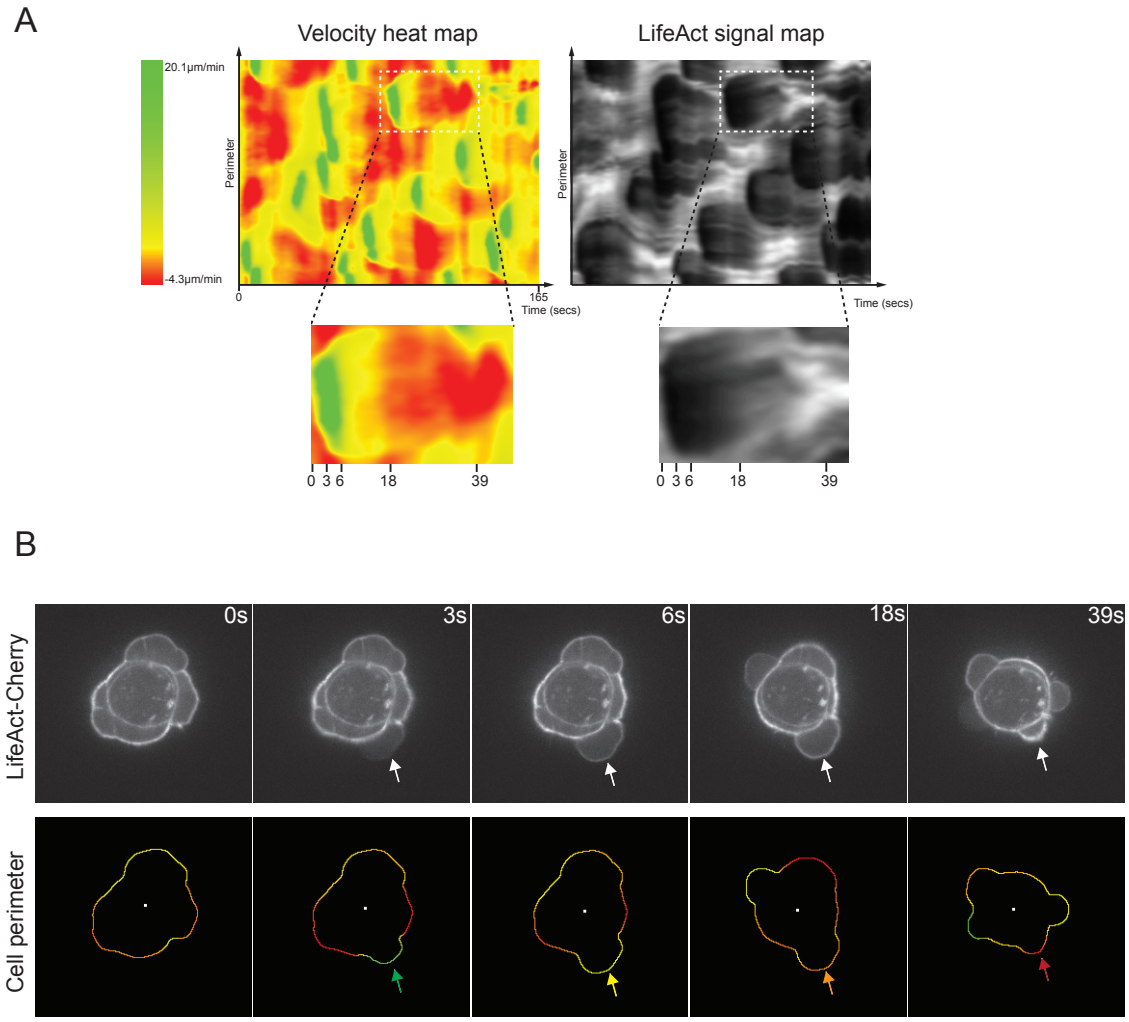

Figure 3.10 The loss and recovery of LifeAct from the membrane during blebbing

A. The velocity heat map from a representative movie of a HeLa cell expressing LifeAct-Cherry and GFP and infected with WR, at 3hpi. The velocity heat map (left hand side) illustrates membrane velocity as a function of the position on the cell perimeter (y-axis) and time (s) (x-axis), where green = positive/protrusive velocity and red = negative/retractive velocity. The LifeAct signal map represents the signal intensity as a function of the position on the cell perimeter (y-axis) and time (s) (x-axis). The zoomed in areas highlight a single bleb over the lifetime of the bleb. (Analysis by David Barry). **B.** The top panel shows still images of the LifeAct-Cherry expressing cell from A. The bottom panel illustrates the cell edge, as determined from the GFP fluorescence. The edge is colour coded according to the membrane velocity. The images are taken at the times indicated by black lines in A. White and coloured arrows indicate the bleb of interest.

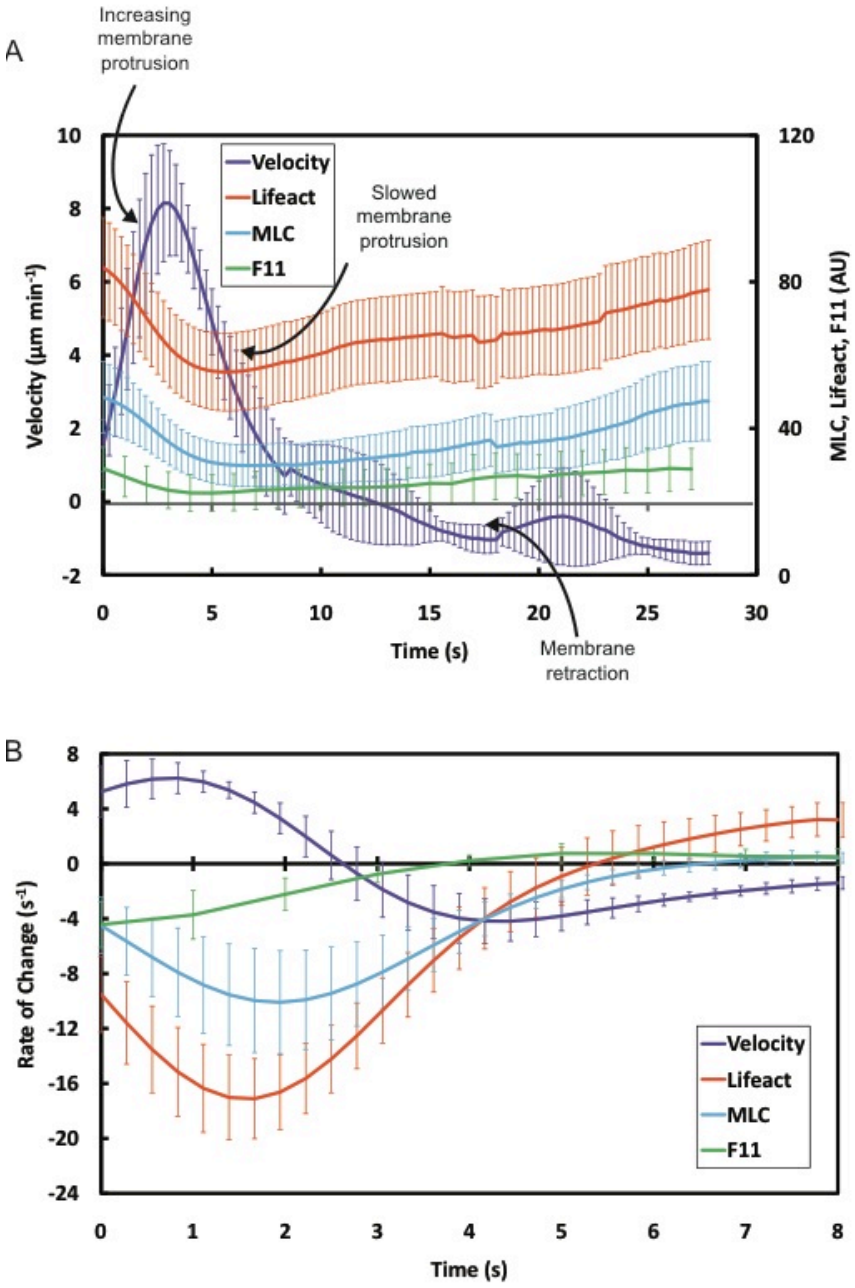

Figure 3.11 The recovery of F11-GFP, LifeAct-Cherry and MLC2-RFP to the membrane during blebbing

A. The graphs show the relationship between the membrane velocity of a bleb (µm/min) (Left hand y-axis) and the fluorescence intensity of F11-GFP, LifeAct-Cherry or MLC2-RFP (arbitrary units) (right hand y-axis) at the membrane as a function of time (s). **B**. The graphs show the rate of change in membrane velocity or signal intensity over time. The time point where the rate of change in signal intensity of F11-GFP, LifeAct-Cherry or MLC2-RFP crosses the x-axis represents the onset of recovery of the signal at the membrane. In both A and B the error bars represent the 95% confidence interval. The purple line is the mean membrane velocity of 435 blebs from 29 cells. Red, blue and green lines are the mean fluorescence intensities of 211 blebs from 17 cells, 224 blebs from 12 cells and 174 blebs from 13 cells, respectively. (Analysis by David Barry).

3.3 Summary

The work presented in this chapter confirms previous suggestions that vaccinia virus stimulates host cell contraction and blebbing during early vaccinia infection. I confirmed that gene expression is required for cell contraction, using UV inactivated virus. In contrast, cell re-spreading following contraction is dependent on the expression of vaccinia late genes. Using a virus that cannot express F11, I showed that F11 is necessary for cell contraction. However, I also showed that F11 is not sufficient, as the rescue of F11 in the attenuated virus MVA does not fully rescue cell contraction. I also suggest that the concentration of F11 protein must decrease sufficiently for re-spreading to occur. F11-GFP (expressed by a recombinant virus) localises to the plasma membrane during cell contraction and blebbing. Expanding bleb membranes are initially devoid of F11-GFP, which is then recruited back to the bleb membrane prior to actin and MLC, further indicating a role for F11 in regulating cell contraction.

Chapter 4.

Vaccinia induced cell contraction is dependent on ROCK but not RhoA

4.1 Introduction

Cell contraction and associated plasma membrane blebbing is often associated with RhoA and ROCK signalling (Gutjahr et al., 2005; Pinner and Sahai, 2008b; Sahai and Marshall, 2003; Sanz-Moreno et al., 2008). Briefly, RhoA activates the kinase activity of ROCK, which then controls the phosphorylation of MLC, either directly or through multiple downstream substrates. MLC phosphorylation activates myosin II mediated contraction of the actin cortex, which can result in plasma membrane blebbing as membrane ruptures from the cortex. I have shown that vaccinia induced cell contraction is dependent on F11. Previous work from this laboratory has shown that F11 can interact with RhoA through a motif highly similar to the Rho binding domain in ROCK (Valderrama et al., 2006). Through this interaction F11 suppresses the activity of RhoA at 8hpi (Cordeiro et al., 2009). In this chapter I explore the contribution of RhoA and ROCK signalling to vaccinia induced contraction.

4.2 Results

4.2.1 Cell contraction is blocked by ROCK inhibition

The kinase activity of ROCK can be effectively blocked with small molecule inhibitors (Davies et al., 2000). Y27632 and H1152 compounds have been used in a variety of studies to investigate the biological effect of ROCK and are classical ROCK inhibitors. However, both molecules can inhibit other kinases as potently as ROCK. *In vitro*, Y27632 inhibits PRK2 (IC50 800nM) and LRRK2 (IC50 1uM) with a similar potency to ROCK2 (IC50 800nM), even though there is limited sequence identity within the kinase domain of these proteins. Additionally Y27632 is less potent but still active towards MSK1 (IC50 8.3uM) and PHK (IC50 19uM) (Davies et al., 2000; Nichols et al., 2009). Similarly, H1152 inhibits PRK2, with similar potency to ROCK2, and LRRK2, albeit 3 fold more weakly than ROCK2. H1152 can also inhibit the *in vitro* activity of Aurora B and Aurora C (Bain et al., 2007; Nichols et al., 2009). The compound GSK429286A is

more specific to ROCK, with the only additional target being MSK1 (Nichols et al., 2009). It is recommended that three or more structurally independent small molecule kinase inhibitors should be used to accurately interpret the biological function of the kinase of interest (Cohen, 2010). To investigate whether ROCK was required for vaccinia-induced contraction, I treated infected cells with GSK429286A, H1152 and Y27632. All inhibitors significantly blocked WR induced cell contraction at 3:40hpi (71.0 ± 4.7, 92.0 ± 6.5, 85.5 ± 0.7% following treatment with GSK429286A, H1152 or Y27632 respectively relative to DMSO alone 25.5 ± 0.2%) (Figures 4.1 B). The effect of the ROCK inhibitors is due to a block in cell contraction rather than a block in virus entry, as treatment with these inhibitors did not block the efficiency of virus infection (Figure 4.1 A). Cell contraction and membrane blebbing is often characteristic of apoptosis, as caspase mediated cleavage of ROCK can render the kinase constitutively active (Sebbagh et al., 2001). The infected cell phenotype is transient so is unlikely to be apoptotic cell death. Nevertheless, to exclude a role for caspase mediated activation of ROCK in WR induced cell contraction, I treated HeLa cells with Z-VAD-fmk (pan-caspase inhibitor) prior to infection with WR (Postigo and Way, 2012). There was no difference in cell contraction in infected cells treated or untreated with Z-VAD-fmk (Figure 4.1 C), indicating that vaccinia induced cell contraction and blebbing is not dependent on the same pathway as apoptotic cell blebbing.

4.2.2 Cell contraction is dependent on ROCK 1 and ROCK 2

There are two isoforms of ROCK, ROCK1 and ROCK2. These kinases have 64% overall sequence identity, with 92% identity in the kinase domains (Leung et al., 1996; Nakagawa et al., 1996). It is not clear whether GSK429286A, H1152 and Y27632 have any preference for ROCK1 or ROCK2, as many of the *in vitro* kinase assays with these inhibitors were performed for ROCK2 only (Bain et al., 2007; Davies et al., 2000; Nichols et al., 2009). I was interested to see if individual or both ROCK proteins were required for vaccinia-induced contraction. I performed siRNA mediated knockdown of each protein individually and simultaneously and followed the efficiency of knockdown by immuno blot. ROCK1 and ROCK2 proteins were not detected in cell lysates following siRNA knockdown, and simultaneous knockdown was as efficient as individual knockdown (Figure 4.2 A). I infected HeLa cells that had been transfected with siRNA oligos for 72 hours with WR. Individual knockdown of either gene had no significant effect on cell contraction at 3:40hpi, whilst simultaneous knockdown of

ROCK1 and ROCK2 blocked contraction (27.7 ± 9.8, 26.1 ± 2.4, 39.4 ± 9.3, 62.6% ± 8.9 for non-targeting control, ROCK1, ROCK2 and both, respectively) (Figure 4.2 B and C). Taken together, the siRNA and inhibitor results suggest that ROCK activity is required for vaccinia induced cell contraction and that ROCK1 and ROCK2 are functionally redundant in this pathway. However, cells lacking both ROCK isoforms did contract later in infection, to 37% of initial cell area at 5:40hpi (Figure 4.2 D). The delay in cell contraction in these cells could be due to residual kinase from inefficient RNAi knockdown, or due to a ROCK independent pathway though which vaccinia stimulates cell contraction. (From this point on any reference to ROCK signifies both ROCK1 and ROCK2.)

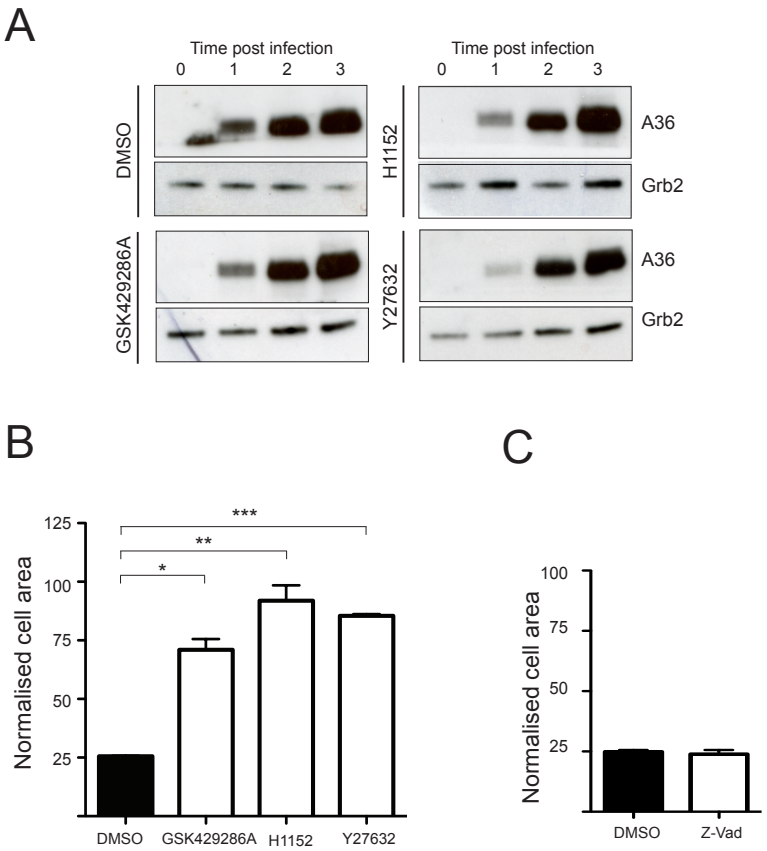

Figure 4.1 The inhibition of ROCK signalling blocks cell contraction

A Immuno blot shows that the three ROCK inhibitors GSK429286A, H1152 or Y27632 do not inhibit the expression of A36 at the indicated times post infection. Grb2 was used as an endogenous loading control. **B** A graph showing the normalised cell area of HeLa cells treated with DMSO or ROCK inhibitors at 3.40hpi with WR. Data is from three independent experiments in which a total of 94, 89, 83 and 83 cells were analysed, respectively. Error bars represent SEM.* P<0.05, ** P <0.01, *** P<0.01 as determined by one-way Anova. **C** A graph showing the normalised area of infected cells treated with z-vad 30 minutes prior to and throughout WR infection. Data is from three independent experiments.

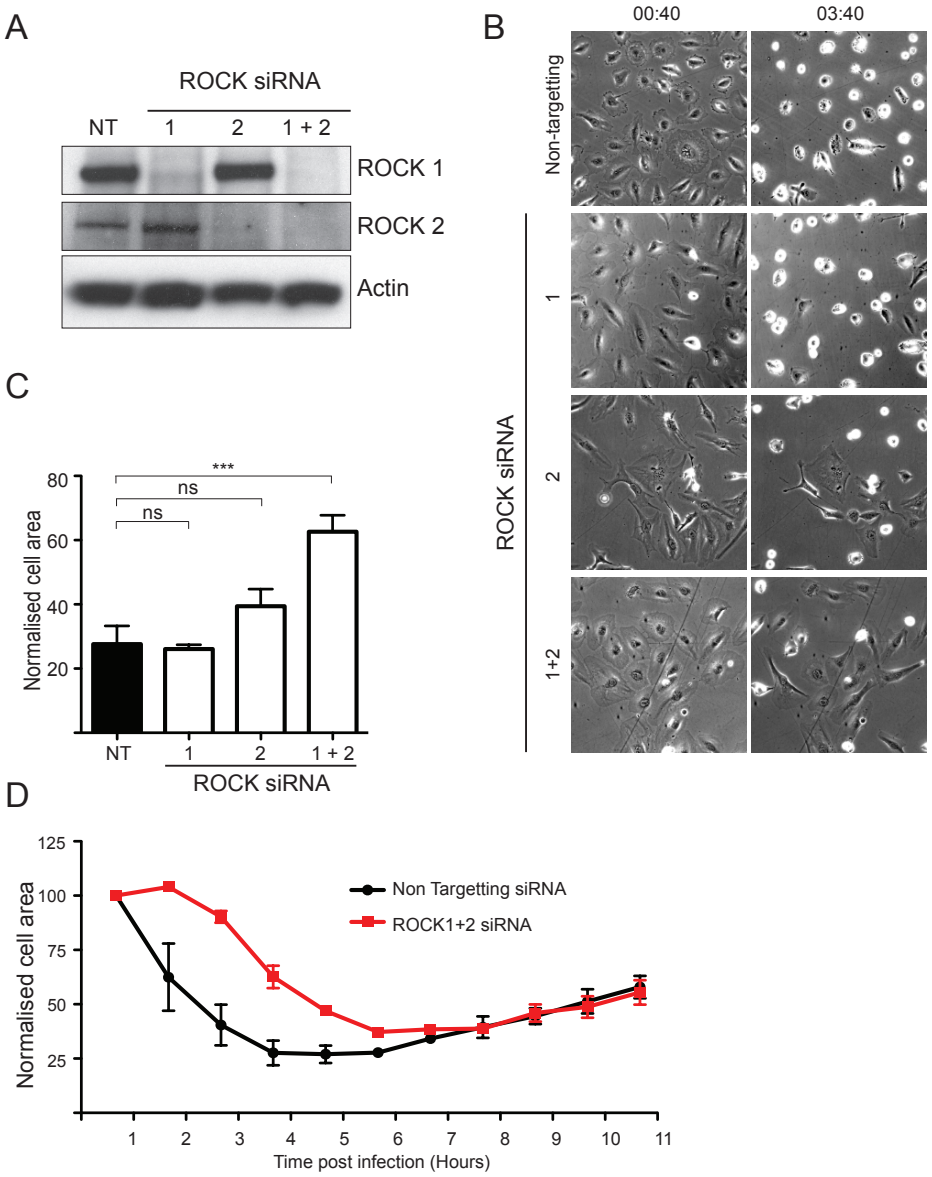

Figure 4.2 RNAi mediated knockdown of ROCK delays cell contraction

A Immuno blot analysis shows the efficiency of RNAi knockdown of ROCK1 and ROCK2 in HeLa cells that have been transfected with the indicated siRNA oligos for 72 hours. **B** Still images from a phase time-lapse movie following WR infection in HeLa cells that had been transfected with the indicated RNAi oligos for 72 hours. **C** A graph showing the area of HeLa cells in B (normalised to cell area at the start of acquisition) at 3:40hpi. Error bars represent SEM. The statistical significance was determined by a one-way Anova and indicated by *** for P value <0.001 or ns for P>0.05. **D** A graph showing the change in area of HeLa cells transfected with the indicated RNAi oligos over the course of infection. The data in C and D is from three independent experiments in which a total 85 cells were analysed in each condition.

4.2.3 RhoA is not required for cell contraction

As ROCK is involved in vaccinia stimulated cell contraction, it is highly likely that RhoA is also required. Previous investigations have shown there is a direct interaction between F11 and RhoA, which is abrogated by mutating a valine and lysine residue in a conserved RhoA binding motif in F11 and ROCK1 (F11-VK mutant) (Cordeiro et al., 2009; Valderrama et al., 2006). The requirement of this interaction for cell contraction was investigated by infecting HeLa cells with a recombinant virus expressing F11-VK. The F11-VK mutant stimulated cell contraction as efficiently as WR (25.3 ± 0.48 and 31.4% ± 5.6 at 3:40hpi with WR or F11-VK, respectively) (Figure 4.3 A and B). These data suggest that the interaction between F11 and RhoA is not important for vaccinia-induced cell contraction. To further investigate a potential role for RhoA, I performed siRNA mediated knockdown of RhoA in HeLa cells. RhoA protein expression was very efficiently blocked in HeLa cells that had been transfected with a pool of four RhoA siRNA oligos for 72 hours, as shown by immuno blot (Figure 4.4 A). HeLa cells depleted of RhoA were infected with WR (Figure 4.4 B and C). There was no significant difference in cell contraction between cells with or without RhoA (21.9 ± 2.5 compared to 32.1 ± 9.2%), indicating that RhoA is not required for contraction.

Previous work has shown that RhoA activity is supressed by F11 expression, at 8 hours post infection (Cordeiro et al., 2009; Valderrama et al., 2006). In contrast, other work has suggested that RhoA activity is supressed by F11 at 3hpi and subsequently recovers by 8hpi (Morales et al., 2008). To exclude the possibility that RhoA was involved in cell contraction I performed RhoA activation assays at 3hpi with WR and F11L. I used Rhotekin assays to measure the activity of RhoA, where the Rho binding domain of Rhotekin is immobilised on beads and selectively interacts with only GTP bound RhoA in the cell lysate. For this assay I used U-2 OS cells, which also contract with WR but not ΔF11L infection (Figure 3.5 A and B), because the detection of RhoA in U-2 OS lysates is more reproducible compared to HeLa lysates. RhoA activity was decreased in vaccinia-infected cells in comparison to uninfected cells, and this was independent of F11 expression because RhoA activity was similarly suppressed in ΔF11L infection (28.4 ± 9.2 and 35.9 ± 5.9 % for WR and ΔF11L, respectively, normalised to uninfected) (Figure 4.4 D). Taken together, these results suggest that RhoA is not required for vaccinia induced cell contraction.

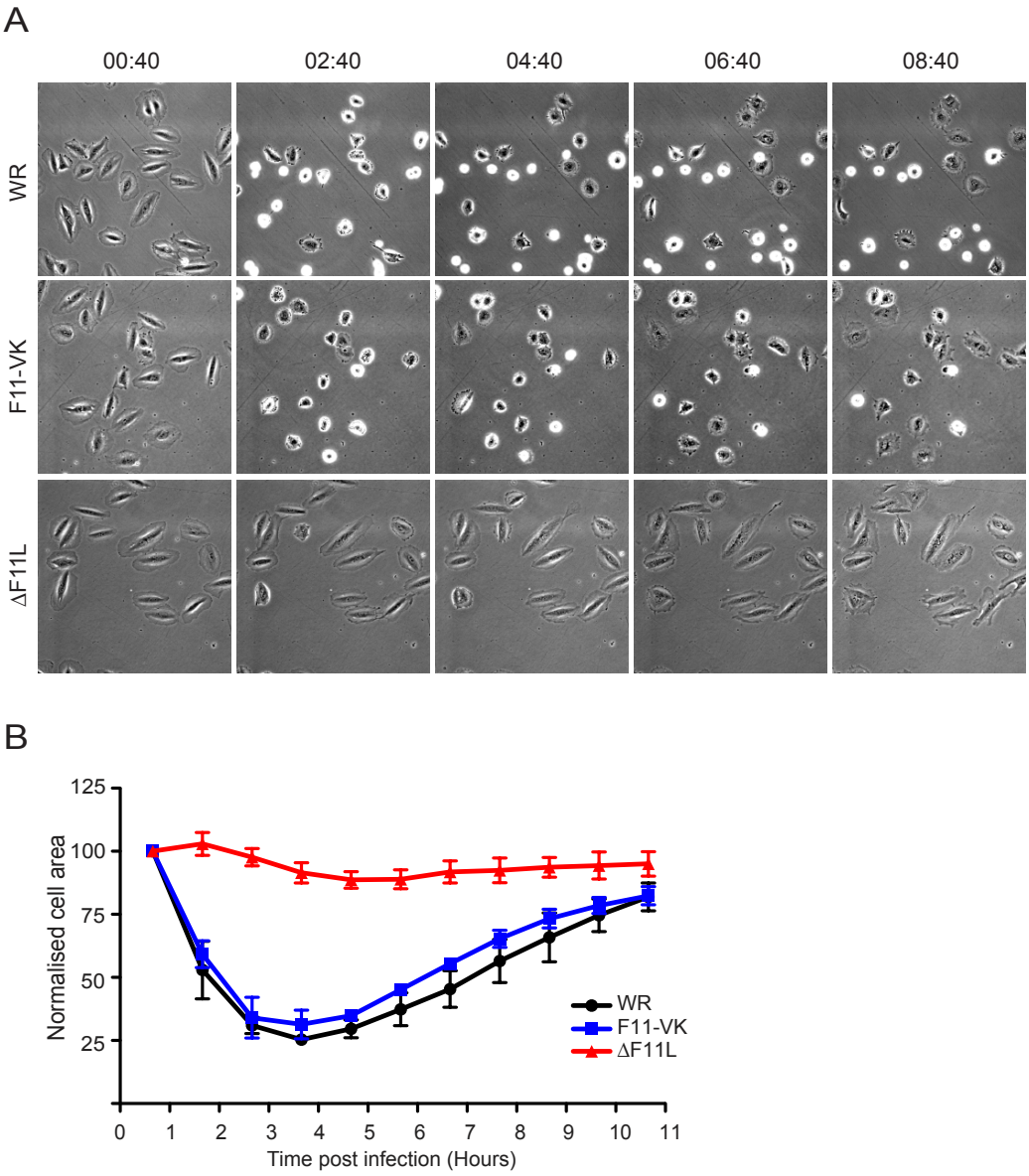

Figure 4.3 F11 binding to RhoA is not required for virus induced cell contraction

A Still images from a time-lapse movie of HeLa cells infected with WR, F11-VK or ΔF11L. **B** A graph to show the normalised cell area over the course of infection with WR, F11-VK or ΔF11L. The data is from three independent experiments, in which a total of between 60 and 70 cells were analysed. Error bars represent SEM.

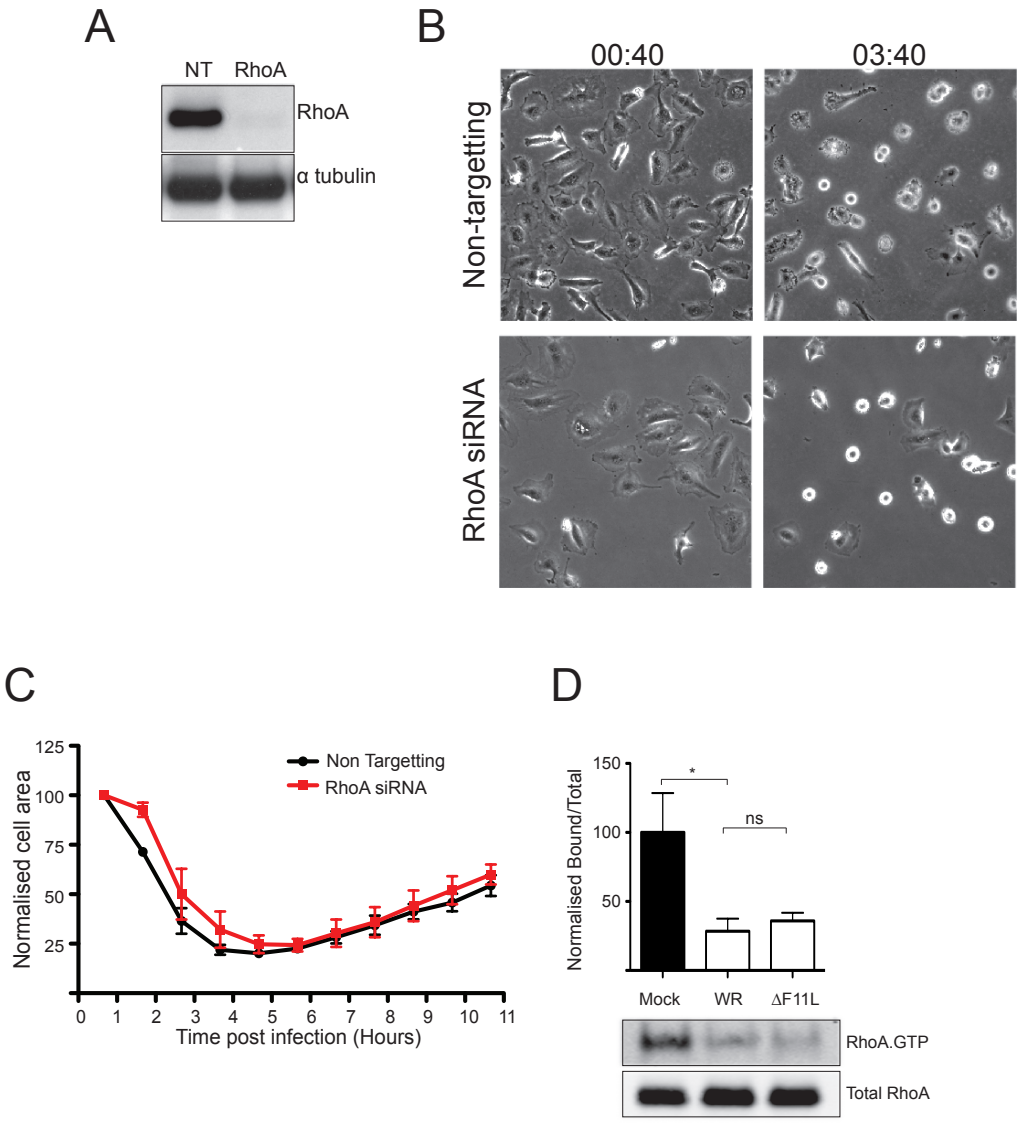

Figure 4.4 RhoA is not required for vaccinia induced cell contraction

A Immuno blot analysis shows the efficiency of RNAi mediated knockdown of RhoA. The cellular loading control was α-tubulin. **B** Still images from a time lapse movie following WR infection in HeLa cells that have been transfected with a pool of four RNAi oligos against RhoA for 72 hours, compared with non targeting control oligos. **C** The graph shows the change in average area of HeLa cells, transfected with the indicated RNAi oligos during the course of infection with WR. The data is from three independent experiments, in which a total of between 80 and 90 cells were analysed. Error bars represent SEM. **D** Rhotekin pull down assay was used to measure that ratio of GTP bound RhoA compared to total RhoA, in U-2 OS cells infected with WR or ΔF11L at 3hpi. Error bars represent SEM from four independent experiments. The immuno blot illustrates a representative assay. The statistical significance was determined by a one-way Anova, indicated by * for P value <0.05 or ns for P>0.05.

4.2.4 Other Rho GTPases are required for cell contraction

Despite no observable role for RhoA, it is possible that other Rho GTPases, particularly RhoB and RhoC, are involved in vaccinia-induced cell contraction. To investigate a potential role for other Rho GTPases, I treated HeLa cells with the *Clostridium botulinium* toxin C3 prior to infection with WR. The C3 transferase toxin is a good tool to study Rho mediated effects as it renders RhoA, RhoB and RhoC biologically inactive by ADP ribosylating asparagine 41 (Aktories et al., 1989; Braun et al., 1989; Chardin et al., 1989; Paterson et al., 1990). C3 transferase blocked cell contraction when added to infected cells (64.5 ± 5.1 compared to control 26.25 ± 3.2%) (Figure 4.5 A and B). C3 treatment does not affect virus entry as shown by immuno blot analysis of A36 (vaccinia protein) expression and so is a specific effect on cell contraction (Figure 4.5 C). This would indicate that although vaccinia-induced cell contraction is independent of RhoA, the other sub family members RhoB or RhoC may be involved. Furthermore, it is clear that the target of C3 is not RhoA, because in cells depleted of RhoA the difference in area between C3 treatment and no treatment is the same as when RhoA is present (Figure 4.5 D). C3 does not affect the biological activity of Rac1 or Cdc42, but the effect of C3 on other Rho GTPases, such as RhoD, Rif or RhoE, has not yet been studied.

4.3 Summary

The work presented in this chapter aimed to identify some of the cellular proteins required for vaccinia induced cell contraction. Using small molecule inhibitors and siRNA mediated knockdown I was able to confirm that ROCK1 and ROCK2 were required for cell contraction in vaccinia infection. I hypothesised that RhoA might be required because of the previously reported interaction between F11 and RhoA. However, using a recombinant F11 mutant virus, I found this interaction was not required. Furthermore, using siRNA and Rhotekin activity assays I showed that vaccinia induced cell contraction was independent of RhoA. However, the Rho subfamily inhibitor C3 blocked cell contraction, which indicates other Rho GTPase could be involved in vaccinia-induced cell contraction.

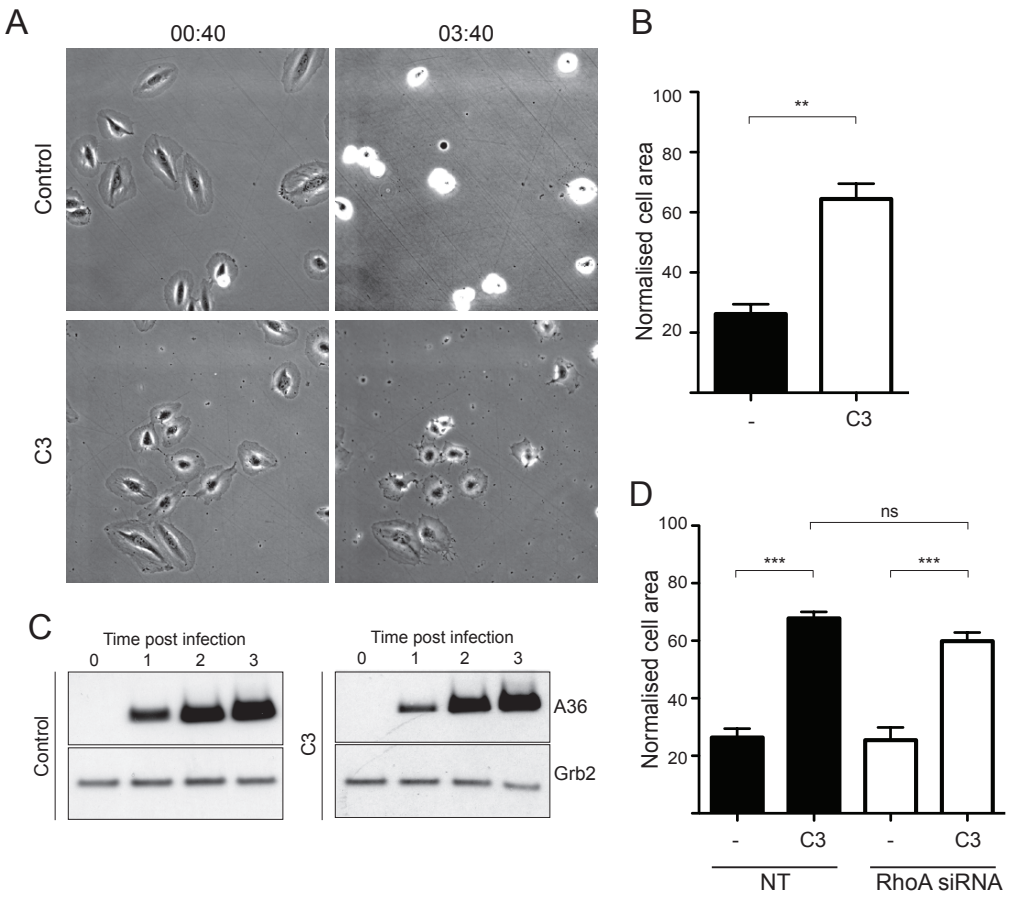

Figure 4.5 C3 blocks cell contraction

A Still images from time lapse movie of HeLa cells treated with cell permeable Rho A, B, C inhibitor C3 for 1 hour prior to and throughout infection with WR. **B** The graph shows the normalised cell area of WR infected HeLa cells with or without C3 treatment at 3.40hpi. The error represents SEM from three independent experiments, in which 100 cells were quantified. The statistical significance was determined by a Students t-test, indicated by ** for P <0.01. **C** Western blot analysis to show the levels of A36 expressed in infected HeLa cells with or without C3 treatment at 0, 1, 2 and 3hpi. **D** The graph shows the normalised cell area of WR infected HeLa cells at 3.40hpi with or without C3 treatment, following transfection with the indicated RNAi oligos for 72 hours. The error represents SEM from three independent experiments, in which approximately 80 cells were quantified. The statistical significance was determined by a one-way Anova, indicated by *** for P value <0.001 or ns for P>0.05.

Chapter 5.

F11 inhibits RhoD to promote RhoC dependent cell contraction

5.1 Introduction

I have found that vaccinia induced cell contraction requires F11 and ROCK but is independent of RhoA. The inhibition of contraction by the Rho inhibitor C3, however, suggests a requirement for other Rho GTPases. A previous PhD student, Joao Cordeiro, discovered that F11 binds additional Rho GTPases including RhoC, RhoD, RhoE and Rif but not RhoB (Figure 5.1 A). Furthermore, in contrast to RhoA, these Rho proteins were pulled down equally well by F11-VK and F11-WT (Figure 5.1 A, B). Each of these Rho proteins has documented roles in regulating the host actin cytoskeleton. RhoC, which can bind and activate ROCK, can mediate similar effects to RhoA (1.1.6.1). RhoD is believed to antagonise RhoA mediated phenotypes such as stress fibre formation, but it is not yet understood how this happens (1.1.6.5). It is well documented that RhoE can inhibit RhoA signalling by activating the RhoA GAP, p190RhoGAP, and inhibiting ROCK (1.1.6.4). Rif can induce filopodia and stress fibre formation (1.1.6.6). Given these documented roles on the actin cytoskeleton I wondered whether these other Rho proteins that can bind F11 are involved in vaccinia induced cell contraction. In this chapter, I investigate this hypothesis using siRNA and overexpression approaches.

Figure 5.1 F11 and F11-VK bind to multiple Rho GTPases

A Immuno blot analysis of a glutathione pull down from infected HeLa cell lysates that expressed GST-F11 and GFP-Rho GTPases. **B** Immuno blot analysis of a glutathione pull down from infected HeLa cell lysates that expressed GST-F11 or GST-F11-VK and GFP-Rho GTPases. Both experiments were performed by João Cordeiro and are published in his PhD thesis Cordeiro, J.V. (2008). Modulation of Rho GTPase signalling during vaccinia virus infection (UCL). *This figure has been removed in the electronic copy of this thesis.*

5.2 Results

5.2.1 siRNA of Rho GTPases

To investigate whether RhoC, RhoD, RhoE and Rif are required for cell contraction, I performed siRNA-mediated knockdown of these proteins (with pools of four siRNA oligos) prior to infection with WR. The efficiency of knockdown of RhoA and RhoC was assessed by immuno blot analysis, which showed extremely efficient depletion of both proteins 72 hours after siRNA treatment (Figure 5.2 A). The loss of RhoA expression by siRNA treatment led to a marked increase in RhoC protein levels. To circumvent the possibility that a phenotype from RhoA siRNA treatment could be masked by the increase in RhoC levels, I performed simultaneous knockdown of both proteins. The simultaneous knockdown of RhoA and RhoC was as efficient as individual knockdowns (Figure 5.2 A). As I lacked the antibodies at the time that worked well for immuno blotting for RhoD, RhoE and Rif, I measured the efficiency of knockdown by quantifying mRNA levels using RT-qPCR. The level of mRNA of the gene of interest was normalised to GAPDH (glyceraldehyde-3-phosphate dehydrogenase), and subsequently normalised to non-targeting control samples using the comparative C_t method (Schmittgen and Livak, 2008). Following siRNA treatment for 72 hours the levels of RhoD, RhoE or Rif mRNA that remained, relative to the control sample, were 7.9%, 6.4% and 35.0% respectively (Figure 5.2 B).

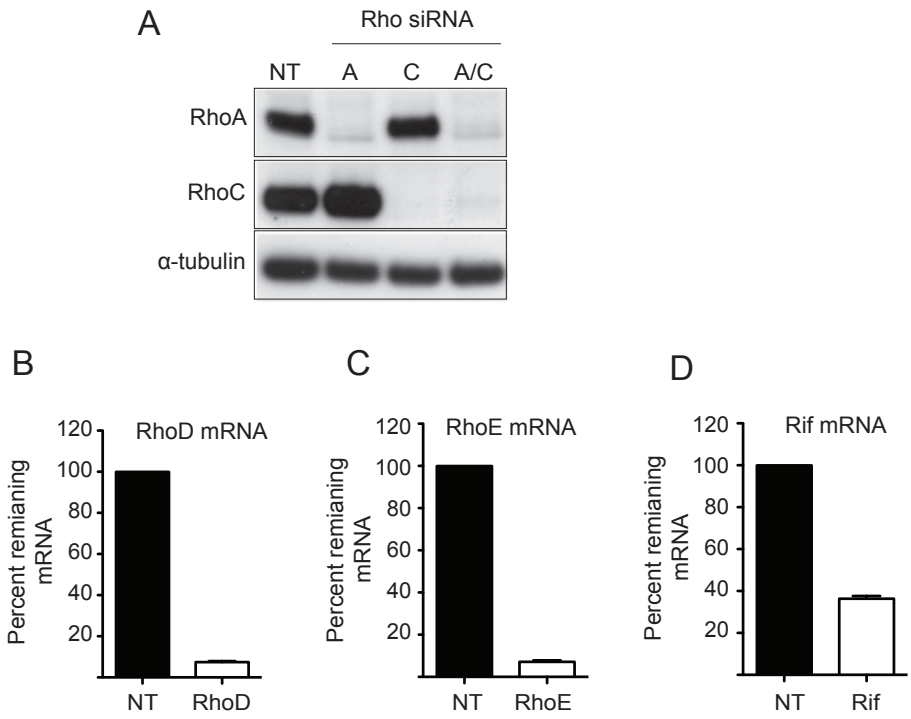

Figure 5.2 RNAi mediated knockdown of Rho GTPases

A Immuno blot analysis showing efficient knockdown of RhoA and/or RhoC following 72 hour treatment with a pool of four siRNA oligos. α-tubulin was used as the cellular loading control. **B-D** The percentage of remaining RhoD, RhoE or Rif mRNA following treatment for 72 hours with siRNA against the indicated proteins. mRNA levels were measured by reverse transcription quantitative PCR (RT-qPCR). The level of mRNA of the gene of interest (GOI) was normalised to GAPDH mRNA and the normalised GOI mRNA in knockdown samples was compared to NT sample using the comparative Ct method. NT= non-targeting siRNA. Error bars represent SEM from two independent experiments.

5.2.2 RhoC is required for efficient cell contraction

HeLa cells were infected with WR 72 hours after siRNA treatment against RhoA, RhoC, RhoD, RhoE or Rif. The change in cell area was followed for 11 hours post infection, which represents a complete replication cycle (Figure 5.3. A-E). Of the five GTPases, knockdown of RhoC substantially altered cell contraction. RhoC depleted cells contracted to 56.2 ± 8.09% of the original area in comparison to non-targeting control treated cells, which contracted to 23.8 ± 2.57% (Figure 5.3 B, F). However, like ROCK siRNA, RhoC depleted cells do eventually contract at 6:40hpi and do not re-spread during the course of imaging (Figure 5.3 B). The simultaneous knock down of RhoA and RhoC did not additionally block cell contraction over RhoC alone (59.0 ± 7.48% and 56.2 ± 8.09%, respectively), this indicated that of the two GTPases only RhoC was required for vaccinia-induced cell contraction (Figure 5.3 A, B and F). The involvement of RhoC in vaccinia-induced cell contraction is perhaps not surprising, as it binds ROCK. A requirement for RhoC could easily explain the observed inhibition of contraction by C3 (Figure 4.5 B). Consistent with this, the target of C3 in vaccinia-induced contraction was not RhoA, as addition of C3 to RhoA depleted cells blocked cell contraction as efficiently as C3 treatment in control cells (Figure 4.5 D and 5.4 A). In contrast, C3 treatment did not further block cell contraction in comparison to DMSO treatment in RhoC depleted cells, where the cell area was 54.75 ± 6.93 and 51.85 ± 2.88% of the original area at 3:40hpi, respectively (Figure 5.4 A). It is very likely that RhoC is the cellular target of C3 in vaccinia-induced cell contraction.

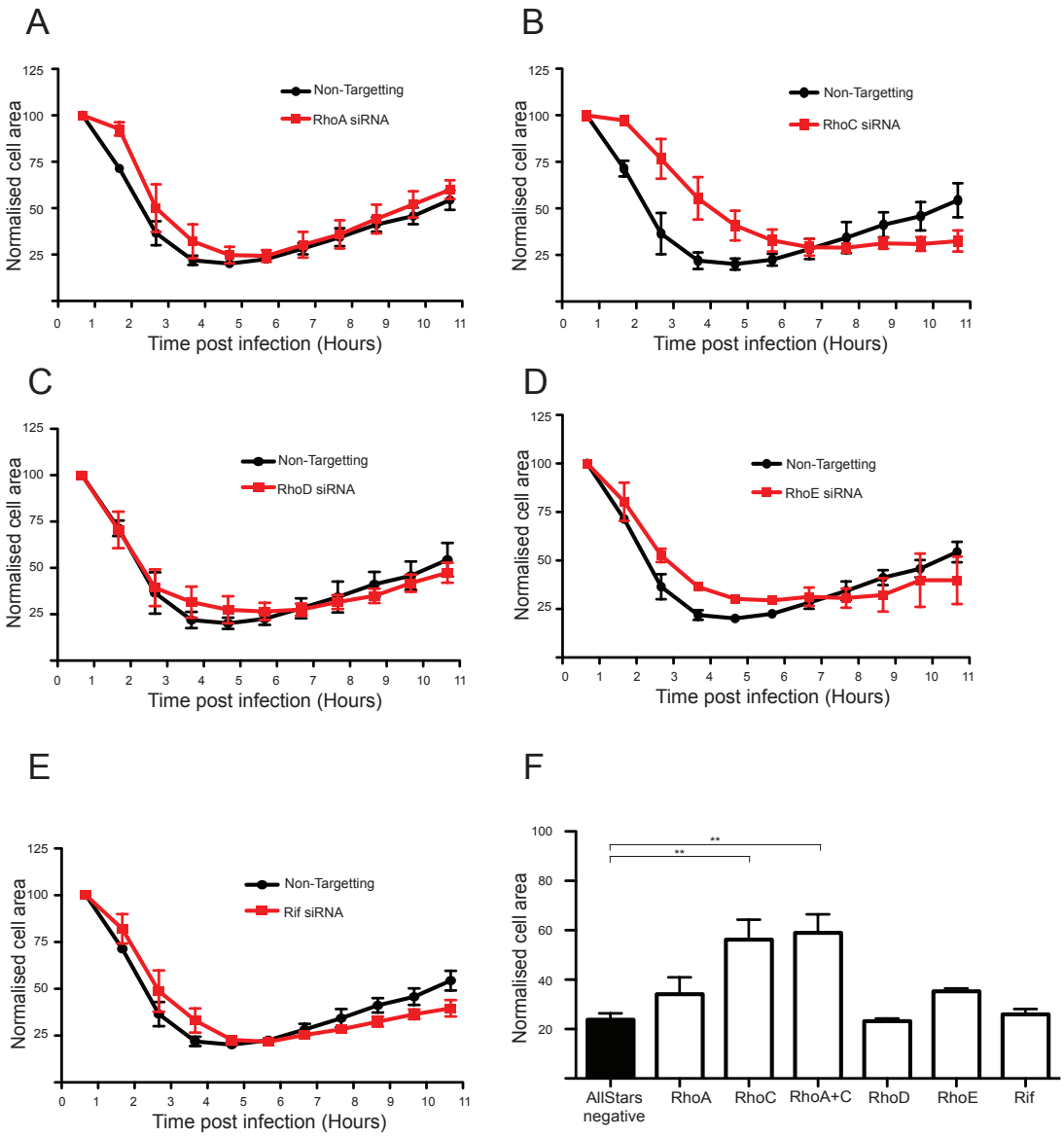

Figure 5.3 Depletion of RhoC reduces the efficiency of vaccinia-induced contraction

A-E Graphs showing the change in area of WR infected HeLa cells that were treated with the indicated pool of four RNAi oligos for 72 hours prior to infection. Error bars represent SEM from four independent experiments, in which approximately 90 cells were analysed. **F** A graph showing the normalised area of HeLa cells, transfected for 72 hours with the indicated pool of four siRNA oligos, at 3:40hpi with WR. Error bars represent SEM from four independent experiments, in which approximately 90 cells were analysed in each condition. The statistical significance was determined by a one-way Anova, indicated by ** for P value <0.01.

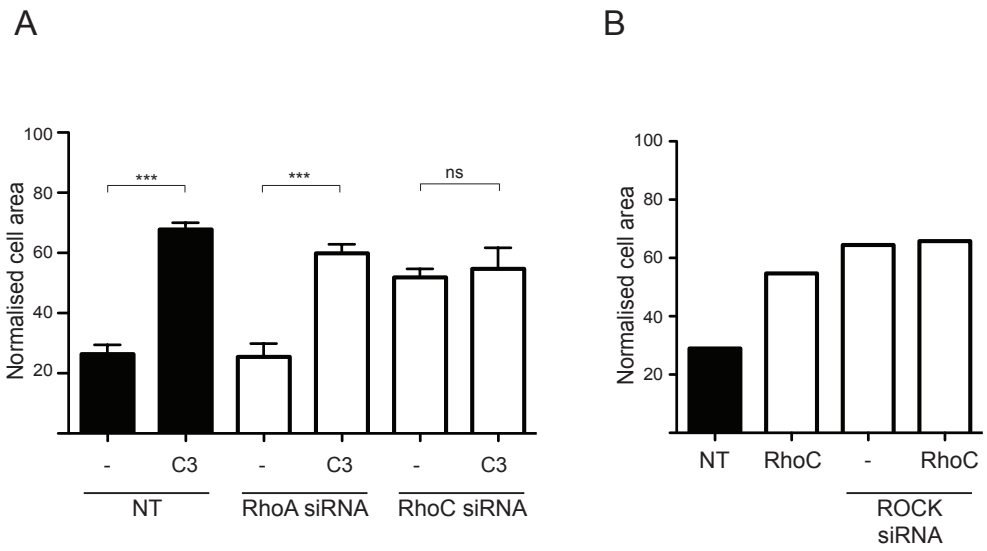

Figure 5.4 Cell contraction is dependent on RhoC-ROCK signalling

A The graph shows the normalised cell area of WR infected HeLa cells at 3.40hpi with or without C3 treatment, following transfection with the indicated siRNA oligos for 72 hours prior to infection. The error represents SEM from three independent experiments, in which approximately 80 cells were quantified. The statistical significance was determined by a one-way Anova, indicated by *** for P value <0.001 or ns for P>0.05. **B** The graph shows the normalised cell area of WR infected HeLa cells at 3:40hpi following transfection with the indicated RNAi oligos for 72 hours. This data is from a single experiment.

To further investigate whether RhoC was in the same pathway as ROCK, I performed simultaneous siRNA mediated knockdown of RhoC and ROCK. At 3:40hpi with WR, cells depleted of RhoC, ROCK or RhoC and ROCK contracted to 54.7%, 64.5% or 65.8% of the original cell area, compared to 28.9% in control cells. RhoC and ROCK appear to be in the same signalling pathway, as depletion of RhoC and ROCK was no more efficient at blocking cell contraction than depletion of ROCK only (Figure 5.4 B). This data is from a single experiment and must be repeated to gain more confidence in the result.

The previous results suggest that HeLa cells must express RhoC for efficient vaccinia induced cell contraction to proceed. Therefore, I was interested whether RhoC activation was required. The expression of constitutively active and dominant negative point mutants of Rho GTPases can be used to address this question. In the

constitutively active mutant of RhoA-related subfamily a valine residue replaces glycine 14 (Rho G14V). Glycine 14 is within the nucleotide-binding pocket and the substitution of a small glycine side chain for the bulky valine side chain sterically hinders GTP hydrolysis and therefore, Rho GTPase inactivation (Ihara et al., 1998). In the dominant negative mutant, the threonine residue at position 19 is mutated to arginine (Rho T19N). This mutant (or the corresponding mutant in Ras) acts as a dominant negative because it binds GEFs with higher affinity than wild type, but the GEF is not displaced because the mutant has low affinity for guanine nucleotides (see 1.1.2). Therefore, the mutant sequesters GEFs and prevents activation of the endogenous Rho GTPase (reviewed in (Feig, 1999)). I transfected HeLa cells with GFP tagged RhoC wild type (WT), G14V and T19N prior to infection with either WR or ΔF11L. It was not possible to examine the effect of G14V as it caused cytotoxicity. In WR infection, there was a slight but insignificant change in the extent of cell contraction in cells expressing GFP-RhoC WT compared to GFP (43.5 ± 0.50 and 35.7 ± 3.00%, respectively). In contrast, RhoC T19N blocked cell contraction as cells expressing GFP-RhoC T19N only contracted to 77.5 ± 4.00% of the original cell area (Figure 5.5 A). Cell contraction was partially induced in HeLa cells infected with ΔF11L and expressing GFP-RhoC WT (63.1 ± 1.90), but not GFP or GFP-RhoC T19N (89.6 ± 5.11 and 92.1 ± 3.41, respectively) (Figure 5.5 B). Taken together, these results suggest that RhoC must be active in WR infection for cell contraction to occur. Furthermore, the expression of RhoC in cells infected with ΔF11L partially rescues cell contraction, this might indicate that in WR infection F11 can activate RhoC. I conducted RhoC Rhotekin assays in HeLa cells infected with WR or ΔF11L to investigate the activation status of RhoC during cell contraction (at 3:40hpi). Infection with both WR and ΔF11L leads to a reduction in GTP bound RhoC levels to 42.2 ± 2.90 and 42.8 ± 9.75% of those seen in uninfected, respectively (Figure 5.5 C). This would suggest RhoC is inhibited during infection, but the inhibition is independent of F11 expression. The siRNA, drug inhibition and overexpression experiments all disagree with this result. Moreover, Rhotekin assays must be interpreted with caution because they measure the activity of RhoC on a global level, which might not be relevant to localised events at the plasma membrane and cortex. However, given that siRNA mediated loss of RhoC, C3 inhibition of RhoC and overexpression of RhoC cDNA complement each other I suggest that RhoC is required for vaccinia-induced cell contraction.

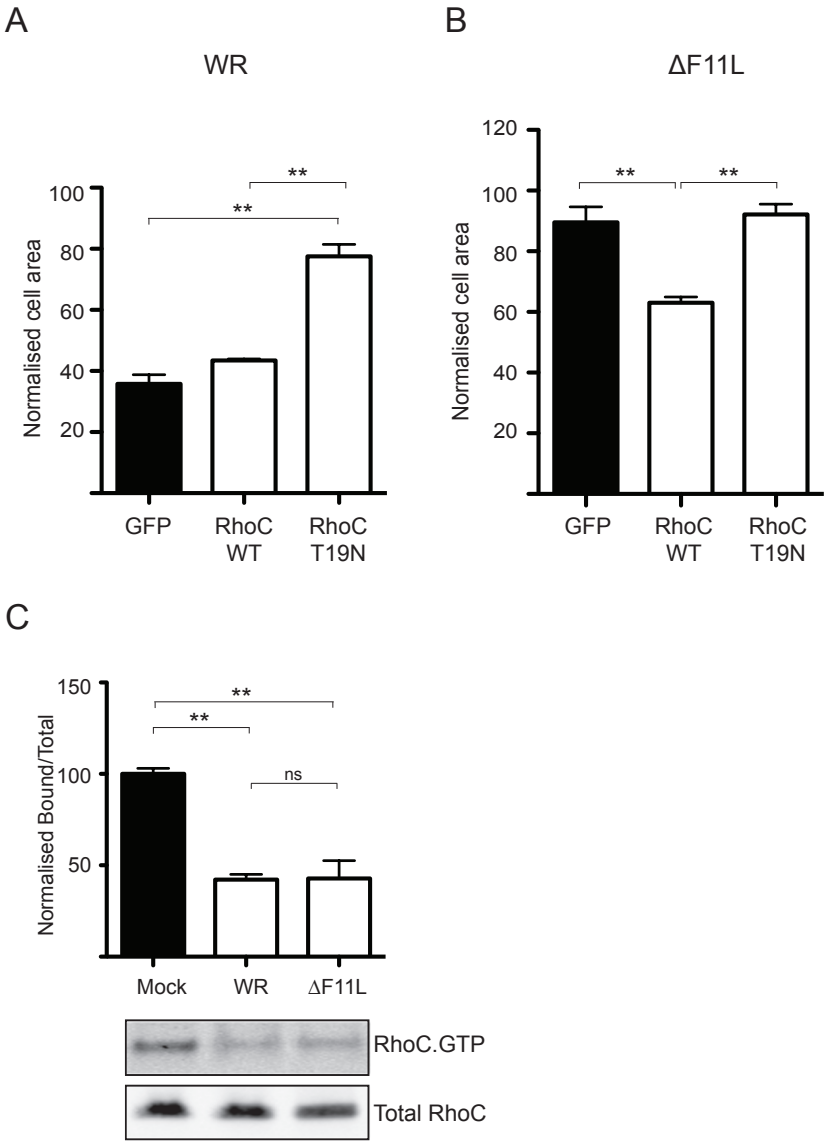

Figure 5.5 RhoC is required for efficient cell contraction

A and B The graphs shows the normalised cell area of HeLa cells expressing GFP, GFP-RhoC WT or GFP-RhoC T19N at 3:40hpi with WR (**A**) or ΔF11L (**B**). Error bars represent SEM from four independent experiments in which approximately 60 cells were analysed. The statistical significance was determined by a one-way Anova, indicated by ** for P value <0.01. **C** Rhotekin pull down assays were used to measure that ratio of GTP bound RhoC compared to total RhoC, in U-2 OS cells infected with WR or ΔF11L at 3hpi. Error bars represent SEM from three independent experiments. The immuno blot illustrates a representative assay. The statistical significance was determined by a one-way Anova, indicated by ** for P value <0.01 or ns for P>0.05.

5.2.3 RhoD negatively regulates cell contraction

The previous experiments attempted to identify positive regulators of vaccinia-induced cell contraction (Figure 5.3). However, this experiment did not consider the possibility that the Rho GTPases may negatively regulate this phenotype. To investigate this possibility, I performed siRNA mediated knockdown of the same five Rho GTPases and infected HeLa cells with ΔF11L virus. I expected the knockdown of a negative regulator to promote cell contraction with this normally contraction deficient virus. Of the five GTPases, only siRNA of RhoD promoted contraction of ΔF11L-infected cells (Figure 5.6 A-F). Furthermore, depletion of RhoD induced transient cell contraction with temporal dynamics similar to that seen in WR infection, albeit not as robust (Figure 3.1, Figure 5.6 C).

The knockdown of the Rho GTPases is performed using a pool of four siRNA oligos. I was concerned that off target siRNA effects of one or multiple siRNA oligos might have caused the cell contraction phenotype. To rule this out, I treated HeLa cells with two individual RhoD siRNA oligos. Following siRNA transfection with oligo 1, oligo 2 or the pool of four, the level of RhoD mRNA that remained was 10.7, 5.3 and 3.7%, respectively, normalised to a non-targeting siRNA control sample (Figure 5.7 A). HeLa cells transfected with RhoD oligos 1 or 2 were able to contract as efficiently as cells treated with the pool of four oligos during ΔF11L virus infection (infected cells contracted to 49.0 ± 2.67, 53.0 ± 1.44, 49.2 ± 7.58% of the original area, respectively, compared to non targeting control of 79.6 ± 3.98) (Figure 5.7 A, B).

In addition, I overexpressed siRNA resistant RhoD in cells depleted of RhoD by siRNA. If ΔF11L induced cell contraction is due to the loss of RhoD expression, then overexpressing RhoD in siRNA treated cells should inhibit cell contraction. I generated siRNA resistant GFP tagged RhoD wild type (WT), constitutively active (G26V) and dominant negative (T31N) mutants using site directed mutagenesis to change the bases within the complimentary region to oligo 2, without altering the amino acid sequence. The G26V and T31N mutants of RhoD correspond to G14V and T19N mutants of RhoC, respectively (Figure 1.12). In cells depleted of RhoD, RhoD WT expression blocked cell contraction during ΔF11L infection (cells area was 82.3 ± 6.25% compared to 44.0 ± 4.90% in non-transfected RhoD depleted cells) (Figure 5.8 A, B). The expression of constitutively active RhoD G26V also blocked ΔF11L induced cell contraction (88.8 ± 4.91%). In contrast, dominant negative RhoD T31N did not

block contraction (51.00 ± 2.22%) (Figure 5.8 A, B). Taken together, these results confirm that ΔF11L induced cell contraction in RhoD siRNA treated cells is due to the loss of RhoD. Furthermore, it indicates that RhoD must be inactivated for cell contraction to occur. If this is the case, then what effect do the RhoD mutants have on cell contraction during WR infection? I expressed GFP-Rho G26V and T31N during WR infection and analysed the extent of cell contraction at 3:40hpi. Activated RhoD prevented WR induced cell contraction while dominant negative RhoD had no effect relative to GFP (59.5 ± 5.45, 30.0 ± 2.69 and 28.69 ± 4.41%, respectively) (Figure 5.9 A and B). My overexpression and siRNA studies with RhoD clearly indicate that RhoD activity is inhibitory to vaccinia induced cell contraction. RhoD activity must be turned off during vaccinia infection to allow efficient cell contraction.

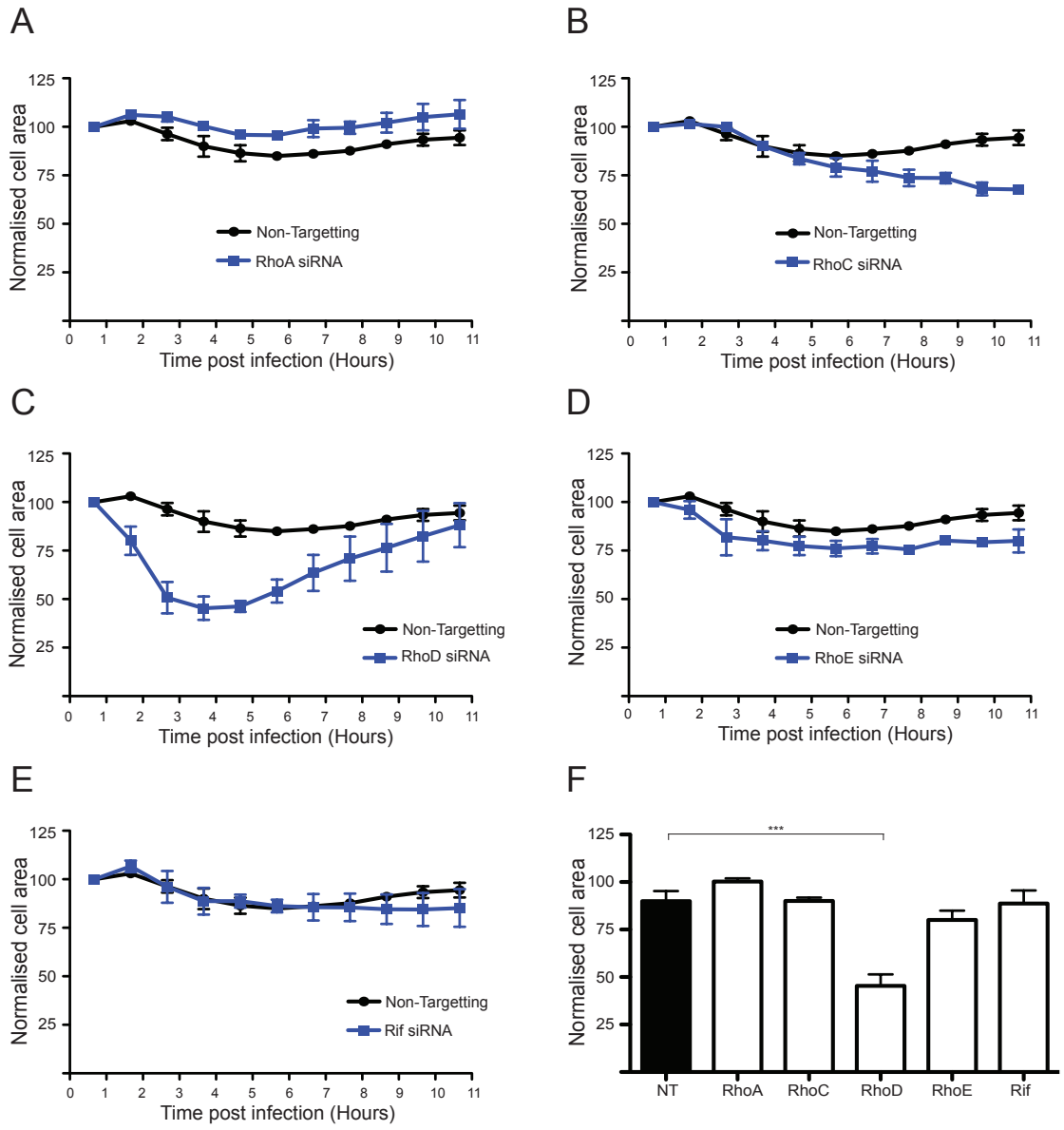

Figure 5.6 Loss of RhoD promotes cell contraction in ΔF11L infection

A-E Graphs showing the change in area of ΔF11L infected HeLa cells that were treated with the indicated pool of four RNAi oligos for 72 hours prior to infection. Error bars represent SEM from four independent experiments, in which approximately 90 cells were analysed. **F** The graph shows the normalised area of HeLa cells, treated for 72 hours with the indicated pool of four siRNA oligos, at 3:40hpi with ΔF11L. Error bars represent SEM from four independent experiments, in which approximately 90 cells were analysed. The statistical significance was determined by a one-way Anova, indicated by *** for P value <0.001.

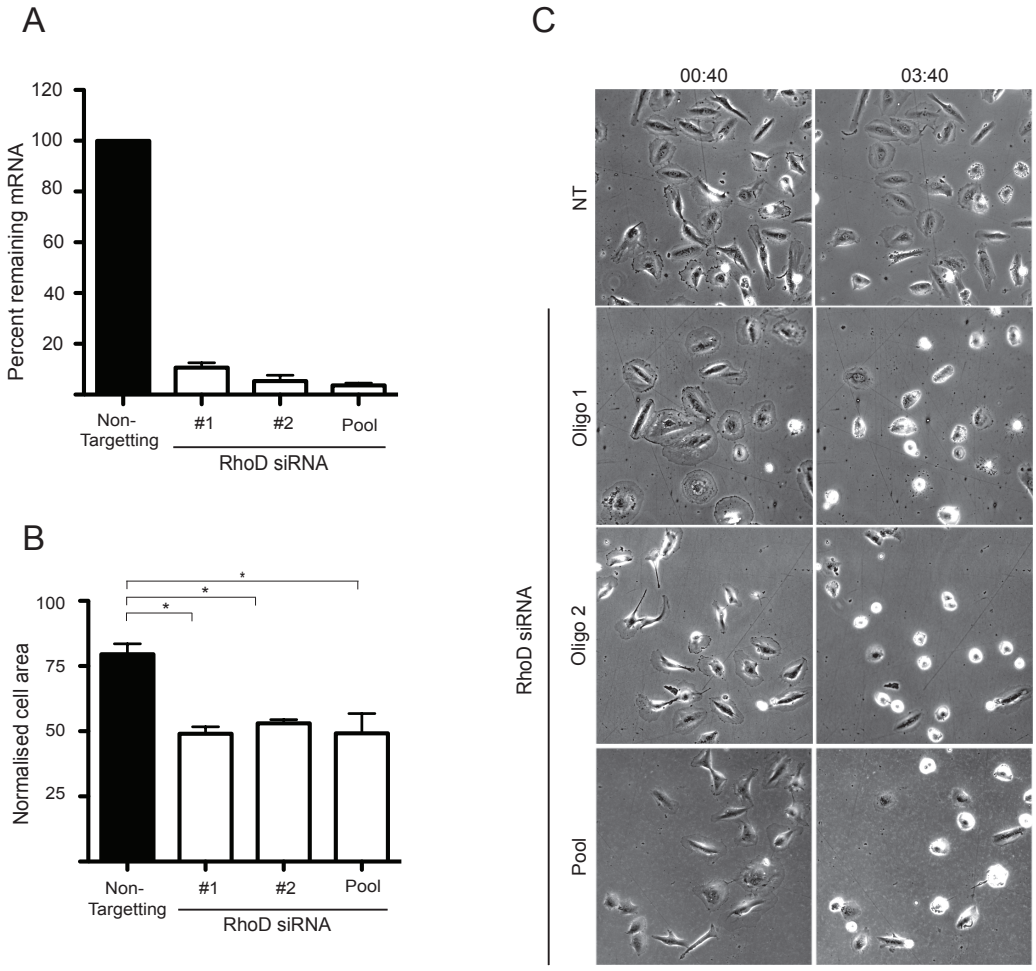

Figure 5.7 ΔF11L can stimulate contraction in cells depleted of RhoD

A The efficiency of RNAi mediated knockdown of RhoD was measured by RT-qPCR. The level of mRNA of the gene of interest was normalised to GAPDH and relative mRNA was calculated using the comparative CT method. Error bars represent SEM from two independent experiments. **B** The normalised area of HeLa cells at 3:40hpi with ΔF11L, following treatment with the indicated siRNA oligos for 72 hours prior to infection. **C** Stills from a time-lapse movie of HeLa cells infected with ΔF11L, following treatment with the indicated siRNA oligos for 72 hours prior to infection. NT = non-targeting oligo. Error bars represent SEM from three independent experiments, in which approximately 60 cells were analysed. The statistical significance was determined by a one-way Anova, indicated by * for P value <0.05.

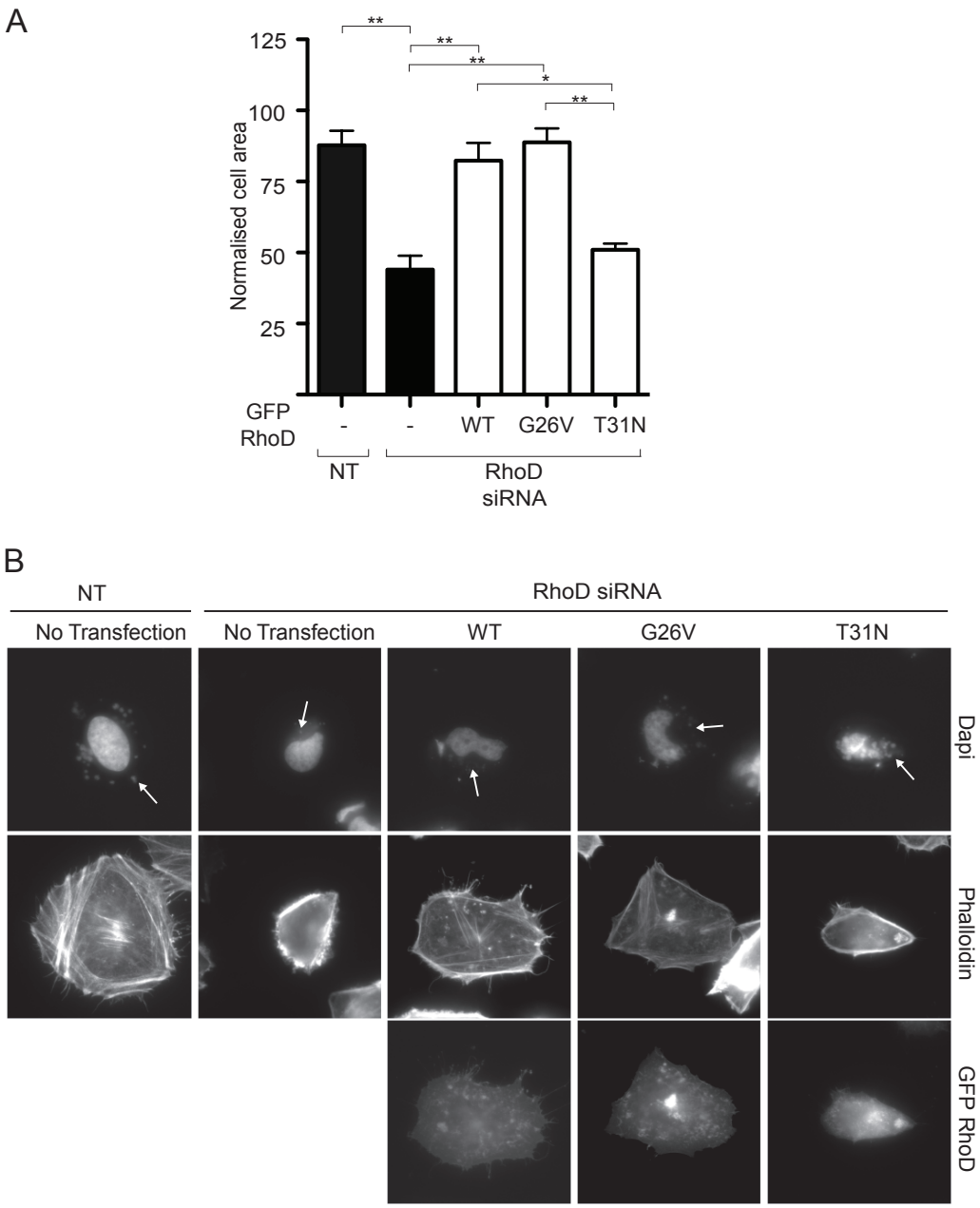

Figure 5.8 RhoD expression blocks ΔF11L stimulated cell contraction

A The graph shows the normalised area of HeLa cells, treated with RhoD siRNA, expressing the indicated GFP-RhoD protein and infected with ΔF11L at 3:40hpi. Error bars represent SEM from three independent time-lapse movies in which approximately 60-70 cells were analysed. The statistical significance was determined by a one-way Anova, indicated by * $P<0.05$ and ** $P<0.01$. **B** Representative immunofluorescence images of HeLa cells expressing the indicated GFP-RhoD protein and infected with ΔF11L at 3:40hpi. F-actin and DNA are stained with phalloidin and DAPI, respectively. White arrows indicate early DNA virus factories.

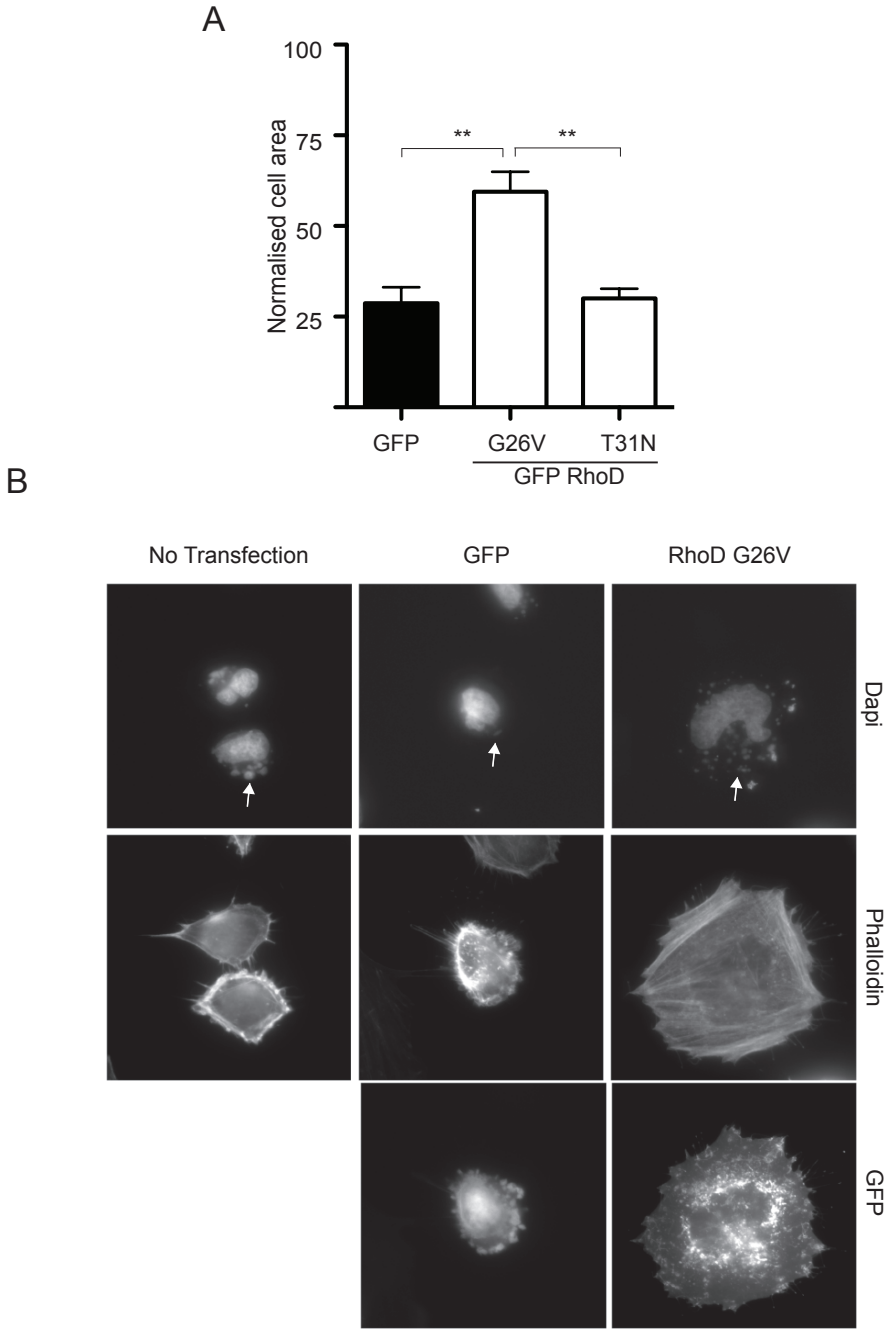

Figure 5.9 Active RhoD blocks WR induced cell contraction

A The graph shows the normalised area of HeLa cells expressing the indicated GFP-RhoD protein and infected with WR at 3:40hpi. Error bars represent SEM from three independent time-lapse movies in which approximately 60-70 cells were analysed. The statistical significance was determined by a one-way Anova, indicated by **P<0.01. **B** Representative immunofluorescence images HeLa cells expressing the indicated GFP-RhoD protein and infected with WR at 3:40hpi. F-actin and DNA are stained with phalloidin and DAPI, respectively. White arrows indicate early DNA virus factories.

5.2.4 How does RhoD repress cell contraction?

Inactivation of RhoD, either by siRNA mediated knockdown or dominant negative mutation, promotes efficient ΔF11L induced cell contraction. To confirm that the cell contraction that resulted from the loss of RhoD expression during ΔF11L infection was through the same signalling mechanism as in WR infection, I treated cells with the ROCK inhibitor, H1152, and Rho inhibitor, C3. To inhibit ROCK I used the inhibitor that was the most efficient at blocking WR induced cell contraction (Figure 4.1 B). In cells depleted of RhoD, H1152 treatment blocked cell contraction in comparison to DMSO treatment (87.9 ± 10.47 and 48.7 ± 0.83%, respectively) (Figure 5.10 A). This is similar to the result I obtained in WR infected cells (Figure 4.1 A and B). In addition, treatment of RhoD depleted cells with C3 blocked ΔF11L-stimulated contraction compared to untreated cells (108.1 ± 6.30 and 47.01 ± 3.94, respectively) (Figure 5.10 B). Both results suggest that ΔF11L induced cell contraction, in cells depleted of RhoD, also proceed via Rho and ROCK. Again, taking into consideration that C3 can inhibit RhoA, RhoB and RhoC, I performed simultaneous knockdown of RhoD and RhoC prior to a ΔF11L infection. siRNA mediated knockdown of both RhoC and RhoD efficiently reduced the expression of both proteins (Figure 5.10 C). RhoD protein levels were observed with a newly available antibody specific for RhoD. The RhoD antibody confirms my previous RT-qPCR result (Figure 5.2). It is worth noting that depletion of RhoC leads to a large increase in RhoD protein levels. This is likely due to increased RhoGDI1 available for RhoD stability in the absence of RhoC (Guilluy et al., 2011). In comparison to siRNA of RhoD alone, little cell contraction was observed in cells treated with siRNA against RhoD and RhoC (39.4 ± 3.40 and 74.0 ± 1.51, respectively) (Figure 5.10 D). Overall, this data demonstrates that ΔF11L stimulated cell contraction in RhoD depleted cells is dependent on RhoC and ROCK.

My data indicates that inhibition of RhoD signalling and activation of RhoC-ROCK signalling is required for WR induced cell contraction. However, it is not clear whether these molecules act in two parallel, independent pathways controlled by F11 that are antagonistic to each other, or if RhoD, RhoC and ROCK are in a single linear pathway (Figure 5.11A). RhoD is suggested to antagonise RhoA signalling but not by interfering with the interaction between RhoA and ROCK (Nguyen et al., 2002; Tsubakimoto et al., 1999). Therefore, it is not clear from these studies whether RhoD is upstream or downstream of RhoA. Yutaka Handa, a post-doctoral researcher in the lab, discovered that overexpression of G26V RhoD reduces the level of RhoA bound to GTP. As RhoA

and RhoC share approximately 85% sequence identity, I decided to test whether the same was true for RhoC. I measured the levels of RhoC bound to GTP in uninfected U-2 OS cells expressing GFP, GFP-RhoD G26V or GFP-RhoD T31N. The relative amount of GTP bound RhoC in each condition was normalised to the GFP control. Overexpression of dominant negative RhoD T31N, led to a 58% increase in the levels of RhoC bound to GTP relative to the GFP control (although this was not significant) (Figure 5.11 B). This indicates that active RhoD antagonises RhoC activity. Confusingly, the transfection of constitutively active RhoD mutant only led to small and insignificant decrease in RhoC activity. Perhaps RhoC activity is sufficiently supressed by endogenous RhoD that additional RhoD activity has no further effect. The effects of a dominant negative RhoD mutant must be interpreted with caution because dominant negative GTPases bind and sequester GEFs. As Rho GEFs can sometimes act on multiple Rho GTPases, RhoD T31N may additionally inactive other Rho GTPases. It may be that in this assays dominant negative RhoD antagonises RhoC activity by sequestering RhoC GEFs. However, it is not known whether RhoC and RhoD share GEFs and the two proteins are sufficiently different that this is unlikely. To confirm this result, I could perform the same RhoC activity assays in cells depleted of endogenous RhoD and investigate whether depletion of RhoD leads to an increase in RhoC activity. During his doctoral studies, João Cordeiro found that F11 binds multiple Rho GTPases in infected cells (Figure 5.1). Furthermore, he found that bacterially expressed purified GST-F11 interacts directly with purified His-RhoD but not RhoC (data not shown). However, correct folding of RhoC was not confirmed as no positive control was used. In conjunction with suspected RhoD antagonism of RhoC activity, the direct interaction of F11 with RhoD but not RhoC is more consistent with a linear pathway involving RhoD, RhoC and ROCK for F11 induced cell contraction. I hypothesise that F11 binds to and inhibits RhoD signalling, this relieves the inhibition of RhoC activity by RhoD and allows ROCK mediated cell contraction.

RhoD interacts with F11 through a small motif that shares sequence identity with one of the only known RhoD effectors, hDia2C (mDia3). João Cordeiro found that mutating the five conserved residues in F11 abrogated RhoD binding (F11 IV-KNS mutant) (Figure 5.12 A and B). I wondered whether the interaction between F11 and RhoD was important for cell contraction. I infected cells with recombinant viruses that expressed F11 IV-KNS or F11 VK/IV-KNS (RhoD binding mutants generated by João Cordeiro) in comparison to WR. HeLa cells infected with F11 IV-KNS were able to contract, but not

as robustly as during infection with WR. There was a small but significant increase in cell area at 3:40hpi between cells infected with F11 IV-KNS or F11 VK/IV-KNS and WR (36.7 ± 2.2, 40.8 ± 3.35 and 25.3 ± 0.48, respectively) (Figure 5.12 C and D). This would suggest that the interaction between F11 and RhoD is not required for cell contraction.

5.3 Summary

In this chapter I investigated the roles of RhoC and RhoD in vaccinia induced cell contraction. In agreement with published data that RhoC activates ROCK, I found that RhoC was required for cell contraction and suggest that RhoC and ROCK lie in the same signalling pathway downstream of F11. I discovered that RhoD activity negatively regulates cell contraction and RhoD activity must be inhibited to allow efficient WR induced cell contraction. I hypothesis that RhoD negatively regulates RhoC activity in ΔF11L infection, while the presence of F11 during WR infection relieves this inhibition. F11 can bind RhoD, however, this interaction is only partially required for cell contraction. It remains to be determined how F11 inhibits RhoD activity, and how RhoD antagonises RhoC.

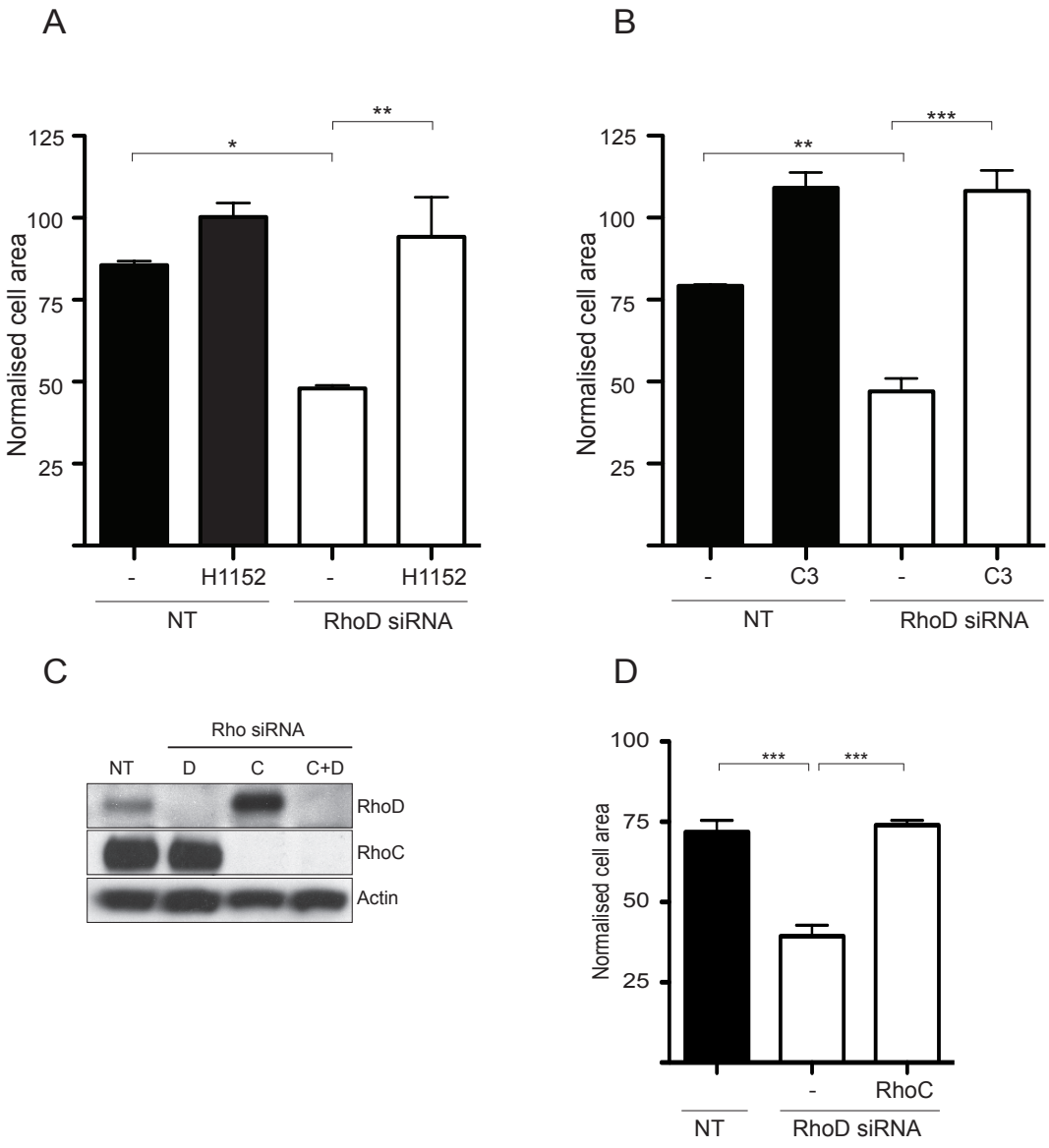

Figure 5.10 Inhibition of ROCK and RhoC blocks ΔF11L induced contraction in RhoD depleted cells

A, B The graph shows the average area of RhoD depleted HeLa cells, with or without H1152 (**A**) or C3 (**B**) treatment, and infected with ΔF11L at 3:40hpi. Error bars represent SEM from three independent experiments in which approximately 70 cells were counted. Statistical significance was determined by a one-way Anova, indicated by * P<0.05, ** P<0.01 and *** P<0.001. **C** Immuno blot analysis of RhoD, RhoC and actin protein levels in HeLa that have been transfected with the indicated siRNA for 72 hours. **D** The graphs shows the average area of HeLa cells depleted of RhoD or RhoD and RhoC. Error bars represent SEM from three independent experiments in which approximately 65 cells were counted in each condition. Statistical significance was determined by a one-way Anova, indicated by *** P<0.001.

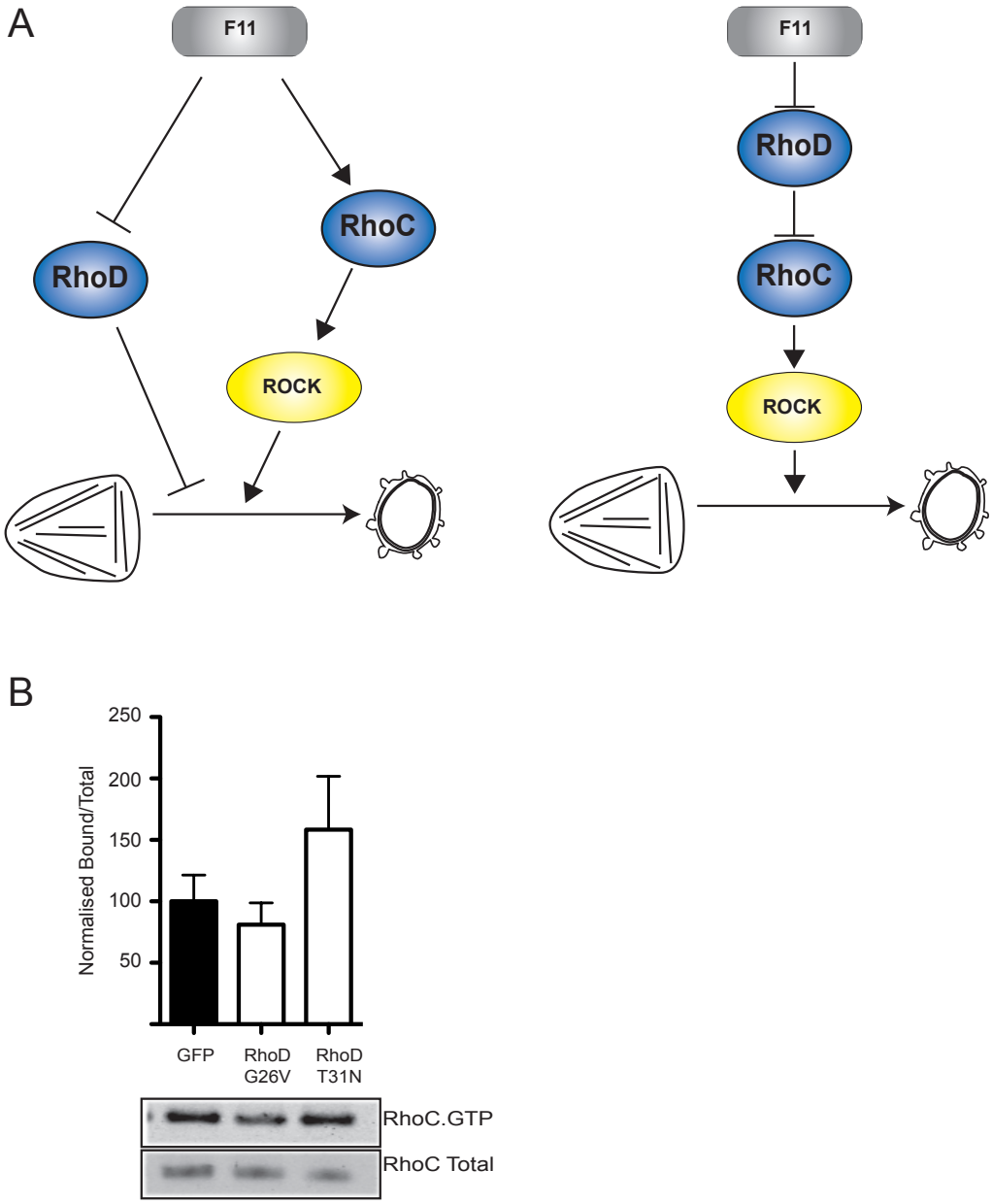

Figure 5.11 Inactivation of RhoD leads to an increase in RhoC activity

A A schematic of F11 stimulating cell contraction through two independent antagonistic pathways or a linear pathway of RhoD, RhoC and ROCK. **B** Rhotekin pull down assays were used to measure that ratio of GTP bound RhoC compared to total RhoC, in uninfected U-2 OS that had been transfected with GFP, GFP-RhoD G26V or GFP-RhoD T31N. U-2 OS cells were serum starved for 24 hours and stimulated with 20% FBS for 5 minutes prior to cell lysis. Error bars represent SEM from four independent experiments. The immuno blot illustrates a representative assay.

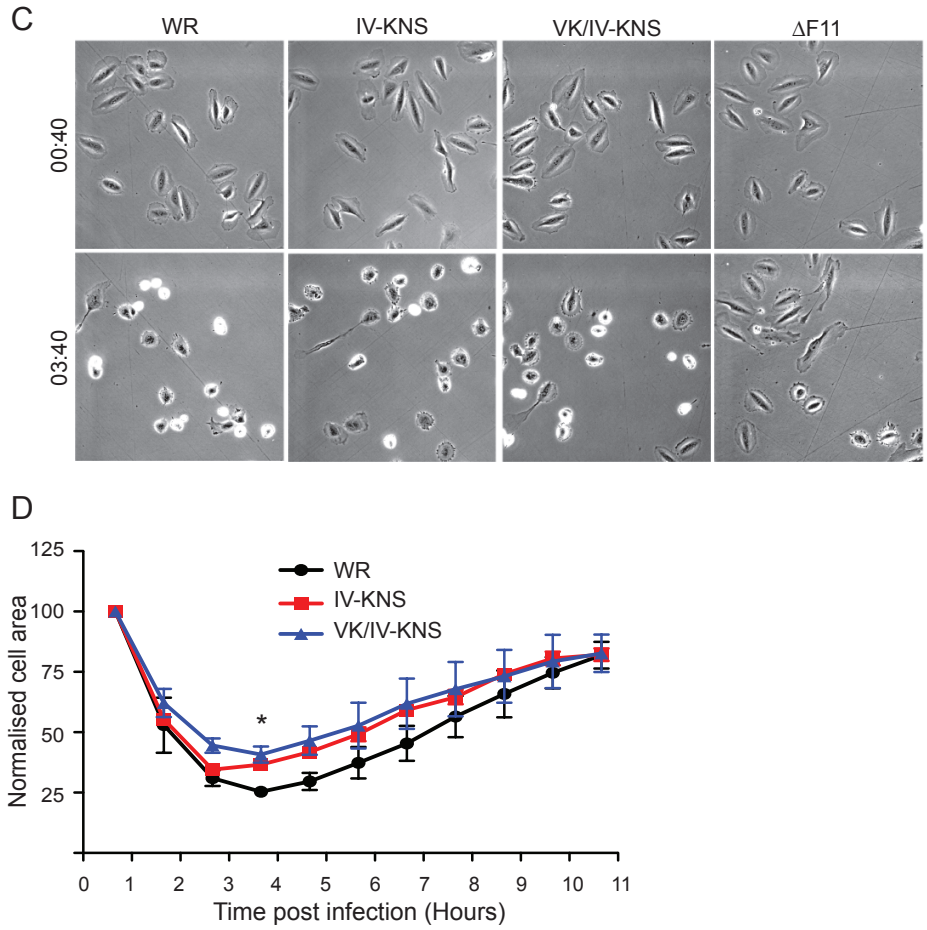

Figure 5.12 The F11 RhoD binding mutant stimulates cell contraction

A The alignment of F11 and the Rho binding domain of the RhoD effector hDia2C (mDia3). **B** Glutathione pull down from infected HeLa cell lysates expressing GST-F11 mutants and GFP-RhoD. The mutation of IV-KNS abrogated RhoD binding. Both A and B are reproduced from the PhD thesis of João Cordeiro. Cordeiro, J.V. (2008). Modulation of Rho GTPase signalling during vaccinia virus infection (UCL). *Parts A and B of this figure have been removed in the electronic copy of this thesis.*
C Still phase images from a time-lapse movie of HeLa cells infected with the indicated virus strains. **D** The graph shows the changes in cell area over time post infection with WR, F11-IV-KNS, F11-VK/IV-KNS. Error bars represent SEM from three independent in which a total of approximately 70 cells were analysed for each virus. Statistical significance was determined by a one-way Anova, indicated by * $P<0.05$.

Chapter 6. Discussion

The aim of this thesis was to characterise vaccinia induced cell contraction and elucidate the vaccinia and cellular components required. I confirmed that cell contraction occurs early during infection and was associated with dynamic plasma membrane blebbing. Using a virus that does not express the vaccinia protein F11, I showed that F11 was required for virus infection to stimulate contraction. However, using the highly attenuated virus rescued with wild type F11, MVA-F11, I found that cell contraction additionally required other vaccinia proteins. Despite previous evidence showing F11 interacts with RhoA, I found that cell contraction was independent of RhoA and instead required RhoC to ROCK signalling. In addition, I discovered that RhoD negatively regulates vaccinia-induced contraction, most likely by inhibiting RhoC activation, and suggest that RhoD signalling is inhibited during infection to allow for efficient cell contraction.

6.1 F11 induced cell contraction

F11 is a vaccinia protein that is expressed early in infection. Previous work from our laboratory showed that F11 binds to RhoA, using a small region of homology with the RhoA binding domain of ROCK (Valderrama et al., 2006). At 8hpi, F11 inhibits RhoA signalling to mDia1 to facilitate the release of progeny virus particles (Arakawa et al., 2007a; Arakawa et al., 2007b; Cordeiro et al., 2009). F11 enhances the spread of WR in vivo, and in confluent monolayers of cells in culture (Cordeiro et al., 2009). F11 also augments the spread of MVA and Myxoma virus (Irwin and Evans, 2012; Zwilling et al., 2010). Initial studies have associated F11 with loss of cell-cell adhesion, cell contraction and cell migration (Cordeiro et al., 2009; Morales et al., 2008; Valderrama et al., 2006). However, there are discrepancies in the potential role for F11 in cell contraction. In a study following vaccinia plaque formation by live cell imaging, cell contraction and loss of cell-cell adhesions was dependent on F11 (Cordeiro et al., 2009). In contrast, sparse Ptk2 cells contracted early in vaccinia infection regardless of F11 expression, however, F11 was required for disrupting cell-cell contracts (Morales et al., 2008). I found that F11 is required for cell contraction in HeLa cells. In agreement with Morales *et al.,* however, I find both WR and ΔF11L viruses induce Ptk2 cell contraction (Morales et al., 2008). In part, the observed differences between HeLa and Ptk2 cells might be due to the cell type specificity. Cell contraction could be

caused by more than one vaccinia protein, and perhaps in Ptk2 cells the F11 induced mechanism is not necessary. Indeed, Ptk2 cells are smaller and more phase bright prior to infection, indicating cell contraction signalling pathways may have a higher basal activity, superseding the requirement for F11. In support of the possibility that more than one vaccinia protein is required, the rescue of F11 into the genome of the attenuated virus MVA (MVA-F11L) only partially rescues HeLa cell contraction. Therefore, F11 is necessary but not sufficient for contraction in HeLa cells, but is not required in Ptk2 cells. Other vaccinia proteins must have a dominant role in Ptk2 cells over F11 to account for contraction in the absence of F11. Another possibility that has not been explored is that cell contraction in Ptk2 cells is actually apoptosis. I have ruled this out in HeLa cells because they respread, WR expresses multiple inhibitors of apoptosis and contraction is not blocked by caspase inhibition (Figure 4.1C). However, in my hands, Ptk2 cells infected with either WR or ∆F11L do not re-spread. It would be interesting to explore whether cell contraction in Ptk2 cells is actually apoptotic cell death induced in response to infection. Investigating if caspase inhibition blocks cell contraction would easily address this.

Although my work has identified one protein required for contraction, future work to identify other virus components would be important. As F11 cannot fully rescue cell contraction in MVA, other vaccinia proteins must be required, that are also absent in MVA. The MVA-F11L virus would be a useful tool to screen for the other proteins. Adding back small portions of the CVA genome (the wild type vaccinia strain from which MVA was derived) to MVA-F11L and screening for efficient contraction, could narrow down which proteins are required. This method was used to initially identify F11L (Valderrama et al., 2006). It is essential to use MVA-F11 for this approach; because it is likely the other proteins are necessary but not sufficient so these would only become apparent in conjunction with F11.

6.2 RhoC is required for cell contraction

The cell contraction phenotype during vaccinia infection is reminiscent of rounded cell migration of cancer cells. We thought that activation of RhoA might be involved, especially given that previous work has shown F11 interacts with GTP bound RhoA (Cordeiro et al., 2009). Interestingly, I found F11-induced cell contraction was independent of RhoA (Figure 4.3-4.5). Instead, the highly related RhoC is required for

cell contraction (Figure 5.2-5.5). Surprisingly, using Rhotekin assays I found that the levels of active RhoC are reduced at 3hpi in vaccinia infection (Figure 5.5C). However, this was the case in the presence and absence of F11, so it is unlikely to be indicative of the signalling that occurs during vaccinia induced cell contraction. Furthermore, Rhotekin assays measure the global level of GTP-bound RhoC averaged across thousands of cells. This may not be relevant to the localised events that happen at the plasma membrane during cell contraction. An alternative method is to study the spatio-temporal activity of RhoC by Förster (Fluorescence) resonance energy transfer (FRET) using a RhoC biosensor. The RhoC biosensor comprises of the GTPase, a donor and acceptor fluorophore (eg, CFP and YFP or GFP and RFP) and the Rho binding domain (RBD) of a suitable effector molecule. Upon activation the GTPase and RBD interact, which brings the donor and acceptor into proximity to allow resonance energy transfer. FRET has been useful to study the spatial and temporal activation of RhoA, Rac and Cdc42 during cell migration (Kurokawa and Matsuda, 2005; Machacek et al., 2009; Pertz et al., 2006). Classically, RhoA is believed to mediate contraction of the cell body, while Rac regulates events at the leading edge. However, in non-stimulated migrating cells FRET revealed RhoA activation at the leading edge during membrane protrusion prior to Rac activation (Heasman et al., 2010; Kurokawa and Matsuda, 2005; Machacek et al., 2009; Pertz et al., 2006). This tight spatial regulation would be impossible to detect with a global Rhotekin pull down assay. Recently, a biosensor was used to describe tight spatial regulation of RhoC activity surrounding, but not within, the core of invadopodia (Bravo-Cordero et al., 2011). This biosensor might give us more accurate information regarding the activation of RhoC at the plasma membrane during WR induced cell contraction. It would also be interesting to study spatial RhoC activation in RhoD depleted cells that are infected with ΔF11L, to see whether this replicates the WR situation.

6.2.1 RhoC and ROCK?

My results in Chapter 4 indicate that ROCK is required for cell contraction. This was expected because it is very well established that ROCKI/II activate myosin II mediated cortical contraction (Amano et al., 1996a; Hagerty et al., 2007; Kawano et al., 1999; Kitazawa et al., 2000). The depletion of the individual ROCK proteins has no significant effect on vaccinia-induced contraction. Instead it was necessary to deplete both genes (Figure 4.2). Therefore, it is probable that ROCKI and ROCKII are functionally

redundant in this phenotype. It is not clear if the three ROCK inhibitors used in this study have different specificities towards ROCKI or ROCKII. Given the 92% identity in the kinase domains it is likely that the compounds inhibit both proteins, especially as they can target several unrelated kinases (Bain et al., 2007; Davies et al., 2000; Leung et al., 1996; Nakagawa et al., 1996; Nichols et al., 2009). From my siRNA data, I have concluded that both ROCK proteins are involved in cell contraction. It is worth noting that siRNA of ROCKII alone has a slightly greater effect than ROCKI (Figure 4.2). This could simply be due to more efficient depletion of ROCKII compared with ROCKI, although this is not discernable by immuno blot. Or perhaps, activating cell contraction through ROCKII is the preferred mechanism but in its absence, vaccinia can still induce cell contraction via ROCKI, albeit less efficiently.

I have assumed that in vaccinia-induced cell contraction, ROCK is the main effector of RhoC. My results certainly suggest they are in the same pathway because depletion of RhoC and ROCK does not have an additive affect in blocking cell contraction (Figure 5.4). Although ROCK is the obvious effector of RhoC in vaccinia-mediated cell contraction, it would be interesting to see if there is any role for specific RhoC effectors. Recently, the formins FMNL2 and FMNL3 were identified as putative RhoC specific effectors (Kitzing et al., 2010; Vega et al., 2011). FMNL2 and FMNL3 both interacted with RhoC, not RhoA and RhoB, and were shown to mediate RhoC specific cell morphology changes (Kitzing et al., 2010; Vega et al., 2011). Interestingly, FMNL2 was important for RhoC driven amoeboid cell migration in 3D invasion assays (Kitzing et al., 2010). Like other members of the formin family, FMNL3 can drive actin nucleation and polymerisation from actin monomers via the FH2 domain (Heimsath and Higgs, 2012). This has not yet been examined for FMNL2. From several functional studies, it has been suggested that other members of the formin family (mDia2, FMNL1 and FHOD1) might mediate the assembly of actin in the cortex (Eisenmann et al., 2007; Han et al., 2009; Hannemann et al., 2008). The studies by Kitzing *et al.,* and Vega *et al.,* suggest that RhoC mediates cell contraction by regulating actin cortex assembly through FMNL2 and/or FMNL3. It would be interesting to examine if FMNL2 and FMNL3 participate in vaccinia-induced cell contraction. This could initially be done by RNAi-mediated silencing of FMNL2 and FMNL2 then possibly extended to the entire formin family.

6.2.2 Do F11 and RhoC interact?

We have previously suggested that F11 binds to RhoA by mimicking the ROCK LxxTxxVxKL motif in the RhoA binding domain (Valderrama et al., 2006). In pull downs from infected cell lysates, mutation of the valine and second lysine in this motif of F11 abrogates binding with RhoA. While under the same conditions, F11 and F11-VK can both interact with RhoC (Figure 5.1) (Cordeiro, 2008). However, this does not necessarily predict direct interactions. Indeed, João Cordeiro performed binding assays with purified recombinant protein and was unable to show a direct interaction between F11 and RhoC. However, F11 was able to directly interact with RhoA, RhoD, RhoE and Rif (Cordeiro, 2008). This would suggest that in contrast to RhoA, F11 must interact with RhoC indirectly via other proteins. However, this experiment lacked a control to show that RhoC was correctly folded when expressed in *E.coli* and under the particular assay conditions. A suitable positive control would be the Rho binding domain of ROCK.

If we assume that F11 and F11-VK both directly interact with RhoC (in agreement with the pull down from cell lysates), this would mean that F11 adopts an alternative mechanism to bind RhoC compared to RhoA. Understanding how would give important insights into the possible mechanisms mediating the specificity of RhoA and RhoC. The crystal structure of RhoA in complex with ROCK1 revealed that the Rho amino acids P36, V38, F39, E40, Q63, D65, Y66, R68, L69 and L72 mediate interactions with ROCK (Dvorsky et al., 2004). These residues are entirely conserved between RhoA and RhoC so it is likely that RhoC interacts with and activates ROCK in the same manner, although the crystal structure for RhoC and ROCK has yet to be determined. This is also true of regions involved in GEF and GAP binding (Figure 1.11). The one exception is at residue 43, which is valine (Val) in RhoA, but isoleucine (Ile) in RhoC. Structural studies have shown that Val43 participates in the interactions of RhoA with some GEFs or the effector PKN1, but not ROCK1 (Dvorsky et al., 2004; Maesaki et al., 1999; Sloan et al., 2012). Substitution of Val43 for Ile showed that the identity of this residue confers specificity of GEFs towards RhoA or RhoC (Sloan et al., 2012). As Ile has a bulkier hydrophobic side chain compared to Val, it is possible that Ile could disrupt binding to certain effectors and GEFs or alternatively mediate RhoC specific binding as this side chain could plug deeper into hydrophobic pockets. Perhaps Ile43 in RhoC is important for mediating an interaction with F11 outside of the LxxTxxVxKL motif. F11 only mimics ROCK within a very small region, otherwise there is no

additional sequence similarity. In contrast to the RhoA:ROCK complex, additional contact sites may exist between F11 and Rho. In binding to RhoA, these sites may provide a minor role compared to the LxxTxxVxKL contact site. Perhaps the additional sites are more important for F11 and RhoC interactions and compensate for the loss of VK within LxxTxxVxKL. RhoA and RhoC are more divergent towards their C-terminus, which might provide some difference in their binding strength with F11.

If the *in vitro* binding assay performed by João Cordeiro does represent the correct result, then F11 does not interact with RhoC. RhoC must therefore be in complex with F11 via intermediate proteins. The same question exists, why can F11 bind RhoA but not the extremely similar RhoC? Again, the difference in binding between RhoA and RhoC could be accounted for by the valine to isoleucine substitution or the C-terminus. In either circumstance the conundrum of F11 interactions with RhoA and RhoC warrants further investigation as this could help understand how the very similar proteins mediate different biological phenotypes during vaccinia infection. It is clear that the difference between RhoA and RhoC binding to F11 is an important determinant for why RhoC, and not RhoA, is required for cell contraction. Future work should concentrate first on confirming if and how F11 and RhoC interact, and if this interaction is important for F11 mediated cell contraction. Ultimately a full molecular understanding of the specificity of F11 for RhoA and RhoC will only come from solving the structure of F11 with each Rho protein.

6.3 RhoD and cell contraction

In Chapter 5 I investigated a potential role for RhoD in cell contraction (Figures 5.6-5.12). In cells depleted of RhoD, the ΔF11L virus can induce cell contraction in a temporal manner reminiscent of WR-induced contraction. Rescuing RNAi treated cells with constitutively active or wild type, but not dominant negative RhoD, reversed this phenotype. Expression of constitutively active RhoD in WR infected cells also blocked cell contraction. Taken together, the results indicate that RhoD inhibits cell contraction and suggest that RhoD signalling must be shut down to allow WR-induced cell contraction.

6.3.1 How does RhoD antagonise RhoC?

In cells depleted of RhoD, cell contraction during ΔF11L infection is dependent on ROCK and RhoC signalling. This led me to hypothesise that RhoD antagonises RhoC/ROCK in uninfected cells as well as during ΔF11L infection. In uninfected cells the expression of dominant negative RhoD (T31N) leads to increased levels of RhoC bound to GTP (Figure 5.11). However, the effects of the RhoD T31N mutant must be interpreted with caution because this mutant could bind and sequester GEFs that act towards multiple Rho GTPases. For example, it is not known if any GEFs stimulate nucleotide exchange in both RhoC and RhoD. If this were the case then the observed increase in RhoC-GTP levels could be an artefact of RhoD T31N sequestering RhoC GEFs. Confidence in a true antagonism of RhoC by RhoD could be verified by investigating RhoC-GTP levels in cells depleted of RhoD.

If RhoD does antagonise RhoC, this raises the question of how crosstalk between the two proteins occurs. There are many examples of crosstalk between members of the Rho GTPase family (see 1.2.6). This can occur at the level of GEFs and GAPs. The upstream Rho GTPase can either modulate the activity of these regulatory proteins by direct interactions or via its effector molecules. (Guilluy et al., 2011). As an example, Rac1 and RhoE can antagonise RhoA activity by binding to and relieving the auto-inhibition of the p190RhoGAP (Bustos et al., 2008; Wennerberg et al., 2003). As p190RhoGAP can also inactivate RhoC, RhoD might employ a similar antagonistic mechanism (Bravo-Cordero et al., 2011). Alternatively, if RhoC and RhoD can be activated by the same GEFs, RhoD could suppress RhoC activity by competitive interactions with the GEF. Currently, there are very few confirmed RhoD effectors (Figure 6.1A). RhoD is proposed to signal through mDia1 and a splice variant of mDia3 (hDia2C), to regulate centrosome duplication and endosome dynamics, respectively (Gasman et al., 2003; Kyrkou et al., 2012). In addition, RhoD can interact with and regulate the localisation of PAK5. Constitutively active RhoD binds particularly well to PAK5 (Wu and Frost, 2006). This raises the possibility that PAK5 is also an effector of RhoD. A post-doctoral researcher in our group, Yutaka Handa, investigated whether RhoD can interact with members of the PAK family, PAK1-6. In pull down experiments from cell lysates, RhoD could bind PAK1 and PAK4-6. It would be interesting to investigate whether these kinases are bona fide effectors of RhoD, by looking for direct interactions that are specific to GTP bound RhoD. There are several known examples of crosstalk between Rac1 and RhoA that involve PAK1 and/or PAK4. Particularly,

PAK1 and PAK4 phosphorylate p115 RhoGEF, GEF-H1, PDZ-RhoGEF and Net1 (Alberts et al., 2005; Barac et al., 2004; Rosenfeldt et al., 2006; Zenke et al., 2004). Phosphorylation inhibits GEFs by mis-localisation or reducing their nucleotide exchange activity. Although, these studies only investigate PAK1 and PAK4 mediated antagonism of RhoA, these GEFs (with the exception of Net1) additionally regulate RhoB and RhoC activity. Therefore, PAK1 and PAK4 are undoubtedly able to antagonise RhoC.

Combining the evidence that RhoD binds PAK family kinases and PAK1/4 are already known to inactivate RhoC GEFs, RhoD antagonism of RhoC via PAK family kinase is the most likely mechanism for crosstalk (Figure 6.1A). Future work will concentrate on characterising the interactions between RhoD and PAK family members and examining a role for PAK in supressing RhoC. In addition we will investigate the effects on vaccinia induced cell contraction by depleting PAK proteins in the presence or absence of F11.

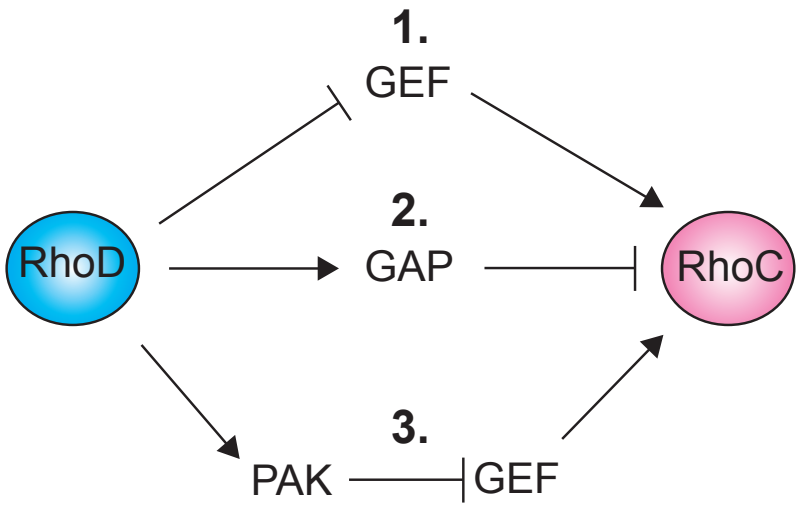

Figure 6.1 The potential mechanisms for RhoD mediated antagonism of RhoC

1) Competitive binding of RhoD with a RhoC GEF. 2) RhoD binds and activates a Rho GAP by relieving intrinsic auto-inhibition. 3) RhoD activates a member of the PAK family, which phosphorylates a GEF to inhibit its activity towards RhoC.

6.3.2 F11 inhibits RhoD to promote RhoC dependent cell contraction

In his PhD studies, João Cordeiro, found that F11 directly interacts with RhoD. This interaction is mediated by an IV-KNS motif, which is also present in a splice variant of mDia3 (hDia2C) that binds RhoD (Figure 5.12). João found that F11 preferentially binds GDP bound RhoD. In addition, João developed a RhoD activation assay, using the RhoD binding motif of mDia3, and found that F11 activates RhoD at 8hpi (Cordeiro, 2008). In contrast, my results indicate that RhoD signalling must be turned off at 3hpi, as it is inhibitory to vaccinia-induced cell contraction. Because cell contraction in the absence of F11 can only occur when RhoD is depleted, and based on the direct interaction between the two proteins, I suggest that F11 could inhibit RhoD in WR infection at 3hpi. This should be confirmed using João's RhoD activation assay. F11 could inhibit RhoD by binding to and sequestering GDP bound RhoD to prevent its activation. However, cell contraction is still induced by the F11-IV-KNS recombinant virus, although it is less efficient than WR. This indicates that an interaction between the two proteins is not required. Perhaps during cell contraction, F11 does not physically inhibit RhoD, rather it protects RhoC from inhibition by RhoD. F11 could do so by recruiting a RhoD specific GAP to the plasma membrane to locally inactivate RhoD in the vicinity. The G26V mutant of RhoD is resistant to GAP mediated GTP hydrolysis, therefore, this mutant is able to supress cell contraction even when F11 is present.

RhoC is required for cell contraction but it is not clear whether RhoC activation is actually mediated by F11. During ΔF11L infection, cell contraction does not occur, presumably because RhoD suppresses RhoC activation. When RhoD is depleted RhoC-dependent vaccinia-induced cell contraction can occur. If preventing RhoD inhibition of RhoC was the only contributing factor to vaccinia-induced cell contraction, then surely RhoD depleted cells would be constitutively contracted regardless of vaccinia infection. However, this is not the case as infection with ΔF11L stimulates temporal contraction, indicating a temporal activation of RhoC. Therefore, it is likely that another vaccinia protein activates RhoC, and that sufficient activation to drive cell contraction is only achieved in addition to RhoD suppression. From studies with MVA-F11, I know that at least one other protein contributes to cell contraction with F11. In this virus perhaps F11 inhibits RhoD to prevent antagonism of RhoC, but robust cell contraction cannot occur because the protein that fully activates RhoC is not expressed.

6.3.3 Working model

From the results in this thesis I suggest the following model for vaccinia induced cell contraction. Early in infection, F11 localises to the plasma membrane where it recruits a RhoD GAP and locally inhibits RhoD activity (Figure 6.2 B). Additionally, F11 recruits RhoC to the vicinity where it is protected from RhoD antagonism and is activated by another vaccinia protein. RhoC activates ROCK activity to stimulate myosin II driven contraction of the actin cortex. When F11 is not present, RhoD antagonises RhoC activity using PAK mediated inactivation of RhoC GEFs.

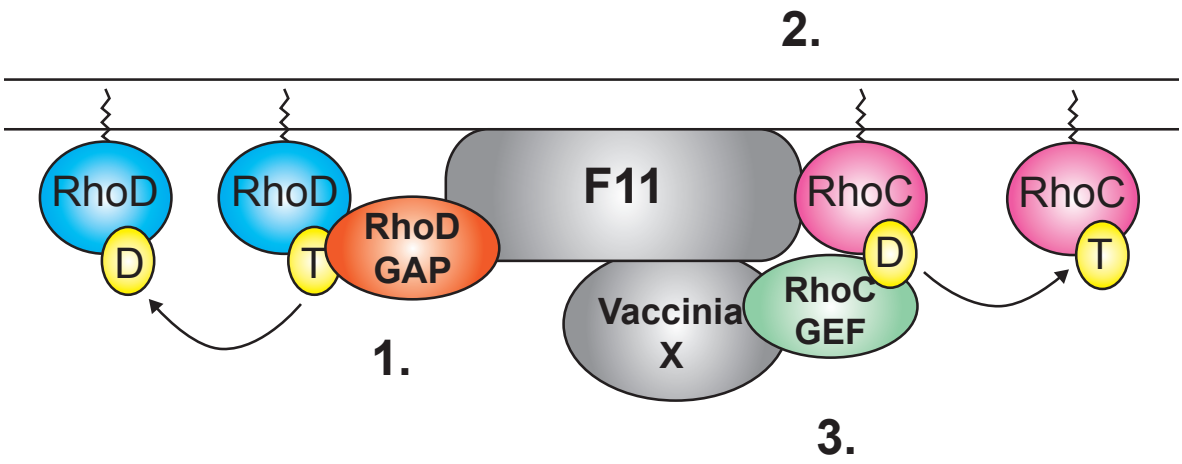

Figure 6.2 A hypothetical model of F11-RhoD-RhoC signalling

1) F11 localises to the plasma membrane and recruits a RhoD GAP. This GAP locally supresses RhoD activity. 2) F11 recruits RhoC to areas where RhoD is supressed. 3) An unidentified vaccinia protein (Vaccinia X) activates RhoC.

The work presented in this thesis concentrates on the signalling pathways that lead to vaccinia induced cell contraction but does not consider how the subsequent re-spreading occurs. I suggest that re-spreading is dependent on the expression of

vaccinia late proteins (Figure 3.3). As yet we do not know the identity of the vaccinia protein/s or how these proteins stimulate re-spreading.

There are two possible mechanisms for re-spreading. Firstly, the expression of late vaccinia proteins could activate a signalling pathway that promotes re-spreading. Rac dependent signalling is a likely mechanism, as Rac can inhibit RhoA signalling (which is presumably also true of RhoC) and induce lamellipodia and cell spreading (Ridley et al., 1992). Treating WR infected cells at 3hpi with Rac inhibitors and measuring the ability of the contracted cells to re-spread could easily test this. Similarly, a candidate based small molecule screen could be conducted to identify additional host proteins required for re-spreading.

Alternatively, the second possible mechanism is that cell re-spreading is not induced but rather cell contraction is turned off. Intriguingly, the levels of F11 protein, as detected by immuno blotting, coincide strikingly with the onset and termination of cell contraction and blebbing (Figure 3.6). The protein is detected from 1:30hpi, most abundant between 3-4hpi and begins to decrease form 5hpi onwards. This could suggest that a threshold level of F11 is required to induce and maintain cell contraction. Indeed, when late gene expression is blocked the level of F11 does not significantly decrease (Figure 3.3). This might explain why when late protein expression is blocked, cell contraction is sustained. It raises the possibility that vaccinia late proteins direct the reduction in F11 levels possibly through degradation or proteolytic cleavage.

6.4 What is the role of contraction in vaccinia spread?

In this thesis I have studied vaccinia-induced cell contraction in cells in culture. Although the purpose of my work was to use vaccinia virus as a tool to understand novel cellular mechanisms that can lead to cell contraction it would be interesting to understand how this contributes to vaccinia infection *in vivo*.

Previous data shows that F11 significantly contributes to virus spread in culture and *in vivo* (Cordeiro et al., 2009; Irwin and Evans, 2012; Zwilling et al., 2010). However, my work now shows that F11 probably has two different functions during vaccinia infection. At early stages of infection F11 stimulates cell contraction, whilst at later stages F11 facilitates virus release by modulating actin cortex and MT dynamics (Arakawa et al.,

2007a; Arakawa et al., 2007b; Cordeiro et al., 2009). Therefore, it is difficult to delineate the contribution of each F11 function to virus spread. The F11-VK virus is a useful tool to help us separate F11 functions. F11-VK stimulates efficient cell contraction but virus release is equally impaired during F11-VK and ∆F11L infections. F11-VK spreads better than ∆F11L in plaque assays and *in vivo*, and this potentially highlights a contribution for cell contraction in virus spread. An alternative approach would be to temporally separate F11 functions. It would interesting to generate a recombinant virus where F11 is expressed from a late vaccinia promoter rather than the endogenous early promoter. If this virus did not stimulate cell contraction, but virus release was not impaired relative to WR then this virus could be used to understand what contribution F11 stimulated cell contraction made to F11 mediated virus spread.

My study does not allow us to determine whether cell contraction is a physiologically relevant mechanism for virus spread and it possible that it is entirely an artefact of cell culture substrates, culturing conditions and/or cell lines used. Cell contraction and associated plasma membrane blebbing has been observed in many cancer cell lines in culture and is thought to contribute to a proteolytic-independent mode of migration *in vivo* (Friedl and Wolf, 2003, 2010; Wolf et al., 2003). Given the visual similarity and its dependence on ROCK signalling it is possible that vaccinia-induced contraction is necessary to facilitate the 3D migration of infected cells in tissues and thereby increase virus spread. However, this is just a hypothesis and we do not have adequate assays to test the relevance of cell contraction, if any, to virus spread. Currently, we can either image virus spread through confluent monolayers of cells seeded onto plastic, or measure the virus titre in different organs following intranasal inoculation of mice (Cordeiro et al., 2009). Both assays have significant limitations, the first assay is too artificial to give us physiological relevant information, while the second does not allow us to gain any information about infection on a single cell level. It would be useful to develop an organotypic cell culture assay that represents the site of vaccinia infection, such as the trachea epithelium or skin (Buller and Palumbo, 1991), while allowing for the imaging resolution required to visualise cell morphology changes.

6.5 Future perspectives

The working model for F11-stimulated cell contraction is based on my results in conjunction with evidence from the literature (Section 6.3.3). But many of the

suggested steps require experimental confirmation. This presents several avenues for future research. If F11 inhibits RhoD activity it is clearly not through a direct interaction, this warrants exploration to identify the mediating regulatory protein. Currently, the regulatory molecules acting on RhoD are not known, therefore solving this could have wider implications in the understanding of the cellular function of RhoD. Potentially RhoD supresses RhoC activity, immediate future work should concentrate on validating this hypothesis and identifying the molecular players. Given that RhoD can bind members of the PAK family, we suspect that PAK mediated inhibition of RhoC GEFs is important. RhoC and ROCK expression often correlate with the metastatic potential of tumours and poor prognosis. If RhoD is a true suppressor of RhoC, is there any evidence that RhoD expression inversely correlates with RhoC in cancers? My work has started to explore the regulatory mechanism for WR induced cell contraction but have not addressed how contraction is turned off. It would be interesting to identify the mechanisms behind cell re-spreading and elucidate how the same cell can display such strikingly different morphologies at different points in vaccinia infection. Answers to this question could contribute to the understanding of how cancer cells achieve similar morphology switches when they encounter different extracellular environments.

Reference List

Abdul-Manan, N., Aghazadeh, B., Liu, G.A., Majumdar, A., Ouerfelli, O., Siminovitch, K.A., and Rosen, M.K. (1999). Structure of Cdc42 in complex with the GTPase-binding domain of the 'Wiskott-Aldrich syndrome' protein. Nature *399*, 379-383.

Abe, H., Kamai, T., Tsujii, T., Nakamura, F., Mashidori, T., Mizuno, T., Tanaka, M., Tatsumiya, K., Furuya, N., Masuda, A*., et al.* (2008). Possible role of the RhoC/ROCK pathway in progression of clear cell renal cell carcinoma. Biomed Res *29*, 155-161.

Abe, T., Kato, M., Miki, H., Takenawa, T., and Endo, T. (2003). Small GTPase Tc10 and its homologue RhoT induce N-WASP-mediated long process formation and neurite outgrowth. J Cell Sci *116*, 155-168.

Adamson, P., Marshall, C.J., Hall, A., and Tilbrook, P.A. (1992a). Post-translational modifications of p21rho proteins. J Biol Chem *267*, 20033-20038.

Adamson, P., Paterson, H.F., and Hall, A. (1992b). Intracellular localization of the P21rho proteins. J Cell Biol *119*, 617-627.

Aktories, K., Braun, U., Rosener, S., Just, I., and Hall, A. (1989). The rho gene product expressed in E. coli is a substrate of botulinum ADP-ribosyltransferase C3. Biochem Biophys Res Commun *158*, 209-213.

Aktories, K., and Hall, A. (1989). Botulinum ADP-ribosyltransferase C3: a new tool to study low molecular weight GTP-binding proteins. Trends in pharmacological sciences *10*, 415-418.

Alberts, A.S. (2001). Identification of a carboxyl-terminal diaphanous-related formin homology protein autoregulatory domain. J Biol Chem *276*, 2824-2830.

Alberts, A.S., Qin, H., Carr, H.S., and Frost, J.A. (2005). PAK1 negatively regulates the activity of the Rho exchange factor NET1. J Biol Chem *280*, 12152-12161.

Amano, M., Chihara, K., Kimura, K., Fukata, Y., Nakamura, N., Matsuura, Y., and Kaibuchi, K. (1997). Formation of actin stress fibers and focal adhesions enhanced by Rho-kinase. Science *275*, 1308-1311.

Amano, M., Chihara, K., Nakamura, N., Kaneko, T., Matsuura, Y., and Kaibuchi, K. (1999). The COOH terminus of Rho-kinase negatively regulates rho-kinase activity. J Biol Chem *274*, 32418-32424.

Amano, M., Ito, M., Kimura, K., Fukata, Y., Chihara, K., Nakano, T., Matsuura, Y., and Kaibuchi, K. (1996a). Phosphorylation and activation of myosin by Rho-associated kinase (Rho-kinase). J Biol Chem *271*, 20246-20249.

Amano, M., Mukai, H., Ono, Y., Chihara, K., Matsui, T., Hamajima, Y., Okawa, K., Iwamatsu, A., and Kaibuchi, K. (1996b). Identification of a putative target for Rho as the serine-threonine kinase protein kinase N. Science *271*, 648-650.

Amano, T., Tanabe, K., Eto, T., Narumiya, S., and Mizuno, K. (2001). LIM-kinase 2 induces formation of stress fibres, focal adhesions and membrane blebs, dependent on its activation by Rho-associated kinase-catalysed phosphorylation at threonine-505. The Biochemical journal *354*, 149-159.

Antoine, G., Scheiflinger, F., Dorner, F., and Falkner, F.G. (1998). The complete genomic sequence of the modified vaccinia Ankara strain: comparison with other orthopoxviruses. Virology *244*, 365-396.

Arakawa, Y., Cordeiro, J.V., Schleich, S., Newsome, T.P., and Way, M. (2007a). The release of vaccinia virus from infected cells requires RhoA-mDia modulation of cortical actin. Cell Host Microbe *1*, 227-240.

Arakawa, Y., Cordeiro, J.V., and Way, M. (2007b). F11L-mediated inhibition of RhoA-mDia signaling stimulates microtubule dynamics during vaccinia virus infection. Cell Host Microbe *1*, 213-226.

Arber, S., Barbayannis, F.A., Hanser, H., Schneider, C., Stanyon, C.A., Bernard, O., and Caroni, P. (1998). Regulation of actin dynamics through phosphorylation of cofilin by LIM-kinase. Nature *393*, 805-809.

Armstrong, J.A., Metz, D.H., and Young, M.R. (1973). The mode of entry of vaccinia virus into L cells. J Gen Virol *21*, 533-537.

Arthur, W.T., Ellerbroek, S.M., Der, C.J., Burridge, K., and Wennerberg, K. (2002). XPLN, a guanine nucleotide exchange factor for RhoA and RhoB, but not RhoC. J Biol Chem *277*, 42964-42972.

Aspenstrom, P., Fransson, A., and Saras, J. (2004). Rho GTPases have diverse effects on the organization of the actin filament system. The Biochemical journal *377*, 327-337.

Aspenstrom, P., Ruusala, A., and Pacholsky, D. (2007). Taking Rho GTPases to the next level: the cellular functions of atypical Rho GTPases. Experimental cell research *313*, 3673-3679.

Assarsson, E., Greenbaum, J.A., Sundstrom, M., Schaffer, L., Hammond, J.A., Pasquetto, V., Oseroff, C., Hendrickson, R.C., Lefkowitz, E.J., Tscharke, D.C.*, et al.* (2008). Kinetic analysis of a complete poxvirus transcriptome reveals an immediate-early class of genes. Proc Natl Acad Sci U S A *105*, 2140-2145.

Bablanian, R., Baxt, B., Sonnabend, J.A., and Esteban, M. (1978). Studies on the mechanisms of vaccinia virus cytopathic effects. II. Early cell rounding is associated with virus polypeptide synthesis. J Gen Virol *39*, 403-413.

Bain, J., Plater, L., Elliott, M., Shpiro, N., Hastie, C.J., McLauchlan, H., Klevernic, I., Arthur, J.S., Alessi, D.R., and Cohen, P. (2007). The selectivity of protein kinase inhibitors: a further update. The Biochemical journal *408*, 297-315.

Baldick, C.J., Jr., and Moss, B. (1993). Characterization and temporal regulation of mRNAs encoded by vaccinia virus intermediate-stage genes. J Virol *67*, 3515-3527.

Barac, A., Basile, J., Vazquez-Prado, J., Gao, Y., Zheng, Y., and Gutkind, J.S. (2004). Direct interaction of p21-activated kinase 4 with PDZ-RhoGEF, a G protein-linked Rho guanine exchange factor. J Biol Chem *279*, 6182-6189.

Baroudy, B.M., and Moss, B. (1982). Sequence homologies of diverse length tandem repetitions near ends of vaccinia virus genome suggest unequal crossing over. Nucleic acids research *10*, 5673-5679.

Bergert, M., Chandradoss, S.D., Desai, R.A., and Paluch, E. (2012). Cell mechanics control rapid transitions between blebs and lamellipodia during migration. Proc Natl Acad Sci U S A.

Berthold, J., Schenkova, K., and Rivero, F. (2008). Rho GTPases of the RhoBTB subfamily and tumorigenesis. Acta pharmacologica Sinica *29*, 285-295.

Bishop, A.L., and Hall, A. (2000). Rho GTPases and their effector proteins. The Biochemical journal *348 Pt 2*, 241-255.

Boriack-Sjodin, P.A., Margarit, S.M., Bar-Sagi, D., and Kuriyan, J. (1998). The structural basis of the activation of Ras by Sos. Nature *394*, 337-343.

Bos, J.L., Rehmann, H., and Wittinghofer, A. (2007). GEFs and GAPs: critical elements in the control of small G proteins. Cell *129*, 865-877.

Boulter, E., Estrach, S., Garcia-Mata, R., and Feral, C.C. (2012). Off the beaten paths: alternative and crosstalk regulation of Rho GTPases. FASEB journal : official publication of the Federation of American Societies for Experimental Biology *26*, 469-479.

Boulter, E., Garcia-Mata, R., Guilluy, C., Dubash, A., Rossi, G., Brennwald, P.J., and Burridge, K. (2010). Regulation of Rho GTPase crosstalk, degradation and activity by RhoGDI1. Nat Cell Biol *12*, 477-483.

Boureux, A., Vignal, E., Faure, S., and Fort, P. (2007). Evolution of the Rho family of ras-like GTPases in eukaryotes. Molecular biology and evolution *24*, 203-216.

Bourne, H.R. (1997). G proteins. The arginine finger strikes again. Nature *389*, 673-674.

Braun, U., Habermann, B., Just, I., Aktories, K., and Vandekerckhove, J. (1989). Purification of the 22 kDa protein substrate of botulinum ADP-ribosyltransferase C3 from porcine brain cytosol and its characterization as a GTP-binding protein highly homologous to the rho gene product. FEBS Lett *243*, 70-76.

Bravo-Cordero, J.J., Oser, M., Chen, X., Eddy, R., Hodgson, L., and Condeelis, J. (2011). A novel spatiotemporal RhoC activation pathway locally regulates cofilin activity at invadopodia. Curr Biol *21*, 635-644.

Bray, D., and White, J.G. (1988). Cortical flow in animal cells. Science *239*, 883-888.

Broyles, S.S. (2003). Vaccinia virus transcription. J Gen Virol *84*, 2293-2303.

Brugnera, E., Haney, L., Grimsley, C., Lu, M., Walk, S.F., Tosello-Trampont, A.C., Macara, I.G., Madhani, H., Fink, G.R., and Ravichandran, K.S. (2002). Unconventional Rac-GEF activity is mediated through the Dock180-ELMO complex. Nat Cell Biol *4*, 574-582.

Buller, R.M., and Palumbo, G.J. (1991). Poxvirus pathogenesis. Microbiological reviews *55*, 80-122.

Burgess, S.A., Yu, S., Walker, M.L., Hawkins, R.J., Chalovich, J.M., and Knight, P.J. (2007). Structures of smooth muscle myosin and heavy meromyosin in the folded, shutdown state. J Mol Biol *372*, 1165-1178.

Bustos, R.I., Forget, M.A., Settleman, J.E., and Hansen, S.H. (2008). Coordination of Rho and Rac GTPase function via p190B RhoGAP. Curr Biol *18*, 1606-1611.

Campellone, K.G., and Welch, M.D. (2010). A nucleator arms race: cellular control of actin assembly. Nature reviews Molecular cell biology *11*, 237-251.

Carlier, M.F., Laurent, V., Santolini, J., Melki, R., Didry, D., Xia, G.X., Hong, Y., Chua, N.H., and Pantaloni, D. (1997). Actin depolymerizing factor (ADF/cofilin) enhances the rate of filament turnover: implication in actin-based motility. J Cell Biol *136*, 1307-1322.

Carter, G.C., Law, M., Hollinshead, M., and Smith, G.L. (2005). Entry of the vaccinia virus intracellular mature virion and its interactions with glycosaminoglycans. J Gen Virol *86*, 1279-1290.

Carter, G.C., Rodger, G., Murphy, B.J., Law, M., Krauss, O., Hollinshead, M., and Smith, G.L. (2003). Vaccinia virus cores are transported on microtubules. J Gen Virol *84*, 2443-2458.

Chang, F.K., Sato, N., Kobayashi-Simorowski, N., Yoshihara, T., Meth, J.L., and Hamaguchi, M. (2006). DBC2 is essential for transporting vesicular stomatitis virus glycoprotein. J Mol Biol *364*, 302-308.

Chang, L., Chiang, S.H., and Saltiel, A.R. (2007). TC10alpha is required for insulin-stimulated glucose uptake in adipocytes. Endocrinology *148*, 27-33.

Chardin, P. (2006). Function and regulation of Rnd proteins. Nature reviews Molecular cell biology *7*, 54-62.

Chardin, P., Boquet, P., Madaule, P., Popoff, M.R., Rubin, E.J., and Gill, D.M. (1989). The mammalian G protein rhoC is ADP-ribosylated by Clostridium botulinum exoenzyme C3 and affects actin microfilaments in Vero cells. EMBO J *8*, 1087-1092.

Charras, G., and Paluch, E. (2008). Blebs lead the way: how to migrate without lamellipodia. Nature reviews Molecular cell biology *9*, 730-736.

Charras, G.T. (2008). A short history of blebbing. Journal of microscopy *231*, 466-478.

Charras, G.T., Coughlin, M., Mitchison, T.J., and Mahadevan, L. (2008). Life and times of a cellular bleb. Biophysical journal *94*, 1836-1853.

Charras, G.T., Hu, C.K., Coughlin, M., and Mitchison, T.J. (2006). Reassembly of contractile actin cortex in cell blebs. J Cell Biol *175*, 477-490.

Charras, G.T., Yarrow, J.C., Horton, M.A., Mahadevan, L., and Mitchison, T.J. (2005). Non-equilibration of hydrostatic pressure in blebbing cells. Nature *435*, 365-369.

Chen, F., Ma, L., Parrini, M.C., Mao, X., Lopez, M., Wu, C., Marks, P.W., Davidson, L., Kwiatkowski, D.J., Kirchhausen, T.*, et al.* (2000). Cdc42 is required for PIP(2)-induced actin polymerization and early development but not for cell viability. Curr Biol *10*, 758-765.

Chen, Z., Medina, F., Liu, M.Y., Thomas, C., Sprang, S.R., and Sternweis, P.C. (2010). Activated RhoA binds to the pleckstrin homology (PH) domain of PDZ-RhoGEF, a potential site for autoregulation. J Biol Chem *285*, 21070-21081.

Chenette, E.J., Mitin, N.Y., and Der, C.J. (2006). Multiple sequence elements facilitate Chp Rho GTPase subcellular location, membrane association, and transforming activity. Mol Biol Cell *17*, 3108-3121.

Cheng, L., Mahon, G.M., Kostenko, E.V., and Whitehead, I.P. (2004). Pleckstrin homology domain-mediated activation of the rho-specific guanine nucleotide exchange factor Dbs by Rac1. J Biol Chem *279*, 12786-12793.

Chiu, W.L., Lin, C.L., Yang, M.H., Tzou, D.L., and Chang, W. (2007). Vaccinia virus 4c (A26L) protein on intracellular mature virus binds to the extracellular cellular matrix laminin. J Virol *81*, 2149-2157.

Chung, C.S., Hsiao, J.C., Chang, Y.S., and Chang, W. (1998). A27L protein mediates vaccinia virus interaction with cell surface heparan sulfate. J Virol *72*, 1577-1585.

Clark, E.A., Golub, T.R., Lander, E.S., and Hynes, R.O. (2000). Genomic analysis of metastasis reveals an essential role for RhoC. Nature *406*, 532-535.

Clarke, S. (1992). Protein isoprenylation and methylation at carboxyl-terminal cysteine residues. Annual review of biochemistry *61*, 355-386.

Cohen, P. (2010). Guidelines for the effective use of chemical inhibitors of protein function to understand their roles in cell regulation. The Biochemical journal *425*, 53-54.

Collett, G.P., Goh, X.F., Linton, E.A., Redman, C.W., and Sargent, I.L. (2012). RhoE is regulated by cyclic AMP and promotes fusion of human BeWo choriocarcinoma cells. PLoS One *7*, e30453.

Corbetta, S., Gualdoni, S., Albertinazzi, C., Paris, S., Croci, L., Consalez, G.G., and de Curtis, I. (2005). Generation and characterization of Rac3 knockout mice. Mol Cell Biol *25*, 5763-5776.

Corbetta, S., Gualdoni, S., Ciceri, G., Monari, M., Zuccaro, E., Tybulewicz, V.L., and de Curtis, I. (2009). Essential role of Rac1 and Rac3 GTPases in neuronal development. FASEB journal : official publication of the Federation of American Societies for Experimental Biology *23*, 1347-1357.

Cordeiro, J.V. (2008). Modulation of Rho GTPase signalling during vaccinia virus infection (UCL).

Cordeiro, J.V., Guerra, S., Arakawa, Y., Dodding, M.P., Esteban, M., and Way, M. (2009). F11-mediated inhibition of RhoA signalling enhances the spread of vaccinia virus in vitro and in vivo in an intranasal mouse model of infection. PLoS One *4*, e8506.

Cote, J.F., and Vuori, K. (2002). Identification of an evolutionarily conserved superfamily of DOCK180-related proteins with guanine nucleotide exchange activity. J Cell Sci *115*, 4901-4913.

Cote, J.F., and Vuori, K. (2007). GEF what? Dock180 and related proteins help Rac to polarize cells in new ways. Trends in cell biology *17*, 383-393.

Cramer, L.P., Siebert, M., and Mitchison, T.J. (1997). Identification of novel graded polarity actin filament bundles in locomoting heart fibroblasts: implications for the generation of motile force. J Cell Biol *136*, 1287-1305.

Cudmore, S., Cossart, P., Griffiths, G., and Way, M. (1995). Actin-based motility of vaccinia virus. Nature *378*, 636-638.

Cyrklaff, M., Risco, C., Fernandez, J.J., Jimenez, M.V., Esteban, M., Baumeister, W., and Carrascosa, J.L. (2005). Cryo-electron tomography of vaccinia virus. Proc Natl Acad Sci U S A *102*, 2772-2777.

Davies, S.P., Reddy, H., Caivano, M., and Cohen, P. (2000). Specificity and mechanism of action of some commonly used protein kinase inhibitors. The Biochemical journal *351*, 95-105.

Davison, A.J., and Moss, B. (1989a). Structure of vaccinia virus early promoters. J Mol Biol *210*, 749-769.

Davison, A.J., and Moss, B. (1989b). Structure of vaccinia virus late promoters. J Mol Biol *210*, 771-784.

DerMardirossian, C., and Bokoch, G.M. (2005). GDIs: central regulatory molecules in Rho GTPase activation. Trends in cell biology *15*, 356-363.

DerMardirossian, C., Schnelzer, A., and Bokoch, G.M. (2004). Phosphorylation of RhoGDI by Pak1 mediates dissociation of Rac GTPase. Molecular cell *15*, 117-127.

Dias, S.M., and Cerione, R.A. (2007). X-ray crystal structures reveal two activated states for RhoC. Biochemistry *46*, 6547-6558.

Didsbury, J., Weber, R.F., Bokoch, G.M., Evans, T., and Snyderman, R. (1989). rac, a novel ras-related family of proteins that are botulinum toxin substrates. J Biol Chem *264*, 16378-16382.

Diz-Munoz, A., Krieg, M., Bergert, M., Ibarlucea-Benitez, I., Muller, D.J., Paluch, E., and Heisenberg, C.P. (2010). Control of directed cell migration in vivo by membrane-to-cortex attachment. PLoS biology *8*, e1000544.

Dobereiner, H.G., Dubin-Thaler, B.J., Hofman, J.M., Xenias, H.S., Sims, T.N., Giannone, G., Dustin, M.L., Wiggins, C.H., and Sheetz, M.P. (2006). Lateral membrane waves constitute a universal dynamic pattern of motile cells. Physical review letters *97*, 038102.

Doceul, V., Hollinshead, M., van der Linden, L., and Smith, G.L. (2010). Repulsion of superinfecting virions: a mechanism for rapid virus spread. Science *327*, 873-876.

Dodding, M.P., Newsome, T.P., Collinson, L.M., Edwards, C., and Way, M. (2009). An E2-F12 complex is required for intracellular enveloped virus morphogenesis during vaccinia infection. Cell Microbiol *11*, 808-824.

Dodding, M.P., and Way, M. (2009). Nck- and N-WASP-dependent actin-based motility is conserved in divergent vertebrate poxviruses. Cell Host Microbe *6*, 536-550.

Domi, A., and Beaud, G. (2000). The punctate sites of accumulation of vaccinia virus early proteins are precursors of sites of viral DNA synthesis. J Gen Virol *81*, 1231-1235.

Dominguez, R., and Holmes, K.C. (2011). Actin structure and function. Annual review of biophysics *40*, 169-186.

Dorseuil, O., Reibel, L., Bokoch, G.M., Camonis, J., and Gacon, G. (1996). The Rac target NADPH oxidase p67phox interacts preferentially with Rac2 rather than Rac1. J Biol Chem *271*, 83-88.

Dvorsky, R., and Ahmadian, M.R. (2004). Always look on the bright site of Rho: structural implications for a conserved intermolecular interface. EMBO reports *5*, 1130-1136.

Dvorsky, R., Blumenstein, L., Vetter, I.R., and Ahmadian, M.R. (2004). Structural insights into the interaction of ROCKI with the switch regions of RhoA. J Biol Chem *279*, 7098-7104.

Eden, S., Rohatgi, R., Podtelejnikov, A.V., Mann, M., and Kirschner, M.W. (2002). Mechanism of regulation of WAVE1-induced actin nucleation by Rac1 and Nck. Nature *418*, 790-793.

Edwards, D.C., Sanders, L.C., Bokoch, G.M., and Gill, G.N. (1999). Activation of LIM-kinase by Pak1 couples Rac/Cdc42 GTPase signalling to actin cytoskeletal dynamics. Nat Cell Biol *1*, 253-259.

Eisenmann, K.M., Harris, E.S., Kitchen, S.M., Holman, H.A., Higgs, H.N., and Alberts, A.S. (2007). Dia-interacting protein modulates formin-mediated actin assembly at the cell cortex. Curr Biol *17*, 579-591.

Eitzen, G. (2003). Actin remodeling to facilitate membrane fusion. Biochim Biophys Acta *1641*, 175-181.

Ellerbroek, S.M., Wennerberg, K., and Burridge, K. (2003). Serine phosphorylation negatively regulates RhoA in vivo. J Biol Chem *278*, 19023-19031.

Ellis, S., and Mellor, H. (2000). The novel Rho-family GTPase rif regulates coordinated actin-based membrane rearrangements. Curr Biol *10*, 1387-1390.

Fan, L., Pellegrin, S., Scott, A., and Mellor, H. (2010). The small GTPase Rif is an alternative trigger for the formation of actin stress fibers in epithelial cells. J Cell Sci *123*, 1247-1252.

Feig, L.A. (1999). Tools of the trade: use of dominant-inhibitory mutants of Ras-family GTPases. Nat Cell Biol *1*, E25-27.

Fernandez-Borja, M., Janssen, L., Verwoerd, D., Hordijk, P., and Neefjes, J. (2005). RhoB regulates endosome transport by promoting actin assembly on endosomal membranes through Dia1. J Cell Sci *118*, 2661-2670.

Forget, M.A., Desrosiers, R.R., Del, M., Moumdjian, R., Shedid, D., Berthelet, F., and Beliveau, R. (2002). The expression of rho proteins decreases with human brain tumor progression: potential tumor markers. Clin Exp Metastasis *19*, 9-15.

Foster, R., Hu, K.Q., Lu, Y., Nolan, K.M., Thissen, J., and Settleman, J. (1996). Identification of a novel human Rho protein with unusual properties: GTPase deficiency and in vivo farnesylation. Mol Cell Biol *16*, 2689-2699.

Fransson, A., Ruusala, A., and Aspenstrom, P. (2003). Atypical Rho GTPases have roles in mitochondrial homeostasis and apoptosis. J Biol Chem *278*, 6495-6502.

Fransson, S., Ruusala, A., and Aspenstrom, P. (2006). The atypical Rho GTPases Miro-1 and Miro-2 have essential roles in mitochondrial trafficking. Biochem Biophys Res Commun *344*, 500-510.

Friedl, P., and Wolf, K. (2003). Proteolytic and non-proteolytic migration of tumour cells and leucocytes. Biochemical Society symposium, 277-285.

Friedl, P., and Wolf, K. (2010). Plasticity of cell migration: a multiscale tuning model. J Cell Biol *188*, 11-19.

Frischknecht, F., Moreau, V., Rottger, S., Gonfloni, S., Reckmann, I., Superti-Furga, G., and Way, M. (1999). Actin-based motility of vaccinia virus mimics receptor tyrosine kinase signalling. Nature *401*, 926-929.

Fujisawa, K., Fujita, A., Ishizaki, T., Saito, Y., and Narumiya, S. (1996). Identification of the Rho-binding domain of p160ROCK, a Rho-associated coiled-coil containing protein kinase. J Biol Chem *271*, 23022-23028.

Gallego-Gomez, J.C., Risco, C., Rodriguez, D., Cabezas, P., Guerra, S., Carrascosa, J.L., and Esteban, M. (2003). Differences in virus-induced cell morphology and in virus maturation between MVA and other strains (WR, Ankara, and NYCBH) of vaccinia virus in infected human cells. J Virol *77*, 10606-10622.

Garcia-Mata, R., Boulter, E., and Burridge, K. (2011). The 'invisible hand': regulation of RHO GTPases by RHOGDIs. Nature reviews Molecular cell biology *12*, 493-504.

Gasman, S., Kalaidzidis, Y., and Zerial, M. (2003). RhoD regulates endosome dynamics through Diaphanous-related Formin and Src tyrosine kinase. Nat Cell Biol *5*, 195-204.

Gauthier-Rouviere, C., Vignal, E., Meriane, M., Roux, P., Montcourier, P., and Fort, P. (1998). RhoG GTPase controls a pathway that independently activates Rac1 and Cdc42Hs. Mol Biol Cell *9*, 1379-1394.

Giang Ho, T.T., Stultiens, A., Dubail, J., Lapiere, C.M., Nusgens, B.V., Colige, A.C., and Deroanne, C.F. (2011). RhoGDIalpha-dependent balance between RhoA and RhoC is a key regulator of cancer cell tumorigenesis. Mol Biol Cell *22*, 3263-3275.

Goebel, S.J., Johnson, G.P., Perkus, M.E., Davis, S.W., Winslow, J.P., and Paoletti, E. (1990). The complete DNA sequence of vaccinia virus. Virology *179*, 247-266, 517-263.

Goh, W.I., Sudhaharan, T., Lim, K.B., Sem, K.P., Lau, C.L., and Ahmed, S. (2011). Rif-mDia1 interaction is involved in filopodium formation independent of Cdc42 and Rac effectors. J Biol Chem *286*, 13681-13694.

Goode, B.L., and Eck, M.J. (2007). Mechanism and function of formins in the control of actin assembly. Annual review of biochemistry *76*, 593-627.

Grizot, S., Faure, J., Fieschi, F., Vignais, P.V., Dagher, M.C., and Pebay-Peyroula, E. (2001). Crystal structure of the Rac1-RhoGDI complex involved in nadph oxidase activation. Biochemistry *40*, 10007-10013.

Gu, Y., Filippi, M.D., Cancelas, J.A., Siefring, J.E., Williams, E.P., Jasti, A.C., Harris, C.E., Lee, A.W., Prabhakar, R., Atkinson, S.J.*, et al.* (2003). Hematopoietic cell regulation by Rac1 and Rac2 guanosine triphosphatases. Science *302*, 445-449.

Gu, Y., Jasti, A.C., Jansen, M., and Siefring, J.E. (2005). RhoH, a hematopoietic-specific Rho GTPase, regulates proliferation, survival, migration, and engraftment of hematopoietic progenitor cells. Blood *105*, 1467-1475.

Gubser, C., Hue, S., Kellam, P., and Smith, G.L. (2004). Poxvirus genomes: a phylogenetic analysis. J Gen Virol *85*, 105-117.

Guilluy, C., Garcia-Mata, R., and Burridge, K. (2011). Rho protein crosstalk: another social network? Trends in cell biology *21*, 718-726.

Gutjahr, M.C., Rossy, J., and Niggli, V. (2005). Role of Rho, Rac, and Rho-kinase in phosphorylation of myosin light chain, development of polarity, and spontaneous migration of Walker 256 carcinosarcoma cells. Experimental cell research *308*, 422-438.

Hagerty, L., Weitzel, D.H., Chambers, J., Fortner, C.N., Brush, M.H., Loiselle, D., Hosoya, H., and Haystead, T.A. (2007). ROCK1 phosphorylates and activates zipper-interacting protein kinase. J Biol Chem *282*, 4884-4893.

Hakem, A., Sanchez-Sweatman, O., You-Ten, A., Duncan, G., Wakeham, A., Khokha, R., and Mak, T.W. (2005). RhoC is dispensable for embryogenesis and tumor initiation but essential for metastasis. Genes & development *19*, 1974-1979.

Hakoshima, T., Shimizu, T., and Maesaki, R. (2003). Structural basis of the Rho GTPase signaling. J Biochem *134*, 327-331.

Hall, A. (1990). The cellular functions of small GTP-binding proteins. Science *249*, 635-640.

Han, Y., Eppinger, E., Schuster, I.G., Weigand, L.U., Liang, X., Kremmer, E., Peschel, C., and Krackhardt, A.M. (2009). Formin-like 1 (FMNL1) is regulated by N-terminal myristoylation and induces polarized membrane blebbing. J Biol Chem *284*, 33409-33417.

Hancock, J.F., Cadwallader, K., and Marshall, C.J. (1991a). Methylation and proteolysis are essential for efficient membrane binding of prenylated p21K-ras(B). EMBO J *10*, 641-646.

Hancock, J.F., Cadwallader, K., Paterson, H., and Marshall, C.J. (1991b). A CAAX or a CAAL motif and a second signal are sufficient for plasma membrane targeting of ras proteins. EMBO J *10*, 4033-4039.

Hancock, J.F., Paterson, H., and Marshall, C.J. (1990). A polybasic domain or palmitoylation is required in addition to the CAAX motif to localize p21ras to the plasma membrane. Cell *63*, 133-139.

Hannemann, S., Madrid, R., Stastna, J., Kitzing, T., Gasteier, J., Schonichen, A., Bouchet, J., Jimenez, A., Geyer, M., Grosse, R.*, et al.* (2008). The Diaphanous-related Formin FHOD1 associates with ROCK1 and promotes Src-dependent plasma membrane blebbing. J Biol Chem *283*, 27891-27903.

Hart, M.J., Eva, A., Evans, T., Aaronson, S.A., and Cerione, R.A. (1991). Catalysis of guanine nucleotide exchange on the CDC42Hs protein by the dbl oncogene product. Nature *354*, 311-314.

Heasman, S.J., Carlin, L.M., Cox, S., Ng, T., and Ridley, A.J. (2010). Coordinated RhoA signaling at the leading edge and uropod is required for T cell transendothelial migration. J Cell Biol *190*, 553-563.

Heimsath, E.G., Jr., and Higgs, H.N. (2012). The C terminus of formin FMNL3 accelerates actin polymerization and contains a WH2 domain-like sequence that binds both monomers and filament barbed ends. J Biol Chem *287*, 3087-3098.

Herrero-Martinez, E., Roberts, K.L., Hollinshead, M., and Smith, G.L. (2005). Vaccinia virus intracellular enveloped virions move to the cell periphery on microtubules in the absence of the A36R protein. J Gen Virol *86*, 2961-2968.

Herrlich, A., and Mayr, A. (1957). [Smallpox vaccine from tissue culture from a bull's tongue; at the same time a contribution to the question of culture vaccines]. Archiv fur die gesamte Virusforschung *7*, 284-296.

Heuser, J. (2005). Deep-etch EM reveals that the early poxvirus envelope is a single membrane bilayer stabilized by a geodetic "honeycomb" surface coat. J Cell Biol *169*, 269-283.

Hiller, G., and Weber, K. (1985). Golgi-derived membranes that contain an acylated viral polypeptide are used for vaccinia virus envelopment. J Virol *55*, 651-659.

Hoffman, G.R., Nassar, N., and Cerione, R.A. (2000). Structure of the Rho family GTP-binding protein Cdc42 in complex with the multifunctional regulator RhoGDI. Cell *100*, 345-356.

Hollinshead, M., Vanderplasschen, A., Smith, G.L., and Vaux, D.J. (1999). Vaccinia virus intracellular mature virions contain only one lipid membrane. J Virol *73*, 1503-1517.

Horiuchi, A., Imai, T., Wang, C., Ohira, S., Feng, Y., Nikaido, T., and Konishi, I. (2003). Up-regulation of small GTPases, RhoA and RhoC, is associated with tumor progression in ovarian carcinoma. Laboratory investigation; a journal of technical methods and pathology *83*, 861-870.

Hsiao, J.C., Chung, C.S., and Chang, W. (1999). Vaccinia virus envelope D8L protein binds to cell surface chondroitin sulfate and mediates the adsorption of intracellular mature virions to cells. J Virol *73*, 8750-8761.

Huang, C.Y., Lu, T.Y., Bair, C.H., Chang, Y.S., Jwo, J.K., and Chang, W. (2008). A novel cellular protein, VPEF, facilitates vaccinia virus penetration into HeLa cells through fluid phase endocytosis. J Virol *82*, 7988-7999.

Huang, M., and Prendergast, G.C. (2006). RhoB in cancer suppression. Histology and histopathology *21*, 213-218.

Hughes, A.L., Irausquin, S., and Friedman, R. (2010). The evolutionary biology of poxviruses. Infection, genetics and evolution : journal of molecular epidemiology and evolutionary genetics in infectious diseases *10*, 50-59.

Hutin, Y.J., Williams, R.J., Malfait, P., Pebody, R., Loparev, V.N., Ropp, S.L., Rodriguez, M., Knight, J.C., Tshioko, F.K., Khan, A.S.*, et al.* (2001). Outbreak of human monkeypox, Democratic Republic of Congo, 1996 to 1997. Emerging infectious diseases *7*, 434-438.

Huxley, H.E. (1963). Electron Microscope Studies on the Structure of Natural and Synthetic Protein Filaments from Striated Muscle. J Mol Biol *7*, 281-308.

Ichetovkin, I., Grant, W., and Condeelis, J. (2002). Cofilin produces newly polymerized actin filaments that are preferred for dendritic nucleation by the Arp2/3 complex. Curr Biol *12*, 79-84.

Ihara, K., Muraguchi, S., Kato, M., Shimizu, T., Shirakawa, M., Kuroda, S., Kaibuchi, K., and Hakoshima, T. (1998). Crystal structure of human RhoA in a dominantly active form complexed with a GTP analogue. J Biol Chem *273*, 9656-9666.

Iiizumi, M., Bandyopadhyay, S., Pai, S.K., Watabe, M., Hirota, S., Hosobe, S., Tsukada, T., Miura, K., Saito, K., Furuta, E.*, et al.* (2008). RhoC promotes metastasis via activation of the Pyk2 pathway in prostate cancer. Cancer Res *68*, 7613-7620.

Ikebe, M., Koretz, J., and Hartshorne, D.J. (1988). Effects of phosphorylation of light chain residues threonine 18 and serine 19 on the properties and conformation of smooth muscle myosin. J Biol Chem *263*, 6432-6437.

Irwin, C.R., and Evans, D.H. (2012). Modulation of the myxoma virus plaque phenotype by vaccinia virus protein F11. J Virol *86*, 7167-7179.

Ishizaki, T., Maekawa, M., Fujisawa, K., Okawa, K., Iwamatsu, A., Fujita, A., Watanabe, N., Saito, Y., Kakizuka, A., Morii, N.*, et al.* (1996). The small GTP-binding protein Rho binds to and activates a 160 kDa Ser/Thr protein kinase homologous to myotonic dystrophy kinase. EMBO J *15*, 1885-1893.

Islam, M., Lin, G., Brenner, J.C., Pan, Q., Merajver, S.D., Hou, Y., Kumar, P., and Teknos, T.N. (2009). RhoC expression and head and neck cancer metastasis. Molecular cancer research : MCR *7*, 1771-1780.

Jung, J.H., and Traugh, J.A. (2005). Regulation of the interaction of Pak2 with Cdc42 via autophosphorylation of serine 141. J Biol Chem *280*, 40025-40031.

Kamai, T., Kawakami, S., Koga, F., Arai, G., Takagi, K., Arai, K., Tsujii, T., and Yoshida, K.I. (2003a). RhoA is associated with invasion and lymph node metastasis in upper urinary tract cancer. BJU international *91*, 234-238.

Kamai, T., Tsujii, T., Arai, K., Takagi, K., Asami, H., Ito, Y., and Oshima, H. (2003b). Significant association of Rho/ROCK pathway with invasion and metastasis of bladder cancer. Clinical cancer research : an official journal of the American Association for Cancer Research *9*, 2632-2641.

Kanzaki, M., and Pessin, J.E. (2003). Insulin signaling: GLUT4 vesicles exit via the exocyst. Curr Biol *13*, R574-576.

Kato, S.E., Greco, F.A., Damaso, C.R., Condit, R.C., and Moussatche, N. (2004). An alternative genetic method to test essential vaccinia virus early genes. Journal of virological methods *115*, 31-40.

Katoh, H., Hiramoto, K., and Negishi, M. (2006). Activation of Rac1 by RhoG regulates cell migration. J Cell Sci *119*, 56-65.

Katoh, H., and Negishi, M. (2003). RhoG activates Rac1 by direct interaction with the Dock180-binding protein Elmo. Nature *424*, 461-464.

Kawano, Y., Fukata, Y., Oshiro, N., Amano, M., Nakamura, T., Ito, M., Matsumura, F., Inagaki, M., and Kaibuchi, K. (1999). Phosphorylation of myosin-binding subunit (MBS) of myosin phosphatase by Rho-kinase in vivo. J Cell Biol *147*, 1023-1038.

Keller, H., Rentsch, P., and Hagmann, J. (2002). Differences in cortical actin structure and dynamics document that different types of blebs are formed by distinct mechanisms. Experimental cell research *277*, 161-172.

Kitazawa, T., Eto, M., Woodsome, T.P., and Brautigan, D.L. (2000). Agonists trigger G protein-mediated activation of the CPI-17 inhibitor phosphoprotein of myosin light chain phosphatase to enhance vascular smooth muscle contractility. J Biol Chem *275*, 9897-9900.

Kitzing, T.M., Wang, Y., Pertz, O., Copeland, J.W., and Grosse, R. (2010). Formin-like 2 drives amoeboid invasive cell motility downstream of RhoC. Oncogene *29*, 2441-2448.

Komander, D., Garg, R., Wan, P.T., Ridley, A.J., and Barford, D. (2008). Mechanism of multi-site phosphorylation from a ROCK-I:RhoE complex structure. EMBO J *27*, 3175-3185.

Kovar, D.R., and Pollard, T.D. (2004). Insertional assembly of actin filament barbed ends in association with formins produces piconewton forces. Proc Natl Acad Sci U S A *101*, 14725-14730.

Kristelly, R., Gao, G., and Tesmer, J.J. (2004). Structural determinants of RhoA binding and nucleotide exchange in leukemia-associated Rho guanine-nucleotide exchange factor. J Biol Chem *279*, 47352-47362.

Kurokawa, K., and Matsuda, M. (2005). Localized RhoA activation as a requirement for the induction of membrane ruffling. Mol Biol Cell *16*, 4294-4303.

Kyrkou, A., Soufi, M., Bahtz, R., Ferguson, C., Bai, M., Parton, R.G., Hoffmann, I., Zerial, M., Fotsis, T., and Murphy, C. (2012). RhoD participates in the regulation of cell-cycle progression and centrosome duplication. Oncogene.

Laliberte, J.P., and Moss, B. (2009). Appraising the apoptotic mimicry model and the role of phospholipids for poxvirus entry. Proc Natl Acad Sci U S A *106*, 17517-17521.

Laliberte, J.P., Weisberg, A.S., and Moss, B. (2011). The membrane fusion step of vaccinia virus entry is cooperatively mediated by multiple viral proteins and host cell components. PLoS pathogens *7*, e1002446.

Langanger, G., Moeremans, M., Daneels, G., Sobieszek, A., De Brabander, M., and De Mey, J. (1986). The molecular organization of myosin in stress fibers of cultured cells. J Cell Biol *102*, 200-209.

Lapouge, K., Smith, S.J., Walker, P.A., Gamblin, S.J., Smerdon, S.J., and Rittinger, K. (2000). Structure of the TPR domain of p67phox in complex with Rac.GTP. Molecular cell *6*, 899-907.

Learned, L.A., Reynolds, M.G., Wassa, D.W., Li, Y., Olson, V.A., Karem, K., Stempora, L.L., Braden, Z.H., Kline, R., Likos, A*., et al.* (2005). Extended interhuman transmission of monkeypox in a hospital community in the Republic of the Congo, 2003. The American journal of tropical medicine and hygiene *73*, 428-434.

Lefkowitz, E.J., Wang, C., and Upton, C. (2006). Poxviruses: past, present and future. Virus research *117*, 105-118.

Lei, M., Lu, W., Meng, W., Parrini, M.C., Eck, M.J., Mayer, B.J., and Harrison, S.C. (2000). Structure of PAK1 in an autoinhibited conformation reveals a multistage activation switch. Cell *102*, 387-397.

Lemmon, M.A. (2008). Membrane recognition by phospholipid-binding domains. Nature reviews Molecular cell biology *9*, 99-111.

Leonard, D., Hart, M.J., Platko, J.V., Eva, A., Henzel, W., Evans, T., and Cerione, R.A. (1992). The identification and characterization of a GDP-dissociation inhibitor (GDI) for the CDC42Hs protein. J Biol Chem *267*, 22860-22868.

Leonard, D.A., Lin, R., Cerione, R.A., and Manor, D. (1998). Biochemical studies of the mechanism of action of the Cdc42-GTPase-activating protein. J Biol Chem *273*, 16210-16215.

Leung, T., Chen, X.Q., Manser, E., and Lim, L. (1996). The p160 RhoA-binding kinase ROK alpha is a member of a kinase family and is involved in the reorganization of the cytoskeleton. Mol Cell Biol *16*, 5313-5327.

Leung, T., Manser, E., Tan, L., and Lim, L. (1995). A novel serine/threonine kinase binding the Ras-related RhoA GTPase which translocates the kinase to peripheral membranes. J Biol Chem *270*, 29051-29054.

Li, F., and Higgs, H.N. (2005). Dissecting requirements for auto-inhibition of actin nucleation by the formin, mDia1. J Biol Chem *280*, 6986-6992.

Li, X., Bu, X., Lu, B., Avraham, H., Flavell, R.A., and Lim, B. (2002). The hematopoiesis-specific GTP-binding protein RhoH is GTPase deficient and modulates activities of other Rho GTPases by an inhibitory function. Mol Cell Biol *22*, 1158-1171.

Li, X.D., Saito, J., Ikebe, R., Mabuchi, K., and Ikebe, M. (2000). The interaction between the regulatory light chain domains on two heads is critical for regulation of smooth muscle myosin. Biochemistry *39*, 2254-2260.

Lin, C.L., Chung, C.S., Heine, H.G., and Chang, W. (2000). Vaccinia virus envelope H3L protein binds to cell surface heparan sulfate and is important for intracellular mature virion morphogenesis and virus infection in vitro and in vivo. J Virol *74*, 3353-3365.

Liu, A., Cerniglia, G.J., Bernhard, E.J., and Prendergast, G.C. (2001). RhoB is required to mediate apoptosis in neoplastically transformed cells after DNA damage. Proc Natl Acad Sci U S A *98*, 6192-6197.

Liu, M., Tang, Q., Qiu, M., Lang, N., Li, M., Zheng, Y., and Bi, F. (2011). miR-21 targets the tumor suppressor RhoB and regulates proliferation, invasion and apoptosis in colorectal cancer cells. FEBS Lett *585*, 2998-3005.

Longenecker, K., Read, P., Derewenda, U., Dauter, Z., Liu, X., Garrard, S., Walker, L., Somlyo, A.V., Nakamoto, R.K., Somlyo, A.P.*, et al.* (1999). How RhoGDI binds Rho. Acta crystallographica Section D, Biological crystallography *55*, 1503-1515.

Lorentzen, A., Bamber, J., Sadok, A., Elson-Schwab, I., and Marshall, C.J. (2011). An ezrin-rich, rigid uropod-like structure directs movement of amoeboid blebbing cells. J Cell Sci *124*, 1256-1267.

Luo, H., Zou, J., Dong, Z., Zeng, Q., Wu, D., and Liu, L. (2012). Up-regulated miR-17 promotes cell proliferation, tumour growth and cell cycle progression by targeting the RND3 tumour suppressor gene in colorectal carcinoma. The Biochemical journal *442*, 311-321.

Lutz, S., Shankaranarayanan, A., Coco, C., Ridilla, M., Nance, M.R., Vettel, C., Baltus, D., Evelyn, C.R., Neubig, R.R., Wieland, T.*, et al.* (2007). Structure of Galphaq-p63RhoGEF-RhoA complex reveals a pathway for the activation of RhoA by GPCRs. Science *318*, 1923-1927.

Machacek, M., Hodgson, L., Welch, C., Elliott, H., Pertz, O., Nalbant, P., Abell, A., Johnson, G.L., Hahn, K.M., and Danuser, G. (2009). Coordination of Rho GTPase activities during cell protrusion. Nature *461*, 99-103.

Madaule, P., and Axel, R. (1985). A novel ras-related gene family. Cell *41*, 31-40.

Maesaki, R., Ihara, K., Shimizu, T., Kuroda, S., Kaibuchi, K., and Hakoshima, T. (1999). The structural basis of Rho effector recognition revealed by the crystal structure of human RhoA complexed with the effector domain of PKN/PRK1. Molecular cell *4*, 793-803.

Maiti, S., Michelot, A., Gould, C., Blanchoin, L., Sokolova, O., and Goode, B.L. (2012). Structure and activity of full-length formin mDia1. Cytoskeleton (Hoboken) *69*, 393-405.

Malacombe, M., Bader, M.F., and Gasman, S. (2006). Exocytosis in neuroendocrine cells: new tasks for actin. Biochim Biophys Acta *1763*, 1175-1183.

Mallardo, M., Schleich, S., and Krijnse Locker, J. (2001). Microtubule-dependent organization of vaccinia virus core-derived early mRNAs into distinct cytoplasmic structures. Mol Biol Cell *12*, 3875-3891.

Manser, E., Leung, T., Salihuddin, H., Zhao, Z.S., and Lim, L. (1994). A brain serine/threonine protein kinase activated by Cdc42 and Rac1. Nature *367*, 40-46.

Matsui, T., Amano, M., Yamamoto, T., Chihara, K., Nakafuku, M., Ito, M., Nakano, T., Okawa, K., Iwamatsu, A., and Kaibuchi, K. (1996). Rho-associated kinase, a novel serine/threonine kinase, as a putative target for small GTP binding protein Rho. EMBO J *15*, 2208-2216.

Mayr, A. (2003). Smallpox vaccination and bioterrorism with pox viruses. Comparative immunology, microbiology and infectious diseases *26*, 423-430.

Mayr, A., Stickl, H., Muller, H.K., Danner, K., and Singer, H. (1978). [The smallpox vaccination strain MVA: marker, genetic structure, experience gained with the parenteral vaccination and behavior in organisms with a debilitated defence mechanism (author's transl)]. Zentralblatt fur Bakteriologie, Parasitenkunde, Infektionskrankheiten und Hygiene Erste Abteilung Originale Reihe B: Hygiene, Betriebshygiene, praventive Medizin *167*, 375-390.

Mazieres, J., Antonia, T., Daste, G., Muro-Cacho, C., Berchery, D., Tillement, V., Pradines, A., Sebti, S., and Favre, G. (2004). Loss of RhoB expression in human lung cancer progression. Clinical cancer research : an official journal of the American Association for Cancer Research *10*, 2742-2750.

McGough, A., Pope, B., Chiu, W., and Weeds, A. (1997). Cofilin changes the twist of F-actin: implications for actin filament dynamics and cellular function. J Cell Biol *138*, 771-781.

Meisinger-Henschel, C., Schmidt, M., Lukassen, S., Linke, B., Krause, L., Konietzny, S., Goesmann, A., Howley, P., Chaplin, P., Suter, M.*, et al.* (2007). Genomic sequence of chorioallantois vaccinia virus Ankara, the ancestor of modified vaccinia virus Ankara. J Gen Virol *88*, 3249-3259.

Meller, J., Vidali, L., and Schwartz, M.A. (2008). Endogenous RhoG is dispensable for integrin-mediated cell spreading but contributes to Rac-independent migration. J Cell Sci *121*, 1981-1989.

Mellor, H., Flynn, P., Nobes, C.D., Hall, A., and Parker, P.J. (1998). PRK1 is targeted to endosomes by the small GTPase, RhoB. J Biol Chem *273*, 4811-4814.

Mercer, J., and Helenius, A. (2008). Vaccinia virus uses macropinocytosis and apoptotic mimicry to enter host cells. Science *320*, 531-535.

Meyer, H., Sutter, G., and Mayr, A. (1991). Mapping of deletions in the genome of the highly attenuated vaccinia virus MVA and their influence on virulence. J Gen Virol *72 (Pt 5)*, 1031-1038.

Michaelson, D., Silletti, J., Murphy, G., D'Eustachio, P., Rush, M., and Philips, M.R. (2001). Differential localization of Rho GTPases in live cells: regulation by hypervariable regions and RhoGDI binding. J Cell Biol *152*, 111-126.

Miki, H., Sasaki, T., Takai, Y., and Takenawa, T. (1998). Induction of filopodium formation by a WASP-related actin-depolymerizing protein N-WASP. Nature *391*, 93-96.

Morales, I., Carbajal, M.A., Bohn, S., Holzer, D., Kato, S.E., Greco, F.A., Moussatche, N., and Krijnse Locker, J. (2008). The vaccinia virus F11L gene product facilitates cell detachment and promotes migration. Traffic *9*, 1283-1298.

Moreau, V., Frischknecht, F., Reckmann, I., Vincentelli, R., Rabut, G., Stewart, D., and Way, M. (2000). A complex of N-WASP and WIP integrates signalling cascades that lead to actin polymerization. Nat Cell Biol *2*, 441-448.

Moriyama, K., Iida, K., and Yahara, I. (1996). Phosphorylation of Ser-3 of cofilin regulates its essential function on actin. Genes to cells : devoted to molecular & cellular mechanisms *1*, 73-86.

Morone, N., Fujiwara, T., Murase, K., Kasai, R.S., Ike, H., Yuasa, S., Usukura, J., and Kusumi, A. (2006). Three-dimensional reconstruction of the membrane skeleton at the plasma membrane interface by electron tomography. J Cell Biol *174*, 851-862.

Morreale, A., Venkatesan, M., Mott, H.R., Owen, D., Nietlispach, D., Lowe, P.N., and Laue, E.D. (2000). Structure of Cdc42 bound to the GTPase binding domain of PAK. Nature structural biology *7*, 384-388.

Moss, B. (2007). Poxviridae: The viruses and their replication, Fifth edition edn (Lippincott, Williams & Williams).

Moss, B. (2012). Poxvirus Cell Entry: How Many Proteins Does it Take? Viruses *4*, 688-707.

Mott, H.R., Owen, D., Nietlispach, D., Lowe, P.N., Manser, E., Lim, L., and Laue, E.D. (1999). Structure of the small G protein Cdc42 bound to the GTPase-binding domain of ACK. Nature *399*, 384-388.

Munemitsu, S., Innis, M.A., Clark, R., McCormick, F., Ullrich, A., and Polakis, P. (1990). Molecular cloning and expression of a G25K cDNA, the human homolog of the yeast cell cycle gene CDC42. Mol Cell Biol *10*, 5977-5982.

Murphy, C., Saffrich, R., Grummt, M., Gournier, H., Rybin, V., Rubino, M., Auvinen, P., Lutcke, A., Parton, R.G., and Zerial, M. (1996). Endosome dynamics regulated by a Rho protein. Nature *384*, 427-432.

Murphy, D.A., and Courtneidge, S.A. (2011). The 'ins' and 'outs' of podosomes and invadopodia: characteristics, formation and function. Nature reviews Molecular cell biology *12*, 413-426.

Naji, L., Pacholsky, D., and Aspenstrom, P. (2011). ARHGAP30 is a Wrch-1-interacting protein involved in actin dynamics and cell adhesion. Biochem Biophys Res Commun *409*, 96-102.

Nakagawa, O., Fujisawa, K., Ishizaki, T., Saito, Y., Nakao, K., and Narumiya, S. (1996). ROCK-I and ROCK-II, two isoforms of Rho-associated coiled-coil forming protein serine/threonine kinase in mice. FEBS Lett *392*, 189-193.

Neudauer, C.L., Joberty, G., Tatsis, N., and Macara, I.G. (1998). Distinct cellular effects and interactions of the Rho-family GTPase TC10. Curr Biol *8*, 1151-1160.

Newsome, T.P., Scaplehorn, N., and Way, M. (2004). SRC mediates a switch from microtubule- to actin-based motility of vaccinia virus. Science *306*, 124-129.

Newsome, T.P., Weisswange, I., Frischknecht, F., and Way, M. (2006). Abl collaborates with Src family kinases to stimulate actin-based motility of vaccinia virus. Cell Microbiol *8*, 233-241.

Nezami, A.G., Poy, F., and Eck, M.J. (2006). Structure of the autoinhibitory switch in formin mDia1. Structure *14*, 257-263.

Nguyen, Q.D., Faivre, S., Bruyneel, E., Rivat, C., Seto, M., Endo, T., Mareel, M., Emami, S., and Gespach, C. (2002). RhoA- and RhoD-dependent regulatory switch of Galpha subunit signaling by PAR-1 receptors in cellular invasion. FASEB journal : official publication of the Federation of American Societies for Experimental Biology *16*, 565-576.

Nichols, R.J., Dzamko, N., Hutti, J.E., Cantley, L.C., Deak, M., Moran, J., Bamborough, P., Reith, A.D., and Alessi, D.R. (2009). Substrate specificity and inhibitors of LRRK2, a protein kinase mutated in Parkinson's disease. The Biochemical journal *424*, 47-60.

Nicole, S., White, P.S., Topaloglu, H., Beigthon, P., Salih, M., Hentati, F., and Fontaine, B. (1999). The human CDC42 gene: genomic organization, evidence for the existence of a putative pseudogene and exclusion as a SJS1 candidate gene. Human genetics *105*, 98-103.

Nimnual, A.S., Taylor, L.J., and Bar-Sagi, D. (2003). Redox-dependent downregulation of Rho by Rac. Nat Cell Biol *5*, 236-241.

Nobes, C.D., and Hall, A. (1995). Rho, rac, and cdc42 GTPases regulate the assembly of multimolecular focal complexes associated with actin stress fibers, lamellipodia, and filopodia. Cell *81*, 53-62.

Nobes, C.D., Lauritzen, I., Mattei, M.G., Paris, S., Hall, A., and Chardin, P. (1998). A new member of the Rho family, Rnd1, promotes disassembly of actin filament structures and loss of cell adhesion. J Cell Biol *141*, 187-197.

Ohta, Y., Hartwig, J.H., and Stossel, T.P. (2006). FilGAP, a Rho- and ROCK-regulated GAP for Rac binds filamin A to control actin remodelling. Nat Cell Biol *8*, 803-814.

Oinuma, I., Kawada, K., Tsukagoshi, K., and Negishi, M. (2012). Rnd1 and Rnd3 targeting to lipid raft is required for p190 RhoGAP activation. Mol Biol Cell *23*, 1593-1604.

Oleksy, A., Opalinski, L., Derewenda, U., Derewenda, Z.S., and Otlewski, J. (2006). The molecular basis of RhoA specificity in the guanine nucleotide exchange factor PDZ-RhoGEF. J Biol Chem *281*, 32891-32897.

Otomo, T., Tomchick, D.R., Otomo, C., Panchal, S.C., Machius, M., and Rosen, M.K. (2005). Structural basis of actin filament nucleation and processive capping by a formin homology 2 domain. Nature *433*, 488-494.

Paluch, E., Piel, M., Prost, J., Bornens, M., and Sykes, C. (2005). Cortical actomyosin breakage triggers shape oscillations in cells and cell fragments. Biophysical journal *89*, 724-733.

Paluch, E., Sykes, C., Prost, J., and Bornens, M. (2006). Dynamic modes of the cortical actomyosin gel during cell locomotion and division. Trends in cell biology *16*, 5-10.

Parker, R.F., Bronson, L.H., and Green, R.H. (1941). Further Studies of the Infectious Unit of Vaccinia. The Journal of experimental medicine *74*, 263-281.

Parrini, M.C., Lei, M., Harrison, S.C., and Mayer, B.J. (2002). Pak1 kinase homodimers are autoinhibited in trans and dissociated upon activation by Cdc42 and Rac1. Molecular cell *9*, 73-83.

Paterson, H.F., Self, A.J., Garrett, M.D., Just, I., Aktories, K., and Hall, A. (1990). Microinjection of recombinant p21rho induces rapid changes in cell morphology. J Cell Biol *111*, 1001-1007.

Paul, A.S., and Pollard, T.D. (2008). The role of the FH1 domain and profilin in formin-mediated actin-filament elongation and nucleation. Curr Biol *18*, 9-19.

Peck, J., Douglas, G.t., Wu, C.H., and Burbelo, P.D. (2002). Human RhoGAP domain-containing proteins: structure, function and evolutionary relationships. FEBS Lett *528*, 27-34.

Pellegrin, S., and Mellor, H. (2005). The Rho family GTPase Rif induces filopodia through mDia2. Curr Biol *15*, 129-133.

Pertz, O., Hodgson, L., Klemke, R.L., and Hahn, K.M. (2006). Spatiotemporal dynamics of RhoA activity in migrating cells. Nature *440*, 1069-1072.

Pinner, S., and Sahai, E. (2008a). Imaging amoeboid cancer cell motility in vivo. Journal of microscopy *231*, 441-445.

Pinner, S., and Sahai, E. (2008b). PDK1 regulates cancer cell motility by antagonising inhibition of ROCK1 by RhoE. Nat Cell Biol *10*, 127-137.

Pommereit, D., and Wouters, F.S. (2007). An NGF-induced Exo70-TC10 complex locally antagonises Cdc42-mediated activation of N-WASP to modulate neurite outgrowth. J Cell Sci *120*, 2694-2705.

Postigo, A., and Way, M. (2012). The vaccinia virus-encoded Bcl-2 homologues do not act as direct Bax inhibitors. J Virol *86*, 203-213.

Pruyne, D., Evangelista, M., Yang, C., Bi, E., Zigmond, S., Bretscher, A., and Boone, C. (2002). Role of formins in actin assembly: nucleation and barbed-end association. Science *297*, 612-615.

Reckmann, I., Higley, S., and Way, M. (1997). The vaccinia virus F17R protein interacts with actin. FEBS Lett *409*, 141-146.

Reis, K., Fransson, A., and Aspenstrom, P. (2009). The Miro GTPases: at the heart of the mitochondrial transport machinery. FEBS Lett *583*, 1391-1398.

Ridley, A.J. (2011). Life at the leading edge. Cell *145*, 1012-1022.

Ridley, A.J., and Hall, A. (1992). The small GTP-binding protein rho regulates the assembly of focal adhesions and actin stress fibers in response to growth factors. Cell *70*, 389-399.

Ridley, A.J., Paterson, H.F., Johnston, C.L., Diekmann, D., and Hall, A. (1992). The small GTP-binding protein rac regulates growth factor-induced membrane ruffling. Cell *70*, 401-410.

Riento, K., Guasch, R.M., Garg, R., Jin, B., and Ridley, A.J. (2003). RhoE binds to ROCK I and inhibits downstream signaling. Mol Cell Biol *23*, 4219-4229.

Riento, K., Totty, N., Villalonga, P., Garg, R., Guasch, R., and Ridley, A.J. (2005). RhoE function is regulated by ROCK I-mediated phosphorylation. EMBO J *24*, 1170-1180.

Rietdorf, J., Ploubidou, A., Reckmann, I., Holmstrom, A., Frischknecht, F., Zettl, M., Zimmermann, T., and Way, M. (2001). Kinesin-dependent movement on microtubules precedes actin-based motility of vaccinia virus. Nat Cell Biol *3*, 992-1000.

Rittinger, K., Walker, P.A., Eccleston, J.F., Smerdon, S.J., and Gamblin, S.J. (1997). Structure at 1.65 A of RhoA and its GTPase-activating protein in complex with a transition-state analogue. Nature *389*, 758-762.

Roberts, A.W., Kim, C., Zhen, L., Lowe, J.B., Kapur, R., Petryniak, B., Spaetti, A., Pollock, J.D., Borneo, J.B., Bradford, G.B.*, et al.* (1999). Deficiency of the

hematopoietic cell-specific Rho family GTPase Rac2 is characterized by abnormalities in neutrophil function and host defense. Immunity *10*, 183-196.

Roberts, K.L., and Smith, G.L. (2008). Vaccinia virus morphogenesis and dissemination. Trends Microbiol *16*, 472-479.

Rodriguez, J.R., Risco, C., Carrascosa, J.L., Esteban, M., and Rodriguez, D. (1998). Vaccinia virus 15-kilodalton (A14L) protein is essential for assembly and attachment of viral crescents to virosomes. J Virol *72*, 1287-1296.

Rohatgi, R., Ho, H.Y., and Kirschner, M.W. (2000). Mechanism of N-WASP activation by CDC42 and phosphatidylinositol 4, 5-bisphosphate. J Cell Biol *150*, 1299-1310.

Rohatgi, R., Ma, L., Miki, H., Lopez, M., Kirchhausen, T., Takenawa, T., and Kirschner, M.W. (1999). The interaction between N-WASP and the Arp2/3 complex links Cdc42-dependent signals to actin assembly. Cell *97*, 221-231.

Rohatgi, R., Nollau, P., Ho, H.Y., Kirschner, M.W., and Mayer, B.J. (2001). Nck and phosphatidylinositol 4,5-bisphosphate synergistically activate actin polymerization through the N-WASP-Arp2/3 pathway. J Biol Chem *276*, 26448-26452.

Rose, R., Weyand, M., Lammers, M., Ishizaki, T., Ahmadian, M.R., and Wittinghofer, A. (2005a). Structural and mechanistic insights into the interaction between Rho and mammalian Dia. Nature *435*, 513-518.

Rose, R., Wittinghofer, A., and Weyand, M. (2005b). The purification and crystallization of mDia1 in complex with RhoC. Acta crystallographica Section F, Structural biology and crystallization communications *61*, 225-227.

Rosenfeldt, H., Castellone, M.D., Randazzo, P.A., and Gutkind, J.S. (2006). Rac inhibits thrombin-induced Rho activation: evidence of a Pak-dependent GTPase crosstalk. Journal of molecular signaling *1*, 8.

Rosenthal, D.T., Zhang, J., Bao, L., Zhu, L., Wu, Z., Toy, K., Kleer, C.G., and Merajver, S.D. (2012). RhoC Impacts the Metastatic Potential and Abundance of Breast Cancer Stem Cells. PLoS One *7*, e40979.

Rossman, K.L., Worthylake, D.K., Snyder, J.T., Cheng, L., Whitehead, I.P., and Sondek, J. (2002). Functional analysis of cdc42 residues required for Guanine nucleotide exchange. J Biol Chem *277*, 50893-50898.

Rossy, J., Gutjahr, M.C., Blaser, N., Schlicht, D., and Niggli, V. (2007). Ezrin/moesin in motile Walker 256 carcinosarcoma cells: signal-dependent relocalization and role in migration. Experimental cell research *313*, 1106-1120.

Rubins, K.H., Hensley, L.E., Bell, G.W., Wang, C., Lefkowitz, E.J., Brown, P.O., and Relman, D.A. (2008). Comparative analysis of viral gene expression programs during poxvirus infection: a transcriptional map of the vaccinia and monkeypox genomes. PLoS One *3*, e2628.

Ruusala, A., and Aspenstrom, P. (2008). The atypical Rho GTPase Wrch1 collaborates with the nonreceptor tyrosine kinases Pyk2 and Src in regulating cytoskeletal dynamics. Mol Cell Biol *28*, 1802-1814.

Sagot, I., Rodal, A.A., Moseley, J., Goode, B.L., and Pellman, D. (2002). An actin nucleation mechanism mediated by Bni1 and profilin. Nat Cell Biol *4*, 626-631.

Sahai, E., and Marshall, C.J. (2002). ROCK and Dia have opposing effects on adherens junctions downstream of Rho. Nat Cell Biol *4*, 408-415.

Sahai, E., and Marshall, C.J. (2003). Differing modes of tumour cell invasion have distinct requirements for Rho/ROCK signalling and extracellular proteolysis. Nat Cell Biol *5*, 711-719.

Sakurai-Yageta, M., Recchi, C., Le Dez, G., Sibarita, J.B., Daviet, L., Camonis, J., D'Souza-Schorey, C., and Chavrier, P. (2008). The interaction of IQGAP1 with the exocyst complex is required for tumor cell invasion downstream of Cdc42 and RhoA. J Cell Biol *181*, 985-998.

Sancho, M.C., Schleich, S., Griffiths, G., and Krijnse-Locker, J. (2002). The block in assembly of modified vaccinia virus Ankara in HeLa cells reveals new insights into vaccinia virus morphogenesis. J Virol *76*, 8318-8334.

Sanders, L.C., Matsumura, F., Bokoch, G.M., and de Lanerolle, P. (1999). Inhibition of myosin light chain kinase by p21-activated kinase. Science *283*, 2083-2085.

Sanderson, C.M., and Smith, G.L. (1998). Vaccinia virus induces Ca2+-independent cell-matrix adhesion during the motile phase of infection. J Virol *72*, 9924-9933.

Sanderson, C.M., Way, M., and Smith, G.L. (1998). Virus-induced cell motility. J Virol *72*, 1235-1243.

Sandgren, K.J., Wilkinson, J., Miranda-Saksena, M., McInerney, G.M., Byth-Wilson, K., Robinson, P.J., and Cunningham, A.L. (2010). A differential role for macropinocytosis in mediating entry of the two forms of vaccinia virus into dendritic cells. PLoS pathogens *6*, e1000866.

Sanz-Moreno, V., Gadea, G., Ahn, J., Paterson, H., Marra, P., Pinner, S., Sahai, E., and Marshall, C.J. (2008). Rac activation and inactivation control plasticity of tumor cell movement. Cell *135*, 510-523.

Saras, J., Wollberg, P., and Aspenstrom, P. (2004). Wrch1 is a GTPase-deficient Cdc42-like protein with unusual binding characteristics and cellular effects. Experimental cell research *299*, 356-369.

Scaplehorn, N., Holmstrom, A., Moreau, V., Frischknecht, F., Reckmann, I., and Way, M. (2002). Grb2 and Nck act cooperatively to promote actin-based motility of vaccinia virus. Curr Biol *12*, 740-745.

Schepis, A., Schramm, B., de Haan, C.A., and Locker, J.K. (2006). Vaccinia virus-induced microtubule-dependent cellular rearrangements. Traffic *7*, 308-323.

Schmelz, M., Sodeik, B., Ericsson, M., Wolffe, E.J., Shida, H., Hiller, G., and Griffiths, G. (1994). Assembly of vaccinia virus: the second wrapping cisterna is derived from the trans Golgi network. J Virol *68*, 130-147.

Schmidt, F.I., Bleck, C.K., Helenius, A., and Mercer, J. (2011). Vaccinia extracellular virions enter cells by macropinocytosis and acid-activated membrane rupture. EMBO J *30*, 3647-3661.

Schmidt, F.I., Bleck, C.K., and Mercer, J. (2012). Poxvirus host cell entry. Current opinion in virology *2*, 20-27.

Schmittgen, T.D., and Livak, K.J. (2008). Analyzing real-time PCR data by the comparative C(T) method. Nature protocols *3*, 1101-1108.

Schramm, B., de Haan, C.A., Young, J., Doglio, L., Schleich, S., Reese, C., Popov, A.V., Steffen, W., Schroer, T., and Locker, J.K. (2006). Vaccinia-virus-induced cellular contractility facilitates the subcellular localization of the viral replication sites. Traffic *7*, 1352-1367.

Sebbagh, M., Renvoize, C., Hamelin, J., Riche, N., Bertoglio, J., and Breard, J. (2001). Caspase-3-mediated cleavage of ROCK I induces MLC phosphorylation and apoptotic membrane blebbing. Nat Cell Biol *3*, 346-352.

Sellers, J.R., Eisenberg, E., and Adelstein, R.S. (1982). The binding of smooth muscle heavy meromyosin to actin in the presence of ATP. Effect of phosphorylation. J Biol Chem *257*, 13880-13883.

Senkevich, T.G., Ojeda, S., Townsley, A., Nelson, G.E., and Moss, B. (2005). Poxvirus multiprotein entry-fusion complex. Proc Natl Acad Sci U S A *102*, 18572-18577.

Shimizu, T., Ihara, K., Maesaki, R., Amano, M., Kaibuchi, K., and Hakoshima, T. (2003). Parallel coiled-coil association of the RhoA-binding domain in Rho-kinase. J Biol Chem *278*, 46046-46051.

Shimizu, T., Ihara, K., Maesaki, R., Kuroda, S., Kaibuchi, K., and Hakoshima, T. (2000). An open conformation of switch I revealed by the crystal structure of a Mg2+-free form of RHOA complexed with GDP. Implications for the GDP/GTP exchange mechanism. J Biol Chem *275*, 18311-18317.

Shinjo, K., Koland, J.G., Hart, M.J., Narasimhan, V., Johnson, D.I., Evans, T., and Cerione, R.A. (1990). Molecular cloning of the gene for the human placental GTP-binding protein Gp (G25K): identification of this GTP-binding protein as the human homolog of the yeast cell-division-cycle protein CDC42. Proc Natl Acad Sci U S A *87*, 9853-9857.

Shutes, A., Berzat, A.C., Chenette, E.J., Cox, A.D., and Der, C.J. (2006). Biochemical analyses of the Wrch atypical Rho family GTPases. Methods Enzymol *406*, 11-26.

Sloan, C.M., Quinn, C.V., Peters, J.P., Farley, J., Goetzinger, C., Wernli, M., Demali, K.A., and Ellerbroek, S.M. (2012). Divergence of Rho residue 43 impacts GEF activity. Small GTPases *3*, 15-22.

Smith, G.L., and Law, M. (2004). The exit of vaccinia virus from infected cells. Virus research *106*, 189-197.

Sugihara, K., Nakatsuji, N., Nakamura, K., Nakao, K., Hashimoto, R., Otani, H., Sakagami, H., Kondo, H., Nozawa, S., Aiba, A.*, et al.* (1998). Rac1 is required for the formation of three germ layers during gastrulation. Oncogene *17*, 3427-3433.

Sumi, T., Matsumoto, K., and Nakamura, T. (2001). Specific activation of LIM kinase 2 via phosphorylation of threonine 505 by ROCK, a Rho-dependent protein kinase. J Biol Chem *276*, 670-676.

Sumi, T., Matsumoto, K., Takai, Y., and Nakamura, T. (1999). Cofilin phosphorylation and actin cytoskeletal dynamics regulated by rho- and Cdc42-activated LIM-kinase 2. J Cell Biol *147*, 1519-1532.

Svitkina, T.M., and Borisy, G.G. (1999). Arp2/3 complex and actin depolymerizing factor/cofilin in dendritic organization and treadmilling of actin filament array in lamellipodia. J Cell Biol *145*, 1009-1026.

Takahashi, K., Sasaki, T., Mammoto, A., Takaishi, K., Kameyama, T., Tsukita, S., and Takai, Y. (1997). Direct interaction of the Rho GDP dissociation inhibitor with ezrin/radixin/moesin initiates the activation of the Rho small G protein. J Biol Chem *272*, 23371-23375.

Tao, W., Pennica, D., Xu, L., Kalejta, R.F., and Levine, A.J. (2001). Wrch-1, a novel member of the Rho gene family that is regulated by Wnt-1. Genes & development *15*, 1796-1807.

Tartaglia, J., Perkus, M.E., Taylor, J., Norton, E.K., Audonnet, J.C., Cox, W.I., Davis, S.W., van der Hoeven, J., Meignier, B., Riviere, M.*, et al.* (1992). NYVAC: a highly attenuated strain of vaccinia virus. Virology *188*, 217-232.

Tcherkezian, J., and Lamarche-Vane, N. (2007). Current knowledge of the large RhoGAP family of proteins. Biology of the cell / under the auspices of the European Cell Biology Organization *99*, 67-86.

Thorne, S.H. (2008). Oncolytic vaccinia virus: from bedside to benchtop and back. Current opinion in molecular therapeutics *10*, 387-392.

Tinevez, J.Y., Schulze, U., Salbreux, G., Roensch, J., Joanny, J.F., and Paluch, E. (2009). Role of cortical tension in bleb growth. Proc Natl Acad Sci U S A *106*, 18581-18586.

Tolonen, N., Doglio, L., Schleich, S., and Krijnse Locker, J. (2001). Vaccinia virus DNA replication occurs in endoplasmic reticulum-enclosed cytoplasmic mini-nuclei. Mol Biol Cell *12*, 2031-2046.

Tomasevic, N., Jia, Z., Russell, A., Fujii, T., Hartman, J.J., Clancy, S., Wang, M., Beraud, C., Wood, K.W., and Sakowicz, R. (2007). Differential regulation of WASP and N-WASP by Cdc42, Rac1, Nck, and PI(4,5)P2. Biochemistry *46*, 3494-3502.

Tooze, J., Hollinshead, M., Reis, B., Radsak, K., and Kern, H. (1993). Progeny vaccinia and human cytomegalovirus particles utilize early endosomal cisternae for their envelopes. European journal of cell biology *60*, 163-178.

Totsukawa, G., Wu, Y., Sasaki, Y., Hartshorne, D.J., Yamakita, Y., Yamashiro, S., and Matsumura, F. (2004). Distinct roles of MLCK and ROCK in the regulation of membrane protrusions and focal adhesion dynamics during cell migration of fibroblasts. J Cell Biol *164*, 427-439.

Townsley, A.C., Weisberg, A.S., Wagenaar, T.R., and Moss, B. (2006). Vaccinia virus entry into cells via a low-pH-dependent endosomal pathway. J Virol *80*, 8899-8908.

Trahey, M., and McCormick, F. (1987). A cytoplasmic protein stimulates normal N-ras p21 GTPase, but does not affect oncogenic mutants. Science *238*, 542-545.

Traut, T.W. (1994). Physiological concentrations of purines and pyrimidines. Molecular and cellular biochemistry *140*, 1-22.

Troeger, A., Johnson, A.J., Wood, J., Blum, W.G., Andritsos, L.A., Byrd, J.C., and Williams, D.A. (2012). RhoH is critical for cell-microenvironment interactions in chronic lymphocytic leukemia in mice and humans. Blood *119*, 4708-4718.

Tsubakimoto, K., Matsumoto, K., Abe, H., Ishii, J., Amano, M., Kaibuchi, K., and Endo, T. (1999). Small GTPase RhoD suppresses cell migration and cytokinesis. Oncogene *18*, 2431-2440.

Tsung, K., Yim, J.H., Marti, W., Buller, R.M., and Norton, J.A. (1996). Gene expression and cytopathic effect of vaccinia virus inactivated by psoralen and long-wave UV light. J Virol *70*, 165-171.

Tu, D., Li, Y., Song, H.K., Toms, A.V., Gould, C.J., Ficarro, S.B., Marto, J.A., Goode, B.L., and Eck, M.J. (2011). Crystal structure of a coiled-coil domain from human ROCK I. PLoS One *6*, e18080.

Tu, H., and Wigler, M. (1999). Genetic evidence for Pak1 autoinhibition and its release by Cdc42. Mol Cell Biol *19*, 602-611.

Upton, C., Slack, S., Hunter, A.L., Ehlers, A., and Roper, R.L. (2003). Poxvirus orthologous clusters: toward defining the minimum essential poxvirus genome. J Virol *77*, 7590-7600.

Valderrama, F., Cordeiro, J.V., Schleich, S., Frischknecht, F., and Way, M. (2006). Vaccinia virus-induced cell motility requires F11L-mediated inhibition of RhoA signaling. Science *311*, 377-381.

Valencia, A., Chardin, P., Wittinghofer, A., and Sander, C. (1991). The ras protein family: evolutionary tree and role of conserved amino acids. Biochemistry *30*, 4637-4648.

Vega, F.M., Colomba, A., Reymond, N., Thomas, M., and Ridley, A.J. (2012). RhoB regulates cell migration through altered focal adhesion dynamics. Open biology *2*, 120076.

Vega, F.M., Fruhwirth, G., Ng, T., and Ridley, A.J. (2011). RhoA and RhoC have distinct roles in migration and invasion by acting through different targets. J Cell Biol *193*, 655-665.

Verkhovsky, A.B., and Borisy, G.G. (1993). Non-sarcomeric mode of myosin II organization in the fibroblast lamellum. J Cell Biol *123*, 637-652.

Vetter, I.R., and Wittinghofer, A. (2001). The guanine nucleotide-binding switch in three dimensions. Science *294*, 1299-1304.

Vicente-Manzanares, M., Ma, X., Adelstein, R.S., and Horwitz, A.R. (2009). Non-muscle myosin II takes centre stage in cell adhesion and migration. Nature reviews Molecular cell biology *10*, 778-790.

Vignal, E., De Toledo, M., Comunale, F., Ladopoulou, A., Gauthier-Rouviere, C., Blangy, A., and Fort, P. (2000). Characterization of TCL, a new GTPase of the rho family related to TC10 andCcdc42. J Biol Chem *275*, 36457-36464.

Vigorito, E., Bell, S., Hebeis, B.J., Reynolds, H., McAdam, S., Emson, P.C., McKenzie, A., and Turner, M. (2004). Immunological function in mice lacking the Rac-related GTPase RhoG. Mol Cell Biol *24*, 719-729.

Vincent, S., Jeanteur, P., and Fort, P. (1992). Growth-regulated expression of rhoG, a new member of the ras homolog gene family. Mol Cell Biol *12*, 3138-3148.

Vinzenz, M., Nemethova, M., Schur, F., Mueller, J., Narita, A., Urban, E., Winkler, C., Schmeiser, C., Koestler, S.A., Rottner, K.*, et al.* (2012). Actin branching in the initiation and maintenance of lamellipodia. J Cell Sci.

Walker, M.P., Zhang, M., Le, T.P., Wu, P., Laine, M., and Greene, G.L. (2011). RAC3 is a pro-migratory co-activator of ERalpha. Oncogene *30*, 1984-1994.

Ward, B.M., and Moss, B. (2004). Vaccinia virus A36R membrane protein provides a direct link between intracellular enveloped virions and the microtubule motor kinesin. J Virol *78*, 2486-2493.

Watanabe, G., Saito, Y., Madaule, P., Ishizaki, T., Fujisawa, K., Morii, N., Mukai, H., Ono, Y., Kakizuka, A., and Narumiya, S. (1996). Protein kinase N (PKN) and PKN-related protein rhophilin as targets of small GTPase Rho. Science *271*, 645-648.

Wells, C.M., and Jones, G.E. (2010). The emerging importance of group II PAKs. The Biochemical journal *425*, 465-473.

Wennerberg, K., and Der, C.J. (2004). Rho-family GTPases: it's not only Rac and Rho (and I like it). J Cell Sci *117*, 1301-1312.

Wennerberg, K., Forget, M.A., Ellerbroek, S.M., Arthur, W.T., Burridge, K., Settleman, J., Der, C.J., and Hansen, S.H. (2003). Rnd proteins function as RhoA antagonists by activating p190 RhoGAP. Curr Biol *13*, 1106-1115.

Wheeler, A.P., and Ridley, A.J. (2004). Why three Rho proteins? RhoA, RhoB, RhoC, and cell motility. Experimental cell research *301*, 43-49.

Wheeler, A.P., and Ridley, A.J. (2007). RhoB affects macrophage adhesion, integrin expression and migration. Experimental cell research *313*, 3505-3516.

Wherlock, M., Gampel, A., Futter, C., and Mellor, H. (2004). Farnesyltransferase inhibitors disrupt EGF receptor traffic through modulation of the RhoB GTPase. J Cell Sci *117*, 3221-3231.

Wittek, R. (1982). Organization and expression of the poxvirus genome. Experientia *38*, 285-297.

Wolf, K., Mazo, I., Leung, H., Engelke, K., von Andrian, U.H., Deryugina, E.I., Strongin, A.Y., Brocker, E.B., and Friedl, P. (2003). Compensation mechanism in tumor cell migration: mesenchymal-amoeboid transition after blocking of pericellular proteolysis. J Cell Biol *160*, 267-277.

Wolfe, C.L., Ojeda, S., and Moss, B. (2012). Transcriptional repression and RNA silencing act synergistically to demonstrate the function of the eleventh component of the vaccinia virus entry-fusion complex. J Virol *86*, 293-301.

Woodrum, D.T., Rich, S.A., and Pollard, T.D. (1975). Evidence for biased bidirectional polymerization of actin filaments using heavy meromyosin prepared by an improved method. J Cell Biol *67*, 231-237.

Worthylake, D.K., Rossman, K.L., and Sondek, J. (2000). Crystal structure of Rac1 in complex with the guanine nucleotide exchange region of Tiam1. Nature *408*, 682-688.

Worthylake, R.A., Lemoine, S., Watson, J.M., and Burridge, K. (2001). RhoA is required for monocyte tail retraction during transendothelial migration. J Cell Biol *154*, 147-160.

Wu, X., and Frost, J.A. (2006). Multiple Rho proteins regulate the subcellular targeting of PAK5. Biochem Biophys Res Commun *351*, 328-335.

Wyatt, L.S., Carroll, M.W., Czerny, C.P., Merchlinsky, M., Sisler, J.R., and Moss, B. (1998). Marker rescue of the host range restriction defects of modified vaccinia virus Ankara. Virology *251*, 334-342.

Xu, Y., Moseley, J.B., Sagot, I., Poy, F., Pellman, D., Goode, B.L., and Eck, M.J. (2004). Crystal structures of a Formin Homology-2 domain reveal a tethered dimer architecture. Cell *116*, 711-723.

Yaffe, M.B. (2002). Phosphotyrosine-binding domains in signal transduction. Nature reviews Molecular cell biology *3*, 177-186.

Yang, J., Zhang, Z., Roe, S.M., Marshall, C.J., and Barford, D. (2009). Activation of Rho GTPases by DOCK exchange factors is mediated by a nucleotide sensor. Science *325*, 1398-1402.

Yoshinaga, C., Mukai, H., Toshimori, M., Miyamoto, M., and Ono, Y. (1999). Mutational analysis of the regulatory mechanism of PKN: the regulatory region of PKN contains an arachidonic acid-sensitive autoinhibitory domain. J Biochem *126*, 475-484.

Zalcman, G., Closson, V., Linares-Cruz, G., Lerebours, F., Honore, N., Tavitian, A., and Olofsson, B. (1995). Regulation of Ras-related RhoB protein expression during the cell cycle. Oncogene *10*, 1935-1945.

Zenke, F.T., Krendel, M., DerMardirossian, C., King, C.C., Bohl, B.P., and Bokoch, G.M. (2004). p21-activated kinase 1 phosphorylates and regulates 14-3-3 binding to GEF-H1, a microtubule-localized Rho exchange factor. J Biol Chem *279*, 18392-18400.

Zhang, B., Zhang, Y., Collins, C.C., Johnson, D.I., and Zheng, Y. (1999). A built-in arginine finger triggers the self-stimulatory GTPase-activating activity of rho family GTPases. J Biol Chem *274*, 2609-2612.

Zhang, Y., and Moss, B. (1992). Immature viral envelope formation is interrupted at the same stage by lac operator-mediated repression of the vaccinia virus D13L gene and by the drug rifampicin. Virology *187*, 643-653.

Zhou, J., Li, K., Gu, Y., Feng, B., Ren, G., Zhang, L., Wang, Y., Nie, Y., and Fan, D. (2011). Transcriptional up-regulation of RhoE by hypoxia-inducible factor (HIF)-1 promotes epithelial to mesenchymal transition of gastric cancer cells during hypoxia. Biochem Biophys Res Commun *415*, 348-354.

Zigmond, S.H., Evangelista, M., Boone, C., Yang, C., Dar, A.C., Sicheri, F., Forkey, J., and Pring, M. (2003). Formin leaky cap allows elongation in the presence of tight capping proteins. Curr Biol *13*, 1820-1823.

Zwilling, J., Sliva, K., Schwantes, A., Schnierle, B., and Sutter, G. (2010). Functional F11L and K1L genes in modified vaccinia virus Ankara restore virus-induced cell motility but not growth in human and murine cells. Virology *404*, 231-239.